CANADIAN THESES ON MICROFICHE

THÈSES CANADIENNES SUR MICROFICHE

National Library of Canada
Collections Development Branch

Canadian Theses on
Microfiche Service

Ottawa, Canada
K1A 0N4

Bibliothèque nationale du Canada
Direction du développement des collections

Service des thèses canadiennes
sur microfiche

NOTICE

The quality of this microfiche is heavily dependent upon the quality of the original thesis submitted for microfilming. Every effort has been made to ensure the highest quality of reproduction possible.

If pages are missing, contact the university which granted the degree.

Some pages may have indistinct print especially if the original pages were typed with a poor typewriter ribbon or if the university sent us an inferior photocopy.

Previously copyrighted materials (journal articles, published tests, etc.) are not filmed.

Reproduction in full or in part of this film is governed by the Canadian Copyright Act, R.S.C. 1970, c. C-30. Please read the authorization forms which accompany this thesis.

AVIS

La qualité de cette microfiche dépend grandement de la qualité de la thèse soumise au microfilmage. Nous avons tout fait pour assurer une qualité supérieure de reproduction.

S'il manque des pages, veuillez communiquer avec l'université qui a conféré le grade.

La qualité d'impression de certaines pages peut laisser à désirer, surtout si les pages originales ont été dactylographiées à l'aide d'un ruban usé ou si l'université nous a fait parvenir une photocopie de qualité inférieure.

Les documents qui font déjà l'objet d'un droit d'auteur (articles de revue, examens publiés, etc.) ne sont pas microfilmés.

La reproduction, même partielle, de ce microfilm est soumise à la Loi canadienne sur le droit d'auteur, SRC 1970, c. C-30. Veuillez prendre connaissance des formules d'autorisation qui accompagnent cette thèse.

THIS DISSERTATION
HAS BEEN MICROFILMED
EXACTLY AS RECEIVED

LA THÈSE A ÉTÉ
MICROFILMÉE TELLE QUE
NOUS L'AVONS REÇUE

NL 339 (r. 86/09)

Canadä

0-315-21280-2

(8)

National Library of Canada
Canadian Theses Division
Ottawa, Canada
K1A 0N4

Bibliothèque nationale du Canada
Division des thèses canadiennes

PERMISSION TO MICROFILM — AUTORISATION DE MICROFILMER

- Please print or type — Écrire en lettres moulées ou dactylographier

Full Name of Author — Nom complet de l'auteur
LORRAINE ANN PATERSON

Date of Birth — Date de naissance 7 FEBRUARY 1959	Country of Birth — Lieu de naissance NEW ZEALAND

Permanent Address — Résidence fixe
23 MARETH ST PANMURE
AUCKLAND, 6
NEW ZEALAND

Title of Thesis — Titre de la thèse
PETROLOGY OF THE TSU LAKE GNEISS IN THE FORT SMITH AREA

University — Université
UNIVERSITY OF ALBERTA

Degree for which thesis was presented — Grade pour lequel cette thèse fut présentée
MSc

Year this degree conferred — Année d'obtention de ce grade 1985	Name of Supervisor — Nom du directeur de thèse D.G.W. SMITH R. St.J. LAMBERT

Permission is hereby granted to the NATIONAL LIBRARY OF CANADA to microfilm this thesis and to lend or sell copies of the film.

The author reserves other publication rights, and neither the thesis nor extensive extracts from it may be printed or otherwise reproduced without the author's written permission.

L'autorisation est, par la présente, accordée à la BIBLIOTHÈQUE NATIONALE DU CANADA de microfilmer cette thèse et de prêter ou de vendre des exemplaires du film.

L'auteur se réserve les autres droits de publication; ni la thèse ni de longs extraits de celle-ci ne doivent être imprimés ou autrement reproduits sans l'autorisation écrite de l'auteur.

Date 17 January 1985	Signature L. A. Paterson

NL-91 (4/77)

THE UNIVERSITY OF ALBERTA

Petrology of the Tsu Lake Gneiss in the Fort Smith Area

by

Ⓒ Lorraine Ann Paterson

A THESIS

SUBMITTED TO THE FACULTY OF GRADUATE STUDIES AND RESEARCH

IN PARTIAL FULFILMENT OF THE REQUIREMENTS FOR THE DEGREE

OF Master of Science

Department of Geology

EDMONTON, ALBERTA

Spring 1985

THE UNIVERSITY OF ALBERTA

RELEASE FORM

NAME OF AUTHOR	Lorraine Ann Paterson
TITLE OF THESIS	Petrology of the Tsu Lake Gneiss in the Fort Smith Area
DEGREE FOR WHICH THESIS WAS PRESENTED	Master of Science
YEAR THIS DEGREE GRANTED	Spring 1985

Permission is hereby granted to THE UNIVERSITY OF ALBERTA LIBRARY to reproduce single copies of this thesis and to lend or sell such copies for private, scholarly or scientific research purposes only.

The author reserves other publication rights, and neither the thesis nor extensive extracts from it may be printed or otherwise reproduced without the author's written permission.

(SIGNED) L.A. Paterson

PERMANENT ADDRESS:

23 MARETH ST
PANMURE, AUCKLAND, 6
NEW ZEALAND

DATED 17 January 1985

THE UNIVERSITY OF ALBERTA

FACULTY OF GRADUATE STUDIES AND RESEARCH

The undersigned certify that they have read, and recommend to the Faculty of Graduate Studies and Research, for acceptance, a thesis entitled Petrology of the Tsu Lake Gneiss in the Fort Smith Area submitted by Lorraine Ann Paterson in partial fulfilment of the requirements for the degree of Master of Science.

Supervisor

R. St J Lambert

Supervisor

H. Baadsgaard

Date 17 January 1985

Abstract

The mineral assemblages of both pelitic and basic rocks from the Tsu Lake area, in the NW Churchill Province, indicate the attainment of granulite facies metamorphic conditions. The pelitic samples show evidence of partial melting while the basic rocks appear to have been unaffected. In contrast rocks from Deskenatlata Lake, which lies 30 km northwest of Tsu Lake, are typical of amphibolite facies grade metamorphism. Compositions of the minerals in the Tsu Lake rocks are consistent with those commonly found in granulite facies rocks and are quite distinct from the compositions of the same phases in Deskenatlata Lake assemblages.

There is little petrographical evidence of lower grade metamorphic overprints in the Tsu Lake rocks. The occurrence of prehnite associated with biotite in the intermediate to basic rocks is the strongest evidence for the existence of another metamorphic event. Compositional data on the granulite facies minerals indicate regular partitioning relations of the major elements between most of the major mineral pairs. The order of preference for Fe over Mg partitioning into the Tsu Lake minerals is in accordance with that predicted for granulite facies conditions. This implies that the granulite facies event has been unaffected by later metamorphic overprinting.

Temperature estimates of 680 - 750°C are suggested for the Tsu Lake area by the presence of hornblende in the basic rocks. Pressures are constrained at 4.5 ±0.5 kb by the assemblage grnt - cord - sill - qtz. Temperatures for the Deskenatlata Lake area are estimated at 600 - 650 °C; based on the absence of the hornblende breakdown reaction and the presence of sphene. Higher fO_2 conditions than at Tsu Lake are inferred for the Deskenatlata Lake area.

The granulite facies metamorphic event at Tsu Lake is assumed to be Archean in age, while the amphibolite facies metamorphism at Deskenatlata Lake is Aphebian. Both areas have been affected by a lower grade greenschist facies metamorphic event, represented by the occurrence of prehnite.

Geochemical data indicate the Tsu Lake rocks show the LIL element patterns characteristic of the metasomatic event which affected the whole of the Athabasca mobile belt. The Tsu Lake granulites do not show the depletion in the LIL element patterns which is

present in several other granulite facies terrains.

REE patterns of the Tsu Lake rocks suggest that the REE are immobile in the basic rocks but have been fractionated in the partially melted pelitic rocks. A study of the REE patterns of granulite facies minerals, from both Tsu Lake and a higher pressure granulite facies terrain, the Scourian complex in NW Scotland, show a similarity to the REE patterns of minerals from dacitic rocks. However, the similarity may be unrelated to igneous processes, as has been implied elsewhere, because there are important differences in the REE partitioning relations between the major minerals and in the REE patterns of the accessory phases.

Acknowledgements

Many people have assisted me in the production of this thesis. Firstly, I would like to thank both of my supervisors, Professors D.G.W. Smith and R. St.J. Lambert, for their financial support and help. I would also like to thank the Department of Geology for a University of Alberta teaching assistantship.

Field work and the collection of samples would not have been possible without financial aid from the Boreal Institute for Northern Studies and the Department of Indian Affairs and Northern Development (DIAND), for which the author is grateful. Additional field support was provided by DIAND and by the Geological Survey of Canada (GSC). Sincere thanks is due to the people who assisted me in the field at various times: A.D. Smith, B. Bowerman and K. Fyten.

Most of the research undertaken in this thesis would not have been possible without the analytical facilities that were made available to me. Use of the electron microprobe facilities in the Department of Geology is gratefully acknowledged. The microprobe facilities are supported by a Natural Sciences and Engineering Research Council (NSERC) grant to D.G.W. Smith. I would like to express my gratitude to the staff of the microprobe facilities, D.A. Tomlinson and S. Launspach, for their co-operation and assistance in the collection of data and subsequent processing. Professor L.G. Stephens-Newsham is thanked for allowing me to use the necessary equipment at the SLOWPOKE reactor facility at the University of Alberta. These facilities are supported, in part, by an NSERC infrastructure grant. The staff of the SLOWPOKE facility have provided me with much assistance, in particular M.J.M. Duke, D. Ng and P. Ford; I am indebted to them. The geochemical laboratories of the GSC in Ottawa are thanked for providing geochemical analyses of some of my samples; this assistance was possible through the support of Dr H.H. Bostock of the GSC. Dr H.H. Bostock has been supportive of this project from the beginning and I take this opportunity to thank him for his assistance. Professor H. Baadsgaard has provided me with invaluable assistance in some aspects of this project for which I express my appreciation.

Lastly, but not the least, I express my gratitude to my friends; P. Metcalfe, M.J.M. Duke, P.A. Cavell and D.A. Tomlinson, who have provided moral support and encouragement without which this thesis would probably not have been completed. P. Metcalfe and M.J.M. Duke are also thanked for the assistance they gave in the final stages of the production of this thesis.

Table of Contents

Page

1. INTRODUCTION 1
Regional Geology 1
NW Churchill Province 3
Fort Smith Area 4
Tsu Lake 7
Deskenatlata Lake 8
Research Procedures 8
2. PETROGRAPHY, MINERALOGY AND ELEMENT PARTITIONING 10
Sampling 10
Petrography 11
Tsu Lake Samples 11
Basic Assemblages 14
Intermediate - Quartzofeldspathic Assemblages 20
Pelitic Assemblages 21
Deskenatlata Lake Assemblages 27
Unusual Features 28
Prehnite Occurrences 28
Monazite and Allanite Occurrences 31
Mineralogy 31
Amphiboles 32
Pyroxenes 37
Orthopyroxene 37
Clinopyroxene 42
Biotite 47
Garnet 53
Feldspars 58
Plagioclase 58
K-feldspar 60

Cordierite 60
Sillimanite 62
Oxides 63
Ilmenite 63
Magnetite 66
Hercynite 66
Sphene and Rutile 68
Prehnite 68
Element Partitioning 71
Distribution Diagrams 71
$Fe^{2+}/(Fe^{2+}+Mg)$ Partitioning 71
Mn Partitioning 82
Ti Partitioning 87
AFM Diagrams 89
Basic Assemblages 90
Basic to Intermediate Assemblages 92
Pelitic Assemblages 92
Mineral-Forming Reactions 94
Pelitic Assemblages 94
Basic to Intermediate Assemblages 96
3. GEOTHERMOMETRY AND GEOBAROMETRY 100
Stability Regions of Critical Mineral Reactions 100
Basic Assemblages 100
Pelitic Assemblages 103
Geothermometry-Geobarometry 107
Exchange Geothermometers 108
Garnet-Biotite 109
Application 111
Garnet-Cordierite 113
Application 114
Orthopyroxene-Clinopyroxene 116

Application 120
Pyroxene-Ilmenite 124
Application 125
Magnetite-Ilmenite 127
Application 129
Two Feldspar 130
Geobarometry 131
Garnet-Cordierite Geobarometer 132
Application 134
Conclusions 136

4. GEOCHEMISTRY 138
Significance of LIL element patterns in granulites 139
Tsu Lake LIL element characteristics 144
REE Geochemistry 151
Whole Rock REE Geochemistry 152
Sample Selection 152
Results 154
Basic Rocks 154
Dolerites 159
Pelitic Rocks I 159
Pelitic Rocks II 163
Granites 165
Mineral REE Geochemistry 167
Mineral Selectivity for the REE 168
Results 169
Orthopyroxene 169
Clinopyroxene 174
Hornblende 178
Plagioclase 179
Apatite 184
Zircon 187

Garnet 190
Mineral / Mineral Pairs 191
Conclusions 200
5. CONCLUSIONS 203
Mineralogy 203
Geochemistry 207
REFERENCES 208
APPENDIX 1 225
ELECTRON MICROPROBE ANALYSIS 226
Pyroxenes 231
Amphiboles 231
Ilmenite 231
Magnetite 231
WHOLE ROCK GEOCHEMICAL ANALYSES 232
INSTRUMENTAL NEUTRON ACTIVATION ANALYSIS 233
Sample Preparation 233
Crushing 233
Mineral Separations 234
Pelletisation 234
Semi-absolute Technique 235
Irradiation - Decay - Counting 236
Detection System 237
Sources of Error 238
Self Absorption 238
Interferences 239
Determination of the Semi-absolute Experimental Parameters 240
Data Processing 240
APPENDIX 2 243
NUMERICAL EXPRESSIONS OF GEOTHERMOMETERS 244
Garnet - Biotite 244
Ferry and Spear (1978) 244

Thompson (1976) 244
Holdaway and Lee (1977) 245
Perchuk and Lavrent eva (1983) 245
Ganguly and Saxena (1984) 245
Garnet - Cordierite 246
Thompson (1976) 246
Holdaway and Lee (1977) 246
Perchuk and Lavrent eva 246
Orthopyroxene - Clinopyroxene 247
Wood and Banno (1973) 247
Wells (1977) 247
Saxena (1976) 247
Kretz (1982) 249
Pyroxene - Ilmenite 249
Bishop (1980) 249
APPENDIX 3 250

List of Tables

Page

Table 3.1. Garnet - biotite geothermometry. 112

Table 3.2. Garnet - cordierite Geothermometry 115

Table 3.3. Orthopyroxene - clinopyroxene geothermometry 122

Table 3.4. Pyroxene - ilmenite geothermometry. 126

Table 3.5. Garnet - cordierite geobarometry. 135

Table 4.1. Whole rock geochemical analyses: metaigneous lithologies. 140

Table 4.2. Whole rock geochemical analyses: metasedimentary lithologies. 141

Table A.1. Electron microprobe standards. 228

Table A.2. Statistical detection limits for EDA. 229

Table A.3. Statistical detection limits for whole rock geochemical data. 232

Table A.4. USGS rock standard REE values. 241

Table I. Amphibole analyses 251

Table II. Orthopyroxene analyses. 255

Table III. Clinopyroxene analyses 258

Table IV. Biotite analyses 260

Table V. Garnet analyses. 266

Table VI. Plagioclase analyses. 269

Table VII. K-feldspar analyses. 274

Table VIII. Cordierite analyses. 276

Table IX. Sillimanite analyses 278

Table X. Ilmenite analyses 279

Table XI. Magnetite analyses. 283

Table XII. Hercynite analyses. 286

Table XIII. Sphene analyses 287

Table XIV. Rutile analyses 288

Table XV. Prehnite, epidote and grandite analyses. 289

Table XVI. REE analyses of whole rocks. 291

Table XVII. REE analyses of minerals. 296

Table XVIII. Whole rock geochemical analyses: metasedimentary lithologies. 301
Table XIX. Whole rock geochemical analyses: metaigneous lithologies. 305
Table XX. Whole rock geochemical analyses: granitic lithologies. 307

List of Figures

Page

Fig. 1.1. Map showing the location of the study area........ 2

Fig. 2.1. Geological map of the Tsu Lake area........ 12

Fig. 2.2. Geological map of the Deskenatlata Lake area........ 13

Fig. 2.3. Compositional variation of the amphiboles........ 33

Fig. 2.4. Variation of Al(IV) and A site contents of amphiboles........ 35

Fig. 2.5. Variation of Al(IV) and Al(VI) contents of amphiboles........ 35

Fig. 2.6. Variation of Al(IV) and Ti contents of amphiboles........ 36

Fig. 2.7. Variation of the Ca, Mg and Fe^{2+} contents of the pyroxenes........ 38

Fig. 2.8. Variation of Mg and Fe^{2+} contents of orthopyroxenes........ 38

Fig. 2.9. Variation of Ca and Mg contents in orthopyroxenes........ 40

Fig. 2.10. Variation of Mg and Si in orthopyroxenes........ 40

Fig. 2.11. Variation of Al(IV) and Al(VI) in orthopyroxenes........ 41

Fig. 2.12. Variation of Ca and Al(VI) in orthopyroxenes........ 41

Fig. 2.13. Variation of Mn and Fe^{2+} in orthopyroxenes........ 43

Fig. 2.14. Variation of Mg and Fe^{2+} in clinopyroxenes........ 43

Fig. 2.15. Variation of Al(IV) and Al(VI) in clinopyroxenes........ 45

Fig. 2.16. Variation of Mg and Ca in clinopyroxenes........ 45

Fig. 2.17. Variation of Mg and Mn in clinopyroxenes........ 46

Fig. 2.18. Variation of Al$_2$O$_3$, FeO and MgO in biotites........ 48

Fig. 2.19. Variation of Al(IV) and Al(VI) in biotites........ 50

Fig. 2.20. Variation of Ti and Al(IV) in biotites........ 50

Fig. 2.21. Variation of Ti and Al(VI) in biotites........ 51

Fig. 2.22. Variation of the calculated total positive charge and Al(VI) in biotites........ 51

Fig. 2.23. Variation of the calculated total positive charge and Ti in biotites........ 54

Fig. 2.24. Variation of Ti versus the Mg/Fe^{2+} ratio in biotites........ 54

Fig. 2.25. Variation of Ca, Mg and Fe^{2+}+Mn in garnets........ 55

Fig. 2.26. Variation of Ca, Mn, and Fe^{2+}+Mg in garnets........ 55

Fig. 2.27. Relationship between the percentage of grossular in garnet and the anorthite

content of coexisting plagioclase. 56
Fig. 2.28. Variation of Ca, Na and K in both plagioclase and K-feldspar. 59
Fig. 2.29. Relationship between the $CaO / (CaO + Na_2O)$ ratio in plagioclase versus that of the rock. 59
Fig. 2.30. Variation of Al(tot) and Si in cordierites. 61
Fig. 2.31. Variation of Al(tot) and Fe+Mg+Mn in cordierites. 61
Fig. 2.32. Variation of Ti, Fe^{2+} and Fe^{3+} in ilmenites. 64
Fig. 2.33. Variation of Fe^{2+}, Mg and Mn in ilmenites. 65
Fig. 2.34. Variation of Ti, Fe^{2+} and Fe^{3+} in magnetites. 67
Fig. 2.35. Variation of Fe^{3+}, Al and Cr+V in magnetites. 67
Fig. 2.36. Variation of Ca, Fe^{3+} and Al in prehnites, epidotes and grandite. 70
Fig. 2.37. Partitioning of $Fe^{2+} / (Fe^{2+}+Mg)$ between orthopyroxenes and clinopyroxenes. 72
Fig. 2.38. Partitioning of $Fe^{2+} / (Fe^{2+}+Mg)$ between orthopyroxenes and hornblendes. 72
Fig. 2.39. Partitioning of $Fe^{2+} / (Fe^{2+}+Mg)$ between clinopyroxenes and hornblendes. 73
Fig. 2.40. Partitioning of $Fe^{2+} / (Fe^{2+}+Mg)$ between orthopyroxenes and biotites. 73
Fig. 2.41. Partitioning of $Fe^{2+} / (Fe^{2+}+Mg)$ between clinopyroxenes and biotites. 75
Fig. 2.42. Partitioning of $Fe^{2+} / (Fe^{2+}+Mg)$ between hornblendes and biotites. 75
Fig. 2.43. Partitioning of $Fe^{2+} / (Fe^{2+}+Mg)$ between the rock and (a) pyroxenes, and (b) biotite. 76
Fig. 2.44. Relationship between the distribution coefficient for the partitioning of $Fe^{2+} / (Fe^{2+}+Mg)$ between orthopyroxene, clinopyroxene and hornblende, and the Al(IV) content of hornblende. 77
Fig. 2.45. Partitioning of $Fe^{2+} / (Fe^{2+}+Mg)$ between garnet and cordierite. 77
Fig. 2.46. Partitioning of $Fe^{2+} / (Fe^{2+}+Mg)$ between garnet and biotite. 79
Fig. 2.47. Partitioning of $Fe^{2+} / (Fe^{2+}+Mg)$ between cordierite and biotite. 79
Fig. 2.48. Partitioning of $Fe^{2+} / (Fe^{2+}+Mg)$ between the rock and (a) garnet and cordierite, and (b) biotite. 80
Fig. 2.49. Partitioning of Mn between orthopyroxenes and clinopyroxenes. 83
Fig. 2.50. Partitioning of Mn between pyroxenes and hornblendes. 83
Fig. 2.51. Partitioning of Mn between pyroxenes and ilmenites. 84
Fig. 2.52. Partitioning of Mn between garnets and ilmenites and cordierites. 84

Fig. 2.53. Partitioning of Mn between cordierites and ilmenites. 85

Fig. 2.54. Partitioning of Mn between the rock and (a) garnet, ilmenite and (b) orthopyroxene, cordierite. 86

Fig. 2.55. Partitioning of Ti between hornblendes, biotites and clinopyroxenes. 88

Fig. 2.56. Partitioning of Ti between magnetites and biotites. 88

Fig. 2.57. AFM diagram of the group 1 to 3 basic samples of Tsu Lake. 91

Fig. 2.58. AFM diagram of the group 5 and 6 pelitic samples of Tsu Lake. 93

Fig. 2.59. Relationship between the $Fe^{2+}/(Fe^{2+}+Mg)$ ratio of hornblendes and the percentage of anorthite in coexisting plagioclases. 98

Fig. 3.1. Stability fields for the hornblende breakdown reaction. 101

Fig. 3.2. Stability regions of the H_2O - saturated minimum melting reactions, H_2O - conserving melting reactions, and dehydration reactions for pelitic rocks. 104

Fig. 3.3. Stability regions for some reactions in the system $FeO - Al_2O_3 - SiO_2 - H_2O$. 106

Fig. 3.4. Calculated site occupancies of orthopyroxene and clinopyroxene. 121

Fig. 4.1. Relationship between K (wt. %) and Rb (ppm) for the Tsu Lake samples. 145

Fig. 4.2. Relationship between K (wt. %) and Sr (ppm) for the Tsu Lake samples. 145

Fig. 4.3. Relationship between K (wt. %) and Ba (ppm) for the Tsu Lake samples. 147

Fig. 4.4. Relationship between Rb (ppm) and Sr (ppm) for the Tsu Lake samples. 147

Fig. 4.5. Relationship between Ba (ppm)) and Rb (ppm) for the Tsu Lake samples. 149

Fig. 4.6. Relationship between Ba (ppm) and Sr (ppm) for the Tsu Lake samples. 149

Fig. 4.7. Chondrite normalised REE patterns of the Tsu Lake group 1 basic rocks. 155

Fig. 4.8. Chondrite normalised REE patterns of the Tsu Lake group 2 basic granulites. 156

Fig. 4.9. Chondrite normalised REE patterns of the Tsu Lake dolerites. 160

Fig. 4.10. Chondrite normalised REE patterns of the Tsu Lake group 4 and group 5 pelitic/restite samples. 161

Fig. 4.11. Chondrite normalised REE patterns of the Tsu Lake group 6 pelitic/migmatitic samples compared to the NASC. 164

Fig. 4.12. Chondrite normalised REE patterns of the Slave Granite, the megacrystic granite, and the biotite granodiorite. 166

Fig. 4.13. Chondrite normalised REE patterns of the Tsu Lake orthopyroxenes compared to orthopyroxenes from other rocks types. 170

Fig. 4.14. REE distribution coefficients for the partitioning of the REE between the orthopyroxene and the bulk rock. 171

Fig. 4.15. Chondrite normalised REE patterns of the Tsu Lake clinopyroxenes compared to the clinopyroxenes from other rock types. 175

Fig. 4.16. REE distribution coefficients for the partitioning of the REE between clinopyroxene and the bulk rock. 176

Fig. 4.17. Chondrite normalised REE patterns of the Tsu Lake hornblendes compared to hornblendes from other rock types. 179

Fig 4.18. REE distribution ccoefficients for the partitioning of the REE between the hornblende and the bulk rock. 180

Fig. 4.19. Chondrite normalised REE patterns of the Tsu Lake plagioclases compared to plagioclases from other rock types. 182

Fig. 4.20. REE distribution coefficients for the partitioning of the REE between the plagioclase and the bulk rock. 183

Fig. 4.21. Chondrite normalised REE patterns of the Tsu Lake apatites compared to apatites from other rock types. 185

Fig. 4.22. REE distribution coefficients for the partitioning of the REE between the apatite and the bulk rock. 186

Fig 4.23. Chondrite normalised REE patterns of a Tsu Lake zircon compared to zircons from other rock types. 188

Fig. 4.24. REE distribution coefficients for the partitioning of the REE between (a) zircon and the bulk rock, and (b) garnet and the bulk rock. 189

Fig. 4.25. Chondrite normalised REE patterns of a Tsu Lake garnet compared to garnets from other rock types. 191

Fig. 4.26. REE distribution coefficients for coexisting orthopyroxene - plagioclase pairs. . 193

Fig. 4.27. REE distribution coefficients for coexisting clinopyroxene - plagioclase pairs. .. 194

Fig. 4.28. REE distribution coefficients for coexisting clinopyroxene - orthopyroxene pairs. 195

Fig. 4.29. REE distribution coefficients for coexisting hornblende - plagioclase pairs. 196

Fig. 4.30. REE distribution coefficients for coexisting orthopyroxene - hornblende pairs. 197

Fig. 4.31. REE distribution coefficients for coexisting clinopyroxene - hornblende pairs. .. 197

Fig. 4.32. REE distributions coefficients for coexisting orthopyroxene - apatite pairs. 198

Fig. 4.33. REE distributions coefficients for coexisting clinopyroxene - apatite pairs. 198

Fig. 4.34. REE distribution coefficients for coexisting hornblende - apatite pairs. 199

List of Plates

Page

Plate I-a.Granoblastic, equigranular textures in a metabasic rock of group 1. 15

Plate I-b. Granoblastic, inequigranular textures in a rock of tonalitic/greywacke composition, lithologic group 3. 15

Plate II-a. Granoblastic, inequigranular textures in a metagabbroic rock........................ 18

Plate II-b. Granoblastic, inequigranular textures in a metabasic rock, group 2a. 18

Plate III-a. Textural relationships between sillimanite, biotite and hercynite in a pelitic rock, group 6. 23

Plate III-b. Textural relationships between sillimanite, garnet and hercynite in a pelitic migmatite. 23

Plate IV-a. Porphyroblast of sillimanite set in a matrix of cordierite from a pelitic migmatite.. 25

Plate IV-b. Bands of platy sillimanite crystals separated by bands of cordierite in a pelitic migmatite.. 25

Plate V-a. Textural relationships between biotite and prehnite in a group 3 Tsu Lake sample. 29

Plate V-b. Textural relationships between biotite, prehnite and grandite in a Deskenatlata Lake sample. 29

List of Abbreviations and Mineral Formulae

Mineral Formulae

cpx	clinopyroxene	$(Ca,Na,Mg,Fe^{2+},Mn,Fe^{3+},Al,Ti)_2(Si,Al)_2O_6$
diop	diopside	$CaMgSi_2O_6$
hed	hedenbergite	$CaFeSi_2O_6$
opx	orthopyroxene	$(Mg,Fe^{2+})_2Si_2O_6$
en	enstatite	$Mg_2Si_2O_6$
fs	ferrosilite	$Fe_2Si_2O_6$
plag	plagioclase	$NaAlSi_3O_8$ - $CaAl_2Si_2O_8$
an	anorthite	$CaAl_2Si_2O_8$
alb	albite	$NaAlSi_3O_8$
ksp	K-feldspar	$(K,Na)AlSi_3O_8$
or	orthoclase	$KAlSi_3O_8$
hbl	hornblende	$(Na,K)_{0-1}Ca_2(Mg,Fe^{2+},Fe^{3+},Al)_5(Si_{6-7}Al_{2-1}O_{22})(OH,F)_2$
biot	biotite	$K_2(Mg,Fe^{2+})_{6-4}(Fe^{3+},Al,Ti)_{0-2}Si_{6-5}Al_{2-3}O_{20})(OH,F)_4$
ann	annite	$K_2Fe_6Si_6Al_2O_{20}(OH)_4$
phl	phlogopite	$K_2Mg_6Si_6Al_2O_{20}(OH)_4$
ilm	ilmenite	$FeTiO_3$
hc	hercynite	$Fe^{2+}Al_2O_4$
mag	magnetite	$Fe^{2+}Fe^{3+}{}_2O_4$
ulvsp	ulvospinel	$Fe^{2+}{}_2TiO_4$
hem	hematite	Fe_2O_3
apat	apatite	$Ca_5(PO_4)_3(OH,F,Cl)$
monaz	monazite	$(Ce,REE,Th)PO_4$
grnt	garnet	$(Ca,Mg,Mn,Fe^{2+})_3(Al,Fe^{3+})_2Si_3O_{12}$
alm	almandine	$Fe^{2+}{}_3Al_2Si_3O_{12}$
py	pyrope	$Mg_3Al_2Si_3O_{12}$
spess	spessartine	$Mn_3Al_2Si_3O_{12}$
gross	grossular	$Ca_3Al_2Si_3O_{12}$
hygr	hydrogrossular	$Ca_3Al_2Si_2O_8(SiO_4)_{1-}\ (OH)_4$

andr	andradite	$Ca_3Fe^{3+}{}_2Si_3O_{12}$
grandite	grossular+andradite	
zirc	zircon	$ZrSiO_4$
cord	cordierite	$Al_3(Mg,Fe^{2+})_2Si_5AlO_{18}$
sill	sillimanite	Al_2SiO_5
preh	prehnite	$Ca_2Al(AlSi_3O_{10})(OH)_2$
qtz	quartz	SiO_2

Abbreviations

□	vacant site
ΔH	change in enthalpy
ΔS	change in entropy
ΔV	change in molar volume
ΔG	change in Gibbs free energy
C(P)	specific heat at constant pressure
μ	chemical potential
fO_2	oxygen fugacity
P	total pressure
T	temperature
K(D)	distribution coefficient
$X(H_2O)$	mole fraction of water
a(X)	activity of X
R	gas constant
A°	Angstroms
kb	kilobars
FWHM	full width half maximum
REE	rare earth element(s)
LIL	large ion lithophile
Ce(N)	chondrite normalised Ce value
Yb(N)	chondrite normalised Yb value

Eu/Eu^*	ratio of measured Eu to theoretical Eu

CHAPTER 1

INTRODUCTION

The study area of this research project around Tsu Lake and Deskenatlata Lake lies at the western extremity of the exposed shield of the Churchill Province, Fig. 1.1. Reconnaissance mapping by Bostock (1980, 1981, 1982) in the Fort Smith district, implied this area would be suitable for a study to define further the complex metamorphic history. Reasons for selecting the Tsu Lake area are given below.

Regional Geology

The Churchill Province is believed to have been involved in both the Kenoran and Hudsonian orogenies, with the predominant evolution occurring during the Hudsonian. It is recognised as a subdivision of the Canadian shield on the basis of structural features and geological evolution. A more complete summary of the geology of the Churchill Province may be found in Davidson (1972).

The NW boundary of the Churchill Province is separated from the Slave Province by the Thelon front. Rocks from the Slave Province suffer increasing deformation towards this front. In the East Arm region of the Great Slave Lake the boundary between the Churchill and the Slave Provinces is assumed to be delineated by the MacDonald Fault (Davidson, 1972; Burwash and Culbert, 1976).

In a 200 - 300 km zone along the boundaries of the Thelon front and the MacDonald Fault zone the Churchill Province consists predominantly of remnant areas of granulite facies rocks, which probably represent a strongly uplifted deep crustal zone. Metamorphism of this area is thought to be related to the tectonic activity along the Thelon front.

The geology of the NW Churchill Province contrasts sharply with that observed in the SE of the Province. Metamorphic grade is variable in this latter region where a crude alternation between fold-belt and greenstone terrain is observed. The geologic variation in this SE part of the Province is thought to be the result of a breakdown in the stability of a

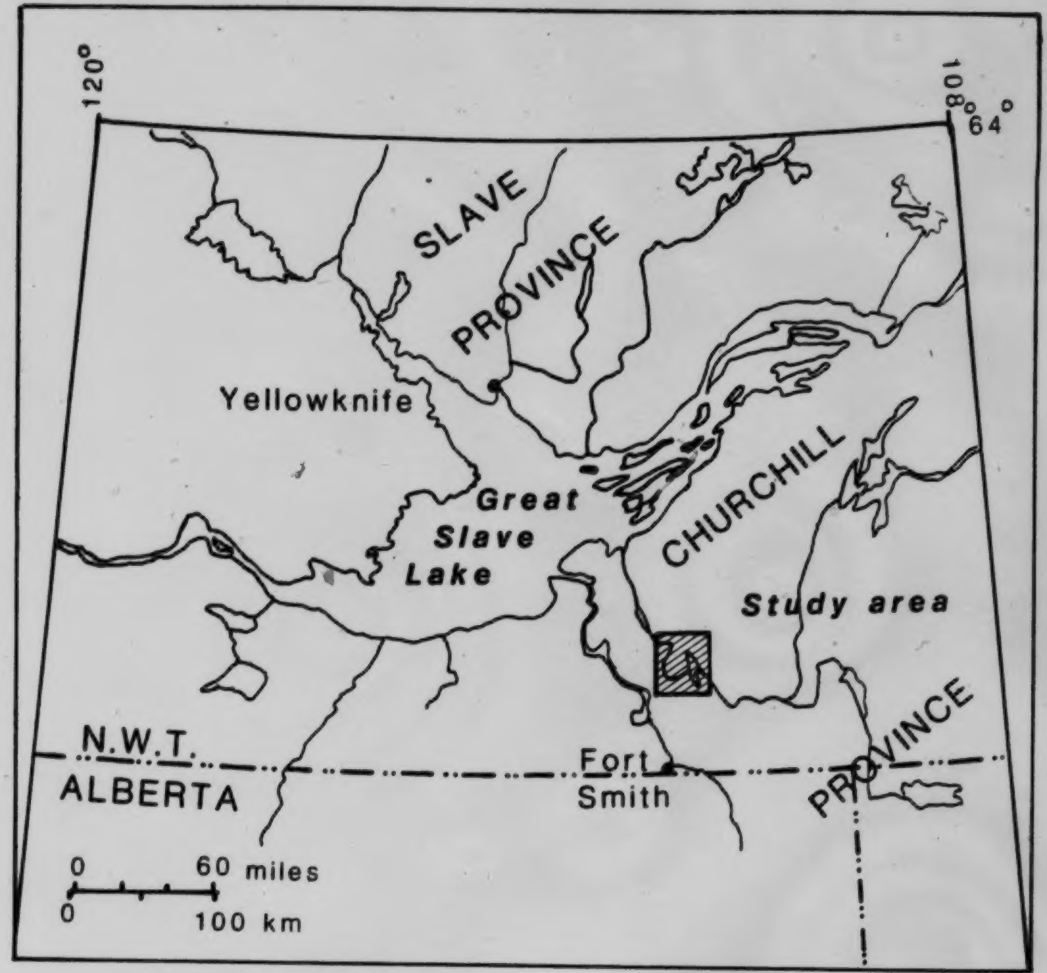
120°
108°
64°
SLAVE
PROVINCE
Yellowknife
Great
Slave
Lake
CHURCHILL
PROVINCE
Study area
N.W.T.
ALBERTA
Fort
Smith
0
60 miles
0
100 km

Fig. 1.1. Map showing the location of the study area (shaded area).

previously continuous Archean crust (Davidson, 1972). The relationship between the NW and SE portions of the Churchill Province still remains enigmatic.

Burwash and Culbert (1976) were able to recognise three tectonic zones within the subsurface extensions of the Churchill Province; (a) the Athabasca mobile zone, (b) the Cree Lake - Calgary belt, and (c) the Kisseynew - Sweetgrass belt. The Athabasca mobile belt corresponds to the NW granulite facies zone of the exposed shield while the other two zones correspond to the SE Churchill zone. The complex geologic history of the Athabasca mobile belt is apparent from the presence of large scale K metasomatism and the polymetamorphic nature of the rocks. The neighbouring Cree Lake - Calgary belt is essentially monometamorphic and the Kisseynew - Sweetgrass belt has only suffered weak K metasomatism and mylonitisation.

NW Churchill Province

The dominant metamorphic events documented for various parts of the NW Churchill Province range in age from Archean to Aphebian. The Archean metamorphism was a high grade event; where recognised it is either of amphibolite or granulite facies grade. The age of this metamorphism is inferred from K-Ar dates, and the continuity of the Archean metavolcanic belts across the Thelon front (Fraser, 1978). Amphibolite facies metamorphism is characterised by the presence of staurolite and/or andalusite. A distinction between the amphibolite facies metamophism and the granulite facies metamorphism is made on the basis of the association of sphene with hornblende. The granulite facies metamorphism is characterised by the assemblage grnt - cord - sill - hc. A diagnostic granulite facies mineral, orthopyroxene, is reported to be sparse, although this may be a reflection of the rarity of rocks of suitable compositions.

Fraser (1978) documented the Archean metamorphic event in three areas: Queen Maud gulf, Armit Lake region and the East Arm area. Reinhardt (1968) described the Thubun Lake region, East Arm, as an area of granulite facies metamorphism. Godfrey and Langenberg (1978) and Nielsen *et al.* (1981) have documented this event in NE Alberta. Estimated pressure - temperature conditions of the Archean granulite facies event are 900±100 °C and 7.5±2 kb (Nielsen *et al.*, 1981). These estimates have been based on the mineralogies of peraluminous rocks.

It is possible that the metamorphism of Archean age represents more than one event. Fraser (1978) found amphibolite facies mafic rocks that were associated with quartzofeldspathic gneisses metamorphosed to granulite facies grade. However, there is little other documentation of similar associations.

The early metamorphism of Archean age has been overprinted by at least two Aphebian events; an amphibolite facies metamorphic event and a late Aphebian cataclastic deformation event. Both of these Aphebian events are believed to be related to the uplift and subsequent cooling of the NW Churchill Province. The amphibolite facies event correlates with the remobilisation of infrastructural materials (Godfrey and Langenberg, 1978). Nielsen *et al.* (1981) estimate the pressure - temperature conditions of this event to be of two stages: (i) 740±30°C and 5±0.7 kb with $X(H_2O)<0.4$; and (ii) 550±55°C and 3.0±0.3 kb with $X(H_2O)>0.4$. Emplacement of extensive granitoid plutons and remobilisation of existing ones occurred during the first stage of this period.

The late Aphebian event is characterised by cataclastic deformation and later recrystallisation under greenschist facies conditions. Geothermal gradients are assumed to have been depressed due to the removal of cover rock during this period. Pressure - temperature conditions of the cataclastic event are not well constrained but are estimated at 260±35°C and 2 kb from the observed assemblages and the closure temperature of Ar loss from biotite (Nielsen *et al.*, 1981).

Many of the mylonite zones in the NW Churchill Province are assumed to have developed because of the brittle response of the rocks to the cataclastic deformation. The presence of greenschist facies assemblages in some of the mylonite zones supports this suggestion. However, from an examination of the differing structural trends of the mylonite zones more than one event is suggested (Fraser, 1978).

Development of the mylonitisation and K metasomatism of the Athabasca mobile belt is believed to have occurred during the late Aphebian (approximately 2000 Ma.) and to have ceased by 1800 Ma.

Fort Smith Area

The geology of the Fort Smith area, map sheet 75D, has been investigated by Bostock (1980, 1981, 1982). The study area around Tsu Lake and Deskenatlata Lake is situated at the western edge of the Fort Smith district.[1] Bostock (1982) delineated six major units which are of importance to this study area. They are: (i) the Slave Granite, (ii) the Tsu Lake Gneiss, (iii) the Granitic Gneiss (Bostock sudivided this unit into two sub-units), (iv) the western granodioritic complexes, (v) the metagabbro and (vi) the megacrystic granitic batholith. Of these units only the megacrystic granite is inferred to be Aphebian in age; the others are of Archean age.

Bostock (1982) recognised three significant structural zones which are important in terms of the geologic relationships between the units listed above. A central uplifted belt is flanked by two depressed lateral belts. The Deskenatlata Lake Fault zone and the Allan Fault, two major shear zones, define the margins of the central zone. The interpretation of an uplift of the central zone relative to the lateral belts was based on a number of factors. The reasons given by Bostock (1982) are:

1. The Slave Granite, which locally preserves granulite facies mineralogy, is confined to the central uplifted belt. (It is likely exposed as a result of uplift.)
2. Retrogressive metamorphism, as indicated by breakdown of iron-magnesium silicates to chlorite is least extensive in the central uplift zone. (Rocks of the lateral belts have been altered in a more hydrous environment closer to the surface.)
3. Ilmenite is the dominant iron oxide of the central zone (Charboneau, 1980) whereas magnetite is dominant in the lateral zones. This reflects low oxidation a potential in the central zone and is responsible for the regional low aeromagnetic anomaly over large parts of it. (The lateral belts have been altered in a more hydrous and oxidising environment closer to the surface.)
4. The megacrystic granite batholith, as opposed to much smaller related eastern stocks, is confined to the central belt. (The central belt was uplifted as a result of emplacement of the megacrystic granite and has consequently undergone more extensive erosion.)
5. The Nonacho Group and Hill Island Lake assemblage lie outside the central uplift and were deposited about the same time as, or before the megacrystic granite was emplaced. (Preservation of these sediments only in the eastern lateral belt suggests that this belt has been depressed with respect to the rocks to the west over most of the interval since deposition.)

Tsu Lake lies within the central belt whereas Deskenatlata Lake lies on the edge of the western lateral belt adjacent to the central belt.

The Slave Granite and the Tsu Lake Gneiss are believed to represent the basement rocks of this area which existed by the end of the Archean. The Slave Granite consists of a leucocratic, medium grained, massive granite. In some areas it is charnockitic, notably to the north of Tsu Lake. Most contacts with the Tsu Lake Gneiss are tectonic although there are a few intrusive contacts. Near Jackfish Lake the granite projects upwards into the Tsu Lake Gneiss and displays cross-cutting relationships with it. Bostock (1981, 1982) believes this reflects local remobilisation of the Slave Granite and so does not discount the possibility of a Slave Granite Archean basement. Godfrey and Langenberg (1978) record that the Slave Granite contains both a granulite facies assemblage and an amphibolite facies overprint, the latter probably related to a remobilisation event. A more recent geochemical study of the Slave Granite suggests that it could have been derived by partial melting of the Granitic Gneiss unit (Goff *et al.*, in prep.).

---

[1] There is a discrepancy in the spelling of the name "Deskenatlata". The topographic sheet, map 75D Fort Smith district, gives the spelling as "Deskenatlata", while Bostock (1982) gives the name as "Deskenetlata". The spelling of the name in accordance with that given on the topographic sheet has been adopted throughout this thesis.

The Tsu Lake Gneiss unit consists of a series of metasediments comprised of pelites, quartzites, calcsilicates and iron formations. Minor amphibolite bands that could be of an igneous or sedimentary origin are also found. Some amphibolites are believed to be derived from iron formations (Bostock, 1982). The Tsu Lake gneiss is found mainly within the eastern Slave Granite domain and as a remnant along the western contact of the Slave Granite and megacrystic granite. Smaller remnants are found elsewhere in the megacrystic granite. Tsu Lake pelitic gneisses within the Slave Granite are reported to contain: sill - cord - ksp - grnt - sp. These assemblages are interpreted as representing Archean granulite facies metamorphism with a relatively "dry" Aphebian amphibolite facies overprint (Bostock, 1982). The age of the Tsu Lake Gneiss is unknown but is thought to be either Archean or early Aphebian. It is intruded by the megacrystic granite and locally intruded by the Slave Granite.

The Granitic Gneiss consists of granitic layers interleaved with medium to fine grained biotite and biotite - hornblende gneiss. Metasedimentary bands of a similar composition to the Tsu Lake Gneiss unit are found within this unit. Bostock (1982) made a distinction between a granitic gneiss unit where the interleaved paragneiss is recognisable as metasedimentary band, and that where the metasedimentary portion is present only as hornblende or biotite-rich schlieren. Pelitic components of the Granitic Gneiss in the central uplifted belt contain remnants of granulite facies assemblages. The age of this unit, therefore, has been interpreted to be Archean (Bostock, 1982).

The biotite granodiorite complex is restricted to west of Deskenatlata Lake. Compositionally it varies from quartz monzonite to diorite. The relative age of the complex is uncertain because of the absence of a granulite facies assemblage. It is believed to be a lateral belt of the Archean terrain which was more deeply buried than the gneisses to the east of it. The unit now contains an amphibolite facies assemblage defined by the association of hornblende and sphene.

A metagabbroic unit found just west of Tsu Lake intrudes the Slave Granite. Both units were folded and metamorphosed together under granulite facies conditions. Therefore, it is likely that the metagabbroic unit is also Archean in age. The metagabbro has the assemblage hbl - plag - opx with the orthopyroxene being a partially altered phase.

The dominant unit in the Fort Smith area is the megacrystic granite, comprising a batholith in which five domains are recognised (Bostock, 1982). Mineralogically the granite consists of potassium feldspar megacrysts and a fine grained matrix of feldspar, quartz, chlorite. Garnet is found and less commonly cordierite, spinel, monazite, zircon, apatite and ilmenite. Hypersthene is found in a highly altered form and is believed to be of a xenocrystic origin. Frequently the contact between the Slave Granite and the megacrystic granite is mylonitised. Where gradational contacts are seen, either intershearing is found, or the Slave Granite is locally megacrystic as a result of K metasomatism. The mylonite zones within the map area may be related to the emplacement of the batholith. They appear to penetrate only the edges of the megacrystic granite.

Tsu Lake

All the major lithologies described in the preceding section, with the exception of the biotite granodiorite complex, are exposed at Tsu Lake. Field relations are obscured between the Slave Granite, Tsu Lake gneiss and megacrystic granite, principally because of the lack of continuous exposures between these lithologies. The Slave Granite is found along the western shore of the lake. Minor exposures occur at the northeastern end and on islands along the centre of the lake. The megacrystic granite is restricted to the eastern shore.

Remnants of the Tsu Lake gneiss are exposed on islands in the lake. The gneisses consist dominantly of pelitic and quartzitic metasediments. Amphibolites of igneous or sedimentary origin are found associated with the gneisses.

Dykes of a much younger age than the megacrystic granite, intrude the metasediments on islands in the centre of the lake. A gabbro with a chilled margin is found associated with them. The metagabbroic body, lying to the west of Tsu Lake, is unrelated to the dykes.

Areas around the lake are intensely sheared. A mylonite zone cuts across the northeast margin of the lake and joins up with the Warren Fault zone. Numerous smaller stockwork breccias are found along the eastern and northern shores of the lake.

Deskenatlata Lake

The bioite granodiorite complex is exposed on the north western shore of Deskenatlata Lake. However, the predominant unit found at this lake is the Granitic Gneiss. The Slave Granite abuts against the Granitic Gneiss along the eastern shore of the lake.

Research Procedures

The Tsu Lake region appeared to be the most feasible place in the Fort Smith district in which to concentrate research on the metamorphism of the area. Tsu Lake is reasonably accessible from Fort Smith and most of the lithologies of interest are exposed here. As it occurs within the central uplifted zone the Archean granulite facies metamorphic event would more likely be preserved. Deskenatlata Lake was chosen as a site for a comparative study with Tsu Lake. Its location in the western lateral depressed belt should provide an example of the lower grade Aphebian metamorphic event, while its proximity to Tsu Lake was convenient for the collection of samples.

The principal objective of the research was to delineate the nature of the metamorphism in the Tsu Lake and Deskenatlata Lake areas. This was to be attempted by examining the mineralogies and compositions of the rocks concerned.

Petrographical examinations of the rocks were made in order to determine if minerals diagnostic of a particular metamorphic facies were present. The rocks were classified into groups based on their mineralogies. Compositional data, obtained by electron microprobe analysis, on the mineral phases permitted evaluations on the mineral forming processes to be made.

Estimates of the pressure - temperature conditions for the various Archean and Aphebian metamorphic events in the NE Albertan area, have been restricted to a consideration of the mineralogical compositions of pelitic or peraluminous rocks. Because suitable assemblages in the basic rocks from Tsu Lake were available, as well those in pelitic rocks, it was intended to examine the pressure - temperature estimates obtained from these two compositionally different systems.

Some calibrations of the geothermometers and geobarometers currently in use are based on inadequate experimental data. Problems arise from the application of other geothermometers to mineral species for which complete compositional data is not available. A literature review and an assessment of some of the problems associated with the use of geothermometers and geobarometers was made for the mineral systems applicable to this study.

The purpose behind the geochemical studies of the Tsu Lake rocks was two-fold. As the Athabasca mobile belt has been shown to be enriched in K and Rb, and depleted in Sr, it was necessary to know to what extent the Tsu Lake rocks have been affected. The large ion lithophile (LIL) element characteristics of the Tsu Lake area may help to define the Archean granulite facies metamorphic event. The nature of LIL element patterns is often cited as a characteristic of intermediate to high-pressure granulite facies terrains. Because there is some controversy over the significance of the granulite facies LIL element patterns, a review of the literature on this subject was undertaken.

An assessment of the usefulness of the rare earth elements (REE) as a petrogenetic tool in high grade metamorphic studies was also attempted. An earlier study on the REE distributions between minerals of granulite facies grade by Pride and Muecke (1981) suggested that the REE were sensitive to granulite facies processes. Selected samples of rocks and minerals from the Tsu Lake area were analysed for their REE concentrations and compared to other relevant published data.

CHAPTER 2

PETROGRAPHY, MINERALOGY AND ELEMENT PARTITIONING

The purpose of this chapter is to discuss the metamorphic petrology of the rocks found at Tsu Lake and Deskenatlata Lake.

The principle objective in examining the petrography and mineralogy of these rocks is to determine the grade of metamorphism. It is important to determine how many metamorphic events the rocks have undergone. Rocks from the Tsu Lake area are compared to rocks from Deskenatlata Lake because it is believed that the grade of metamorphism is different for the two localities (Bostock, 1982). The chapter is divided into the following sections: method of sampling, petrography, mineralogy, element partitioning and mineral-forming reactions. Each succeeding section deals with a progressively more detailed view of the petrology.

Lithological classification and mineralogical textural relations are discussed in the petrography section. The mineralogy section describes the variations in the composition of each of the major phases and compares and contrasts this to the same minerals from other areas which have experienced similar conditions of metamorphism. The purpose of the section on element partitioning is to determine how the major and minor elements are partitioned between the minerals, and the extent to which this is indicative of equilibrium/disequilibrium conditions. The final section on mineral-forming reactions collates information from the preceding sections and relate this to mineral-forming processes.

Sampling

Most of the field work was undertaken at Tsu Lake during two, one-month field seasons, in 1982 and 1983. Mapping of the geology included a confirmation of the boundaries designated by Bostock (1982), which were found to be accurate. The lithologic units defined on a map scale are: the Slave Granite, Tsu Lake Gneiss, Granitic Gneiss, Megacrystic Granite and Metagabbro, Fig. 2.1 (the names are in accordance with those adopted by Bostock, (1982)). No attempt was made to differentiate the Tsu Lake Gneiss unit into pelitic and basic sub-units because the two lithologies are too closely associated in the field.

The most extensive outcrops of the Tsu Lake Gneiss, at Tsu Lake, are confined to islands. The rocks have been severely folded and in some cases, migmatised. Because of the structurally deformed nature of the rocks and the lack of continuous exposures, the mapping of mineral isograds was not feasible.

Fig. 2.1 shows the localities of the samples collected. These were collected predominantly from lakeshore outcrops. The sampling was carried out so as to ensure that as wide a range as possible of the lithologies were collected. In total approximately 300 samples were obtained from the Tsu Lake area. Of these only about 70 were selected, on the basis of the mineralogy visible in hand specimen, for thin-section preparation. The emphasis of selection was placed on those assemblages most useful for geothermometry and geobarometry studies. 40 of the 70 samples were prepared for electron microprobe analysis.

Field work at Deskenatlata Lake concentrated on the collection of samples for a comparison with the Tsu Lake collection. Mineral isograds could not be discerned because of the paucity of outcrops. Fig. 2.2 shows the sample localities. A total of 34 samples were collected, of which approximately 15 were actually thin-sectioned, again with the emphasis of selection being placed on those samples with minerals diagnostic of the temperature - pressure conditions of metamorphism.

Petrography

Tsu Lake Samples

To facilitate description the Tsu Lake Gneiss rocks have been divided into lithologic groups based on their assemblages. These group classifications will be used throughout the thesis. The groups are as follows, with the minerals listed in order of decreasing modal amounts:

1. cpx + opx + plag + ilm ± biot, hbl, qtz, apat (○)
2. a. hbl + opx + cpx + plag + ilm ± biot, qtz, apat (●)
   b. hbl + cpx + hc ± plag, biot (●)

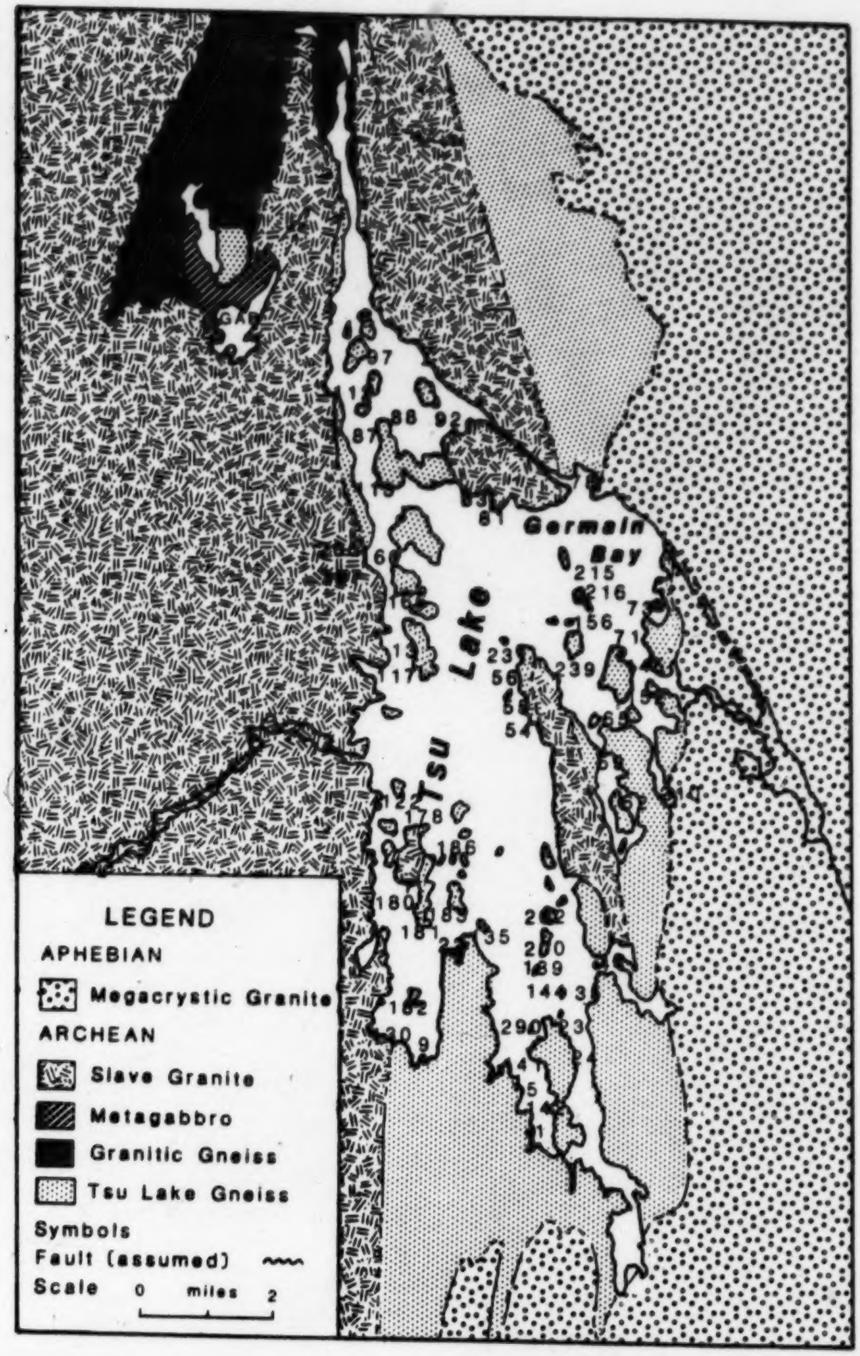
Germain Bay
Tsu Lake
LEGEND
APHEBIAN
Megacrystic Granite
ARCHEAN
Slave Granite
Metagabbro
Granitic Gneiss
Tsu Lake Gneiss
Symbols
Fault (assumed)
Scale 0 miles 2
215
216
56
239
178
180
35
144
169
87
88
92

Fig. 2.1. Geological map of the Tsu Lake area showing the sampling localities. Geological boundaries after Bostock (1982).

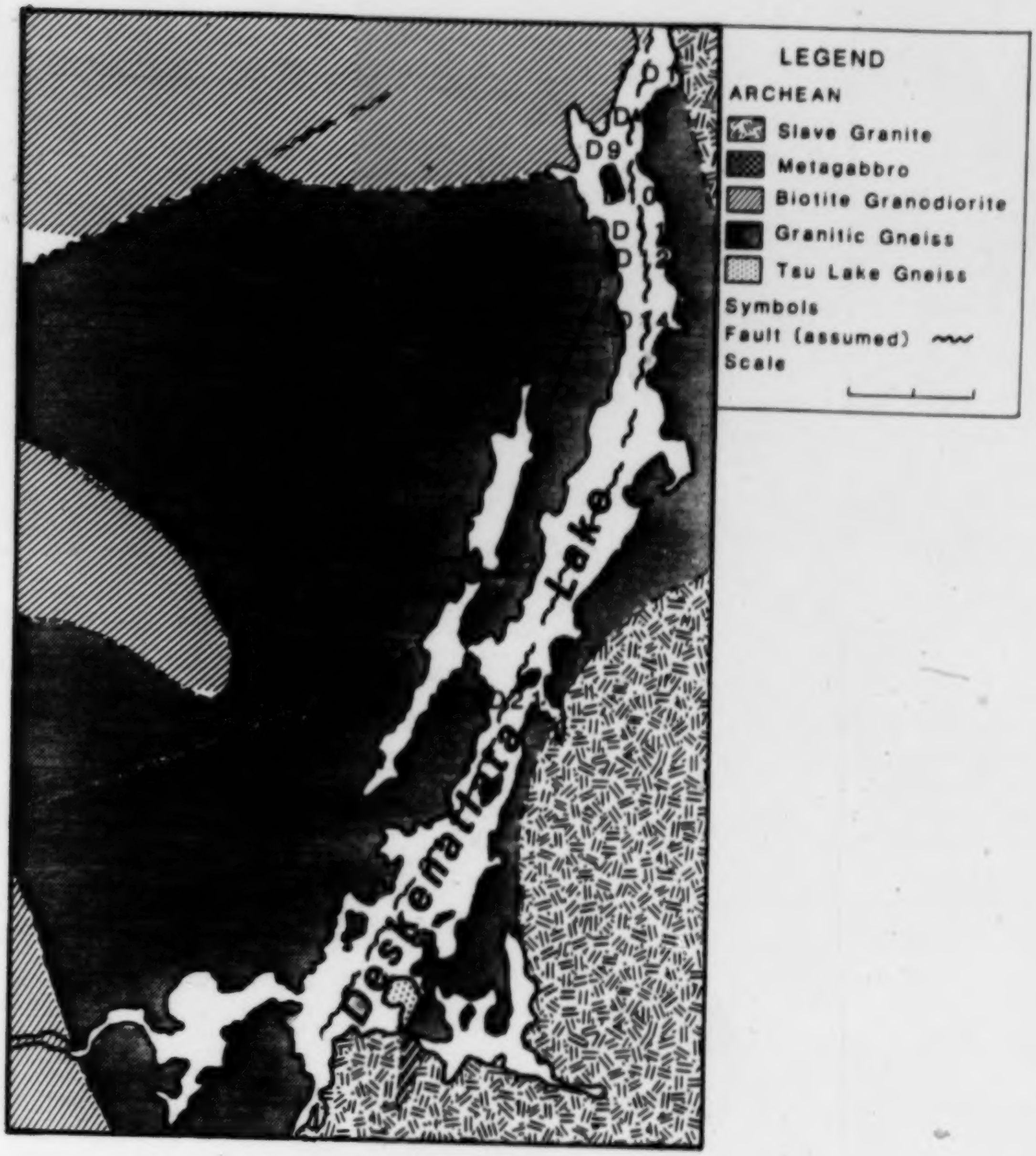
LEGEND
ARCHEAN
Slave Granite
Metagabbro
Biotite Granodiorite
Granitic Gneiss
Tsu Lake Gneiss
Symbols
Fault (assumed)
Scale
D9
D10
Deskenatlata Lake

Fig. 2.2. Geological map of the Deskenatlata Lake area showing the sampling localities. Geological boundaries after Bostock (1982).

c. hbl + opx + plag + ilm ± apat (●)

3. opx + plag + biot + qtz + ilm ± ksp, apat, grnt (◆)

4. plag + biot + grnt + qtz + ilm ± opx, zirc (◇)

5. grnt + cord + hc ± plag, qtz, biot, monaz (×)

6. sill + cord + biot + plag + ksp + qtz + hc ± grnt, monaz (+).

The symbols in brackets following each assemblage are used in diagrams throughout this chapter to denote the samples belonging to each group.

As many fewer samples from Deskenatlata Lake were studied, it is difficult to assign the samples to lithologic groups. The predominant assemblages are:

1. hbl + plag + biot ± qtz
2. biot + plag + qtz ± opx
3. biot + sill + cord + grnt + plag + ksp + qtz.

Deskenatlata Lake samples are depicted in diagrams by the symbol (□).

In all the textural descriptions the terminology suggested by Winkler (1974) is adopted.

Basic Assemblages.

Group 1 and 2 samples have the mineralogies of basic rocks. According to the classification scheme in Winkler (1974) the rocks should be called enderbitic granolites or hypersthene pyroclases. The listed assemblages do not necessarily imply stable coexistence of all phases.

Group 1

Samples of the group 1 assemblage are few; most of the basic rocks collected belong to the group 2 assemblage. The group 1 assemblage is divided into two types: (a) opx + cpx + hbl, and (b) opx + cpx + biot.

Type 1(a) rocks have a granoblastic, equigranular texture and are normally quite coarse-grained (av. 0.5 - 1 mm), Plate Ia. The pyroxenes usually show interlobate crystal boundaries with the surrounding plagioclases. Both types of pyroxene exhibit a weak pleochroism: for the orthopyroxene the pleochroic scheme is from pale brown, colourless to pale pink, and for the clinopyroxene the pleochroism is from pale green, colourless to pale brown. Exsolution is evident only in the clinopyroxene, and is in the

Plate I-a. Granoblastic, equigranular textures in a metabasic rock of group 1, sample 141B. Orthopyroxene - o, clinopyroxene - c, hornblende - h, and plagioclase - p. Plane polarised light. Scale bar is 1 mm long.

Plate I-b. Granoblastic, inequigranular textures in a rock of tonalitic / greywacke composition, lithologic group 3, sample 22L. Orthopyroxene - o, biotite - b, plagioclase - p. Plane polarised light. Scale bar is 1 mm long.

Plate I

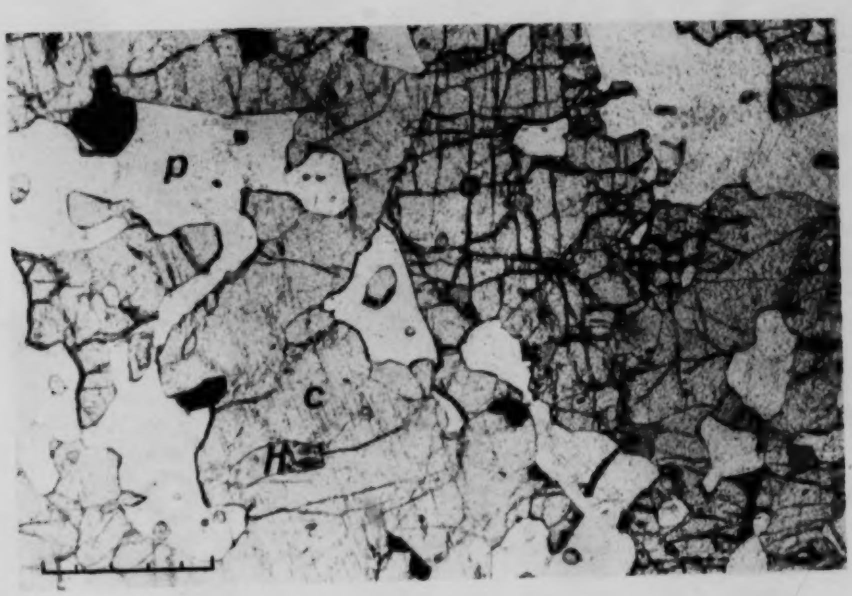

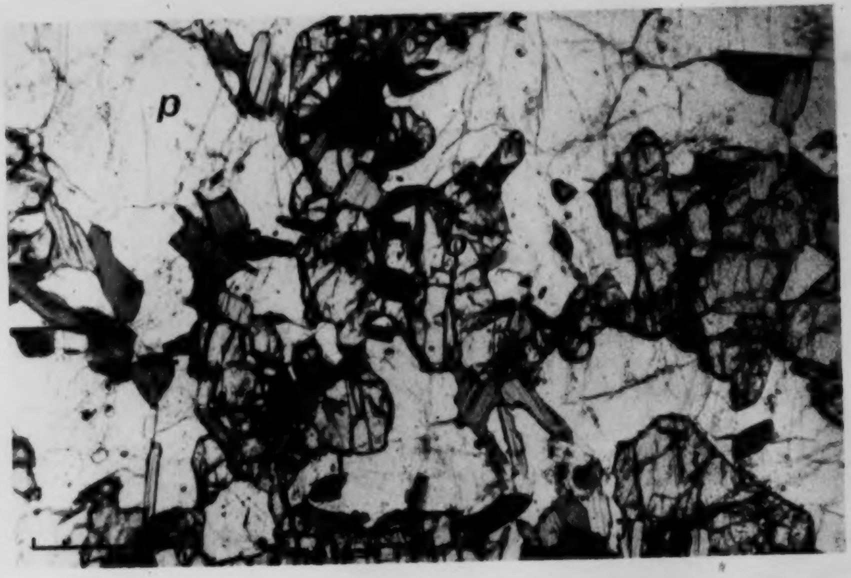

form of thin lamellae. The relationship between the two pyroxenes could be described as a "pseudo-adcumulate" texture, with the clinopyroxene partially surrounding the orthopyroxene. Hornblende, when present, is included in the clinopyroxene rather than the orthopyroxene. Strong pleochroism is shown by the hornblende, with colours ranging from pale green, brownish green to greenish yellow. Opaque phases, normally ilmenite, occur along the edges of, or are included in orthopyroxene crystals.

Type 1(b) rocks are somewhat finer grained than the type 1(a) rocks (average grain size 0.2 mm). They exhibit an equigranular, granoblastic texture with polygonal to interlobate grain boundaries. Both pyroxenes show pleochroism with the same scheme as in type 1 (a). Again, only clinopyroxene shows exsolution features. Biotite occurs as anhedral crystals with irregular outlines, and appears to be replacing both pyroxenes. It is pleochroic in dark brown, reddish-brown and yellowish-brown.

In one of the type 1(b) samples, 200A, biotite comprises the matrix of the rock, with the pyroxenes partially included in this phase. Plagioclase in this rock has been completely altered to sericite. Thus the textural evidence suggests that there are two modes of formation for the group 1 assemblage.

Group 2.

Most of the basic rocks contain the assemblage 2(a). In several other amphibolites, including the metagabbro unit, type 2(b) prevails. The type 2(c) assemblage is rare; only one occurrence of this ultramafic unit has been found at Tsu Lake.

The type 2(a) amphibolites are coarse grained (average grain size 1 - 1.5 mm), granoblastic and equigranular, Plate IIb. Some of the samples exhibit a poorly-defined compositional banding with the pyroxenes being concentrated between layers rich in hornblende. Contacts between subhedral crystals of hornblende and the pyroxenes are either polygonal or interlobate. Plagioclases have a tendency to form amoeboid grain boundaries, although most are interlobate. Hornblende is closely associated with both pyroxenes, and normally surrounds them. It frequently has irregular, corroded crystal outlines, suggesting instability of this phase. Pyroxenes may occasionally show minor uralitisation of the grain boundaries, Plate IIa or IIb. Hornblende, orthopyroxene and clinopyroxene are all pleochroic in the colours described for these phases in the group 1 assemblages. Apatite, when present, is normally included in hornblende. Ilmenite, or the

Plate II-a. Granoblastic, inequigranular textures in a metagabbroic sample of lithologic group 2b. Note the alteration around the rims of orthopyroxene grains. Orthopyroxene - o, hornblende - h. Crossed nicols. Scale bar is 1 mm long.

Plate II-b. Granoblastic, inequigranular textures in a metabasic rock of lithologic group 2a. Orthopyroxene - o, clinopyroxene - c, hornblende - h, plagioclase - p. Plane polarised light. Scale bar is 1 mm long.

Plate II

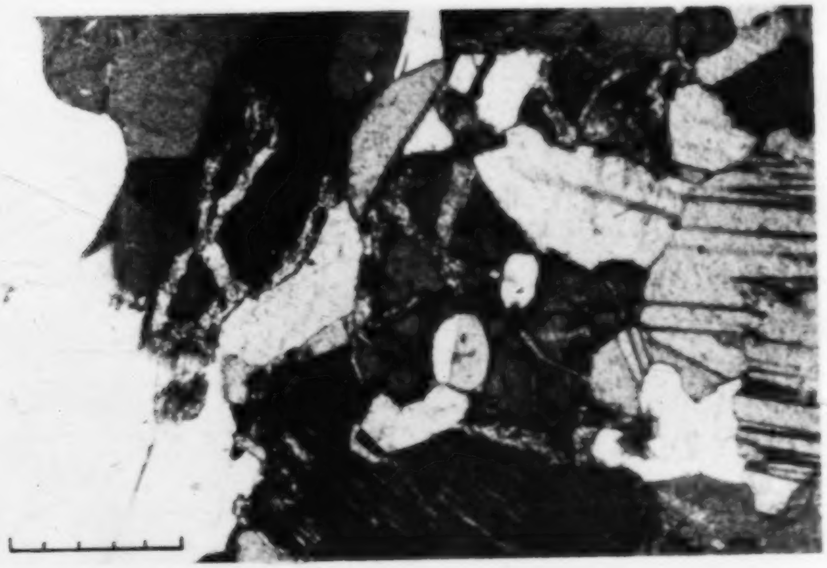

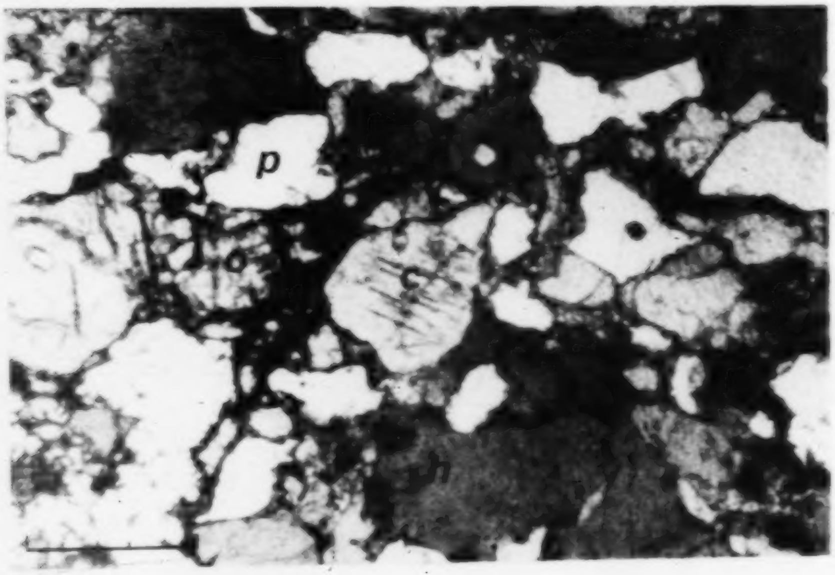

oxide phase, is associated with the mafic minerals. The oxide phase shows green, semi-transparent colours in plane polarised light and has been identified as hercynite. Biotite occurs as a retrograde phase associated with hornblende.

Type 2(b) samples are very similar in appearance to type 2(a) rocks, Plate IIb. The largest difference is that orthopyroxene is invariably heavily uralitised around the edges. Grain boundaries tend to be interlobate rather than polygonal.

Type 2(c) rocks are granoblastic and equigranular, with polygonal crystal boundaries (average size 1 mm). There is a tendency for the mafic minerals, clinopyroxene and hornblende, to form monomineralic layers. Hercynite is associated with hornblende, not clinopyroxene. Biotite occurs rarely, apparently replacing hornblende.

Intermediate - Quartzofeldspathic Assemblages.

Group 3

The group 3 assemblages indicate rocks of a tonalite/greywacke composition. They are generally granoblastic and equigranular to inequigranular (average grain size 1.5 mm), Plate Ib. The size variation is determined primarily by the orthopyroxene which may be porphyroblastic, or equal in size to the rest of the matrix. Porphyroblastic orthopyroxene shows interlobate crystal boundaries with the surrounding matrix, such that it has a "skeletal" appearance. Orthopyroxene is pleochroic in pale pink, pale blue and pale yellow. The matrix is composed of quartz and feldspar, usually with amoeboid grain boundaries. The plagioclase is often antiperthitic. The exsolved K-feldspar phase in the antiperthite shows the cross-hatch twinning patterns of microcline. Biotite is also strongly pleochroic, with colours ranging from dark brown, reddish-brown to yellowish-brown. Biotite crystals are usually corroded in outline. Orthopyroxene is found surrounded by biotite, a texture suggesting biotite is replacing orthopyroxene. Biotite crystals may also be found rimming plagioclase laths. Apatite tends to be dispersed throughout the rock rather than included in a particular phase. The rare garnets are found in contact with orthopyroxene, exhibiting straight grain boundaries, thus suggesting equilibrium for this pair.

Group 4

A wide range of varying textures is encompassed by rocks with the group 4 assemblage. Inequigranular granoblastic and flaser textures are the most common but mylonitic textures have developed in some instances. The rocks are generally composed of two compositionally different bands; a felsic layer, and a mafic layer. The felsic layer consists of porphyroblasts of plagioclase (average crystal size 4 mm), which is often antiperthitic, set in a finer grained matrix of quartz and plagioclase (average grain size 0.5 mm). The phases in the fine grained matrix have amoeboid grain boundaries. The mafic layers are composed of garnet and biotite. Garnet is anhedral and is completely surrounded, and included with, biotite. The grain boundaries of biotite are irregular and ragged, suggesting it is an unstable phase. The feldspar, quartz and biotite phases sometimes show evidence of strain, in the form of undulose extinction. Orthopyroxene, when occurring, is associated with the felsic layers and is extensively altered to chlorite. Accessory phases, zircon and apatite, are included in biotite.

Pelitic Assemblages.

Both the group 5 and 6 pelitic lithologies show field evidence of partial melting. With the group 6 samples the rock shows a division into dark lenses of restite material which are set in a matrix of felsic material. For group 5 lithologies the evidence is less direct. Bands composed of garnet-cordierite are bordered by quartzite or other felsic material. Inclusions of the garnet-biotite unit in the garnet-cordierite unit imply that the garnet-biotite unit, group 4, is the source material of the rock enclosing it.

Group 5

The texture in the group 5 assemblages is predominantly granoblastic, although the grain size ranges from equigranular to inequigranular (average grain size 2 mm). Crystals of garnet and cordierite both tend to be glomeroporphyroblastic, although this is more evident with garnet. Grain boundaries between garnet and cordierite are usually interlobate, while grain boundaries between individual cordierite crystals are polygonal. Cordierite may show some alteration to pinite. This alteration appears as a yellow discolouration of the normally, colourless cordierite. Where the alteration has been extensive sericite may have developed. Hercynite is invariably closely associated with cordierite and is found between cordierite crystals in an "intercumulate-like" texture. It shows the same optical properties of the group 2 hercynite described earlier. Other oxide phases, ilmenite or magnetite, are associated with garnet. Biotite replaces garnet or cordierite. Quartz, if present, occurs in veins between the garnet-cordierite bands, showing amoeboid grain boundaries. Some rocks show a compositional banding with layers of garnet-cordierite isolated from layers of garnet-plagioclase by quartz veins.

Group 6

Distinct compositional bands are developed in the group 6 assemblages. These are characterised as garnet-rich or garnet-absent bands, separated by felsic layers. The predominant texture, as a result of the banding, is an inequigranular flaser type (the grain size range is from 0.05 to 2 mm). The most usual composition of the bands is: (a) grnt + cord + biot, and (b) sill + biot + cord. However, sillimanite may occur in either of the mafic bands. Sillimanite exhibits platy, euhedral crystals with polygonal grain boundaries, instead of its characteristic fibrous habit. Bucher-Nurminen and Droop (1983) conclude that such a habit could be indicative of paramorphic replacement of kyanite. Only in the equivalent assemblage at Deskenatlata Lake does sillimanite assume a fibrous habit. Sillimanite is closely associated with the oxide phases in both mafic bands, Plate IIIa. Where it occurs with garnet, the oxide phase usually separates the two phases, Plate IIIb. Occasionally sillimanite is included in garnet. More frequently however, it is associated with cordierite in the bands devoid of garnet. Here it tends to form bimineralic clusters with the oxides, usually separated from cordierite by a layer of biotite, Plate IVa and IVb. The two modes of occurrence of sillimanite, with cordierite or with garnet, and the association with hercynite, imply incompatible assemblages in the system (Fe,Mg)O - Al_2O_3 - SiO_2. The presence of these two assemblages may have arisen because of slight changes in the concentration of a component not considered in the above system. That these assemblages may occasionally occur within a single rock makes the above suggestion slightly implausible. Cordierite usually forms monomineralic layers of anhedral crystals with polygonal contacts. Cordierite exhibits the same habit when it associated with garnet. Biotite may be associated with either sillimanite in the garnet-free bands, or replacing garnet in the other mafic band. Corroded grain boundaries characterise the usual

Plate III-a. Textural relationships between sillimanite (s), biotite (b) and hercynite (black mineral) in a pelitic rock, group 6, sample 239B. Plane polarised light. Scale bar is 1 mm long.

Plate III-b. Textural relationships between sillimanite (s), garnet (g) and hercynite (black mineral separating the previous two phases) in a pelitic migmatite, sample 44. Plane polarised light. Scale bar is 1 mm long.

Plate III

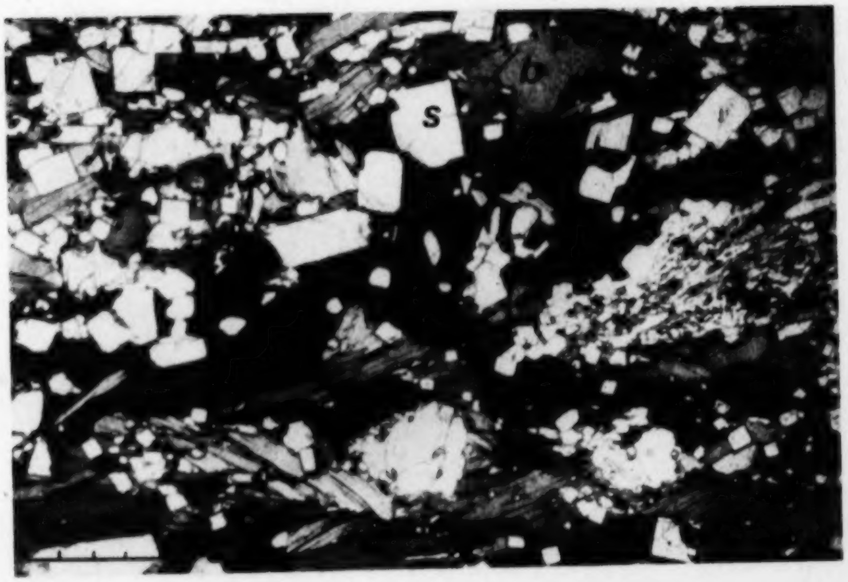

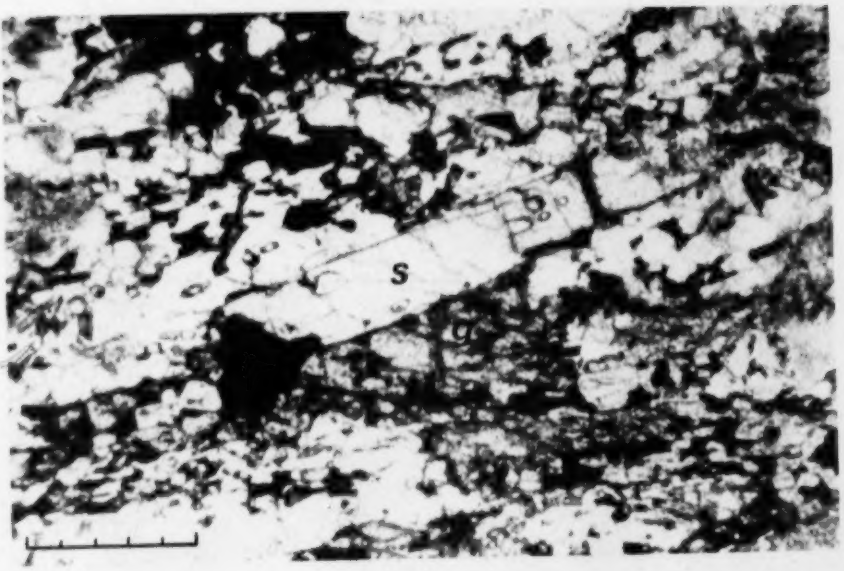

Plate IV-a. Porphyroblast of sillimanite (s) set in a matrix of cordierite (cd) from a pelitic migmatite, sample 44. The sillimanite is partially surrounded by hercynite (black mineral). Plane polarised light. Scale bar is 1 mm long.

Plate IV-b. Bands of platy sillimanite (s) crystals separated by bands of cordierite (cd) in a pelitic migmatite, sample 210B. Crossed nicols. Scale bar is 1 mm long.

Plate IV

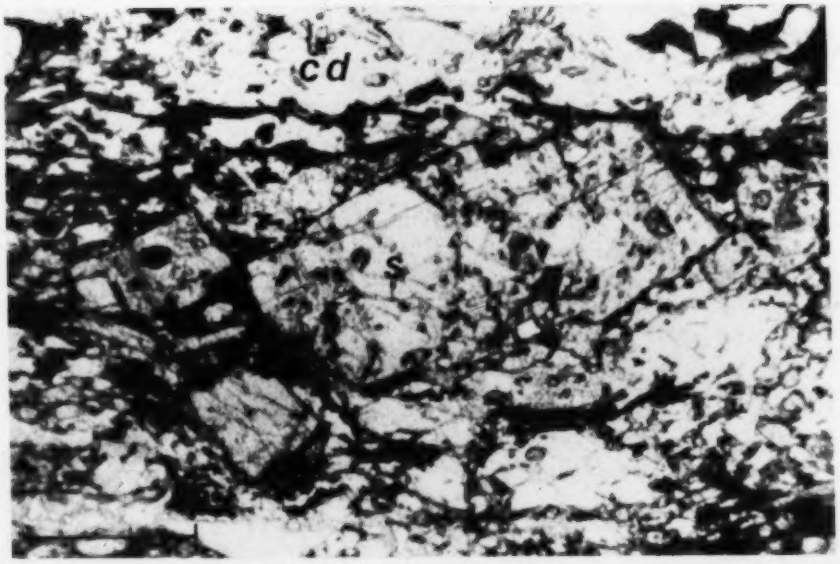

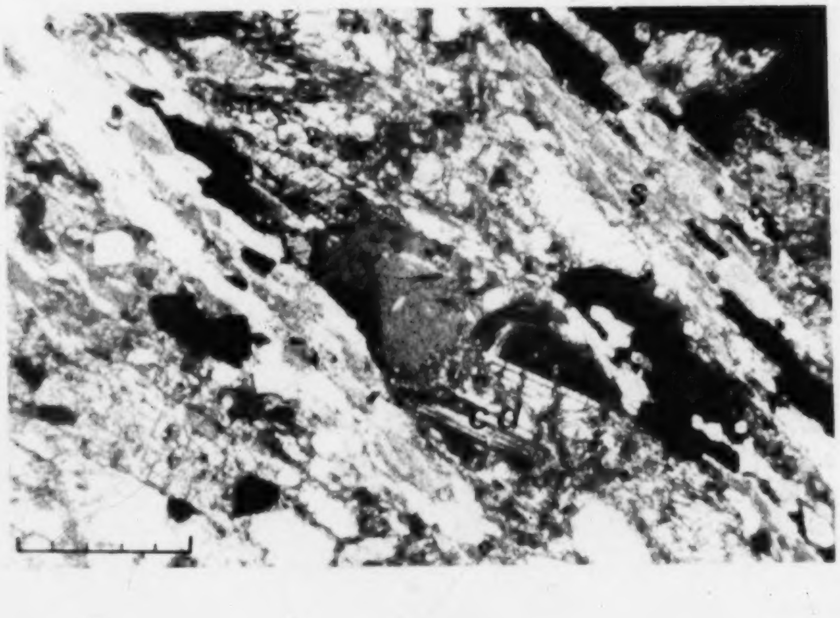

appearance of biotite. This contrasts with the generally anhedral shape of the other non-felsic phases. The intervening layers of felsic material are composed of quartz, plagioclase and K-feldspar. Occasional porphyroblasts of plagioclase or K-feldspar are often present. All phases in these layers have amoeboid grain boundaries.

Deskenatlata Lake Assemblages

The Deskenatlata Lake assemblages are dominated by the hydrous phases, hornblende and biotite. Both minerals are strongly pleochroic. The main difference in appearance between the Deskenatlata Lake and Tsu Lake amphiboles and biotites is in colour. The Deskenatlata Lake hornblende is a bluish-green colour as opposed to the green of the Tsu Lake hornblende. The difference in colour is probably due to the increased proportion of Ti in the Tsu Lake amphiboles. The Deskenatlata Lake biotites are characterised by a more orange-brown colour as opposed to the red-brown Tsu Lake biotites; the colour difference being attributed to differences in the Ti content.

The hornblende-bearing assemblage has an equigranular to inequigranular granoblastic texture (average grain size 1 mm). Hornblende crystals show interlobate grain boundaries with the crystals in the plagioclase-quartz matrix. When biotite is associated with hornblende, they appear to be in equilibrium with one another. Alteration of biotite to chlorite is sometimes seen. Magnetite is associated with the mafic minerals. Apatite is dispersed throughout the rock.

Some rocks with hornblende and biotite show compositional banding. Where this is the case, hornblende is associated with quartz and biotite is associated with plagioclase. Epidote and allanite are both associated with and are usually included in biotite.

The predominantly biotite-bearing assemblage has an inequigranular flaser texture. "Skeletal" crystals of biotite surround porphyroblasts of plagioclase. Both phases have interlobate crystal boundaries. This biotite differs distinctly from biotite in the other Deskenatlata Lake assemblages by being pleochroic in greenish-brown, green and yellowish-brown.

One occurrence of orthopyroxene was found at Deskenatlata Lake. The rock consists predominantly of biotite, approximately 70 modal percent. Both orthopyroxene and hornblende occur as "relict" crystals with hornblende surrounding the orthopyroxene. Rare porphyroblasts of plagioclase are enclosed by biotite.

The only other occurrence of pyroxenes, diopside, is in a calc-slicate rock. That rock contains the assemblage: calcite + cpx + sph + ksp + epi + allanite. The diopside is associated with epidote in a matrix of calcite and K-feldspar. Sphene occurs around the edges of diopside and epidote crystals.

The pelitic assemblage is distinctly different from the Tsu Lake assemblages. The texture is inequigranular flaser. Fibrous sillimanite surrounds lenses of cordierite. This band is bordered by biotite. Garnet occurs in the felsic bands between the sill-cord-biot layers. Quartz shows amoeboid grain boundaries.

Unusual Features

Prehnite Occurrences.

The occurrence of prehnite was not mentioned earlier as it does not appear to be restricted to a particular lithology, nor does it appear to be part of the primary metamorphic assemblage. It occurs throughout the non-pelitic assemblages of Tsu Lake, groups 1 to 4, and Deskenatlata Lake.

Its occurrence has important implications for the conditions of metamorphism in both areas. The upper stability limit for prehnite is approximately 400 °C at 5 kb (Liou, 1971). This is much lower than the conditions suggested by assemblages described earlier. There is little other evidence of a greenschist facies overprint. Chlorite appears only as an alteration product of biotite, in some of the Deskenatlata Lake samples, but not as a pervasive alteration. The development of sphene and rutile replacements of ilmenite also suggests low grade metamorphic conditions. This feature will be discussed later.

The mode of occurrence of prehnite is distinctive. Sheaf-like aggregates of prehnite occur between the cleavage planes of biotite, Plate Va. Biotite appears to be pushed apart by the growth of prehnite. The deformation of biotite is seen in the curved cleavage traces. Only in some of the Deskenatlata Lake assemblages is prehnite found in the matrix, physically independent of biotite.

Prehnite appears to have formed in biotite independently of the surrounding matrix. Biotite in matrices of plagioclase or of hornblende, most commonly contains prehnite. No other phase is associated with prehnite development, in terms of reaction products.

Plate V-a. Textural relationships between biotite (b) and prehnite (pr) in a group 3 Tsu Lake sample, 22L. Plane polarised light. Scale bar is 0.1 mm long.

Plate V-b. Textural relationships between biotite (b), prehnite (pr) and grandite (gr) in a Deskenatlata Lake sample, D10A. Plane polarised light. Scale bar is 0.1 mm long.

Plate V

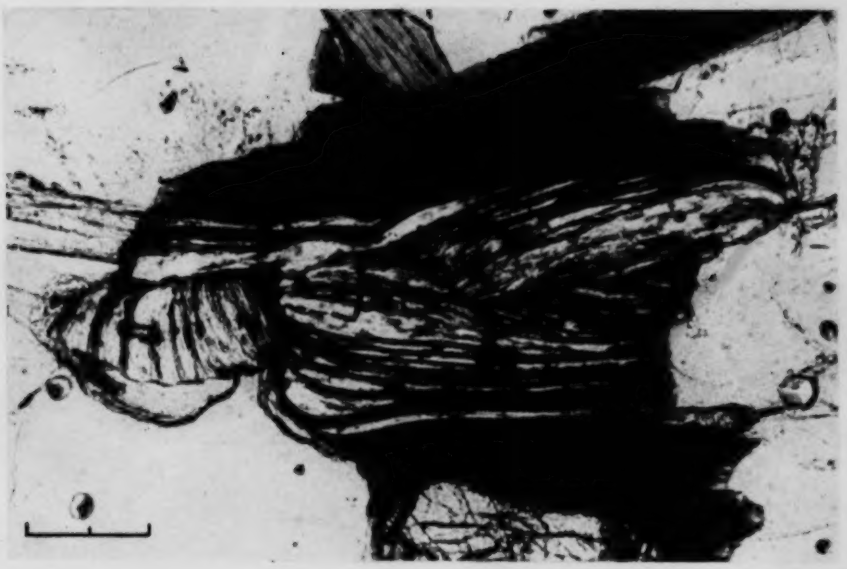

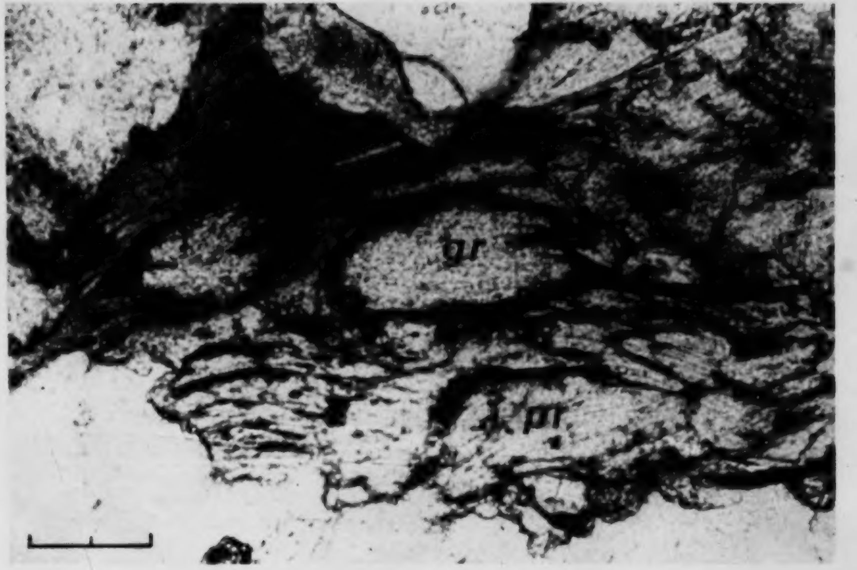

A grandite-hydrogrossular phase was observed in association with prehnite in one sample, (D10A). The grandite forms pods of small crystals, almost amorphous in appearance, in the centre of sheaves of prehnite, Plate Vb. It differs from the recorded occurrence of grandite by Tulloch (1979) in that it appears to push apart the prehnite cleavage planes, analogous to the prehnite growth in biotite. Epidote is associated with prehnite in several other Deskenatlata Lake samples. These two additional Ca-Al silicates appear to represent an advanced stage in the development of the prehnite-biotite association.

Monazite and Allanite Occurrences.

The occurrence of the REE-bearing accessory phases at Tsu Lake and Deskenatlata Lake is noteworthy. Monazite is the common accessory REE-phase in the group 5 and 6 lithologies. It also occurs in the group 4 lithologies. Allanite is the predominant REE-bearing phase in the Deskenatlata Lake rocks although one occurrence of monazite has been observed. The difference in the type of the REE-bearing phase could be related to either the metamorphic conditions, or the composition of the rocks. As no compositional data is available for the Deskenatlata Lake rocks, it is impossible to comment further on this observation.

Mineralogy

Representative analyses of the phases in the assemblages discussed in the previous section, are presented in the appendices. All mineral compositions were determined using the electron microprobe. A section in appendix 1, describes the technique used. Some problems pertinent to microprobe analyses, i.e., determination of ferric iron concentrations and H_2O estimates, are discussed there.

Except in the cases where there is zoning present only one analysis of each phase in a sample is shown..For the most part this analysis represents the average of at least three separate analyses taken from several different grains. Averaging of these analyses was undertaken after the elemental concentrations had been calculated for each analysis. Rim and core compositions of zoned phases are indicated.

Amphiboles

The classification of amphiboles is difficult when the ferric iron content is unknown. The $Mg^{2+}/(Mg^{2+}+Fe^{2+})$ ratio is needed in order to define the Mg and Fe end-members. But more importantly, the amount of ferric iron affects the calculated occupancies of all the cation sites. Most affected are the estimated amounts of Na in the M_4 and A sites. The scheme proposed by Leake (1978) utilises the occupancy of the A site as a classification component; hence the scheme is extremely sensitive to errors in the estimated ferric iron content.

In this study the maximum and minimum amounts of the ferric iron component in the amphibole were calculated. With a maximum ferric iron concentration, the Na content of the M_4 site is maximised, resulting mainly in a magnesio-hornblende classification (Leake, 1978). The method of estimating the minimum amount of ferric iron excludes all Na from the M_4 site, therefore the classification of the amphiboles is forced away from a hornblende component toward that of edenite. Compositional fields shown in Fig. 2.3, represent the end-member components of the "true" amphibole compositions because the actual ferric iron content must lie between the two extremes.

Compositional variation is limited mainly to changes in the $Mg^{2+}/(Mg^{2+}+Fe^{2+})$ ratio. However, there appears to be a significant difference in the Al(IV)/Al(VI) ratio between amphiboles from Tsu Lake and Deskenatlata Lake. It is unlikely that whole rock compositions alone, are responsible for the observed compositional difference.

Amphibole compositional variations due to whole rock compositions are accommodated in the structure by simple substitution mechanisms. If the amphiboles from both areas have equilibrated under the same conditions then they should display the same substitution trends.

Substitution reactions are best considered as replacements to the tremolite formula $\square Ca_2Mg_5Si_8O_{22}(OH)_2$ ($\square$, the A site, is the only site with permissible vacancies, Spear (1981)). The following reactions represent the probable substitutions:

i. Mg = Fe

ii. A + Si(IV) = Na(A) + Al(IV) edenite

iii. 2Si(IV) + 2Mg(VI) = 2Al(IV) + 2Al(VI) tschermakite

iv. 2Si(IV) + 2Mg(VI) = 2Al(IV) + $2Fe^{3+}$(VI) ferri-tschermakite

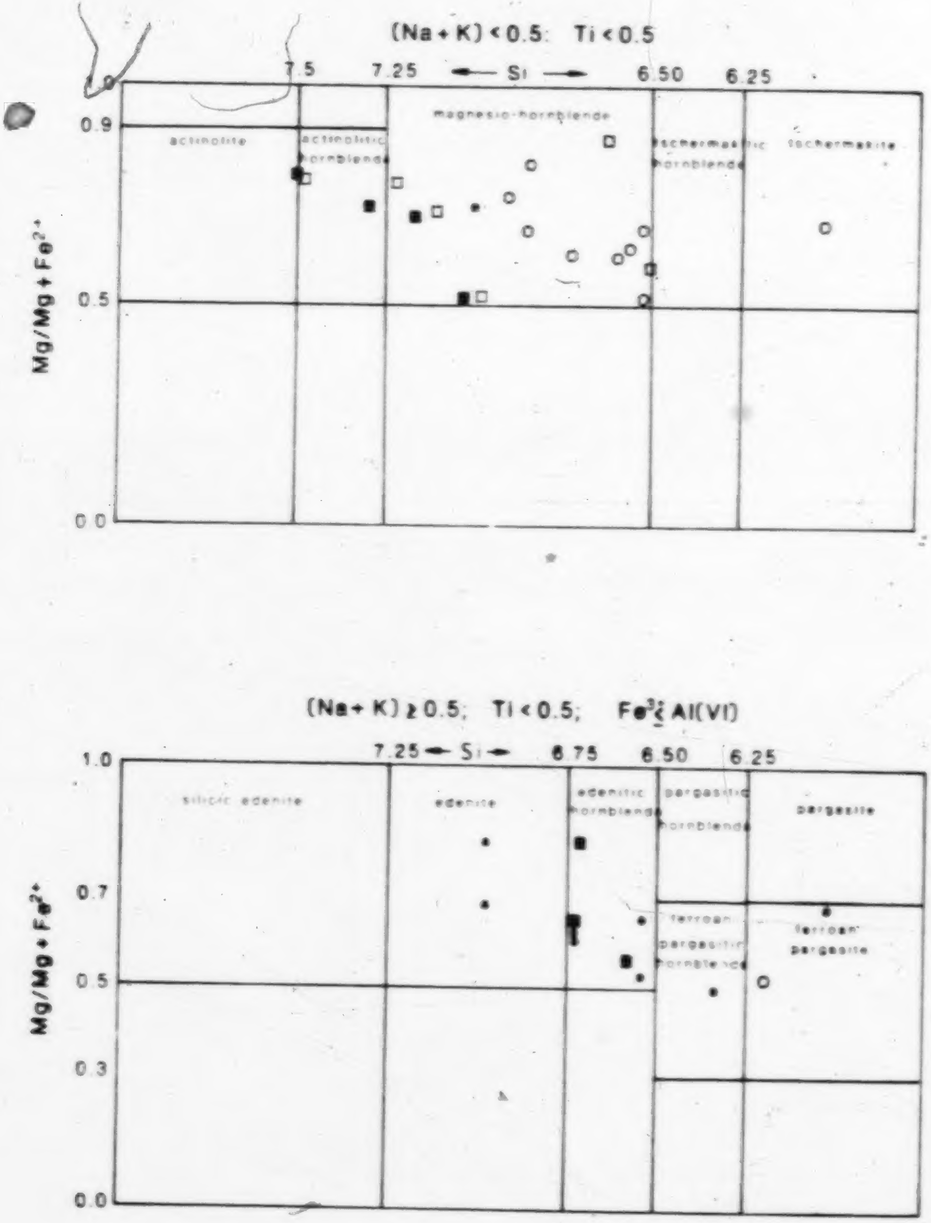

Fig. 2.3. Compositional variation of the amphiboles, using the classification scheme of Leake (1978). Initial normalisation was on the basis of 23 oxygens, excluding H_2O concentrations. Subsequent normalisation procedures gave estimates of the maximum Fe^{3+} content (open symbols) and the minimum Fe^{3+} content (closed symbols). Circles represent Tsu Lake amphibole compositions, squares represent Deskenatlata Lake compositions.

v. $2Ca(M_4) + 2Mg(VI) = 2Na(M_4) + 2Al(VI)$ glaucophane

vi. $2Ca(M_4) + 2Mg(VI) = 2Na(M_4) + 2Fe^{3+}(VI)$ riebeckite

vii. $2Si(IV) + Mg(VI) = 2Al(IV) + Ti(VI)$ Ti-tschermakite

viii. $A + Ca(M_4) = Na(A) + Na(M_4)$ richterite

Other substitutions may be possible by combining two or more of these reactions. For example, pargasite is a combination of the edenite and tschermakite substitutions; hence

ix. $A + Mg(VI)\ 2Si(IV) = Na(A) + Al(VI)\ 2Al(VI)$.

Of these reactions pargasite and Ti-tschermakite are probably the predominant substitutions in the Tsu Lake amphiboles, and pargasite only in the Deskenatlata Lake amphiboles. Figs. 2.4 to 2.6 demonstrate the reasoning behind this conclusion.

Fig. 2.4 shows the variation in Al(IV) with A site occupancy. The calculated site occupancies are given for both ferric iron estimates (as is the case with all the relevant diagrams). One trend (the minimum ferric iron estimate) is close to that expected for pargasite, while the other lies halfway between the tschermakite and pargasite trends. An intercept of approximately 0.1 Al(IV) suggests the involvement of Al(IV) in other substitution reactions.

Fig. 2.5 shows that the substitution mechanism is closer to that of pargasite than tschermakite (both estimates). A difference in composition and/or metamorphic conditions is indicated by the division of the data (minimum ferric iron estimates) into two parallel trends, the groupings corresponding to the two different localities. The division is less pronounced for the maximum ferric iron estimates. The intercept of 0.46 for the Tsu Lake amphiboles suggests Al(IV) is not totally coupled to Al(VI) whereas it is with the Deskenatlata Lake amphiboles. In turn this implies that the Al(IV) - A site coupling of Fig. 2.4, for Deskenatlata Lake, is not real. The considerable scatter shown by the maximum ferric iron estimates in both Figs. 2.4 and 2.5 suggests that perhaps the "true" ferric iron concentration is closer to the value predicted by the minimum estimate.

Ti-tschermakite substitution is possible in the Tsu Lake amphiboles, as is illustrated in Fig. 2.6. The slope of approximately 4:1, twice that expected for ideal Ti-tschermakite substitution, agrees with the conclusions drawn from Figs. 2.4 and 2.5 in that Al(IV) participates in several different substitution reactions. The independence of Al(IV) from Ti for the Deskenatlata Lake amphiboles, suggests that different metamorphic conditions

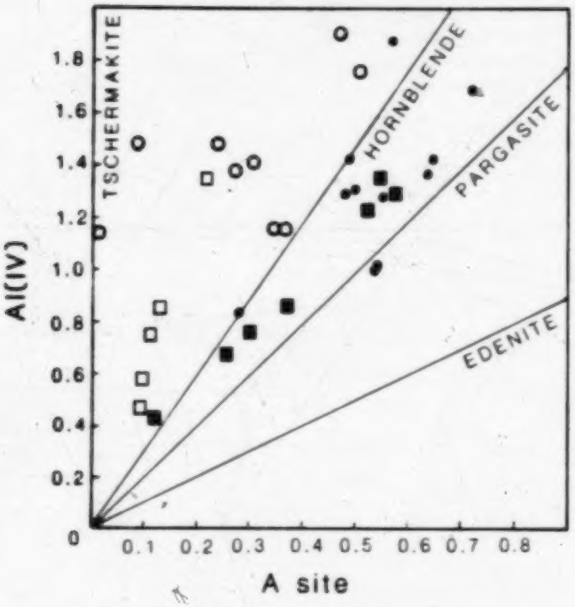

Fig. 2.4. Variation of Al(IV) and A site contents of amphiboles. Initial normalisation was on the basis of 23 oxygens, excluding H_2O concentrations. Subsequent normalisation procedures gave estimates of the maximum Fe^{3+} content (open symbols) and the minimum Fe^{3+} content (closed symbols). Circles represent Tsu Lake amphibole compositions, squares represent Deskenatlata Lake compositions.

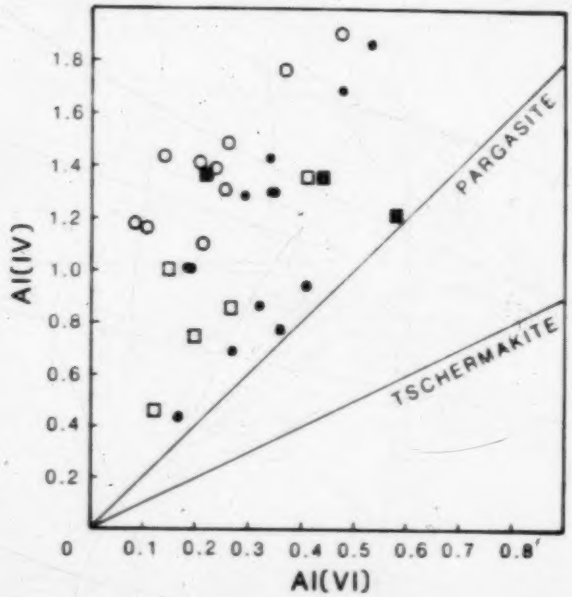

Fig. 2.5. Variation of Al(IV) and Al(VI) contents of amphiboles. Normalisation procedures are as described for Fig. 2.4. Symbols: Tsu Lake amphiboles, maximum Fe^{3+} (open circles); Tsu Lake amphiboles, minimum Fe^{3+} (closed circles); Deskenatlata Lake amphiboles, maximum Fe^{3+} (open squares); Deskenalata Lake amphiboles, minimum Fe^{3+} (closed squares).

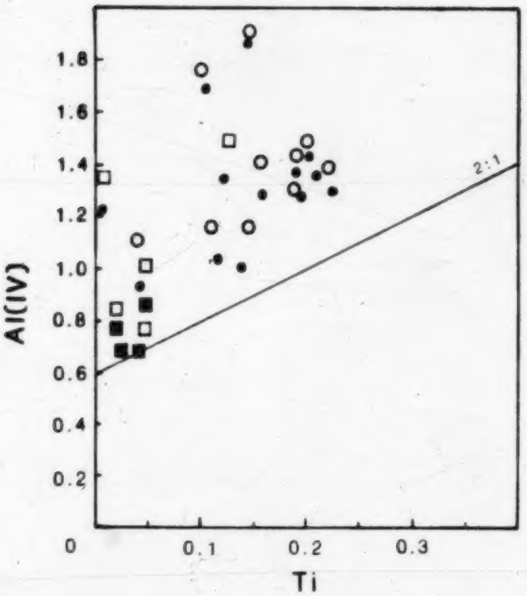

Fig. 2.6. Variation of Al(IV) and Ti contents of amphiboles. Symbols as for Fig. 2.5.

could be responsible for the apparent amphibole compositions of the two localities.

The amphiboles from both areas are similar in many aspects, except for the reaction involving Ti. Unfortunately no whole rock composition data are available to substantiate this, but it is unlikely that Ti, in the Deskenatlata Lake rocks, is sufficiently depleted to exclude the partitioning of significant Ti into the amphibole phase. The presence of sphene as the Ti bearing phase mitigates against a Ti depletion theory. As Ti has been shown to partition more easily into hornblende with increasing temperature (Leake 1965), it is likely that the different amphibole compositions are due to higher temperatures at Tsu Lake than at Deskenatlata Lake.

Pyroxenes

Orthopyroxene.

The compositional range exhibited by the orthopyroxenes is shown in Fig. 2.7. The end-members for the Ca, Mg and Fe system were calculated using the method recommended by Cawthorn and Collerson (1974). Wollastonite is excluded as an end-member for the Tsu Lake orthopyroxenes by this calculation. All Ca is assumed to be present as the Ca-tschermakite molecule. Later it will be shown that this is incorrect. However, it is the function of the diagram to show the maximum compositional variance, i.e., in Mg and Fe, and to show the relationship of the orthopyroxene to any coexisting clinopyroxene.

The range of compositions in orthopyroxenes, from Fs_{26} to Fs_{58}, is not unusual. Howie (1955) reported orthopyroxenes of a similar compositional range from the Madras granulites. Compositions of orthopyroxenes from Tsu Lake and Deskenatlata Lake appear to be mainly a function of the whole rock compositions. Samples which could be classified as charnockites, contain the most Fe-rich orthopyroxenes: Fs_{55} to Fs_{58}, while the ultramafic rocks contain the most Mg rich orthopyroxenes, Fs_{26}.

Three types of orthopyroxene are recognised petrographically, the differences are exemplified quite strongly by the compositions. The types are defined as:

I. orthopyroxene coexisting with clinopyroxene, or with hornblende, groups 1 and 2;
II. orthopyroxene coexisting with biotite and plagioclase, group 3;
III. "relict" orthopyroxene, group 4.

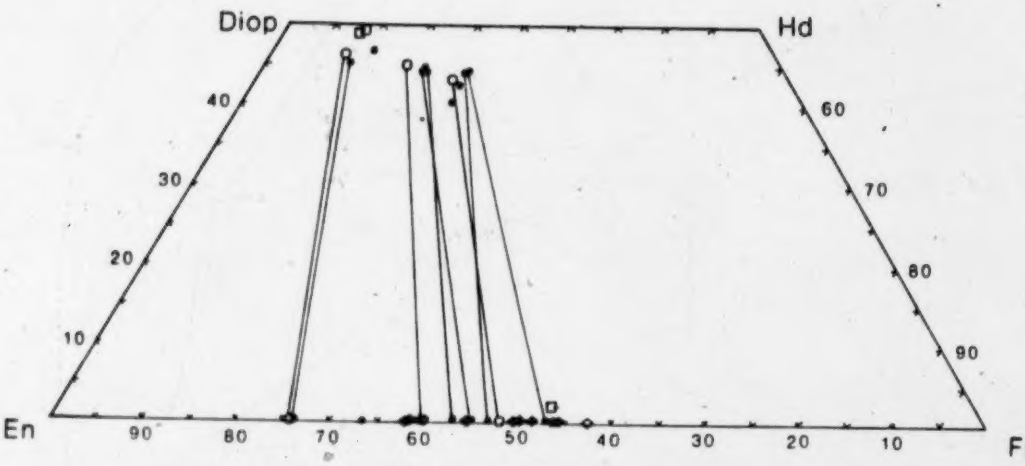

Fig. 2.7. Variation of the Ca, Mg and Fe^{2+} contents of the pyroxenes. Symbols for the Tsu Lake pyroxenes: group 1 (open circles), group 2 (closed circles), group 3 (closed diamonds), group 4 (open diamonds). Symbols for the Deskenatlata Lake pyroxenes: open squares.

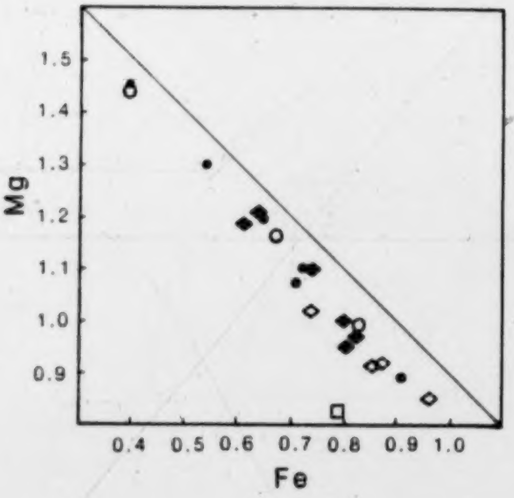

Fig. 2.8. Variation of Mg and Fe^{2+} contents of orthopyroxenes. The line drawn on the diagram represents the expected variation for ideal sustitution between these two elements. Symbols as in Fig. 2.7.

The "relict" orthopyroxene occurs only in the most silicic rocks. It differs distinctly from the other two types in that it occurs as a minor phase, less than 5%, and is quite extensively altered around the grain boundaries. Chlorite is the predominant alteration product.

The chemical differences are most easily described in terms of substitution reactions. The theoretical substitutions to the enstatite molecule, $Mg_2Si_2O_6$ (arbitarily chosen), are:

i. (Ca,Fe,Mn) + Mg = Mg + Mg
ii. (Ca,Fe,Mn) + (Ca,Fe,Mn) = Mg + Mg
iii. (Ca,Fe,Mn) + Al(VI) + Al(IV) = 2Mg + Si
iv. (Ca,Fe,Mn) + Fe^{3+}(VI) + Fe_{3}^{+}(IV) = 2Mg + Si
v. (Ca,Fe,Mn) + Ti(VI) = Mg + Si

Figs. 2.8 to 2.12 illustrate the substitutions which have taken place. The variation of Mg with Fe^{2+} is shown in Fig. 2.8. The line drawn on the diagram represents that which would be expected if reaction (ii) occurred (if Fe^{2+} was the only substituting cation). The data plot below this line, therefore other reactions involving Fe^{2+} have probably occurred, or other cations (Ca,Mn) have replaced Mg.

The Ca variation with Mg illustrates the three orthopyroxene types, Fig. 2.9. A trend of a decreasing Ca content with an increasing amount of Mg is shown for types (I) and (III) orthopyroxenes. The type (II) orthopyroxenes show the reverse trend, increasing Ca with increasing Mg. These variations suggest that Ca is coupled with Fe for types (I) and (iii), and with Mg for type (II). The variation of Ca with Fe^{2+} (not shown), is the exact reverse of Fig. 2.9, supporting the suggestion above.

The presence of substitution (iii) should be shown by the variation of Mg with Si, Fig. 2.10. Type (I) orthpyroxenes display the independence of the Mg content from the amount of Si, implying the absence of the tschermakite reaction. However, the trends for both types (II) and (III) indicate the occurrence of this reaction. In the case of type (II), Fe^{2+} is probably coupled to Al(VI) and Al(IV); in the case of type (III) it is Mg which forms the tschermakite molecule.

Support for the existence of the tschermakite reaction (III) is shown in Fig. 2.11. Types (II) and (III) exhibit the expected tschermakite trend. The absence of this reaction in

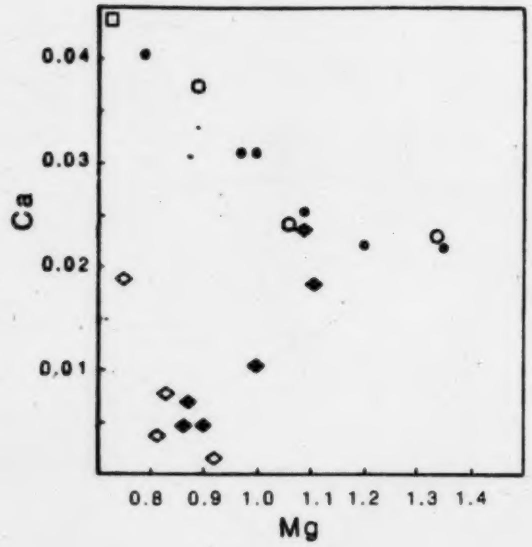

Fig. 2.9. Variation of Ca and Mg (cationic proportions) in orthopyroxenes. Symbols as in Fig. 2.7.

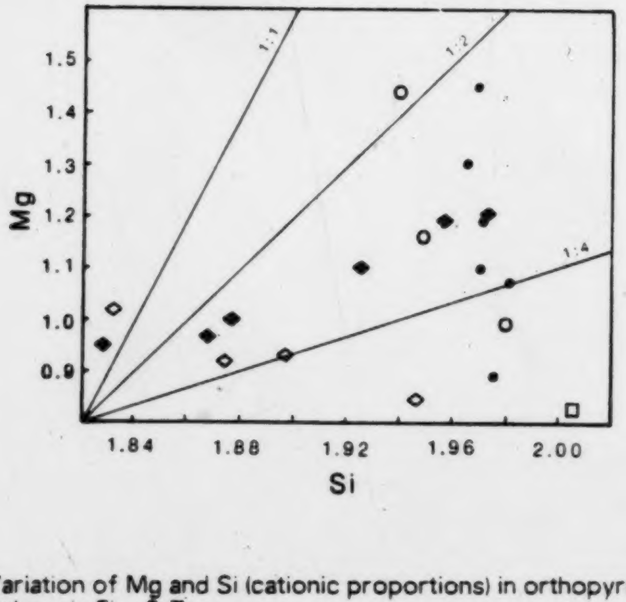

Fig. 2.10. Variation of Mg and Si (cationic proportions) in orthopyroxenes. Symbols as in Fig. 2.7.

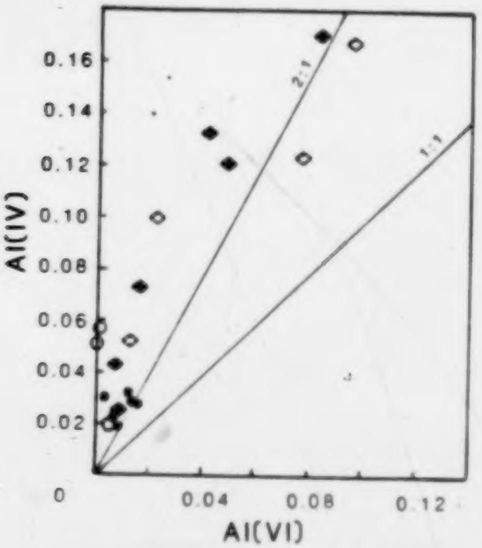

Fig. 2.11. Variation of Al(IV) and Al(VI) (cationic proportions) in orthopyroxenes. Symbols as Fig 2.7.

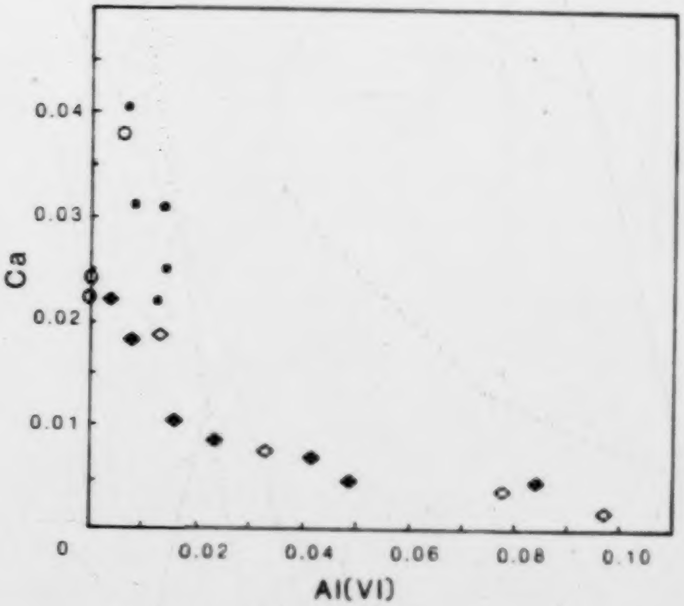

Fig. 2.12. Variation of Ca and Al(VI) (cationic proportions) in orthopyroxenes. Symbols as in Fig. 2.7.

type (I) orthopyroxenes may, in part, be attributed to their very low total Al content. However it is more likely that the low Al content is caused by the reaction which formed the orthopyroxene.

Ca does not appear to be involved in the tschermakite substitution. The variations shown in Fig. 2.12, Ca versus Al(VI), are indications of the coupling of Ca to Mg or Fe^{2+}.

The behaviour of Mn is less clearly defined than that of the other divalent cations. The variations of Fe^{2+}, Fig. 2.13, and Mg with Mn tend to suggest that Mn is coupled to Mg for types (I) and (III), and to Fe^{2+} for type (II).

In summary, the following reactions occur:

a. type (I)
  i. $Ca + Fe^{2+} = Mg + Mg$
  ii. $Mn = Mg$

b. type (II)
  i. $Ca = Mg$
  ii. $Fe^{2+} + Al(VI) + Al(IV) = 2Mg + Si$
  iii. $Mn + Fe = Mg + Mg$

c. type (III)
  i. $Ca + Fe^{2+} = Mg + Mg$
  ii. $Mn = Mg$
  iii. $Mg + Al(VI) + Al(IV) = 2Mg + Si$.

The differences of the type (ii) orthopyroxene compositions from the other two types is enigmatic. It is possible that the switch of roles for Mg and Fe^{2+} in type (ii) is, in some way, related to the coexistence with biotite.

Clinopyroxene.

The compositions of the clinopyroxenes are typical of those found in granulite facies rocks, Fig. 2.7, (Deer *et al.*, 1978). It is apparent that the whole rock compositions are significant in controlling pyroxene compositions. The ultramafic rocks from Tsu Lake have diopsidic compositions similar to clinopyroxenes from the Madras ultrabasic granulites (Deer *et al.*, 1978). The less mafic rocks contain clinopyroxenes with compositions in the augite field. Clinopyroxenes from calc-silicate rocks of Deskenatlata

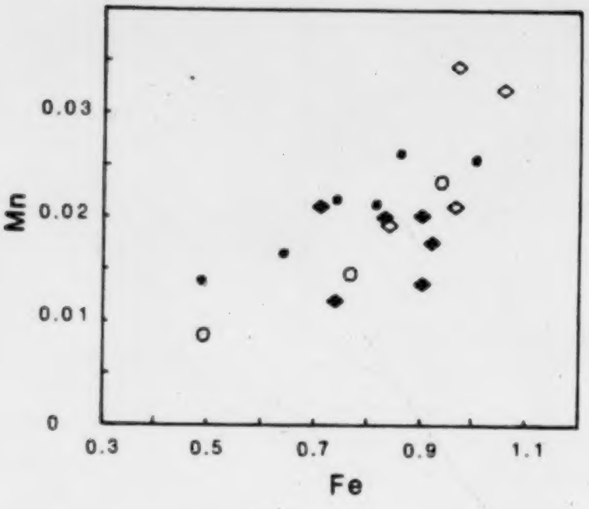

Fig. 2.13. Variation of Mn and Fe²⁺ (cationic proportions) in orthopyroxenes.
Symbols as in Fig. 2.7.

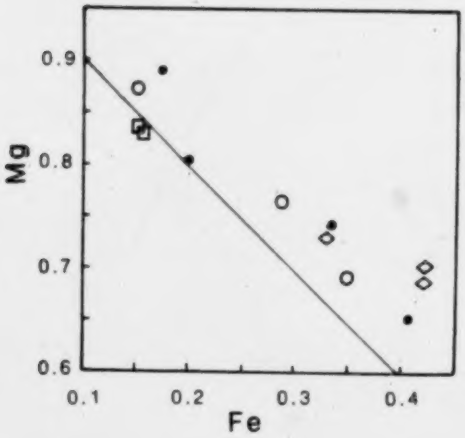

Fig. 2.14. Variation of Mg and Fe²⁺ (cationic proportions) in clinopyroxenes.
Symbols as in Fig. 2.7.

Lake are diopsidic in composition.

Augite compositions of a majority of the clinopyroxenes contrast with the salitic compositions expected for amphibolite facies conditions. The increased solubility of Mg and Fe^{2+} in the diopside-hedenbergite series is a indication of the higher temperatures of metamorphism.

Unlike the orthopyroxenes, there are no discernible differences in the compositions of the clinopyroxenes. Except for the calc-silicate clinopyroxenes and two clinopyroxenes from ultramafic amphibolites, all clinopyroxenes coexist with an orthopyroxene. Therefore the lack of any obvious optical differences and the similarity of the clinopyroxene compositions suggests all the clinopyroxenes were formed by the same reaction. In turn this implies that the differences observed in the orthopyroxenes are a function of the orthopyroxene-forming reaction.

The composition of the clinopyroxenes is described by substitution reactions used for the orthopyroxenes. The variation of Mg and Fe^{2+}, Fig. 2.14 shows that the substitution between these two elements is not ideal. This indicates that Mg or Fe^{2+} participate in a reaction other than reaction (i).

Examination of Fig. 2.15, Al(VI) versus Al(IV), shows scattered data points with no clearly defined tschermakite trend. Mg is independent of the Si content, which is expected in the absence of the tschermakite reaction.

Fig. 2.16 suggests that the Ca content is coupled to Mg; only the diopsidic clinopyroxenes show a Ca independence of Mg or Fe. The opposite trend, of Fe^{2+} content decreasing with increasing Ca (not shown), was found. Mn behaves in an analogous manner to Ca, Fig. 2.17.

The substitution mechanisms that have been identified are:

i. $Ca + Fe^{2+} = Mg + Mg$

ii. $Mn + Fe^{2+} = Mg + Mg$

These two substitutions are the reverse of the substitutions found for the coexisting type (I) orthopyroxenes. It implies that clinopyroxene exerts a control over the partitioning of Ca and Mn into orthopyroxene. The absence of clinopyroxene in the assemblage containing type (II) orthopyroxene assemblages explains the switch of partitioning relations found there.

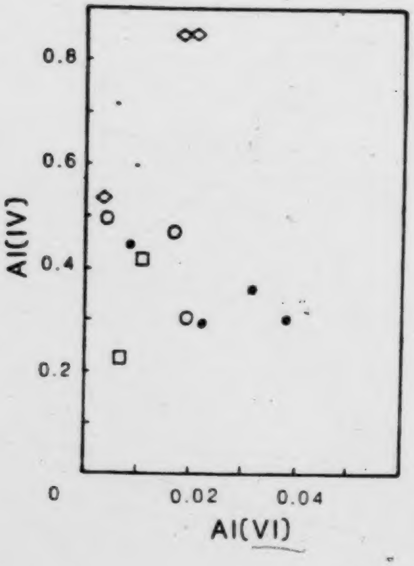

Fig. 2.15. Variation of Al(IV) and Al(VI) (cationic proportions) in clinopyroxenes. Symbols as in Fig. 2.7.

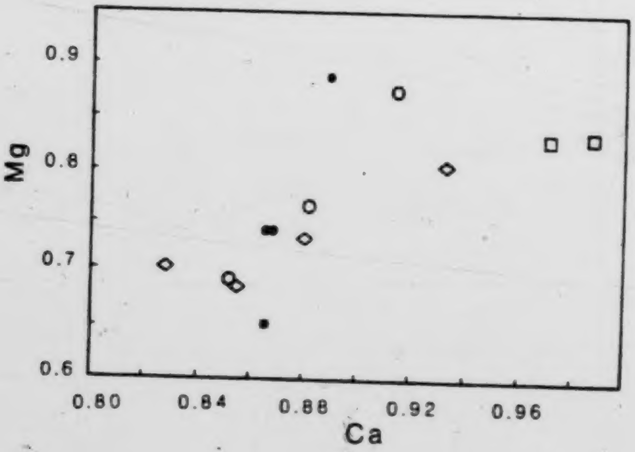

Fig. 2.16. Variation of Mg and Ca (cationic proportions) in clinopyroxenes. Symbols as in Fig. 2.7.

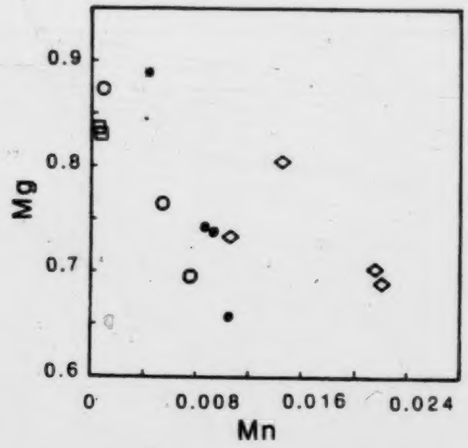

Fig. 2.17. Variation of Mg and Mn (cationic proportions) in clinopyroxenes. Symbols as in Fig. 2.7.

The Deskenatlata Lake clinopyroxenes show a similar composition to those of the Tsu Lake clinopyroxenes, but with a much higher Ca content. This difference merely reflects the control of the whole rock compositions.

Biotite

Compositional variation of the major elements in biotites, is shown in Fig. 2.18 (all Fe is represented as Fe^{2+}). The dependence of the biotite composition on the type of assemblage, and hence whole rock composition, is seen. Biotites in basic or intermediate rocks, i.e., those associated with pyroxenes, have the lowest Al_2O_3 contents. Their compositional variation is restricted to changes in the Mg/Fe ratio. Biotites coexisting with garnet contain approximately the same Al_2O_3 as the biotites from basic rocks, but have a smaller range of Mg/Fe ratios. Aluminous rocks contain biotites with the highest Al_2O_3 concentrations and with a restricted range of Mg/Fe ratios.

The Deskenatlata Lake biotites have compositions similar to Tsu Lake biotites of the same or similar assemblages, except that their compositions lie at the extreme end of the group ranges. The compositional trends seen here match the Al saturation trend reported by Dymek (1983) for biotites in the Lango granulite facies gneisses of Greenland.

Compositional substitutions that are possible in the phlogopite-annite series $K(Mg,Fe)(Si_3,Al)O_{10}(OH)_2$, are defined below (Dymek, 1983).

i. $R^{2+}(VI) + Si^{4+}(IV) = Al^{3+}(VI) + Al^{3+}(VI)$

ii. $3R^{2+}(VI) = 2\,Al^{3+}(VI) + (\square)(VI)$

iii. $R^{2+}(VI) + 2Si^{4+}(IV) = Ti^{4+}(VI) + 2Al^{3+}(IV)$

iv. $Al^{3+}(VI) + Si^{4+}(IV) = Ti^{4+}(VI) + Al^{3+}(IV)$

v. $2Al^{3+}(VI) = Ti^{4+}(VI) + R^{2+}(VI)$

vi. $2R^{2+}(VI) = Ti^{4+}(VI) + (\square)(VI)$

vii. $R^{2+}(VI) + 2OH^- = Ti^{4+}(VI) + 2(O^{2-}) + H_2$

viii. $R^{2+}(VI) + Si^{4+}(IV) = Fe^{3+}(VI) + Al^{3+}(IV)$

ix. $Fe^{2+} + (OH^-) = Fe^{3+} + O^{2-} + 1/2H_2$

x. $K^+(A) + Al^{3+}(IV) = (\square)(A) + Si^{4+}(IV)$

The substitution mechanisms of Ti are particularily important because the presence of this element in biotite appears to increase its stability field (Rutherford, 1973).

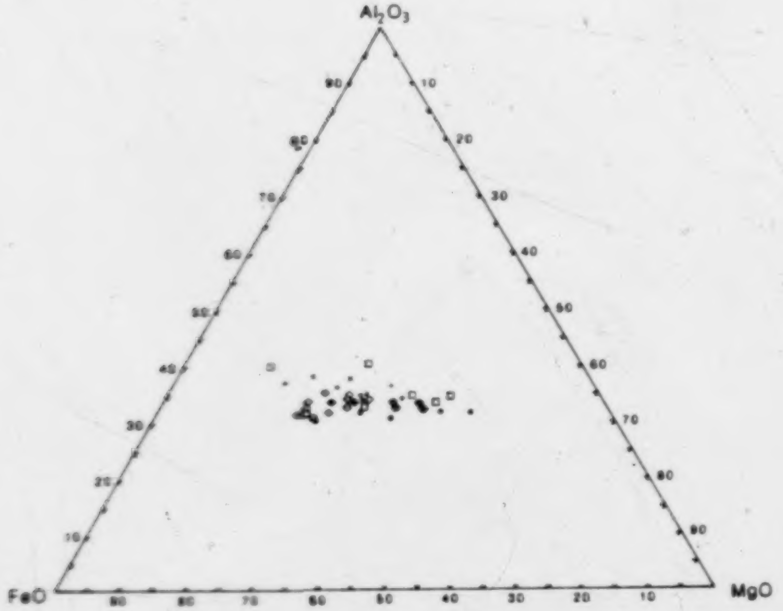

Fig. 2.18. Variation of Al_2O_3, FeO and MgO in biotites. Symbols: Tsu Lake biotites, group 1 (open circles), group 2 (closed circles), group 3 (closed diamonds), group 4 (open squares), group 5 (diagonal crosses), group 6 (vertical crosses). Deskenatlata Lake biotites (open squares). Normalisation is based on 22 oxygens, excluding H_2O contents.

The relationship between Al(IV) and Al(VI), Fig. 2.19, is not a simple linear one. A positive 1:1 relationship would indicate the presence of the Al tschermakite substitution (reaction (i)), but Al(VI) and Al(IV) appear to be independent of one another. The data plots below the 1:1 line, therefore the presence of Al(IV) is not balanced by Al(VI). It is probable that this is merely a reflection of the method of normalisation of the structural formula. The data in Fig. 2.19 are the result of a normalisation using 22 oxygens. A normalisaton procedure based on 14 cations can be used, but by this method only some of the data, namely those biotites richest in Al, are shifted above the 1:1 line.

Examination of Fig. 2.20 reveals a possible linear relationship between Ti and Al(IV). Biotites from groups 1 to 4 show a slope of 1, indicative of substitution reaction (iv). For the Al-rich biotites the relationship is less clear. The absence of the Ti-tschermakite reaction is indicated by the lack of a Ti:Al 1:2 correlation.

The variation of Ti with Al(VI), Fig. 2.21, tends to support the relationship seen in Fig. 2.20. Groups 1 to 4 biotites show a negative slope of approximately 1:1, again the data for the Al-rich biotites is inconclusive.

The lack of any correlation between the total positive charge and Al(VI), Fig. 2.22, suggests that Al(VI) is not involved in a vacancy-forming substitution, reaction (ii). The data does show the Al saturation trend, with the biotites from the same lithologies clustering together.

The relationship between the total positive charge and Ti was examined, Fig. 2.23. Any data which falls on the line labelled: charge excess = 2Ti, suggests the presence of either reaction (vi) or (vii). Most of the data seems to scatter about this line, although groups 1, 2 and 4 biotites have a significantly lower excess charge than the rest. This implies that not all of the Ti, in these three biotite groups, is involved in reactions (vi) or (vii), and supports the conclusions reached regarding substitution (iv).

The relationship between Al(IV) and Al(VI) may now be reviewed. It is possible that several conflicting factors are responsible for the observed results. Al(IV) appears to be involved in substitution (iv), at least for some of the biotites, and this should cause a trend of decreasing Al(VI) with increasing Al(IV). If either substitution (i) or (iii) is involved then an opposing trend should be superimposed on the reaction (iv) trend.

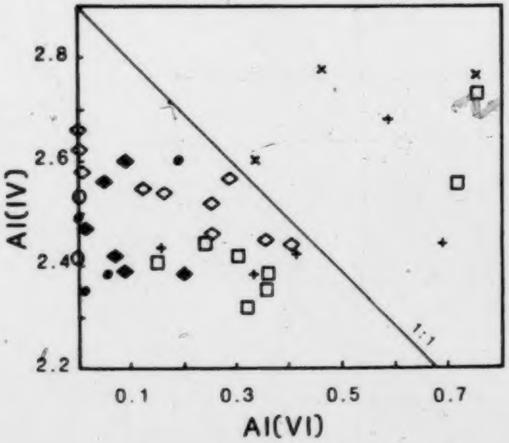

Fig. 2.19. Variation of Al(IV) and Al(VI) (cationic proportions) in biotites. Normalisation procedure and symbols as described in Fig. 2.18.

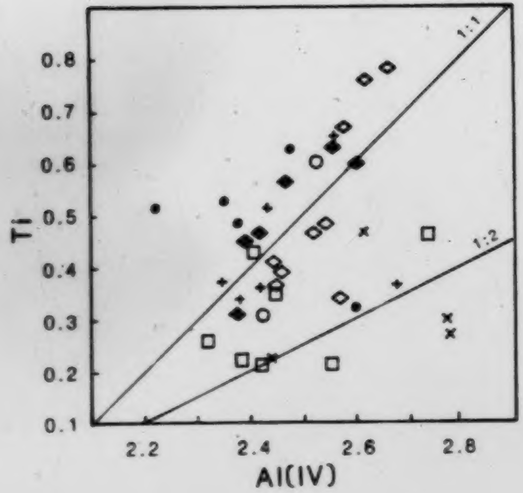

Fig. 2.20. Variation of Ti and Al(IV) (cationic proportions) in biotites. Symbols as in Fig. 2.18.

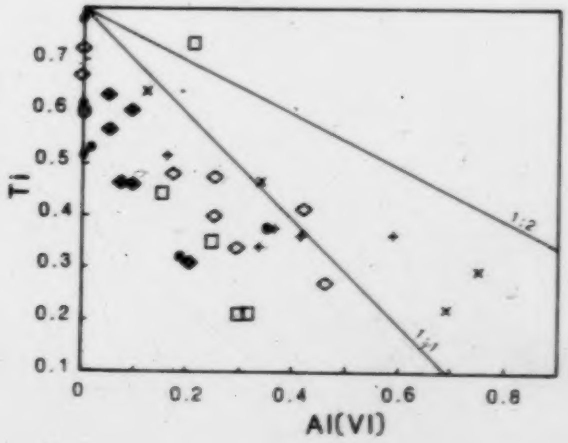

Fig. 2.21. Variation of Ti and Al(VI) (cationic proportions) in biotites. Symbols as in Fig. 2.18.

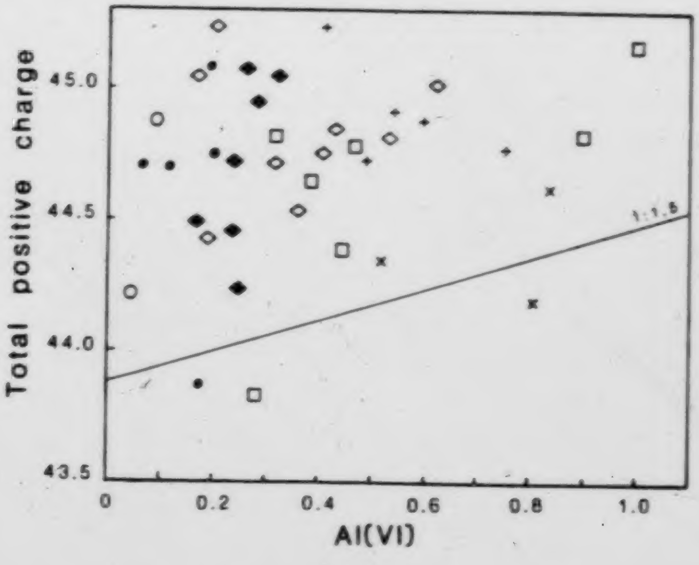

Fig. 2.22. Variation of the calculated total positive charge with Al(VI) (cationic proportion) in biotites. Symbols as in Fig. 2.18.

One other factor may contribute to the observed Al results. If substitution (viii) occurred, then Al(IV) would not be balanced exactly by Al(VI). The presence of Fe^{3+} is suggested by the application of the recommended normalisation procedure of Dymek (1983). The negative amount of "excess" Al(VI) implies the presence of Fe^{3+}.

It is important to note the Ti substitution mechanisms in the Tsu Lake biotites compared to those in other granulite facies biotites. The substitutions (iv), (vi) and (vii) prevail for the Tsu Lake biotites. It is not possible to distinguish between substitutions (vi) and (vii) when only microprobe analyses are available because the OH^- contents are unknown. Substitution (iv) occurs only in the less aluminous biotites. These conclusions are in conflict with the reported observations of Dymek (1983). The Lango biotites show only reaction (vi) or (vii). Dallmeyer's (1974) biotite data indicated the presence of substitution (i) in addition to the Ti substitutions. Bohlen *et al.* (1980) report that Ti in a biotite from the Adirondack granulites occurred by substitutions (iii), (vi) and (vii).

The differences in the Ti substitution reactions for the various granulite facies areas are probably a function of the differing metamorphic conditions. The presence of substitution (iv) for the Tsu Lake group 1 to 4 biotites is probably an indication of both whole rock chemistry and the temperature of crystallisation. The high Al content of the other Tsu Lake biotites may prevent the inclusion of a large amount of Ti and hence prevents the occurrence of substitution (iv).

Dymek (1983) showed that Ti is enriched in biotites of granulite facies grade relative to those of amphibolite facies grade. Ghent (1984) suggested also that Ti partitioning into biotite is controlled more by temperature than by Ti activity. However, there is also a crystal-chemical constraint on the Ti substitution. High Mg/Fe ratios favour increased substitution of Ti into the biotite structure (Dymek, 1983). This relationship for the Tsu Lake biotites is shown in Fig.2.24. Again the differences in the compositions of biotites, due to the Al contents, are exemplified.

The preceding discussion concentrated mainly on the composition of the Tsu Lake biotites. Results for the Deskenatlata Lake biotites do not differ appreciably. The most significant factor is the apparent similarity of the Ti concentrations for the Deskenatlata Lake biotites and the aluminous biotites from Tsu Lake.

However, examination of Fig. 2.24 indicates that the Deskenatlata Lake biotites are richer in Mg than the aluminous Tsu Lake biotites and therefore, should show a higher concentration of Ti. Crystal-chemical and temperature control on the composition of the biotites is indicated by the lower Ti contents of the Deskenatlata Lake biotites. The lower temperature of crystallisation for the Deskenatlata Lake biotites agrees with the conclusions reached regarding the Deskenatlata Lake amphiboles.

Garnet

Figs. 2.25 and 2.26 show the compositional ranges for the garnets of this study. The garnet end-members were calculated assuming negligible andradite. Calculation of the Fe^{3+} content of the garnets by assuming stoichiometry, suggested that the andradite component was insignificant. The main variation is in Fe^{2+} and Mg, both within the phase and between lithologies. The Fe concentration is within the range expected for granulite facies garnets (Deer *et al.*, 1982). There is no correlation between the almandine content of the garnet and the SiO_2 content of the rock. Deer *et al.* (1982) suggested that this was a factor in determining Fe concentrations in garnet.

Each garnet group is characterised by variation in the minor elements. Group 4 garnets differ from the other two in having the highest range of grossular contents from 7 to 3%, Fig. 2.25. Grossular, in garnets of the other groups is limited to less than 3%.

The grossular content of a garnet is probably a function of the composition of any coexisting plagioclase. Fig. 2.27 illustrates the relationship. There is a strong correlation between the percentage of grossular in the garnet and the percentage of anorthite in the plagioclase for the group 4 garnets. The relationship is different and less well defined for the group 6 garnets, but still shows a dependency on the plagioclase composition.

The diagram shows what appears to be a lower limit for the grossular concentration in garnet. It would appear that a certain amount of grossular will be present in garnets of the almandine-pyrope series at granulite facies conditions if Ca is present in the rock system. This is likely a reflection of a reaction between garnet and plagioclase which is temperature or pressure dependent. A geobarometer is based on the reaction:

anorthite = grossular + sillimanite + quartz (Newton, 1983).

In the group 4 assemblages garnet does not coexist with sillimanite. It is probable that a reaction similar to the one described above has occurred but with another phase

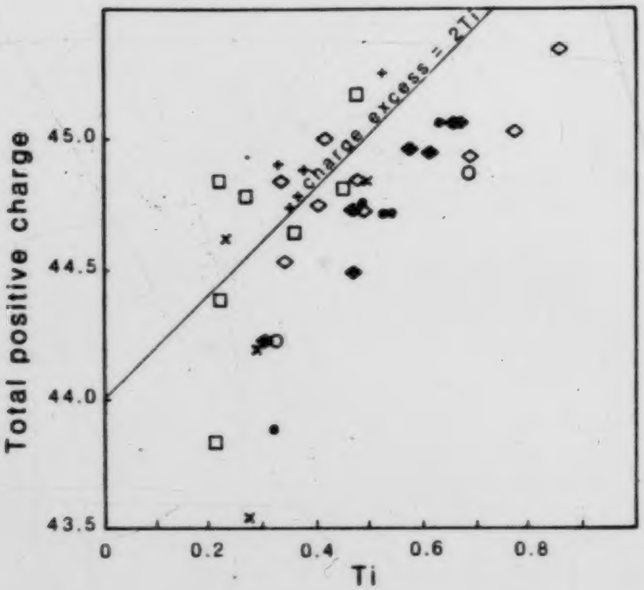

Fig. 2.23. Variation of the calculated total positive charge and Ti in biotites. Symbols as in Fig. 2.18.

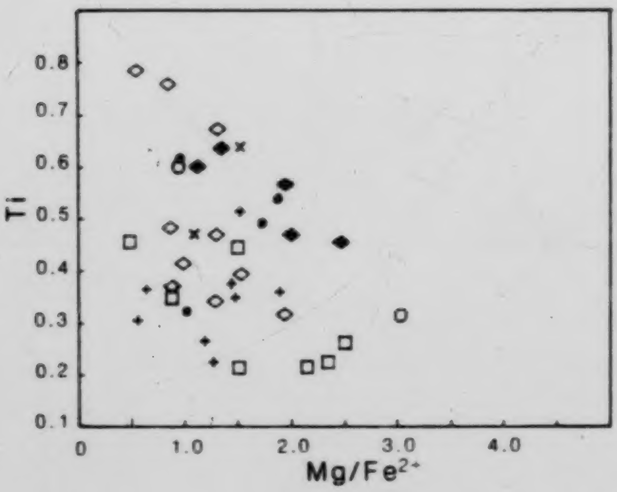

Fig. 2.24. Variation of Ti versus the Mg/Fe^{2+} ratio in biotites. Symbols as in Fig. 2.18.

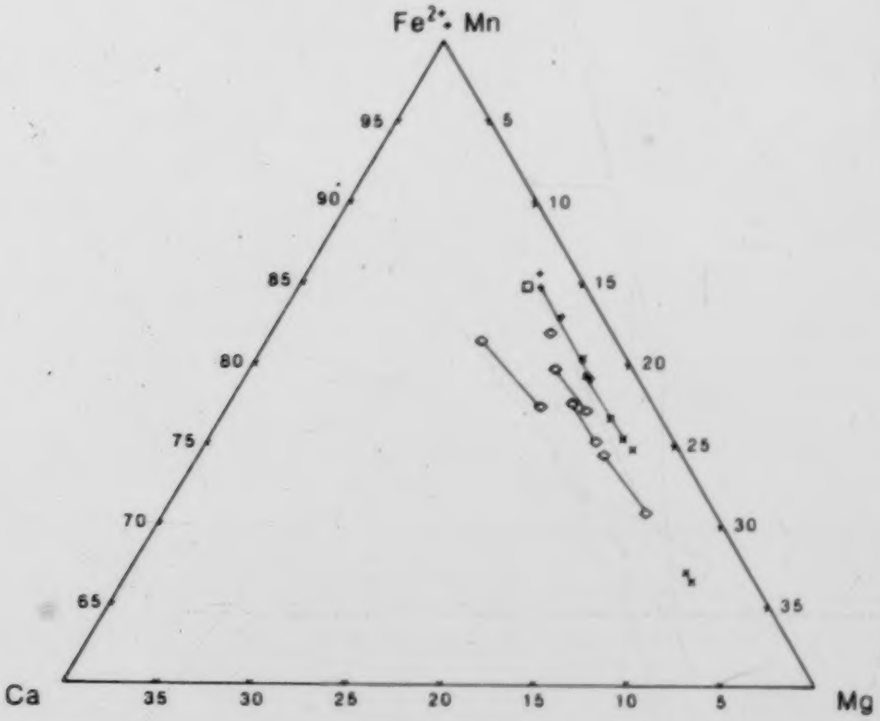

Fig. 2.25. Variation of Ca, Mg and Fe^{2+}+Mn (cationic proportions) in garnets. Symbols: Tsu Lake: group 4 (open diamonds); group 5 (diagonal crosses); group 6 (vertical crosses).

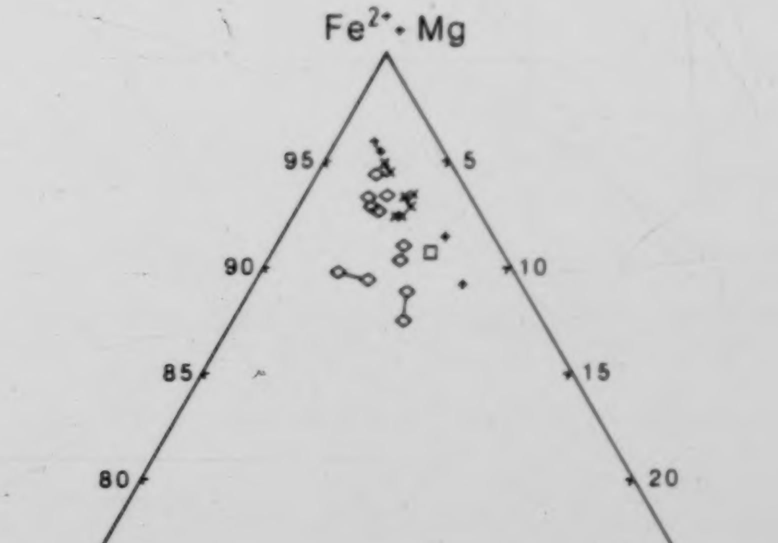

Fig. 2.26. Variation of Ca, Mn, and Fe^{2+}+Mg (cationic proportions) in garnets. Symbols as in Fig. 2.25.

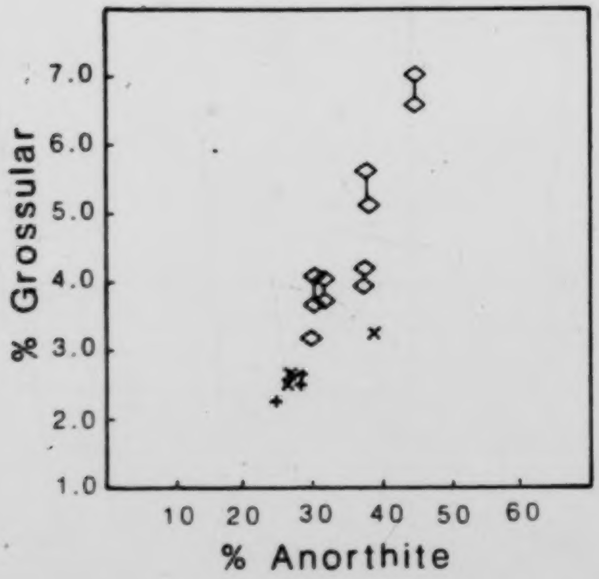

Fig. 2.27. Relationship between the percentage of grossular in garnet and the anorthite content of coexisting plagioclase. Symbols as in Fig. 2.25.

participating in place of sillimanite. The lack of a correlation between the whole rock and garnet Ca values supports the contention that the grossular component of garnet is a function of a pressure dependent reaction.

The spessartine component exhibits a wider range of values in the group 4 and group 6 garnets than it does in the group 5 garnets. Like the grossular component, the spessartine component never falls below a minimum concentration.

Fig. 2.25 indicates the extent of the zoning observed. Undoubtedly this does not represent the actual maximum range because of the analytical difficulty in finding core compositions. Cores are richer in Mg and the rims are richer in Fe.

Both Mn and Ca show a slight degree of zoning although the zoning profiles are variable, showing enrichment in either rim or core. As the concentration of both elements is low, (for most of the garnets the difference between rim and core is only 0.1 weight percent of the oxide), it is thought that the variation is not real but a function of the statistical deviation expected for the analytical method.

The zoning patterns observed reflect the physical conditions of growth. Variations in Mg and Fe are directly related to the type of coexisting phases. The degree of Fe partitioning into garnet, relative to biotite or cordierite, is greater than that of Mg. The zoning profiles may reflect either prograde or retrograde metamorphic conditions. However, whether retrograde metamorphic conditions can actually be recorded in the zoning profiles is a controversial topic. Richardson (1974) and Loomis (1975) presented theories on this subject that are in direct conflict with one another. Loomis (1975) suggested that garnets were unlikely to equilibrate with retrograde reaction products except at the extreme edges of the grain. Richardson (1974) suggested that retrograde diffusion was possible and that zoning profiles of garnets in rocks which had undergone retrograde metamorphism reflected this exchange.

Preservation of the zoning is an indication of the failure of garnet to reequilibrate to changing conditions (Anderson and Olimpio, 1977). Mineral assemblages indicate that temperatures of peak metamorphism were around 700 °C. Woodsworth (1977) indicated that zoning at those temperatures is usually obliterated by diffusion. However, Hollister (1977) considered such zoning to be indicative of rapid uplift, or contact metamporhism where the high temperatures are maintained for only a short period of time.

Feldspars

Plagioclase.

The plagioclase compositions are consistent with lithologic types, Fig. 2.28. Plagioclases from groups 1 and 2 show the widest range of compositions, from An_{86} to An_{43}. The other pyroxene-bearing rocks, group 3, display a more restricted compositional range from An_{40} to An_{46}, although two samples fall outside these limits, having compositions of An_{75} and An_{81}. Group 4 plagioclases fall in the compositional range of An_{30} to An_{46}. Deskenatlata Lake plagioclases have a range of compositions similar to that of group 4.

Only one plagioclase sample from all the pyroxene lithologies showed optically visible antiperthitic textures. Conversly a large percentage of the group 4 plagioclases are antiperthites. Plagioclases of a composition similar to those of group 4 are the most susceptible to antiperthite development (Ribbe, 1975).

Two samples in group 6 contained a plagioclase of approximately An_{25} and an albite, An_2. These compositions straddle the peristerite miscibility gap. However, the feldspars in question do not occur as coexisting phases. The albite is associated with a K-feldspar; in one instance as an exsolved phase of a perthite. There is usually some physical separation, on the order of several mm., between the plagioclase and the albite, as the feldspars are found in separate layers in these rocks. These textures probably resulted during the slow cooling of the partially melted rocks.

The relationship between the Ca/(Ca+Na) ratio of the rock and the plagioclase, illustrated in Fig. 2.29, shows that the Ca/(Ca+Na) ratio of plagioclase is almost independent of that of the rock. As the plagioclases from the same lithologies are recognisable as compositional groups, the compositional range of each group can be said to be controlled by the overall whole rock compositions, not the Ca/(Ca+Na) ratio.

A wide range of compositions exists for the plagioclases from basic rocks; in particular those plagioclases coexisting with hornblende. This is additional evidence for the attainment of granulite facies conditions. Spear (1980) noted the presence of a miscibility gap, An_{38} to An_{86}, in the compositions of plagioclases coexisting with hornblende from amphibolite facies rocks. He predicted, on the basis of plagioclase compositions from the

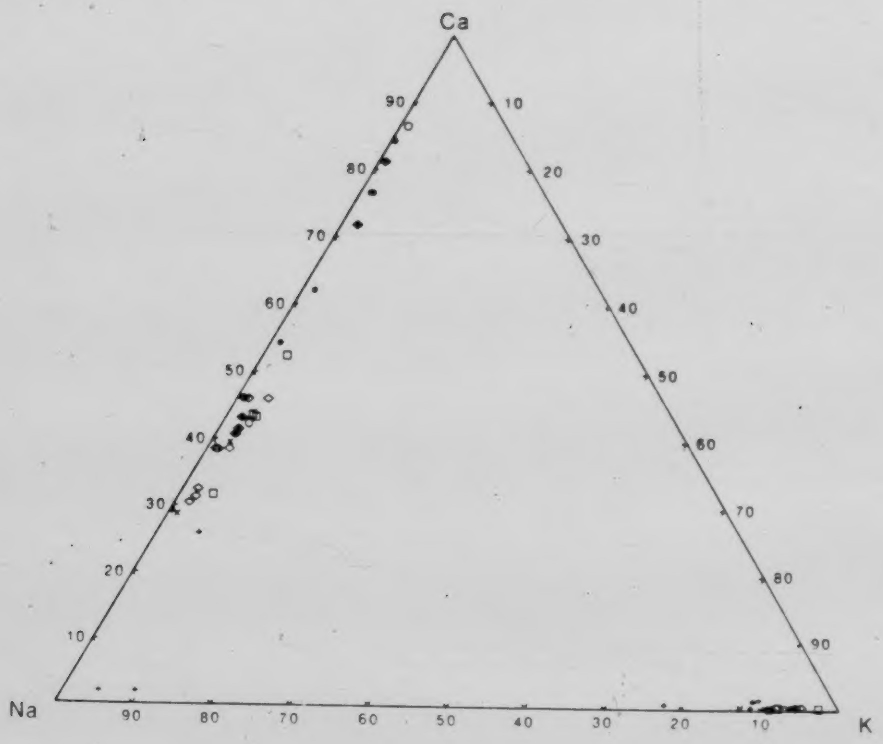

Fig. 2.28. Variation of Ca, Na and K (cationic proportions) in plagioclase and K-feldspar. Symbols: Tsu Lake, group 1 (open circles), group 2 (closed circles), group 3 (closed diamonds), group 4 (open diamonds), group 5 (diagonal crosses), group 6 (vertical crosses); Deskenatlata Lake (open squares).

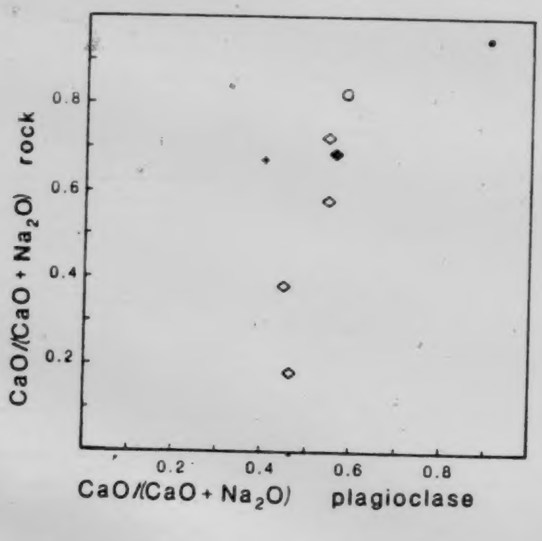

Fig. 2.29. Relationship between the CaO / (CaO + Na$_2$O) ratio in plagioclase versus that of the rock. Symbols as in Fig. 2.28.

Adirondack granulites, this gap would disappear with granulite facies conditions. That the Deskenatlata Lake plagioclases show compositions within the range of the miscibility gap, suggests that the metamorphic conditions at Deskenatlata Lake were only of a slightly lower grade than at Tsu Lake, perhaps on the boundary between the amphibolite and granulite facies grades.

K-feldspar.

The compositional range exhibited by the K-feldspars is narrow, from Or_{88} to Or_{97}, with two exceptions: Or_{77} and Or_{99}. Texturally the K-feldspars, both the primary and the exsolved phases, show the cross-hatch twinning patterns of microcline. Only a slight distinction between K-feldspars of different lithologies is discernible, Fig. 2.28. Notably the group 6 K-feldspars have the lowest Or content.

For any one sample with antiperthite, there is a small difference between the primary metamorphic K-feldspar and the exsolved antiperthite phase. The maximum difference is 6% Or; where the primary K-feldspar is Or_{87} and the exsolved phase is Or_{93}. The exsolved K-feldspar phases are richer in Or than the primary K-feldspar, with Na being retained in the host plagioclases.

Cordierite

The main variation in the compositions of the cordierites is confined to changes in the $Fe^{2+}/(Fe^{2+}+Mg+Mn)$ ratio. A range of 0.44 to 0.65 $Fe^{2+}/(Fe^{2+}+Mg+Mn)$ exists.

Small, subtle variations amongst Si, Al(tot) and the divalent cations, Fe, Mg and Mn, are apparent, Figs. 2.30 to 2.31. A noticeable difference in the Si and Al(tot) concentrations occurs between most of the group 6 and group 5 lithologies. Two of the group 6 samples fall on the same trend as the group 5 samples. A similar pattern is observed for the Al(tot) versus Fe+Mg+Mn variation. These results show that the Al(tot) content of most of the group 6 lithologies, is significantly higher than the rest of the cordierites. The Al(tot) content shows a positive correlation with the Si content, and a negative correlation with the divalent cations.

The separation of the cordierites into two groups based on the Al(tot) content is correlated to the H_2O contents. The samples which fall into the group 6 class, have H_2O contents varying from 0.6 to 1.4 weight percent; the rest of the cordierites have H_2O

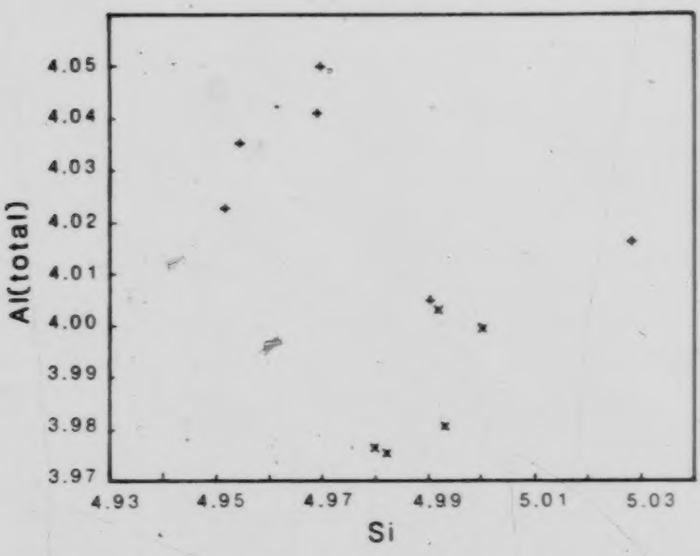

Fig. 2.30. Variation of Al(tot) and Si (cationic proportions) in cordierites. Symbols: Tsu Lake: group 5 (diagonal crosses), group 6 (vertical crosses).

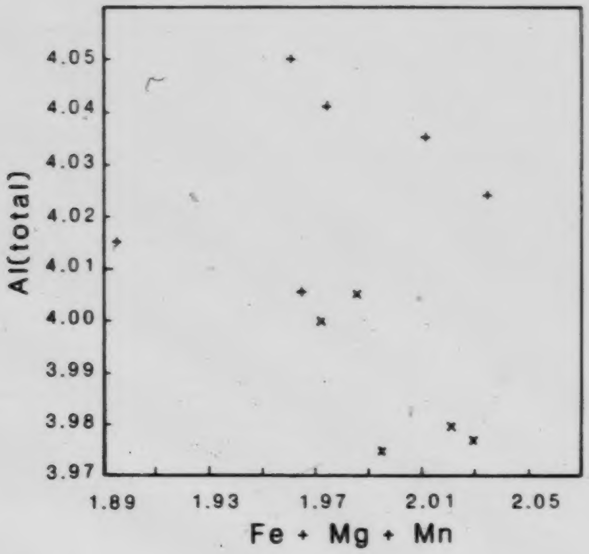

Fig. 2.31. Variation of Al(tot) and Fe+Mg+Mn (cationic proportions) in cordierites. Symbols as in Fig. 2.30.

contents from 1.6 to 2.9 weight percent. There is likely to be considerable error in the H_2O concentrations as these are merely calculated by difference from 100 percent. The Al(tot) content of the group 6 cordierites shows a negative correlation to the H_2O content, suggesting that the compositional difference between the cordierites may not be real. If the low H_2O contents of the group 6 class are the result of large analytical errors then it is to be expected that the Al contents would be affected.

It could be suggested that the compositional differences are the result of differing degrees of pinitisation. An extensively pinitised cordierite from Deskenatlata Lake (analysis not shown in appendix 3) showed very high concentrations of both H_2O and alkalis, implying that such concentrations are the result of the alteration. The Tsu Lake cordierites, in contrast, exhibit low alkali concentrations that do not correlate with the H_2O contents, which suggests the analyses represent unaltered cordierites. During analysis altered grains of cordierite were carefully avoided. It is believed that the compositional difference is real, although this cannot be proven conclusively here. Significantly the cordierites of the group 6 class do not coexist with garnet.

Sillimanite

Sillimanites contains from 0.76 to 1.50 weight percent of Fe_2O_3. Grew (1980) reports that sillimanites do not usually contain more than 1.8 weight percent Fe_2O_3. A significant difference in th Fe_2O_3 content of sillimanites from Tsu Lake and Deskenatlata Lake is observed.

An increase in the mole fraction of Fe^{3+} in sillimanite with an increase in the mole fraction of Fe^{3+} in ilmenite, should be observed if the mineral pair is in equilibrium (Grew, 1980). A regular distribution of Fe^{3+} between sillimanite and ilmenite, is absent from these samples. The Fe_2O_3 values for ilmenite are much lower than those of granulite facies rocks reported by Grew (1980). This indicates the reequilibration of ilmenite to lower grade metamorphic conditions.

The unit cell parameters for two sillimanite samples were measured by the powder photograph technique with the following conditions: Debye-Sherrer camera, Cu Kα radiation with a Ni filter, fine collimators, irradiation time 10 hours, capillary mounts. The cell parameters were calculated using a least squares program of Evans *et al.* (1963). The unit cell dimensions for the two samples are:

171B, a = 7.479 A$^\circ$, b = 7.670 A$^\circ$, c = 5.768 A$^\circ$, and V = 330.839 A$^{\circ 3}$.

210B, a = 7.483 A$^\circ$, b = 7.671 A$^\circ$, c = 5.770 A$^\circ$, and V = 331.19 A$^{\circ 3}$.

Grew (1980), from a compilation of ten sillimanites, obtains the following unit cell dimensions for an iron-free sillimanite:

a = 7.4830 A$^\circ$, b = 7.6708 A$^\circ$, c = 5.7694 A$^\circ$ and V = 331.15 A$^{\circ 3}$.

The unit cell dimensions should increase with the substitution of Fe$_2$SiO$_5$ into sillimanite. The reported unit cell dimensions of sillimanite in Ribbe (1980) are slightly larger than those of Grew (1980). The Tsu Lake sillimanite unit cell parameters are close to those of an iron-free sillimanite but do not show the expected increase in the cell dimensions due to the dissolved Fe^{3+}.

Oxides

The mode of occurrence of the oxide phases differs in each of the lithologic groups. Groups 1 to 4 are characterised by the presence of ilmenite; magnetite is occasionally an associated primary phase. In groups 5 and 6 magnetite is rarely absent, and hercynite, an additional phase, may occur. Exsolution features in the oxides are more common in groups 5 and 6 but may be found in the other groups as well. Frequently observed types of exsolution are:

i. magnetite and rutile exsolved from ilmenite;

ii. ilmenite exsolved from magnetite,

iii. magnetite and corundum exsolved from hercynite.

Secondary alteration products, sphene and rutile, may also be present.

Details on the Fe^{2+}:Fe^{3+} calculation procedure are given in appendix 1.

Ilmenite.

Fig.2.32 shows the compositional range of the major components of ilmenite. A very restricted range of Fe^{3+} values is observed, implying limited solubility of the hematite molecule within ilmenite. This is a feature suggesting the reequilibration of ilmenite to retrograde metamorphic conditions, as ilmenites from granulites usually show much higher hematite contents (Rumble, 1976). A relatively wide range of Fe^{2+} and Ti^{4+} values is shown. Most of the group 5 and 6 ilmenites cluster together around 48 to 50% Ti^{4+}, while the rest of the ilmenites show between 50 and 55% Ti^{4+}.

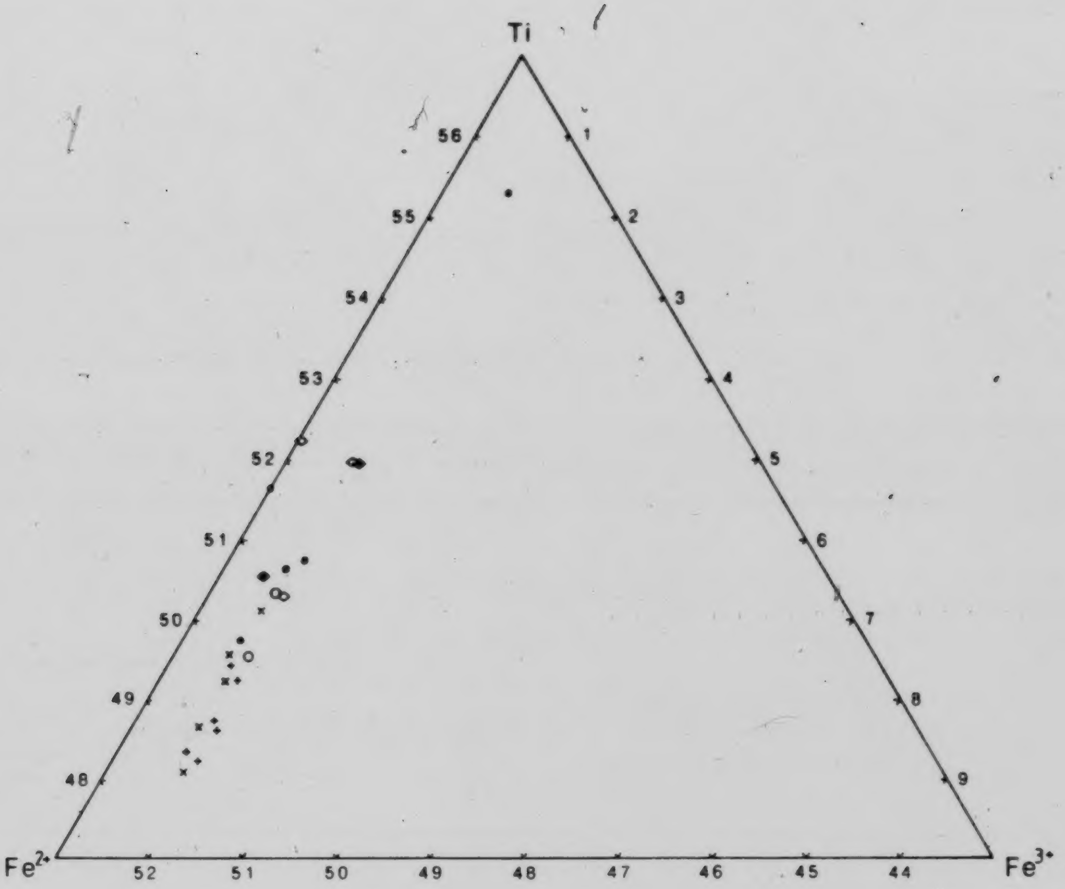

Fig. 2.32. Variation of Ti, Fe^{2+} and Fe^{3+} (cationic proportions) in ilmenites. Symbols: Tsu Lake; group 1 (open circles), group 2 (closed circles), group 3 (closed diamonds), group 4 (open circles), group 5 (diagonal crosses), group 6 (vertical crosses).

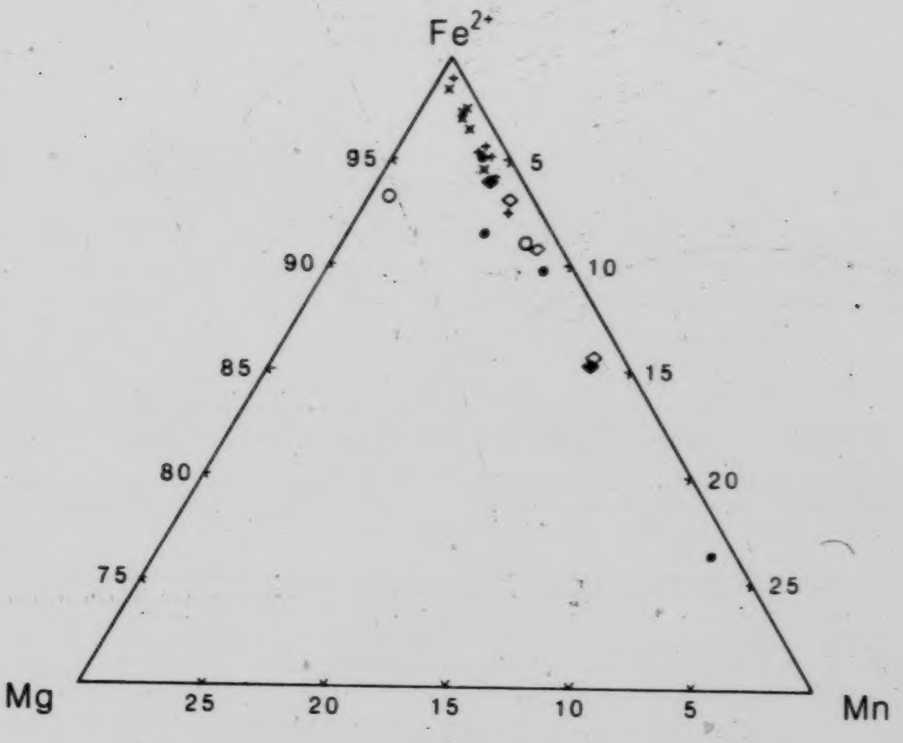

Fig. 2.33. Variation of Fe^{2+}, Mg and Mn (cationic proportions) in ilmenites. Symbols as in Fig. 2.32.

The reason for the apparent lack of stoichiometry (Fe^{2+} should exactly balance Ti^{4+} in the absence of hematite) in the group 1 to 4 ilmenites is obvious from Fig. 2.33. A considerable proportion of the pyrophanite molecule ($MnTiO_3$) is present in the ilmenites which show greater than 50% Ti^{4+}. Of the minor elements Mn is the only one present in significant amounts; Mg shows only very limited substitution.

Mn substitution into ilmenite, in igneous rocks, is controlled by both temperature and the Mn content of the magma (Haggerty, 1976). In metamorphic rocks, the controlling factors are likely to be temperature and the composition of the rock, both of which partially control the type of phases that are present. The abundance of garnet in groups 5 and 6; and the lack of other, similar Mn-bearing phases in the other lithologies can explain the significant difference in the Mn contents of the ilmenites.

Magnetite.

The extent of the ulvospinel solubility in the magnetites is shown in Fig. 2.34. There does not appear to be any correlation between the Ti content of magnetite and the lithologic type.

The other substitutions which are possible, involve the trivalent cations which may replace Fe^{3+}. Ilmenites by contrast show preferential divalent cation substitutions. The degree of these additional substitutions is displayed in Fig. 2.35, with the greatest variation being in the Cr and V concentrations.

From the limited data available, the amount of V substitution into magnetite, as much as 2 weight percent V_2O_5 in the Tsu Lake magnetites, becomes significant during metamorphism at granulite facies grades (Rumble, 1976). Most published analyses of magnetites do not report V concentrations, therefore further comment on the validity of these observations is not possible. It is only since the introduction of the energy dispersive microprobe technique that V has been routinely determined.

Hercynite.

Hercynites found in the Tsu Lake rocks fall into two distinct compositional groups: those which are found with cordierite in group 5 lithologies, and those which coexist with sillimanite in group 6 lithologies. The group 5 hercynites have a larger spinel component,

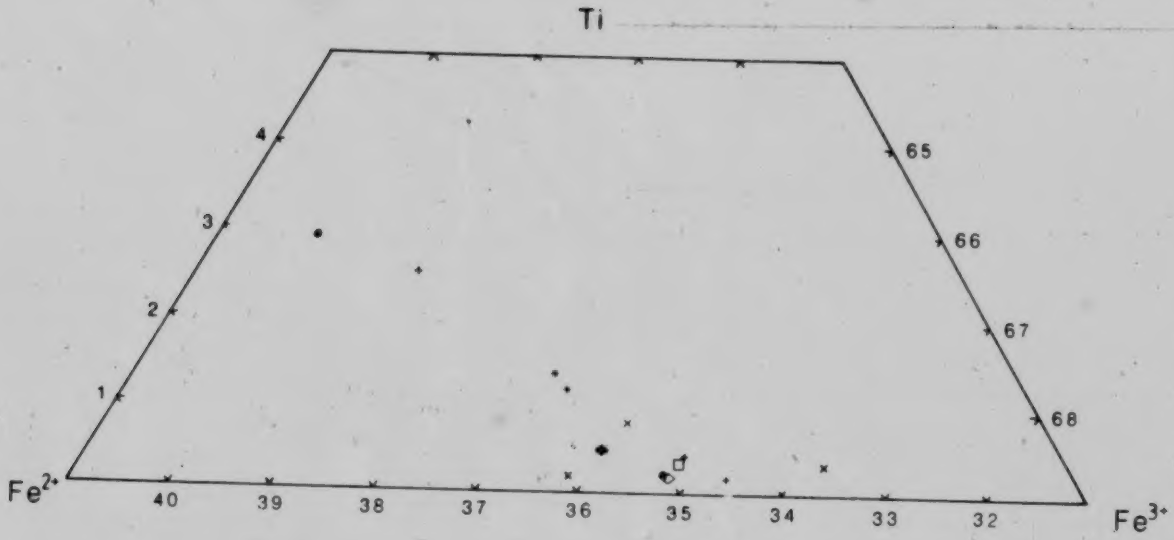

Fig. 2.34. Variation of Ti, Fe²⁺ and Fe³⁺ (cationic proportions) in magnetites. Symbols as in Fig. 2.32.

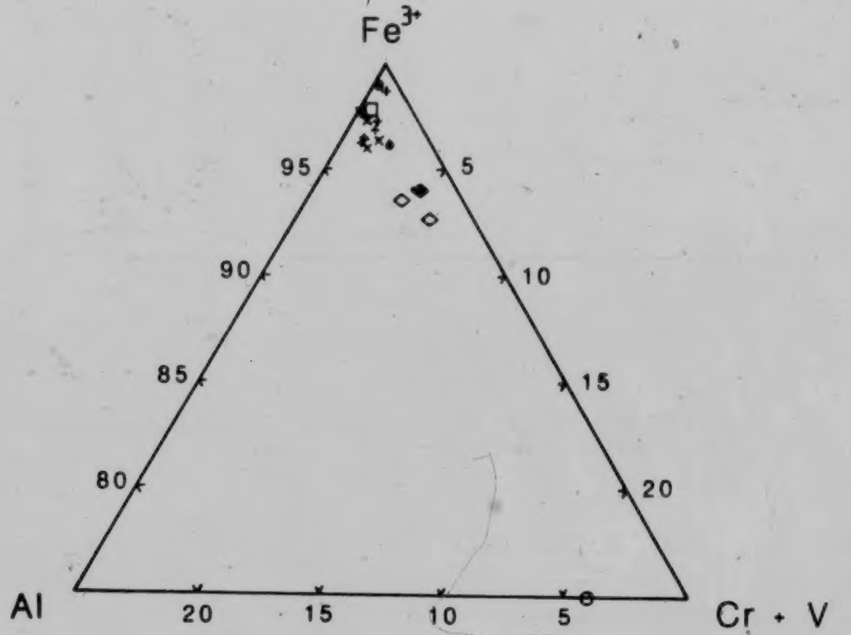

Fig. 2.35. Variation of Fe³⁺, Al and Cr+V (cationic proportions) in magnetites. Symbols as in Fig. 2.32.

up to 10 weight percent MgO, as opposed to the average 2 weight percent MgO for the group 6 hercynites. Group 5 hercynites also have larger amounts of Cr and Zn. Henry (1974) suggests that elements like Fe, Cr and Zn are concentrated in hercynite more readily than in cordierite. An increasing concentration of these elements as the modal ratio of cordierite to hercynites increases, is indicative of a reaction between these two phases:

$$\text{spin(Mg,Fe)} + \text{plag} + H_2O\text{(Fe,Mg)} = \text{cord} + \text{spin(Fe)} + H_2O\text{(Na,Ca)}.$$

The higher relative concentrations of Cr and Zn in the group 5 hercynites is a reflection of the cordierite-forming reaction.

Sphene and Rutile.

Sphene and rutile, which are apparently metasomatic reaction products of ilmenite, are found in a number of samples. Haggerty (1976) reports that "sphenitization" is common in low-grade metamorphic terrains and also in deep-seated intrusives. The development of sphene, in association with ilmenite, is believed to be a product of autometasomatism, by the reaction of residual liquids/fluids with ilmenite. Sphenes formed by this process are usually low in Fe. As much as 2.6 weight percent FeO is observed in the sphenes found in this study. Primary metamorphic sphenes from Deskenatlata Lake have much lower FeO contents, about 0.9 weight percent FeO. A redistribution of the excess iron, from ilmenite, between other iron-bearing phases has not occurred.

Prehnite

The association of prehnite with biotite has been recorded from a number of places in rocks subjected to greenschist facies metamorphism (Phillips and Rickwood, 1975; Moore, 1976; Tulloch, 1979; Kay, 1983). The rock types in which this association is found range from granitic to gabrroic. Most rocks have suffered secondary alteration, with the phases sericite, chlorite, sphene and epidote recorded. Either hornblende or plagioclase, or both, are reported to be always present.

Phillips and Rickwood (1975) and Moore (1976) believe that prehnite formation is a secondary process resulting from deuteric reactions. Biotite only provides suitable nucleation sites for the growth of prehnite, hence the intimate association. Tulloch (1979) and Kay (1983) suggest that prehnite is replacing the host biotite in the metasomatic reaction:

$$\text{plag} + \text{biot} + H_2O = \text{preh} + \text{chl} + \text{ksp} + \text{sph} \pm \text{mus}$$

Arguments against a biotite replacement reaction are strengthened by the lack of other reaction products between prehnite and biotite. Both Tulloch (1979) and Kay (1983) record the presence of these reaction products in the close vicinity of the biotite-prehnite association. However the texture of the prehnite-biotite association, in these two cases, is different from those of examples cited by Phillips and Rickwood (1979) and Moore (1976). In the former case, prehnite is interleaved with undeformed biotite cleavages, in the latter cases, prehnite forms an epitaxial growth with biotite, growing between the biotite cleavage planes. It is possible there is more than one mechanism of prehnite formation.

The mode of association of prehnite with biotite in the rocks of this study suggests formation by deuteric processes. In several cases biotite and prehnite are included in crystals of hornblende. Possibly the presence of a Ca-bearing phase, such as hornblende or plagioclase, is required to provide a source of Ca.

Several prehnites from different lithologies were analysed. Major element variation of Ca, Al and Fe^{3+}, Fig. 2.36, suggests there is a slight compositional difference between the Tsu Lake and Deskenatlata Lake prehnites. The variation is in the $Fe^{3+}/(Fe^{3+}+Al)$ ratio. Deskenatlata Lake prehnites have higher $Fe^{3+}/(Fe^{3+}+Al)$ ratios than the Tsu Lake prehnites. Kuniyoshi and Liou (1976) suggested that this ratio increases with an increase in metamorphic grade. However, Tulloch (1979) and Kay (1983) observe that the $Fe^{3+}/(Fe^{3+}+Al^{3+})$ ratio of prehnite is dependent on the $Fe^{3+}/(Fe^{3+}+Fe^{2+})$ ratio of biotite. No correlation was found between these ratios for the samples of this study. This agrees with the petrographical observations which suggest that prehnite is not replacing biotite. The difference in the $Fe^{3+}/(Fe^{3+}+Al)$ ratio is probably related to the composition of the fluid phase responsible for the formation of prehnite.

Representative analyses of the epidotes and the grandite found with prehnite are shown in Fig. 2.36. All three Ca-Al silicate phases have compositions comparable to those of the same phases reported by Tulloch (1979) and Kay (1983).

Element Partitioning

The discussion of the mineralogy so far has concentrated on the chemical characteristics of each mineral group. Little has been said about the chemical relationships between the phases. The distribution of major and minor elements can give a reasonable indication of the physical conditions of growth. There should be a systematic distribution if equilibrium has been attained.

Of several possible approaches to the presentation of partitioning data, two have been chosen here. The distribution of an element between two phases is dependent on: (i) temperature and pressure of crystallisation, and (ii) availability of the element within the rock, (assuming solubility of the element in the phases concerned). Therefore distribution diagrams for pairs of phases may reveal equilibrium conditions if constant temperatures for the different sampling localities can be assumed. AFM diagrams, on the other hand, portray the relationships between the rock composition and the mineral assemblages and thus examine mineral compatibilities and possible continuous - discontinuous reactions.

Distribution Diagrams

$Fe^{2+}/(Fe^{2+}+Mg)$ Partitioning.

Basic to Intermediate Assemblages

Partitioning of Fe^{2+} and Mg between the major ferromagnesian silicate phases is shown in Figs. 2.37 to 2.42. Good correlations are found between opx-cpx, opx-hbl and cpx-hbl.

The distribution coefficient for the two pyroxene pairs, 1.77, is close to that observed for granulite facies conditions (Davidson, 1968, Kretz, 1981). Only two points depart from the average value of the distribution coefficient, Fig. 2.37; significantly these are samples in which the pyroxenes coexist with biotite rather than with hornblende. Fig. 2.43 shows that variation in $Fe^{2+}/(Fe^{2+}+Mg)$ between individual pairs, is related to the $Fe^{2+}/(Fe^{2+}+Mg)$ ratio of the rock. The consistent value for the distribution coefficient and the whole rock data suggests that equilibrium has been attained for the mineral pair.

The $Fe^{2+}/(Fe^{2+}+Mg)$ partition between opx-hbl and cpx-hbl, Figs. 2.38 and 2.39, show some scatter about the average distribution coefficient. This is due either to

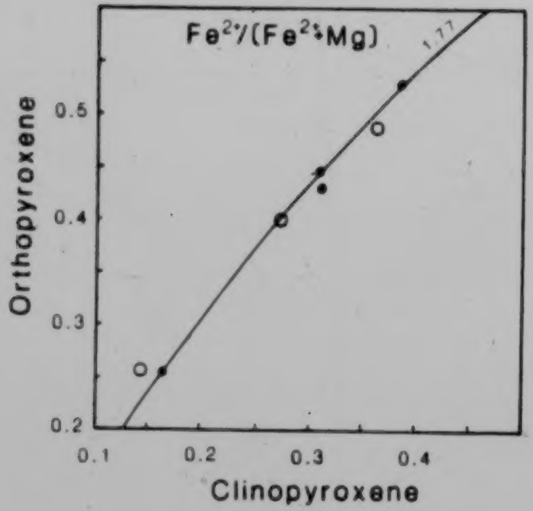

Fig. 2.37. Partitioning of Fe^{2+}/(Fe^{2+}+Mg) between orthopyroxenes and clinopyroxenes. Line represents the average distribution coefficient. Symbols: Tsu Lake, group 1 (open circles), group 2 (closed circles).

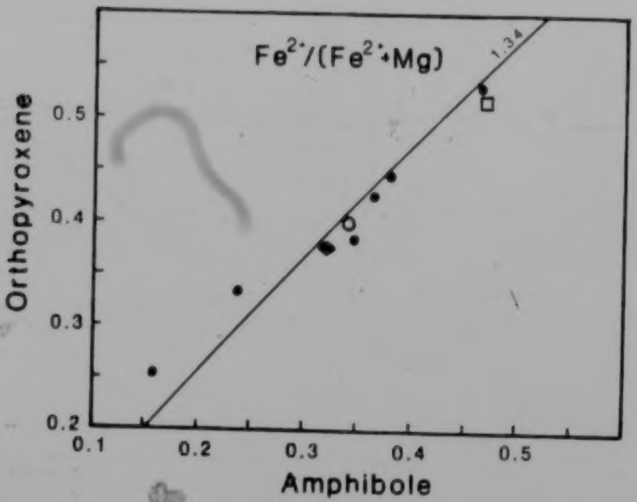

Fig. 2.38. Partitioning of Fe^{2+}/(Fe^{2+}+Mg) between orthopyroxenes and hornblendes. For hornblendes the maximum Fe^{2+} content is given. Line represents the average distribution coefficient. Symbols as in Fig. 2.37.

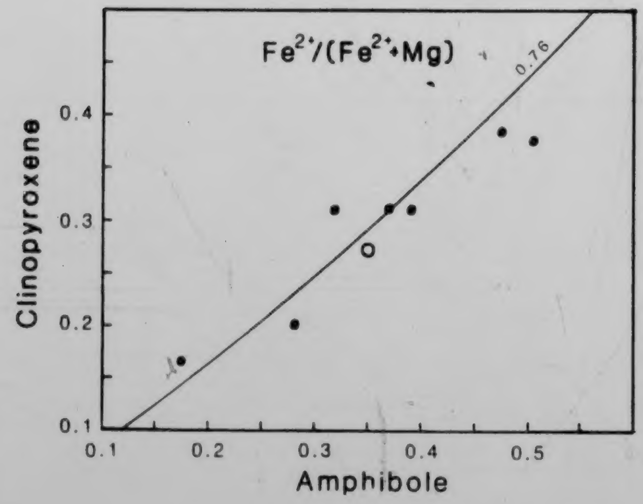

Fig. 2.39. Partitioning of $Fe^{2+}/(Fe^{2+}+Mg)$ between clinopyroxenes and hornblendes. For hornblendes the maximum Fe^{2+} content is given. Line represents the average distribution coefficient. Symbols as in Fig. 2.37.

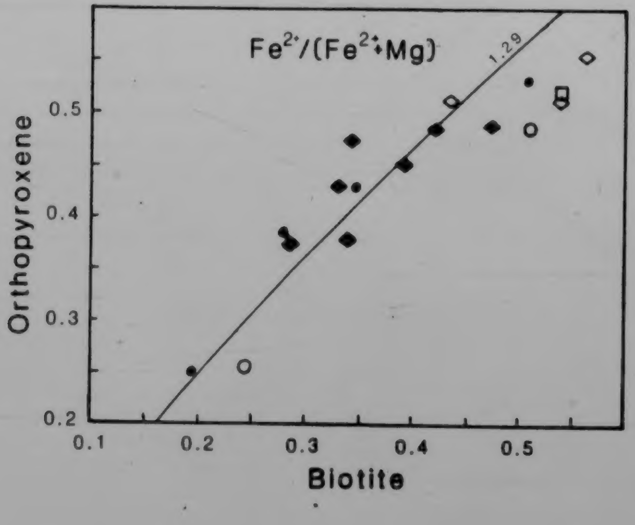

Fig. 2.40. Partitioning of $Fe^{2+}/(Fe^{2+}+Mg)$ between orthopyroxenes and biotites. Line represents the average distribution coefficient. Symbols: Tsu Lake: group 1 (open circles), group 2 (closed circles), group3 (closed diamonds), group 4 (open diamonds).

analytical uncertainty, i.e., unknown ferric iron content, or to disequilibrium. A plot of the partitioning using maximum Fe^{3+} estimates in hornblende (not shown) does not significantly alter the distribution. It is concluded that the slight scatter of the data is due a departure from equilibrium conditions.

The $Fe^{2+}/(Fe^{2+}+Mg)$ partitioning relations between hornblende and pyroxenes, both ortho- and clino-, have been shown to be affected by the hornblende composition; in particular the Al(IV) content (Sen, 1970; Sen, 1973; Kretz and Jen, 1978). Positive correlations between the distribution coefficients and the hornblende Al(IV) content, found for samples in this study, are shown in Fig. 2.44. These trends are in accordance with the observations of Sen (1973).

The hornblende Al(IV) content exerts a stronger control over the clinopyroxene $Fe^{2+}/(Fe^{2+}+Mg)$ ratio than that of orthopyroxene, although both are affected. An important consequence of this is a restriction in the range of values of the distribution coefficient for the opx-cpx exchange. This is observed for granulite facies pyroxenes where a distribution coefficient of 1.8 is consistently noted (Kretz, 1981). The departure of the two points from the opx-cpx distribution curve, noted earlier, is probably a function of the lack of horblende in these samples.

Kretz and Jen (1978) note that the average distribution coefficient for cpx-hbl in rocks transitional between amphibolite and granulite facies is approximately 0.63, whereas in granulite facies rocks it is much higher, about 0.77. An average distribution coefficient of 0.77 was observed for the Tsu Lake cpx-hbl pairs suggesting metamorphic conditions were above the amphibolite - granulite facies boundary.

Partitioning relations of $Fe^{2+}/(Fe^{2+}+Mg)$ between orthopyroxene, clinopyroxene and biotite are more complex. For clinopyroxene the data is scattered about the average distribution coefficient, Fig. 2.41, although this is based on a limited number of samples. The opx-biot distributions show considerable scatter, Fig. 2.40. However, biotite occurs predominantly in two modes in the pyroxene-bearing rocks: (i) in group 1 and 2 associated with hornblende and occasionally in contact with the pyroxenes; (ii) in group 3 samples in association with orthopyroxene. Compared with the group 1 and 2 samples orthopyroxenes and biotites from group 3 samples show very restricted ranges of $Fe^{2+}/(Fe^{2+}+Mg)$ ratios. For orthopyroxenes this varies from 0.4 to 0.5 and for biotite,

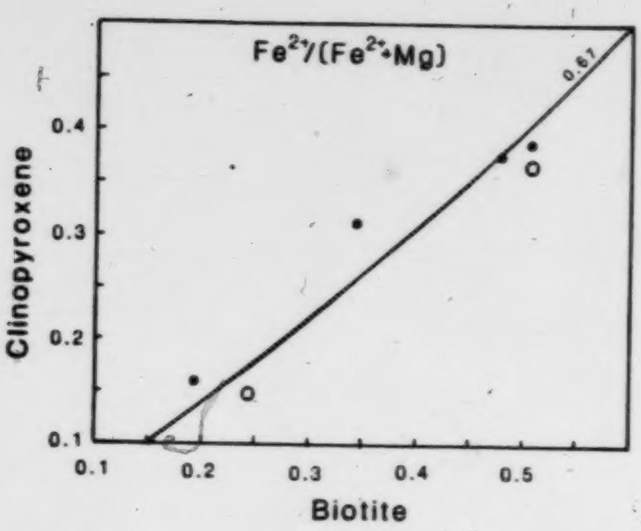

Fig. 2.41. Partitioning of $Fe^{2+}/(Fe^{2+}+Mg)$ between clinopyroxenes and biotites. Line represents the average distribution coefficient. Symbols as in Fig. 2.40.

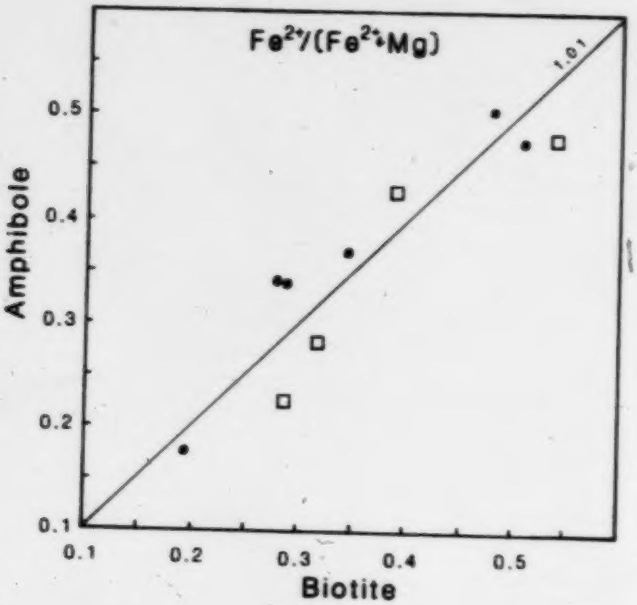

Fig. 2.42. Partitioning of $Fe^{2+}/(Fe^{2+}+Mg)$ between hornblendes and biotites. For hornblendes the maximum Fe^{2+} content is given. Line represents the average distribution coefficient. Symbols: Tsu Lake; group 2 (closed circles), group 3 (closed diamonds), group 4 (open diamonds); Deskenatlata Lake (open squares).

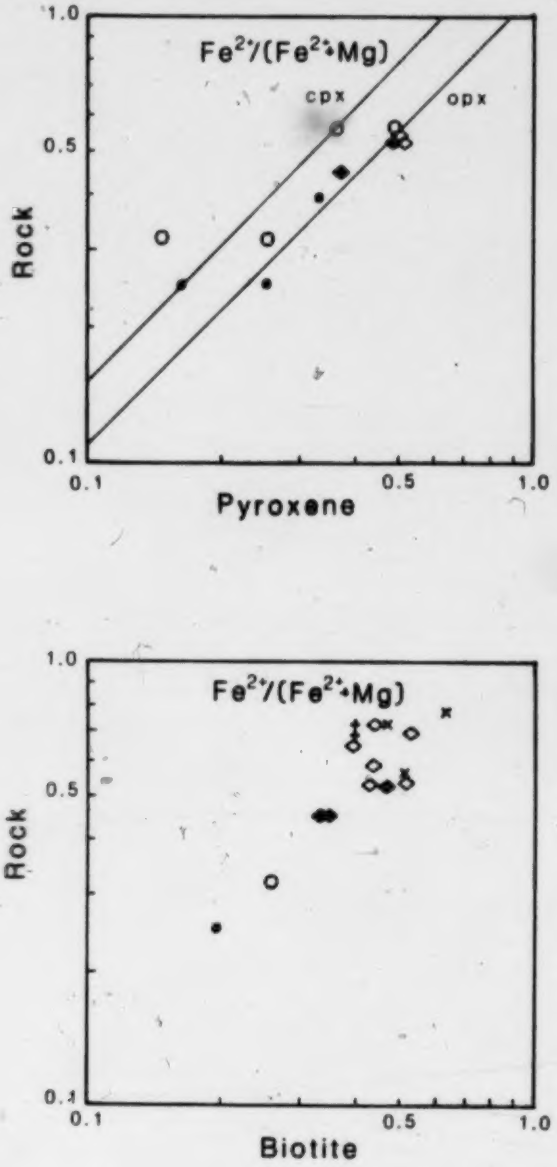

Fig. 2.43. Partitioning of $Fe^{2+}/(Fe^{2+}+Mg)$ between the rock and (a) pyroxenes, (b) biotite. Symbols as in Fig. 2.40.

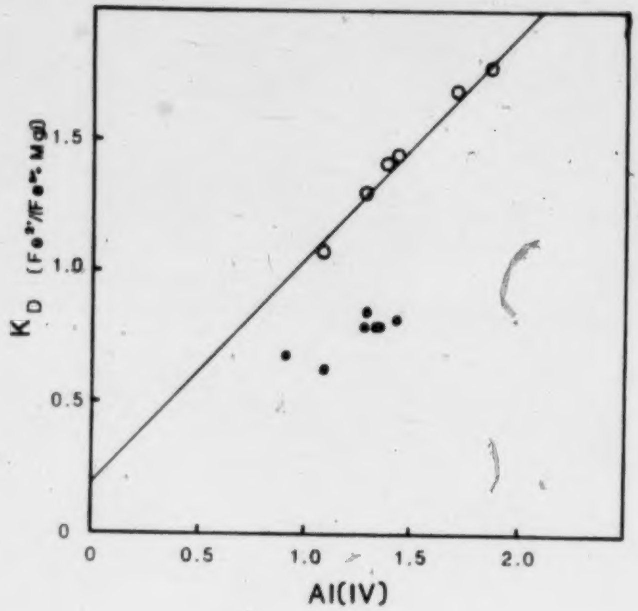

Fig. 2.44. Relationship between the distribution coefficient for the partitioning of $Fe^{2+}/(Fe^{2+}+Mg)$ between orthopyroxene, clinopyroxene and hornblende and the Al(IV) (cationic proportion) of hornblende. Symbols: opx-hbl (open circles), cpx-hbl (closed circles).

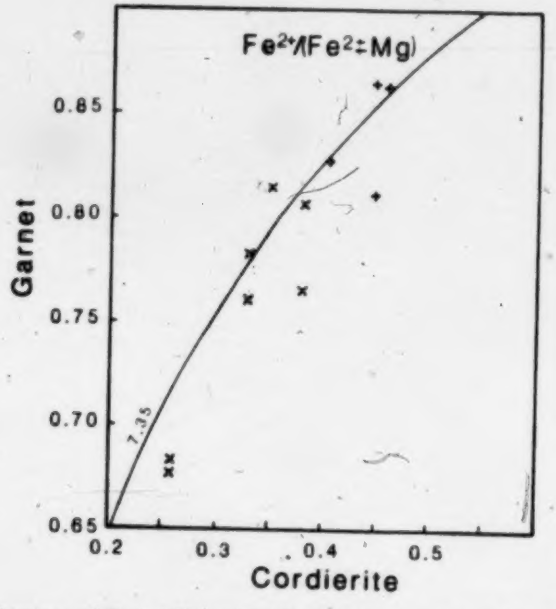

Fig. 2.45. Partitioning of $Fe^{2+}/(Fe^{2+}+Mg)$ between garnet and cordierite. Core and rim compositions of garnet are shown where available, otherwise values for garnet represent the rim compositions. Symbols: Tsu Lake: group 4 (open diamonds), group 5 (diagonal crosses), group 6 (vertical crosses).

from 0.3 to 0.45.

It appears that the group 3 opx-biot equilibrium has been affected by a variation in intensive variables, perhaps a change in fluid composition or oxygen fugacity, that has not affected other lithologies. A knowledge of the ferric iron content of biotite could perhaps be useful in assessing which of these factors is the most probable. These conclusions imply that the group 3 lithologies are closed systems with respect to H_2O and/or oxygen acitivity.

Data for the hbl-biot $Fe^{2+}/(Fe^{2+}+Mg)$ exchange show a similar type of pattern to the cpx-biot exchange, in terms of deviation from the average distribution coefficient, Fig. 2.42. This suggests that the relations observed for group 1 and 2 orthopyroxene, clinopyroxene and biotite exchanges are reasonable.

Pelitic Assemblages

The $Fe^{2+}/(Fe^{2+}+Mg)$ relationships between garnet, cordierite and biotite are shown in Figs. 2.45 to 2.47. Since garnet is appreciably zoned in Fe and Mg the extent of these variations has been depicted. A regular distribution between garnet rims (highest $Fe^{2+}/(Fe^{2+}+Mg)$ ratio) and corderite is observed, Fig. 2.45. Equilibrium does not appear to have been maintained between garnet cores and cordierite.

The distribution between garnet and biotite, for both rim and core compositions, suggests a lack of equilibrium, Fig. 2.46. A few of the samples display a pattern that can be described by a regular distribution model, but the majority of the samples depart from this pattern. There is no correlation between lithologic type and deviation from the distribution curve. Some scatter could be expected for this mineral pair, due to an overestimation of the $Fe^{2+}/(Fe^{2+}+Mg)$ ratio of biotite as a result of the unknown ferric iron content. It is doubtful, though, that this would account for the observed distribution.

The garnet-biotite Fe-Mg exchange is said to be affected by the composition of biotite and of garnet, i.e., other components present in these two phases (Dahl, 1969). The Ti content of biotite is reported to have the most serious effect. As the biotites in these samples are rich in Ti, the relationship between the distribution coefficient and the mole fraction of Ti and Al(VI) in biotite was examined but no correlation was found (not shown).

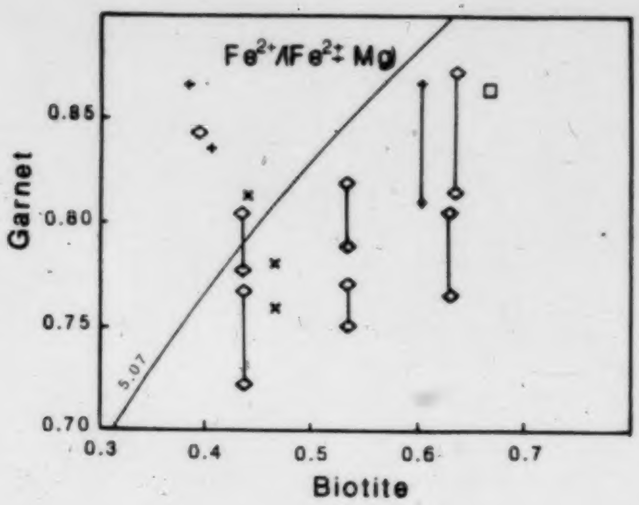

Fig. 2.46. Partitioning of Fe^{2+}/(Fe^{2+}+Mg) between garnet and biotite. Core and rim compositions of garnet where available. Symbols as in Fig. 2.45.

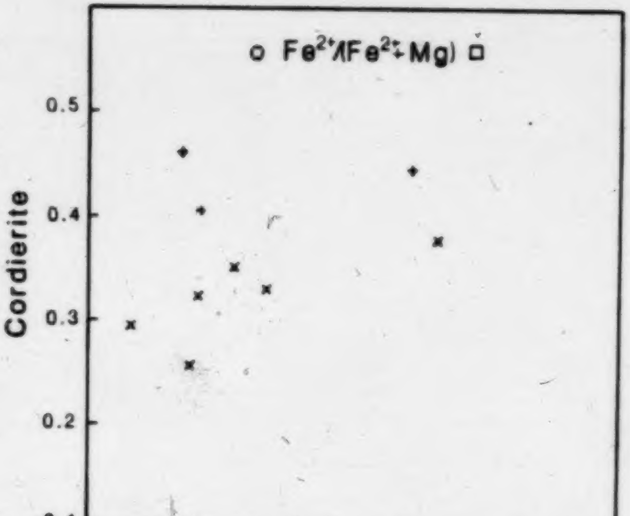

Fig. 2.47. Partitioning of Fe^{2+}/(Fe^{2+}+Mg) between cordierite and biotite. Line drawn represents the average distribution coefficient. Symbols as in Fig. 2.45.

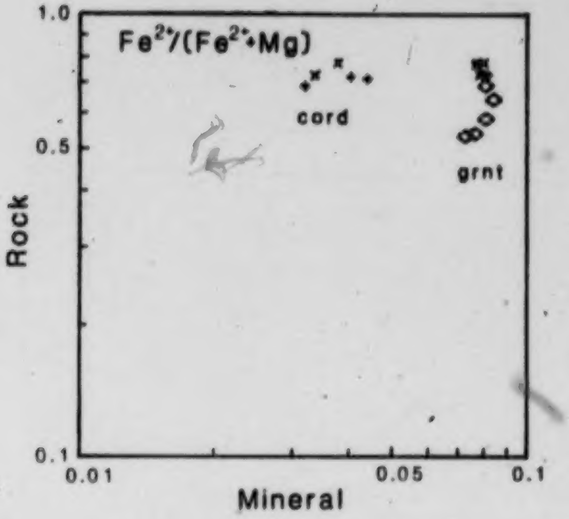

Fig. 2.48. Partitioning of $Fe^{2+}/(Fe^{2+}+Mg)$ between the rock and (a) garnet and cordierite (compositional fields labelled) Symbols as in Fig. 2.45.

The cord-biot $Fe^{2+}/(Fe^{2+}+Mg)$ partition also shows considerable scatter, Fig. 2.47. As cordierite has similar partitioning properties to biotite, for $Fe^{2+}/(Fe^{2+}+Mg)$, there should almost be a 1:1 relationship. The data for both the garnet- and cordierite-biotite pairs suggests that biotite is not in equilibrium with either of these phases.

Fig. 2.48 illustrates the partitioning of Fe and Mg between the rock and garnet, cordierite and biotite respectively. Garnet and cordierite $Fe^{2+}/(Fe^{2+}+Mg)$ ratios for groups 5 and 6 are independent of the rock's $Fe^{2+}/(Fe^{2+}+Mg)$ ratio, although this observation is based on only a few data points. Group 3 garnet $Fe^{2+}/(Fe^{2+}+Mg)$ ratios reflect those of the rock.

The $Fe^{2+}/(Fe^{2+}+Mg)$ ratio of biotite shows a dependence on the rock's $Fe^{2+}/(Fe^{2+}+Mg)$ ratio for most of the lithologic types. Like cordierite and garnet, biotites of group 5 and 6 show a $Fe^{2+}/(Fe^{2+}+Mg)$ ratio which is independent of that of the rock.

The reason for the divergence of group 5 and 6 minerals from the trends shown by minerals from other groups may be related to the mode of formation of the mineral assemblages in these rocks. It is believed that group 5 and 6 samples have experienced partial melting and the assemblages quoted are the restite portions of the rock. The felsic portion, or liquid fraction, has not been removed from the system. These conclusions are based mainly on field observations. As the whole rock compositional data represents the total rock, both the restite and felsic portions, it is conceivable that the $Fe^{2+}/(Fe^{2+}+Mg)$ ratio for the restite portion could be significantly different from that of the whole rock. It was not possible to separate these two fractions for individual analysis.

Overall the partitioning data for Fe and Mg may be summarised, in terms of decreasing order of preference for Fe, as follows:

grnt > opx > hbl > biot > cpx > cord.

These data have implications for the composition of the metamorphic fluid. Eugster and Ilton (1983) compiled data on solid-solid and solid-fluid Fe-Mg partitioning and derived the following order of preference for Fe, for phases in equilibrium with a chloride rich aqueous solution at 600°C:

grnt > opx > hbl > cpx > biot > cord.

The only significant difference between Eugster and Ilton's (1983) data and that observed for this study is the partitioning behaviour of biotite, clinopyroxene and hornblende. The Tsu Lake minerals were probably in equilibrium with the metamorphic fluid at about 700 - 750 °C, (see discussion in the next chapter), approximately 100 °C higher than that for Eugster and Ilton's data. This implies that the preference for Fe over Mg increases in biotite, and decreases in hornblende and clinopyroxene, with increasing temperature. As the data of Kretz and Jen (1978) suggest, the distribution coefficient for cpx/hbl decreases in the temperature range of formation of samples in this study. Therefore the rate of change for hornblende is greater than it is for clinopyroxene. Eugster and Ilton (1983) conclude that the Mg preference over Fe by the solid phases increases with increasing temperature. This is observed here, with the exception of biotite.

Mn Partitioning.

The data for Mn partitioning is presented here rather simply in Figs. 2.49 to 2.53. Rather than express the concentration of Mn as a mole fraction, the data is plotted using the cationic proportion of Mn in each phase. It does not appear to have altered the relationships substantially.

Basic Assemblages

In the basic and intermediate assemblages Mn shows equilibrium partitioning. The distributions between opx-cpx, opx-hbl and cpx-hbl, Figs. 2.49 to 2.50, are regular enough to suggest maintenance of equilibrium conditions. For the opx-ilm Mn exchange two regular but diverging trends are seen, Fig. 2.51. The reason for this is not apparent. Mn partition between cpx-ilm does not show a linear trend, Fig.2.51. Because ilmenite is associated with orthopyroxene rather than with clinopyroxene, the partitioning relations suggest that the association of cpx-ilm is incompatible. In samples where orthopyroxene is absent, ilmenite is found with hornblende rather than with clinopyroxene.

Pelitic Assemblages

Mn is distributed regularily between the grnt-cord, grnt-ilm and cord-ilm pairs, Figs. 2.52 to 2.53. There is, however, a certain amount of scatter for all three pairs. Part of the scatter may be attributed to the nature of the ilmenite. In many samples, particularily in groups 5 and 6, it was difficult to ascertain whether the ilmenite was a primary metamorphic phase or a secondary product resulting from oxidation-exsolution of

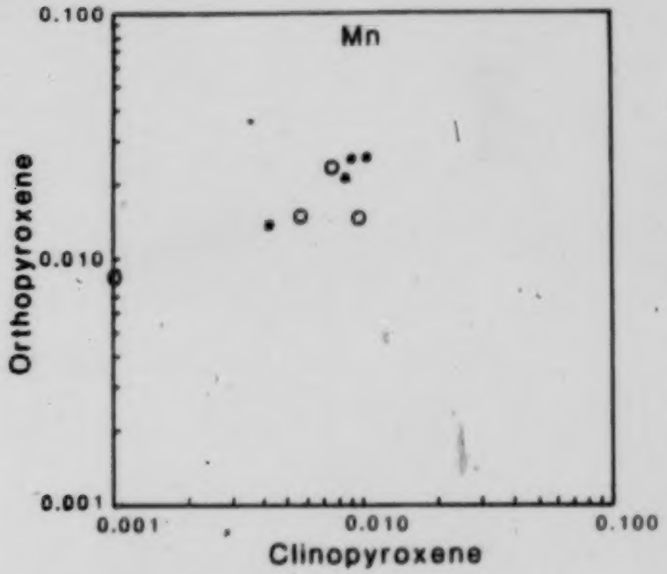

Fig. 2.49. Partitioning of Mn between orthopyroexenes and clinopyroxenes. Symbols as in Fig. 2.37.

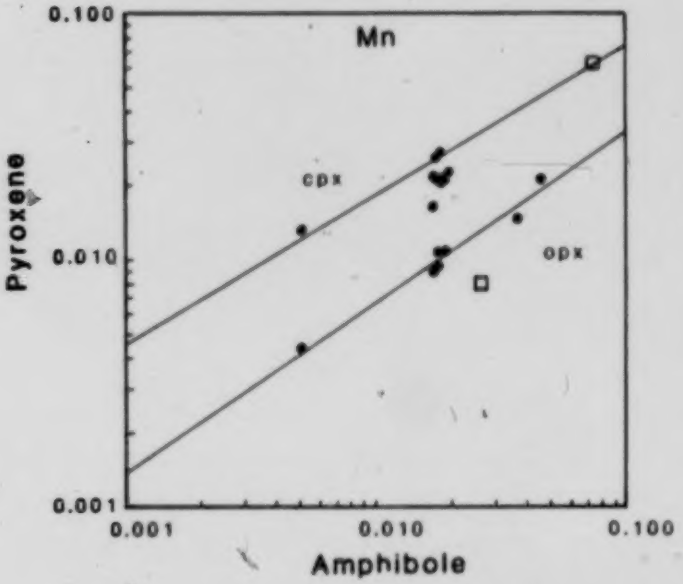

Fig. 2.50. Partitioning of Mn between pyroxenes and hornblendes. Compositional fields of orthopyroxene and clinopyroxene are indicated. Symbols as in Fig. 2.37.

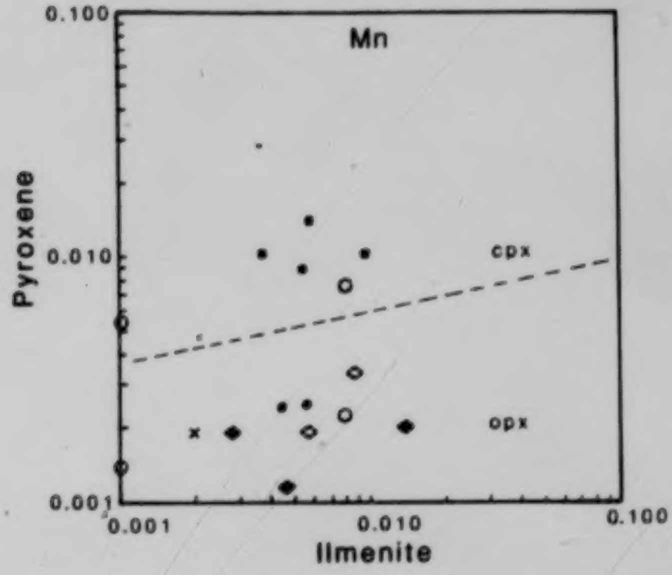

Fig. 2.51. Partitioning of Mn between pyroxenes and ilmenites. Compositional fields of orthopyroxene and clinopyroxenes are indicated. Symbols as in Fig. 2.37.

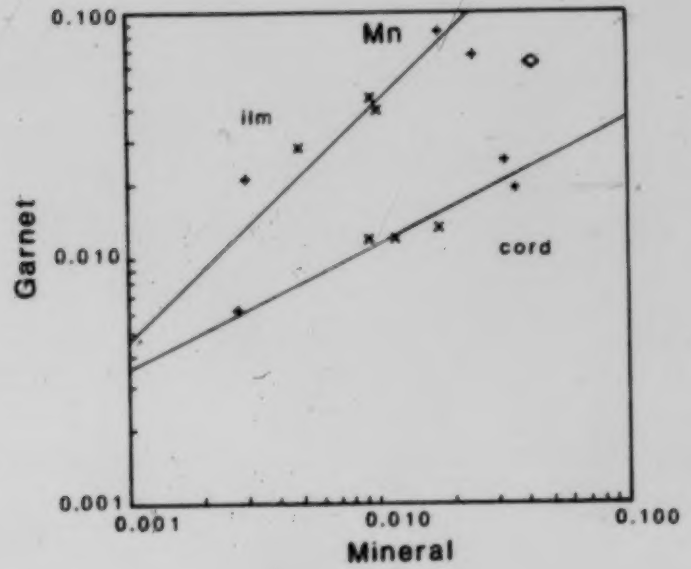

Fig. 2.52. Partitioning of Mn between garnets and ilmenites and cordierites. Compositional fields of ilmenite and cordierite are indicated. Symbols as in Fig. 2.45.

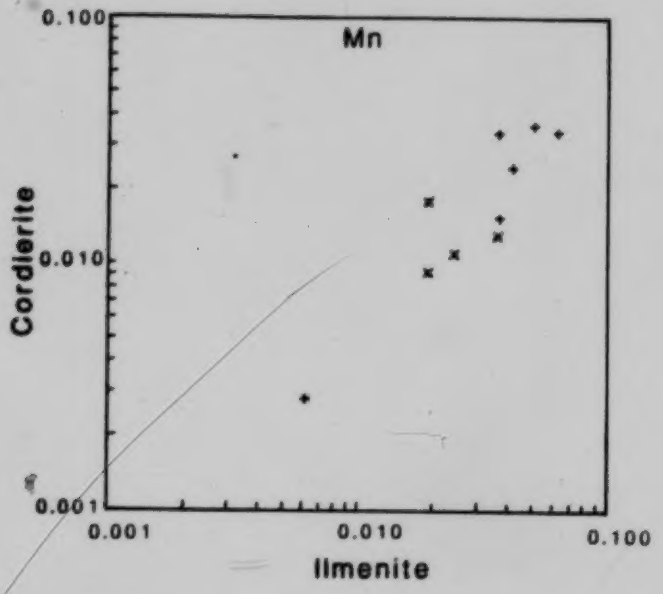

Fig. 2.53. Partitioning of Mn between cordierites and ilmenites. symbols as in Fig. 2.45.

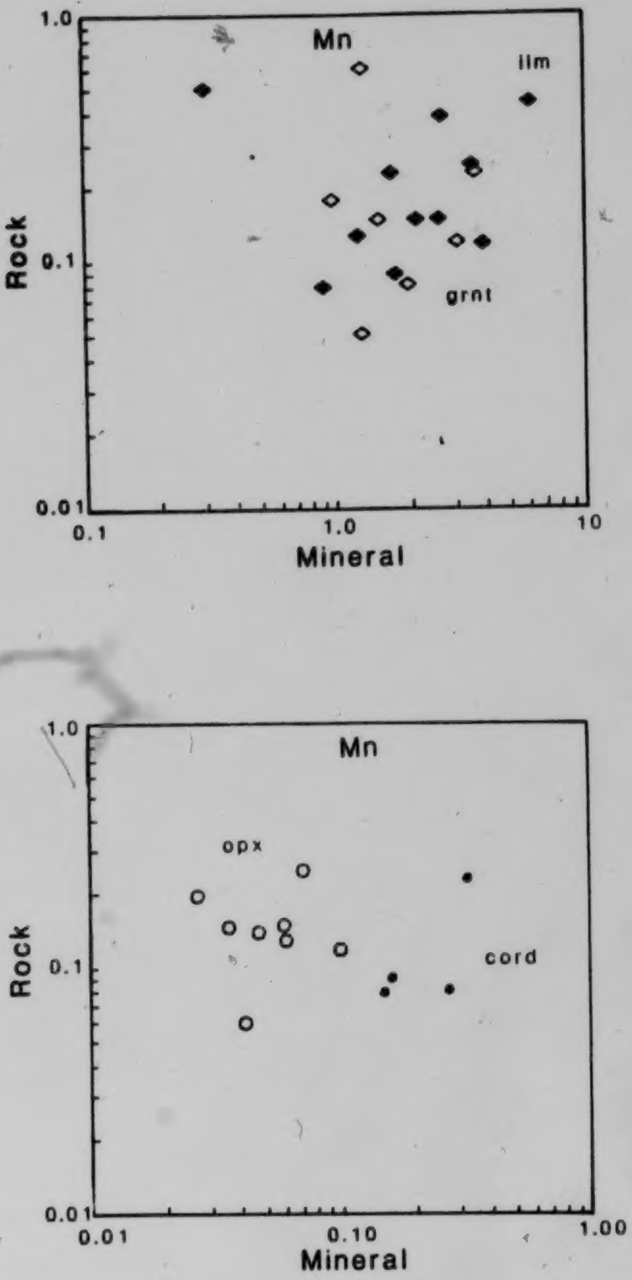

Fig. 2.54. Partitioning of Mn between the rock and (a) garnet, ilmenite and (b) orthopyroxene, cordierite. Compositional fields of each mineral are indicated. Symbols: garnet - open diamonds, ilmenite - closed diamonds, orthopyroxene - open circles, cordierite - closed circles.

magnetite. Obvious "exsolved" ilmenite has been excluded from the element partitioning diagrams. As Mn is a minor component, part of the scatter may also be attributed to analytical errors associated with the determination of this element.

Except for a few samples, Mn is excluded from biotite and magnetite, or at least is below the detection limit of the analytical method used. Stephenson (1977) noted that the Mn content of both hornblende and biotite decreases with increasing temperatures. At granulite facies grades this is due to the occurrence of pyroxenes, and the preferential partitioning of Mn into these phases. The absence Mn from biotite, suggests the metamorphic conditions at Tsu Lake were considerably higher than those experienced by the rocks studied by Stephenson (1977). It is not unusual that Mn is absent or in very low concentrations in biotites of granulite facies grade, as the biotite analyses reported by Dymek (1983) show. The absence of Mn in magnetite indicates the preferential substitution of Mn into ilmenite relative to magnetite at these temperatures.

The distributions of Mn between the rock and the minerals for basic, intermediate and pelitic assemblages display little correlation, Fig. 2.54. Cordierite is the only phase in which the Mn content correlates with that of the rock. Garnet and orthopyroxene appear to show a negative correlation. For ilmenite the data is scattered.

The order of preference for Mn in the minerals may be described as follows:

grnt > ilm > cord > opx > hbl > cpx > biot.

Ti Partitioning.

A few minerals show appreciable concentrations of Ti; ilmenite, biotite, hornblende, clinopyroxene and magnetite. Ti is absent, or in very low concentrations in orthopyroxene and garnet. Of the three phases where Ti is a minor component, only the hbl-biot Ti exchange shows a positive correlation, Figs. 2.55 to 2.56. Biotite has a much stronger affinity for Ti than does hornblende. The data for the mag-biot Ti exchange shows extreme scatter, possibly a reflection of the nature of magnetite. Some magnetites have exsolved ilmenite, thus altering their primary metamorphic composition.

The partitioning of Ti between the rock and each of the phases, would reveal little about the partitioning relations. Because Ti is partitioned strongly into a phase of its own, ilmenite, rather than being dispersed over several phases, the partitioning of Ti between

7

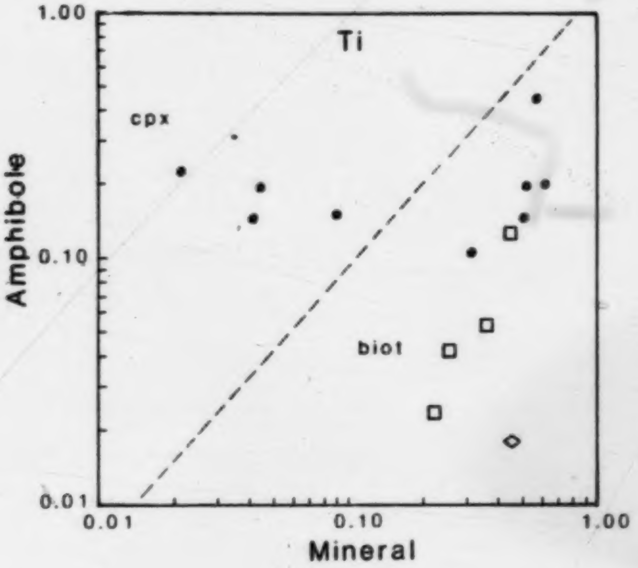

Fig. 2.55. Partitioning of Ti between hornblendes and biotites and clinopyroxenes. Compositional fields of biotite and clinopyroxene are indicated. Symbols as in Fig. 2.37.

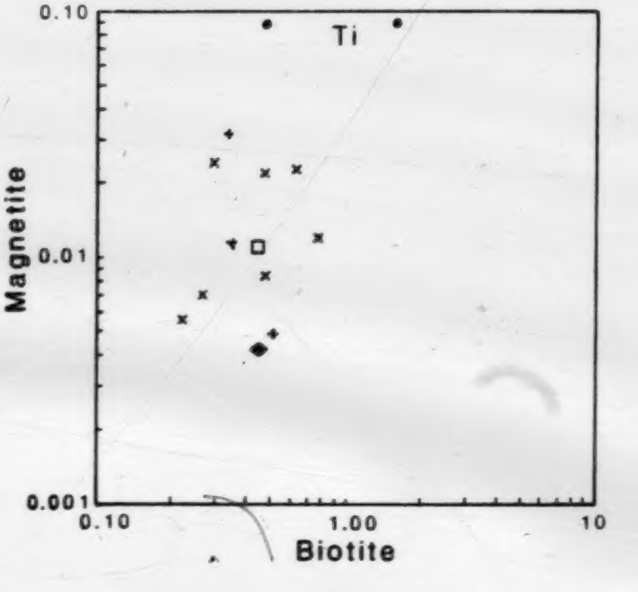

Fig. 2.56. Partitioning of Ti between magnetites and biotites. Symbols as in Fig. 2.37.

the rock and other phases reflects only the modal percentage of ilmenite in the rock.

AFM Diagrams

The means by which the composition of a rock system can be portrayed graphically in relation to its mineral phases, are rather limited. The multicomponent system must be reduced to 3 or 4 components, in order to view the system in simple terms, i.e., as a triangular or tetrahedral diagram. If a component has a fixed chemical potential then it may be omitted from any graphical representations, as it does not affect the relations between the phases being represented. Examples of components with fixed chemical potentials are SiO_2, in quartz, $Fe_2O_3.FeO$, in magnetite, and $FeO.TiO_2$, in ilmenite. Any phase which has a constant composition is said to have a fixed chemical potential.

For a pelitic system which is represented by 10 major components (SiO_2, Al_2O_3, TiO_2, Fe_2O_3, FeO, MgO, CaO, Na_2O, K_2O and H_2O), the number of components may be reduced if quartz, K-feldspar, magnetite and ilmenite are always present (Thompson, 1957). Hence the system is expressed in terms of three components by projecting through the components SiO_2, $Fe_2O_3.FeO$, $FeO.TiO_2$ and K_2O. Thus the three components are:

$A = Al_2O_3 - K_2O$

$F = FeO - (Fe_2O_3 + TiO_2)$

$M = MgO$

Temperature; pressure and uH_2O are assumed constant for all rocks represented.

Other projections can be constructed for rocks of non-pelitic composition. Reinhardt (1968, 1969) used a projection through plagioclase of a constant composition, to display the rock and mineral relationships in felsic granulites. The components in such a system are:

$A = Al_2O_3 - (Na_2O + CaO + K_2O)$

$F = FeO - (Fe_2O_3 + TiO_2)$

$M = MgO$

where quartz, K-feldspar, magnetite, ilmenite and plagioclase are always present. For rocks devoid of K-feldspar the components become:

$A = Al_2O_3 - (Na_2O + CaO)$

$F = FeO - (Fe_2O_3 + TiO_2)$

$M = MgO$

(Froese, 1978).

The Tsu Lake assemblages have been projected onto AFM diagrams, Figs. 2.57 to 2.58. The plagioclase projection has been used for the basic rocks, while the K-feldspar and plagioclase projections have been used for the pelitic and quartzo-feldspathic compositions. The plagioclases which are represented, are not of a constant composition. Naturally this affects the relationships between the minerals and between the minerals and rock compositions. The implications of this will be discussed later.

Basic Assemblages.

Most of the rocks from groups 1 and 2 can be represented in Fig. 2.57 which shows the three phase triangle of orthopyroxene, clinopyroxene and hornblende. Only two samples from group 1, 186A and 200A, cannot be represented as biotite is the phase which coexists with the pyroxenes, rather than hornblende.

The most noticeable feature of Fig. 2.57 is the shift of the three phase triangles and the two phase lines along the F-M axis, at constant A. Because of limited whole rock compositional data, it is difficult to assess if this feature is due to small variations in components not considered by the AFM projection.

The rock compositional data available plot outside the boundary of the three phase triangles or two phase lines. However, the displacement of the rock compositions relative the phase boundaries appears to be systematic, suggesting that a factor common to all assemblages is responsible for the shift. This would tend to rule out variations in components not represented by the AFM projection.

Other alternative explanations for the shift in compositions can be sought in the following areas: (i) non-equilibrium assemblages, (ii) differing pressure - temperature conditions and (iii) compositional differences in the fluid phase and/or oxygen fugacities in equilibrium with each assemblage. Data from the distribution diagrams suggest, at least for these assemblages, that equilibrium has been attained. If the pressure - temperature conditions are assumed to be constant over the areas from which the samples were collected, then the differences in the mineral compositions are likely to be the result of differences in the fluid composition or oxygen fugacity. Grew (1981) and Reinhardt (1968) have explained similar shifts in the compositions of pelitic assemblages as resulting

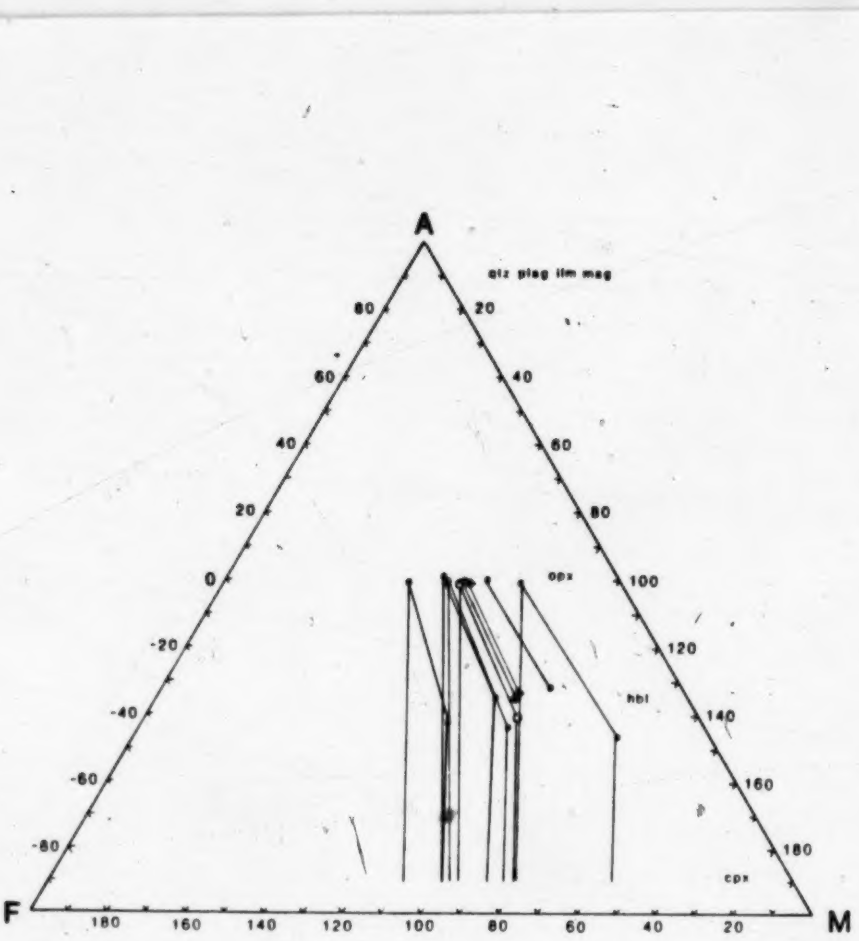

Fig. 2.57. AFM diagram of the group 1 to 3 basic samples of Tsu Lake. Tie lines join coexisting phases. Symbols: group 1 - open circles, group 2 - closed circles, group 3 - closed diamonds.

from changes in uH_2O, and fO_2, respectively. Similarly Rumble (1978) has documented changes in uH_2O in different rock layers from a single outcrop. This would tend to imply that each of the basic rock units has retained its original premetamorphic composition and there was no external control on the composition of the fluid phase.

The hornblende compositions of the three phase assemblages, hbl-cpx-opx, show variations in the A component. The two phase lines, hbl-opx or hbl-cpx, show a relatively constant A component. The best explanation of this variation lies in the differences in the plagioclase compositions seen amongst the samples of the hbl-cpx-opx assemblages.

Basic to Intermediate Assemblages.

The assemblages containing opx-cpx-biot, or opx-biot cannot be adequately represented by an AFM projection. Almost all of these assemblages contain plagioclase or antiperthite but no K-feldspar. Unfortunately the plagioclase AFM projection cannot represent the biotite compositions as K_2O, an important component of biotite, is ignored in the projection.

Pelitic Assemblages.

The stable assemblage of the group 6 lithologies is assumed to be garnet-sillimanite-cordierite. Biotite, on the basis of conclusions drawn from the distribution diagrams and textural observations, is a retrograde product, or least has been substantially affected by later metamorphic events. The pelitic assemblages are believed to be the result of the partial melting of pelitic sediments. If this is the case then the assemblages projected onto the AFM diagram should not show any variation in compositions as the restite assemblages have all been in equilibrium with a minimum melt of the same composition. Fig. 2.58 shows this conclusion appears to be correct. Certainly there is not the compositional variation shown by the basic assemblages. Grew (1981) reports grnt-biot-sill assemblages, that are not the result of partial melting, and these show noticeable variations in composition. Most of the group 5 lithologies cannot be represented on an AFM diagram because K-feldspar and plagioclase are missing.

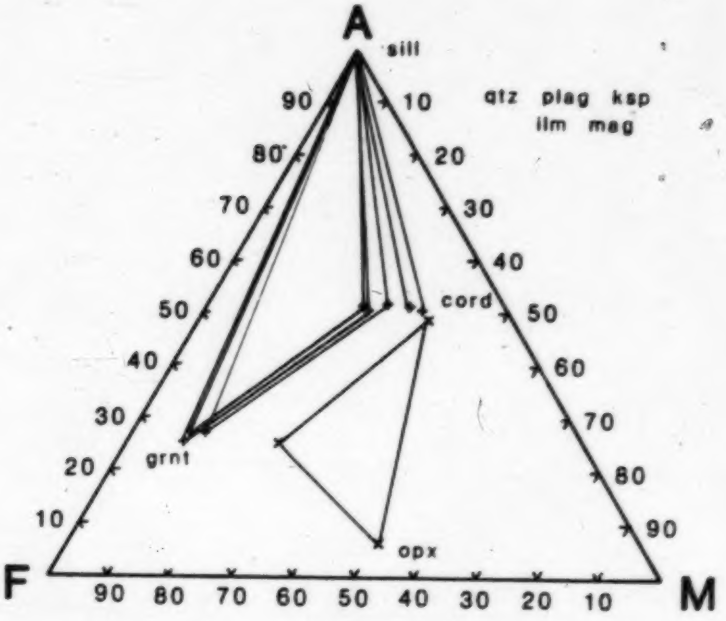

Fig. 2.58. AFM diagram of the group 5 and 6 pelitic samples of Tsu Lake. Tie lines join coexisting phases. Symbols: group 5 - diagonal crosses, group 6 - vertical crosses.

Mineral-Forming Reactions

Pelitic Assemblages

From the earlier discussions on petrography, mineralogy and partitioning data it was concluded that the pelitic lithologies had undergone partial melting. Studies on pelitic systems suggest that the pressure-temperature regime for extensive melting occurs at about 650 - 700 °C and 4 - 6 kb, the pressure-temperature conditions which the Tsu Lake granulites have apparently experienced.

For the CaO + K_2O + $NaAlO_2$ + Al_2O_3 + SiO_2 + H_2O (CKNASH) system partial melting occurs in the region of overlap between the dehydration and melting curves (Thompson and Tracy, 1979). The dehydration reactions are:

mus + alb(Or-Ab) + qtz = sill + ksp(Or-Ab) + H_2O

mus + anr(Or-An) + qtz = sill + kfs(Or-An) + H_2O

The minimum melting curves are:

mus + alb + ksp + qtz + H_2O = liq

mus + or + qtz + H_2O = liq

Beyond the intersection of these two sets of curves it is possible to have the H_2O-conserving melt reactions:

mus + alb + qtz = ksp + sill + liq

mus + qtz = or + sill + liq

Melting occurring via the reactions above is known as dehydration-melting (Thompson and Tracy, 1979). The release of H_2O from the dehydration of muscovite induces melting. Separation of the felsic melt from the restite portion is usually inhibited by the melt's high viscosity.

The dehydration-melting reactions in the CKNASH system are modified by the presence of other components. The assemblage, mus + feld + qtz, will melt at lower temperatures in the presence of a ferromagnesian phase (Thompson, 1982). The melting sequence in the K_2O + FeO + MgO + Al_2O_3 + SiO_2 + H_2O (KFMASH) system, when ferromagnesians other than biotite are present, is determined by the concentrations of FeO and MgO relative to Al_2O_3. Mg-rich and Fe-rich pelites will undergo partial melting before pelites of intermediate Fe-Mg compositions. The H_2O-conserving melt reactions:

biot + sill + qtz = cord + grnt + ksp + liq

Fe-grnt + sill + qtz = Fe-cord + liq
biot + sill + qtz = cord + ksp + liq
biot + cord + qtz = ksp + grnt + liq
biot + sill + qtz = grnt + ksp + liq

control the evolution of most pelitic migmatites (Thompson, 1982).

The group 5 Tsu Lake assemblages of grnt + cord + hc ±plag, qtz, are spatially associated in the field with rocks bearing the assemblage grnt + biot + plag + qtz. Although sillimanite is no longer present, the reaction:

biot + sill + qtz = cord + ksp + liq

is suggested by these two assemblages. The assemblage for sample 182A, grnt + cord + biot + opx + ksp + plag, may have been generated by the reaction:

biot + grnt + qtz + plag + H_2O = cord + opx + ksp + liq

This reaction is believed to record the highest grade of metamorphism attained at Tsu Lake.

The presence of hercynite in close association with cordierite in the group 5 lithologies suggests the reaction:

qtz + sp = cord (Bucher-Nurminen and Droop, 1983)

or

sp(Mg,Fe) + plag + H_2O(Fe,Mg) = cord + sp(Fe) + H_2O(Na,Ca) (Henry, 1974).

From the textural relations, the second reaction is the most probable one.

The assemblages of the group 6 lithologies can be divided into main types:

i. grnt + cord ± biot
ii. sill + cord + biot + hc

Sillimanite, however, is sometimes found in association with garnet, but usually separated from it by hercynite. The association of grnt - sill - hc and sill - cord - hc in the same rock implies that the temperature was above the reactions:

staur = cord + hc + sill
staur = alm + hc + sill.

The two reactions are separated in P-T space by an invariant point in the system FeO - Al_2O_3 - SiO_2 - H_2O (Schreyer, 1976)

The presence of a melting reaction is more evident in the group 6 lithologies than the group 5 lithologies, as the felsic melt fractions are closely associated with the restite portions. The reaction described earlier for the group 5 lithologies may not have gone to completion. A more reasonable explanation is that the group 6 lithologies are of a more intermediate composition than the group 5 lithologies; hence they should begin to melt at a later stage than the group 5 pelites. The reaction:

biot + sill + qtz = cord + grnt + ksp + liq

is a discontinuous one and heralds the beginning of melting in the intermediate Fe-Mg pelites.

The role of biotite in the mineral-forming reactions for the Tsu Lake pelites is uncertain. In the reactions cited above biotite occurs as a primary phase. If the reactions have gone to completion then the presence of biotite implies a retrograde reaction.

Basic to Intermediate Assemblages

A number of reactions have been proposed to account for the observed assemblages in the hornblende-bearing granulites. De Waard (1965) suggested the following bivariant reactions:

i. hbl + grnt + qtz = opx + plag + H_2O
ii. opx + plag = cpx + grnt + qtz
iii. hbl + qtz = opx + cpx + plag + H_2O
iv. hbl + plag + qtz = cpx + grnt + H_2O
v. hbl + opx + plag = cpx + grnt + H_2O

The intersection of the bivariant reactions corresponds to the invariant reaction:

vi

hbl + grnt + plag + qtz = opx + cpx + H_2O (Carmichael, 1974; Jen and Kretz, 1981).

Reactions (ii) and (v) mark the boundary between the hornblende and pyroxene granulite facies, while reaction (iii) marks the boundary between the amphibolite and granulite facies.

The absence of garnet in any of the hornblende-bearing basic assemblages from Tsu Lake precludes the existence of reactions (i), (ii), (iv), and (v). The assemblage of reaction (iii), however, is very common. This implies that the Tsu Lake area has experienced metamorphic conditions just above the amphibolite-granulite facies boundary but below the pyroxene-granulite facies boundary.

The most realistic format of reaction (iii), proposed by Sen (1970) and Sen and Ray (1971), are:

$$Na_{0.5}Ca_2(Mg,Fe^{2+})_4Al_{2.5}Si_{6.5}O_{22}(OH)_2 + 2SiO_2 = 1.5(Mg,Fe^{2+})_2Si_2O_6 + Ca(Mg,Fe^{2+})Si_2O_6 + CaAl_2Si_2O_8.Na_{0.5}Al_{0.5}Si_{0.5}O_4 + H_2O$$

and $$Na_{0.5}Ca_2(Mg,Fe^{2+})_4Al_{2.5}Si_{6.5}O_{22}(OH)_2 + 1.5SiO_2 = 1.25(Mg,Fe^{2+})_2Si_2O_6 + 1.5Ca(Mg,Fe^{2+})Si_2O_6 + Na_{0.5}Ca_{0.5}Al_{1.5}Si_{2.5}O_8 + 0.5Al_2O_3 + H_2O.$$

The compositions of the Tsu Lake hornblendes are close to that suggested for reaction (iii), except for the Al concentrations which are lower. Jen and Kretz (1981) also report low Al values for hornblendes from the Adirondack granulites.

It was suggested by Jen and Kretz (1981) that there should be a correlation between the $Fe^{2+}/(Fe^{2+}+Mg)$ ratio in hornblende and the composition of the plagioclase if reaction (iii) has occurred. They note, for the Adirondack granulites, that the $Fe^{2+}/(Fe^{2+}+Mg)$ ratio of the amphibole increases as the An content of the plagioclase decreases. The relationship for the Tsu Lake granulites is not as well defined but appears as though the $Fe^{2+}/(Fe^{2+}+Mg)$ ratio of hornblende increases as the An content of plagioclase increases, Fig. 2.59. Since a correlation does occur it implies that equilibrium for reaction (iii) has been attained. Also shown on the same diagram are assemblages in which only one pyroxene, orthopyroxene, coexists with hornblende. The correlation between the hornblende and the plagioclase, for these samples, is the same as that observed by Jen and Kretz (1981).

Possible reactions for biotite-bearing basic to intermediate granulites are:

i. biot + qtz = opx + alm + kspar + H_2O

ii. biot + hbl + qtz = opx + plag + kspar + H_2O

iii. biot + alm + cpx + qtz = opx + kspar + plag (Froese and Jen, 1979; Jen and Kretz, 1981),

iv. biot + qtz = opx + ksp + H_2O (Sen and Ray, 1971).

For lithologies of greywacke composition the assemblage biot + opx + plag + qtz, is important in the Tsu Lake area. The assemblage, biot + opx + alm + plag + qtz, is present but very rare. In all the samples biotite is replacing orthopyroxene. The presence of reactions (i) and (iv) are suggested by these assemblages and this implies that K-feldspar should be present. Its absence in the Tsu Lake rocks is puzzling.

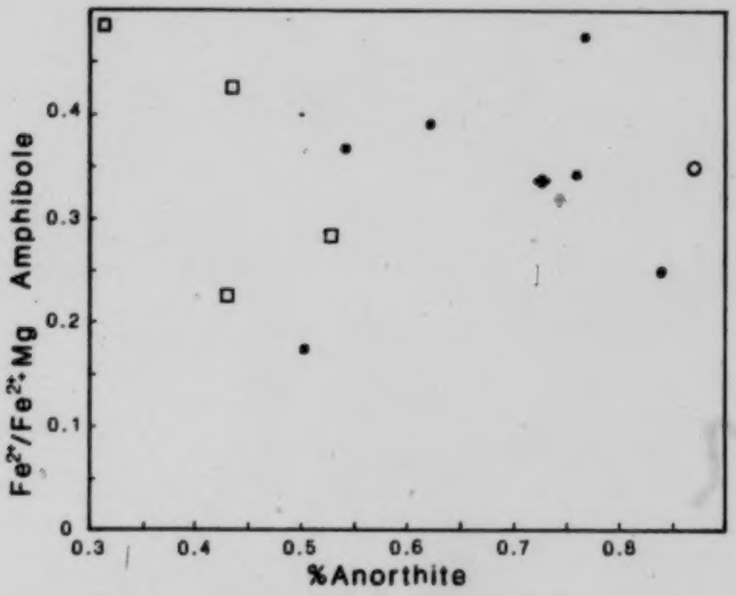

Fig. 2.59. Relationship between the $Fe^{2+}/(Fe^{2+} + Mg)$ratio of hornblendes and the percentage of anorthite in coexisting plagioclases. Symbols as in Fig. 2.37.

Two of the basic granulites contain the assemblage, opx + cpx + biot + plag, although the mode of occurrence of biotite is quite different in each of these samples. In sample 186A, the biotite appears to be replacing both orthopyroxene and clinopyroxene, in a similar manner as in the group 3 lithologies. A possible reaction for this assemblage could be:

biot + plag = opx + cpx + kspar + H_2O.

In sample 200A biotite comprises the matrix of the rock and texturally does not seem to be replacing the pyroxenes.

Sen and Ray (1971) suggest that the evolution of hornblende-bearing granulites is controlled by the activity of SiO_2. Hornblende-bearing granulites are undersaturated with respect to SiO_2, accounting for the paucity of free quartz in such rocks; while hornblende-poor biotite granulites are saturated with respect to SiO_2. Partial melting of pelitic rocks is suggested as the source of the SiO_2 necessary to convert hornblende-granulites to biotite-granulites.

It is unlikely that the SiO_2 activity is responsible for the occurrence of biotite granulites at Tsu Lake. The hornblende-granulites appear to be a closed system with respect to H_2O, and hence are probably closed with respect to SiO_2.

CHAPTER 3

GEOTHERMOMETRY AND GEOBAROMETRY

The previous chapter discussed the mineralogical and petrological characteristics of the rocks found at Tsu Lake and Deskenatlata Lake. Some of the Tsu Lake assemblages carry minerals diagnostic of granulite facies metamorphism. The partitioning relationships between certain phases indicate that, in general, granulite facies conditions have been preserved and not seriously affected by lower-grade overprints. It is intended, in this chapter, to attempt to establish the pressure-temperature conditions of metamorphism. This will be done in two ways: one, by estimating the approximate position in P-T space of a particular mineral reaction; two, by using mineralogical geothermometers and geobarometers to constrain further the pressure-temperature conditions.

Stability Regions of Critical Mineral Reactions

Basic Assemblages

Constraints on the pressure-temperature conditions experienced by the basic rocks are possible from a consideration of the hornblende stability reaction:

$$hbl + qtz = opx + cpx + plag + H_2O$$

Spear (1981) determined the hornblende stability regions under the conditions of the hematite-magnetite (HM), quartz-fayalite-magnetite (QFM) and wustite-magnetite (WM) buffers for $P(H_2O) = P(tot)$. The oxygen fugacity (fO_2) conditions during metamorphism of the of the Tsu Lake rocks are believed to be close to that of the QFM buffer because of the compositions of coexisting magnetite and ilmenite (to be discussed later) and the nature of other mafic minerals. Under the conditions of the QFM buffer hornblende breaks down to form clinopyroxene at 768 °C and 1 kb, and to orthopyroxene at 795 °C, 1 kb, Fig. 3.1. With less hydrous conditions hornblende will breakdown to the pyroxenes at lower temperatures. The calculated stability boundary of the amphibole-pyroxene reaction for $X(H_2O)$ of 0.5, is given in Fig. 3.1.

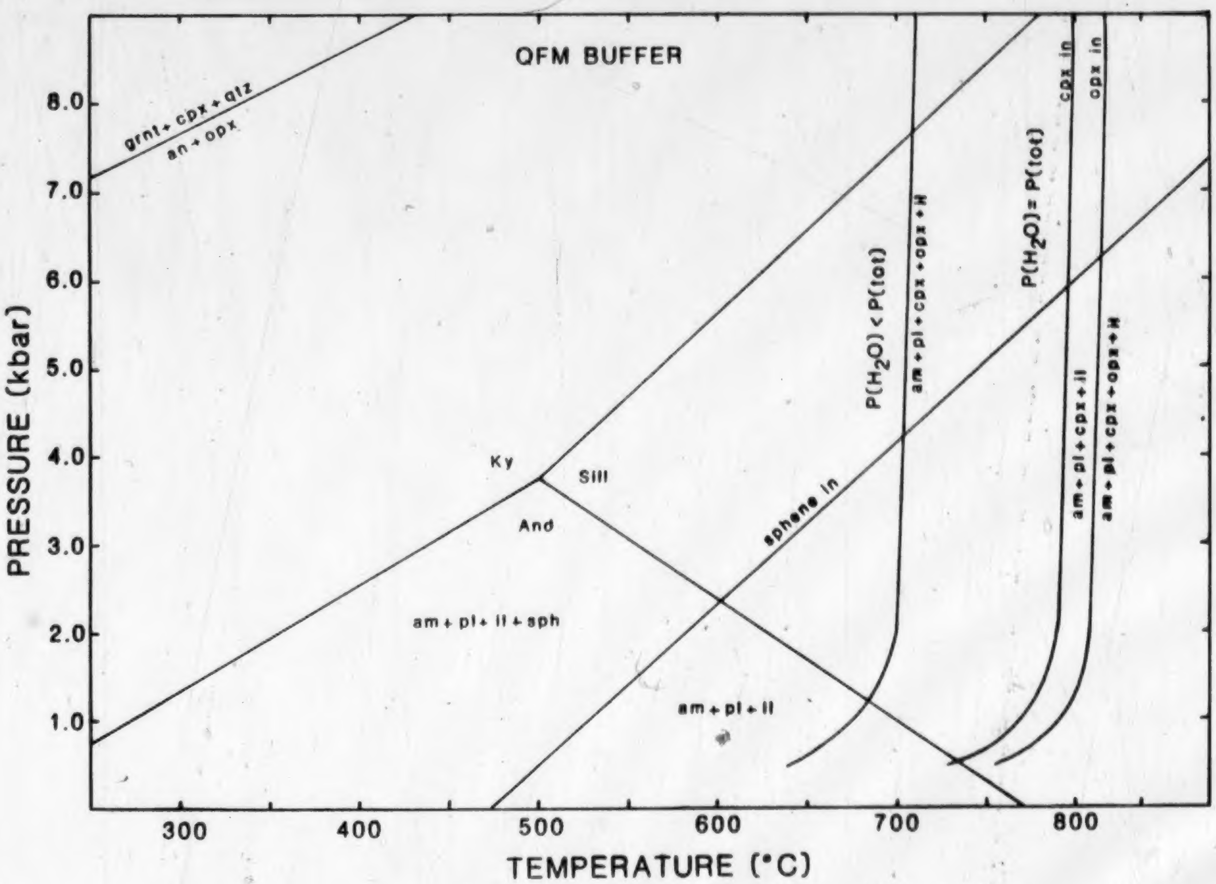

Fig. 3.1. Stability fields for the hornblende breakdown reaction for $XH_2O = 1$ and $XH_2O = 0.5$. Data taken from Spear (1981). The Al-silicate stability fields are given for reference (data from Holdaway, 1971). The stability field of the garnet - pyroxene - plagioclase reaction is given for reference (data from Hansen, 1981).

Aside from the influence of fH_2O on the pressure-temperature conditions of the hornblende stability reaction, the activity of SiO_2 also affects this reaction. The experiments of Spear (1981) indicate that SiO_2 saturation may decrease the temperature of the first occurrence of orthopyroxene. Amphiboles unsaturated with respect to quartz are stable to higher temperatures than those which are saturated, hence the reason for the pargasitic component in hornblendes of granulite facies grade.

If it is assumed that $P(H_2O) \overset{=}{<} P(tot)$, then the Tsu Lake rocks could have been equilibrated at temperatures as low as 700 °C. The Deskenatlata Lake assemblages indicate much lower temperatures. Unfortunately it is not possible to constrain the lower limit of temperature at Deskenatlata Lake because of the lack of suitable temperature indicator assemblages.

Hornblende coexists with ilmenite under the conditions of the QFM buffer. Sphene is only stable at low temperatures, high pressures and high fO_2. However, its presence in the Deskenatlata Lake calc-silicate rocks maybe accounted for by the bulk composition, which is also an important control on the stability of sphene (Helz, 1973).

The role of garnet in granulite facies basic assemblages is uncertain. Some authors believe that its appearance is controlled by bulk composition (Sen, 1973; Manna and Sen, 1974); others cite the occurrence of garnet with coexisting clinopyroxene as an indication of high pressures of metamorphism (Savage and Sills, 1980; Hansen, 1981; Newton, 1983). The occurrence of a sequence of assemblages, indicative of a transition from amphibolite to garnet granulite facies conditions, within individual dykes, led Glassley and Sorensen (1980) to suggest an alternative solution to the garnet stability problem. The following reactions may be applicable by variations in μH_2O and μSiO_2 during prograding metamorphic conditions (Glassley and Sorensen, 1980):

i. hbl = ab + cpx + grnt
ii. hbl = ab + cpx + opx + grnt
iii. opx + an = cpx + grnt
iv. hbl + an + opx = cpx + grnt + ab
v. hbl = ab + an + cpx + opx
vi. hbl + grnt = ab + an + opx

Thus, the absence of garnet in all but one of the basic to intermediate Tsu Lake assemblages may only be a reflection of the lack of suitable μH_2O and/or μSiO_2 (conditions) for its formation.

No pressure estimates could be obtained from the Tsu Lake or Deskenatlata Lake basic assemblages.

Pelitic Assemblages

As was discussed in the previous chapter, the intersection of the melting and dehydration reactions defines the region where anatectic melting can begin in pelitic rocks. The pressure-temperature conditions for the KNASH system shown in Fig. 3.2. (data taken from Thompson (1982)) are listed below.

a. The H_2O - saturated minimum melting curves:
   i. Fe-mus + alb + Fe-biot + ksp + qtz + H_2O = liq
   ii. Fe-mus + Fe-biot + ksp + qtz + H_2O = liq.

b. The H_2O - conserving melting reactions:
   i. Fe-mus + alb + qtz = Fe-biot + ksp + sill + liq
   ii. Fe-mus + qtz = Fe-biot + sill + ksp + liq.

c. The dehydration reactions:
   i. Fe-mus + alb + qtz = Fe-biot + ksp + sill + H_2O
   ii. Fe-mus + qtz = Fe-biot + ksp + sill + H_2O.

The overlap between these curves extends from temperatures of 650 to 700 °C, at 3.5 to 6 kb. For the rocks with intermediate Fe-Mg pelitic compositions the relevant reactions are shown in Fig. 3.2. These reactions are:

d. the H_2O - conserving melt reactions;
   FeMg-biot + sill + qtz = FeMg-cord + FeMg-grnt + ksp + liq,

e. the dehydration reactions;
   FeMg-biot + sill + qtz = FeMg-cord + FeMg-grnt + ksp + H_2O

Temperatures of initial melting could be as high as 700 to 750 °C, depending on the position of the minimum melting curve for rocks of this composition. Other reactions, such as those documented in the previous chapter, can modify further the phase relations beyond the intersection region.

A constraint on the pressure-temperature conditions in the overlap regions is available from a consideration of the reactions in the system, $FeO - Al_2O_3 - SiO_2 - H_2O$. The

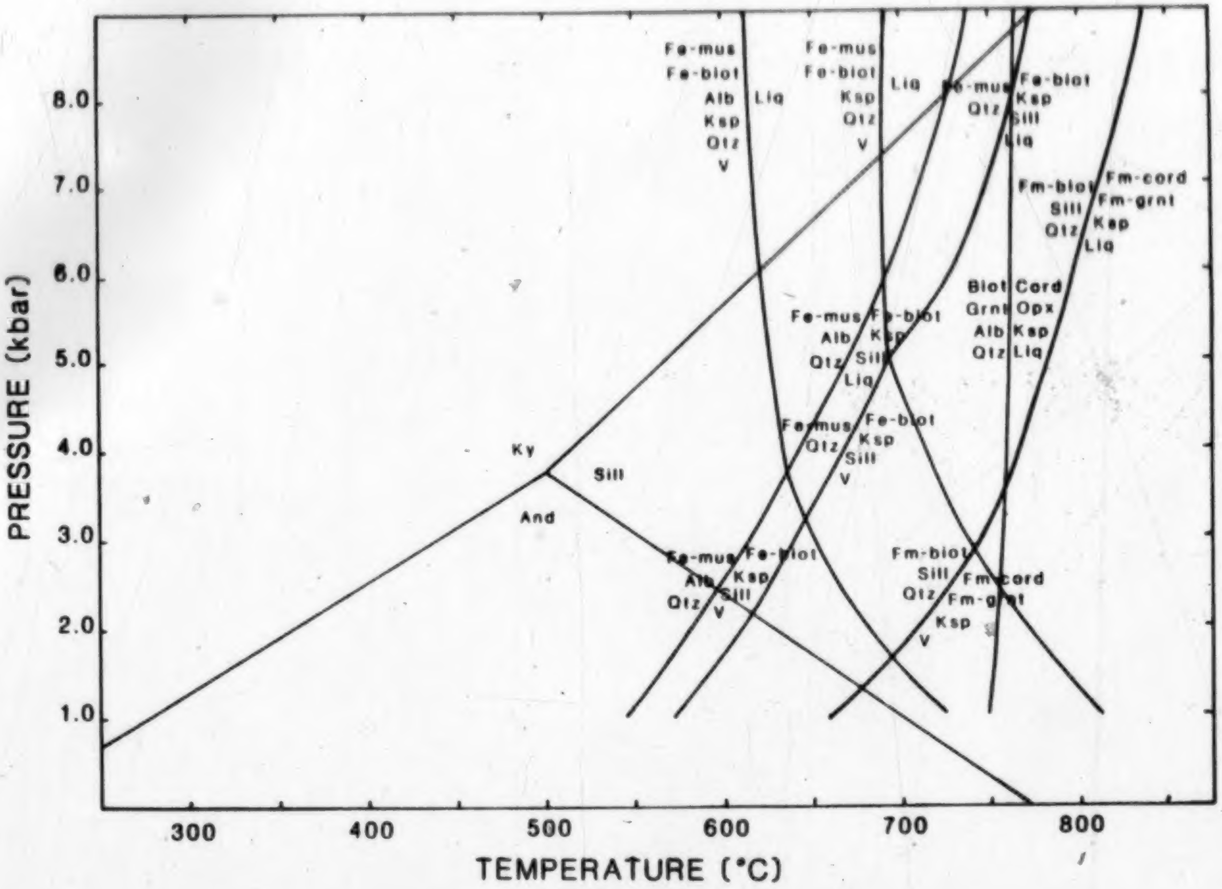

Fig. 3.2. Stability regions of the H_2O - saturated minimum melting reactions, H_2O - conserving melting reactions, and dehydration reactions for pelitic rocks (data from Thompson (1982)). Al - silicate stability fields are given for reference.

melting of a pelitic rock would leave the restite sufficiently depleted in alkalis for this system to be applicable to the Tsu Lake group 6 lithologies. Reactions such as those listed below are suggested by the presence of the reaction products, alm + sill + hc, and alm + cord.

i. staur + qtz = alm + sill + mt

ii. staur = alm + sill + hc

iii. staur = cord + sill + hc

iv. staur + cord = alm + sill

v. staur + qtz + mt = cord + sill

That staurolite is not present, and the lack of any evidence of it ever having been present, implies that the pressure-temperature conditions must have been above the boundary for reaction (i), and possibly reaction (ii). The pressure-temperature conditions for the reactions listed above, under the QFM buffer, are given in Fig. 3.3. (data from Greenwood, 1976; Schreyer, 1976). From this, it is seen that the assemblage, grnt + sill + hc, can be stable at approximately 680 to 690°C, above 3.5 kb of pressure. Modification of the restite assemblage, which would have resulted from the H_2O-conserving melt reaction, appears to have occurred.

Based on the restite assemblages of the group 5 and 6 lithologies listed earlier, the minimum temperature estimate for the Tsu Lake rocks, is 680±30°C; while the maximum temperature estimate is approximately 750±30°C.

The upper temperature limit is harder to constrain because the sequence of melting, and hence the type of unmodified restite assemblage, is dependent on the composition of the original pelitic sediment. An upper limit of 750°C is assigned for two reasons. Reaction (d) marks the beginning of melting in pelitic rocks of intermediate composition. The most Fe-rich pelites, group 5 lithologies, show evidence of extensive melting to the point where the melt has partially separated from the restite; whereas the Fe-Mg intermediate pelites do not show the same degree of melting. The second reason is because of the assemblage observed in sample 182A, grnt + biot + cord + opx + ksp + plag. The pressure-temperature conditions of the reaction:

grnt + biot + plag + qtz = cord + opx + liq (Grant, 1973)

suggests an upper limit of 750 °C for the melting of pelites at Tsu Lake.

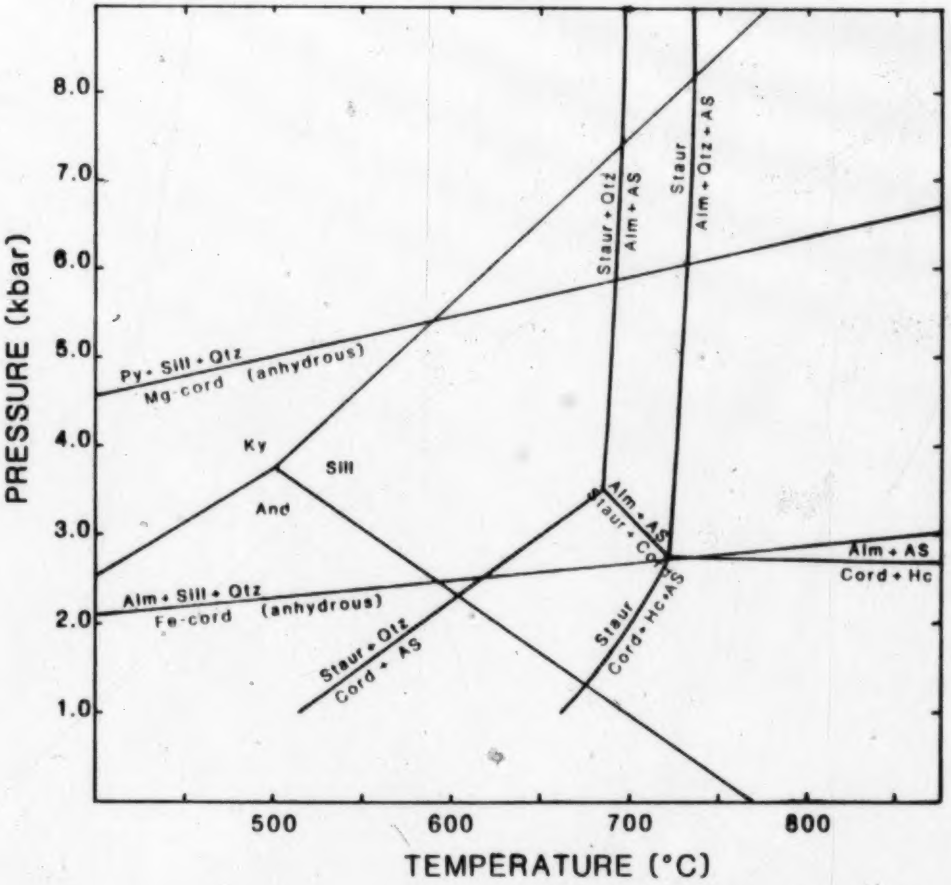

Fig. 3.3. Stability regions for some reactions in the system FeO - Al_2O_3 - SiO_2 - H_2O (data from Greenwood (1976); and Schreyer (1976)). The stability fields for the breakdown reactions of the anhydrous Fe-Mg cordierite end-members (data from Martignole and Sisi, 1981) and the Al-silicates (data from Holdaway, 1971) are also given.

The Deskenatlata Lake pelites have an upper temperature limit of 680 °C, although this estimate is based on one sample only.

Pressure estimates are rather difficult to assign because of the lack of suitable pressure defining reactions. The grnt - rut - sill - ilm - qtz (GRAIL) reaction (Bohlen *et al.*, 1983) is not applicable to the Tsu Lake rocks because of the absence of rutile. The assemblage listed below is pressure dependent.

cord = grnt + sill + qtz

The limits for the anhydrous Mg and Fe end member reactions are given in Fig. 3.3. An increase in $P(H_2O)$ increases the stability of this reaction with respect to pressure. For the pelitic lithologies, the pressure must have been about 4 kb, lower limit, to 6 kb, upper limit.

Geothermometry-Geobarometry

Further refinement of the pressure - temperature conditions may be achieved. A particular assemblage maybe more tightly constrained in P-T space than the mere association of critical assemblages, or phases, would suggest. An analysis of the activities of the components of a reaction can be refined to give a single temperature and/or pressure.

The equilibrium constant, K(D), which describes the relationship between the activities of the components, is defined in P-T space by the equation:

$$\Delta H - T\Delta S + (P - 1)\Delta V^{\circ} = - RT\ln K(D) \qquad (1)$$

where ΔH, ΔS and ΔV are the enthalpy, entropy and volume changes for pure components of the reaction. This only applies to chemically simple systems; a more rigorous treatment is needed for natural systems.

Differentiating equation (1) (Wood and Fraser, 1980) gives:

$$\frac{\delta \ln K(D)}{\delta T} = \frac{\Delta H \;+\; (P-1)\Delta V}{RT^2} \qquad \text{(2) at constant P}$$

$$\frac{\delta \ln K(D)}{\delta P} = \frac{-\Delta V}{RT} \qquad \text{(3) at constant T}$$

Hence if ΔH in equation (2) is much larger than ΔV in equation (3) then K(D) is more dependent on temperature than pressure, and the reaction can be used as a geothermometer. Similarly if ΔV is much larger than ΔH the reaction may be used as a geobarometer. Equation (1) is only valid as a geothemometer if it is assumed that C(p) equals zero.

Exchange Geothermometers

One type of geothermometer involves the exchange of two or more elements either between different crystalline sites in a phase or between different phases. In simple systems the volume change for such an exchange is normally very small thus temperature estimates for the reaction at equilibrium depend on enthalpy and entropy changes. Calculations of these thermodynamic data are normally derived from experiments involving variations of K(D) versus temperature. Because the experimental reactions are, of necessity, chemically simple, application of the derived geothermometer to complex natural systems is difficult. Consideration must be given to the effects of other components on the K(D) of the pure solid solution series of the exchanging phases, i.e., on the kinetics of the exchange reaction. Frequently this aspect is ignored, or modelled on insufficiently known data. Other problems arise from the necessity of extrapolating experimental data taken at high temperatures down to the realistic temperatures of the natural system. Difficulties in analysing all the components of a phase add a third uncertainty factor.

The most common type of exchange reaction geothermometer is that involving Fe^{2+} and Mg. Suitable mineral pairs for this study data include: garnet - biotite, garnet - cordierite, orthopyroxene - ilmenite, clinopyroxene - ilmenite and orthopyroxene - clinopyroxene. Other types of exchange reactions include: Fe-Ti in oxides and Ca-Na in feldspars.

In the following sections each of the geothermometers that are to be used on the Tsu Lake rocks, are discussed separately. The emphasis of the discussion is placed on the factors outlined above. Mathematical derivations of each geothermometer are listed in appendix 2.

Garnet-Biotite

The geothermometer is based on the reaction:

$$\underset{\text{annite}}{KFe_3Si_3AlO_{10}(OH)_2} + \underset{\text{pyrope}}{Mg_3Al_2Si_3O_{12}} = \underset{\text{phlogopite}}{KMg_3Si_3AlO_{10}(OH)_2} + \underset{\text{almandine}}{Fe_3Al_2Si_3O_{12}}$$

and $K(D) = (Xpy)^3(Xan)^3 / (Xalm)^3(Xphl)^3$

The main problems to consider are:

i. the effect of Ca and Mn in garnets on the K(D);

ii. the effect of Al and Ti in biotites on the K(D);

iii. the susceptibility of the above reaction to reequilibration during retrograde metamorphism.

Four calibrations of this geothermometer were considered: Thompson(1976), Goldman and Albee(1977), Ferry and Spear(1978) and Perchuk and Lavrent'eva (1983). In addition modifications of the Ferry and Spear (1978) geothermometer by Ganguly and Saxena (1984) are evaluated.

Thompson (1976) based his calibration on a compilation of natural compositions with temperatures estimated from independent sources, i.e., other phases present in the garnet-biotite assemblages for which experimental thermodynamic data are available. While his calibration avoids some of the compositional effects an experimental system might experience, it is strongly dependent on the accuracy of other data. His main assumption is that the other "systems" equilibrated at the same time and temperature as the Fe-Mg system. Thompson notes a dependency of the K(D) on the mole fraction of Ti in biotite.

Goldman and Albee (1977) used essentially the same approach as Thompson (1976). However, they based their temperature estimates on the quartz-magnetite oxygen isotope exchange equilibrium. Their derived equations clearly show the dependence of the K(D) on the Ti and Al contents in biotite and the other components in garnet. It has been suggested elsewhere that the oxygen isotopic system equilibrates at lower temperatures than the cation exchanges. This would imply that the Goldman and Albee calibration is offset towards lower temperatures. This would appear to be the case when the calibration is compared with the experimentally calibrated system of Ferry and Spear (1978). Neither the Thompson nor the Goldman and Albee calibrations consider the effect of pressure on the system.

The alternative approach is to examine the equilibrium dependence on temperature directly. Ferry and Spear (1978) attempted this for the pure Fe-Mg end-members of the garnet-biotite system. Their experiments, using synthetic starting materials, were run between temperatures of 550 - 880 °C at 2 kb. Because garnet reacts sluggishly they preferred to maintain garnet at a constant composition while changing the composition of the biotite in order to achieve a range of K(D)'s. The authors note their calibration is unlikely to be suitable for garnets with more than $0.2(Ca+Mn)/(Ca+Mn+Fe^{2+}+Mg)$ or biotites with more than $0.15(Ti+Al)/(Ti+Al+Fe^{2+}+Mg)$.

In an attempt to account for the garnet compositional effect, Ganguly and Saxena (1984) have applied their model of the mixing properties of garnet to the Ferry and Spear calibration. As will be seen in a later section, this has the effect of lowering the estimated temperatures by about 50°C. Clearly this shows the magnitude of the garnet compositional effect. However, the means by which this effect can be corrected is unclear because a correction would depend on the validity of the mixing model which is used.

In a more recent experimental calibration Perchuk and Lavrent'eva (1983) used natural minerals as starting materials. They tackled the equilibration problem by approaching the equilibrium composition from opposite sides, i.e., the compositions of the garnet and the biotite were on opposite sides of the predicted equilibrium position. From this they were able to construct histograms which determined the direction of chemical shift, and hence the equilibrium compositions. Unfortunately the starting materials limited the compositional range studied so experiments at high Mg mole fractions could not to be performed. All experiments were run at 6 kb pressure and in the temperature range of 575 - 950 °C. Perchuk and Lavrent'eva predict the lnK(D) will change with the mole fraction of Al in biotite. They also note the dependence of ΔV on the X(Al-biot), a factor which was kept constant during their experiments. There is a discrepancy in the published values of ΔV for the garnet-biotite reaction which results in a difference of 40 °C in the estimated temperatures at P = 1 bar. This difference decreases to 0 as P approaches 6 kb. Note that Ferry and Spear did not allow for this error in their calibration.

Application.

The results of the temperature estimates of five of the calibrations discussed, are presented in Table 3.1. For each sample data from three pairs of garnet - biotite grains were collected. In every case the garnet and biotite phases were in contact. The data presented in Table 3.1 represent estimates that were obtained by using the average compositions of the three garnet analyses and the same for the biotite. This method does not alter the temperature estimate which would be obtained if the temperatures were calculated for each of the pairs and then the temperature estimates averaged. The ferric iron content of the biotites is unknown. A crude estimate of the ferric iron content for phases such as pyroxenes may be obtained from calculations of the charge balances necessary to achieve ideal stoichiometry. However, for a microprobe analysis of a biotite such a calculation is pointless; both the water and the ferric iron content are unknown quantities. There are also other elements which may be present but which cannot be detected by energy dispersive electron microprobe analysis, e.g., F. Hence calculations are performed with all the iron in the divalent state.

Examination of Table 3.1 reveals the extreme scatter of the results. In the worst case there is a temperature range of 600°C; in the best case a temperature range of 300 °C. It is thought that the extreme range shown by the results of the Ferry and Spear (1978) geothermometer is due in part to the calibration based only on the Fe-Mg end-members. The modifications of the Ferry and Spear calibration accounting for the non-ideality of the garnet solid solution, does little to the reduce the scatter.

Other explanations could be sought in the non-ideal solution of Ti in biotite and in the pressure influence on the calibration caused by variation in the Al atomic fraction of biotite. Some of the biotites contain as much as 7 wt. % TiO_2, or the equivalent of 0.140 X(Ti). Coupled with Al this exceeds the limit recommended by Ferry and Spear (1978) as suitable for the application of their geothermometer. Unfortunately there is no apparent correlation between X(Ti), X(Al), X(Al+Ti) and lnK(D), or X(Ti) and $Fe^{2+}/(Fe^{2+}+Mg^{2+})$, which is expected if these factors were the cause of the scattered results.

Possibly biotite and garnet do not represent an equilibrium assemblage. Evidence for this is found in the textural relationships between biotite and garnet; in some samples biotite appears to be replacing garnet. The inhomogeneous nature of the biotite and the

Table 3.1
Garnet - Biotite Geothermometry

	K(D)	1.	2.	3.	4.	5.
8B	3.02	906	806	788	758	741
8E	4.50	677	611	635	628	639
9D	2.59	1000	950	846	807	778
13D	2.52	970	984	822	787	763
23C	4.24	699	627	651	641	650
24B	5.93	575	544	561	562	586
44	7.80	508	509	509	516	547
54A	4.24	709	698	658	648	656
87A	8.55	460	446	471	482	518
135B	4.31	684	682	640	632	643
182A	3.52	802	664	721	702	697
183B	5.53	593	557	574	575	597
239B	10.74	418	434	438	452	491
D11	3.52	809	841	725	706	701
Range h	2.59	1000	984	846	807	778
l	10.74	418	434	438	452	491

1. - Ferry and Spear (1978)
2. - Ganguly and Saxena (1984)
3. - Thompson (1976)
4. - Holdaway (1977)
5. - Perchuk and Lavrent'eva (1983)

* - all temperature estimates in °C

irregular $Fe^{2+}/(Fe^{2+}+Mg^{2+})$ distribution between garnet and biotite, discussed earlier, reinforce this suggestion. Some of the samples are mylonitic or pegmatitic, and conceivably have experienced local reequilibration due to the introduction of a hydrous phase of a different composition to the granulite facies metamorphic fluid.

The non-ideality of the garnet solution model influences the calibration of the geothermometer. Perhaps the non-ideality of Ti in biotite, is also responsible, although this cannot be proven here.

Garnet-Cordierite

The exchange reaction :

$$Mg_3Al_2Si_3O_{12} + Fe_2Al_4Si_5O_{18} = Fe_3Al_2Si_3O_{12} + Mg_2Al_4Si_5O_{18}$$

where K = (Xpy)(XFe-cord) / (Xalm)(XMg-cord).

forms the basis of the garnet-cordierite geothermometer.

Considerable controversy has arisen over the thermodynamics of this reaction. This is mainly the result of conflicting experimental data. Currie (1971, 1974) reported a K(D) dependence on temperature (negative slope for dT / dlnK(D)) which is the reverse of that observed by other workers experimentally, and in natural assemblages (Hensen and Green, 1973; Thompson, 1976; Hensen, 1977; Holdaway and Lee, 1977; Perchuk and Lavrent'eva, 1983). Inadequate experimental conditions may have been used by Currie (1971). Currie's experiments were conducted under hydrous conditions, whereas Hensen and Green's experiments were for anhydrous cordierite only. The K(D) may be dependent on the water content of corderite (Wood, 1973). For a more complete discussion see Hensen (1977).

Data on the role of water in the exchange reaction is also controversial. For a K(D) dependence on $X(H_2O)$, differential absorption of H_2O by the respective cordierite end-members is required (Lonker, 1981). However, the cordierite "hydration" model of Martignole and Sisi (1981) suggests that such an effect, if present, is unlikely to affect the K(D) seriously. Experiments by Gunter (1977) confirm this statement. More recent experimental data of Aranovich and Podlesskii (1983), using hydrous conditions, reveal the independence of $X(H_2O)$ on the Fe / Mg ratio of cordierite.

Another implication of studies of the role of water was postulated by Newton and Wood (1979). Their experiments on the system cordierite-garnet-sillimanite-quartz suggest that the K(D) is nearly independent of temperature, pressure and X(H_2O), implying that the exchange reaction is useless as a geothermometer. Arguments disputing their data will be discussed in the section on the garnet-cordierite-sillimanite-quartz geobarometer.

The calibrations of Thompson (1976), Holdaway and Lee (1977) and Perchuk and Lavrent'eva (1983) are used in the assessment of pressure and temperature conditions at Tsu Lake. Thompson (1976) derived the garnet-cordierite calibration in an analogous manner to that of his garnet-biotite calibration. Holdaway and Lee (1977) used the same approach as Thompson (1976) but with modifications to the calibration at the low temperature end. The experimental approach used by Perchuk and Lavrent'eva (1983) in the garnet-biotite calibration was also used for the garnet-cordierite calibration, again using natural mineral starting materials.

The compositional dependence of Ca and Mn in garnet and Mn in cordierite imposes limitations to the calibrations discussed above.

Application.

Temperature estimates of averaged mineral pair compostions for each sample are presented in Table 3.2. The influence of the Mn content of cordierite on the K(D) has been ignored because it is believed to be insignificant. No correlation between the K(D) and the X(Mn) was found.

Similarly the application of a regular solution model to the components in garnet was not tested. As cordierite has similar partition properties to biotite, a comparison with the garnet-biotite results shows that the effect should be to lower the estimated temperatures by a maximum of 50 °C. Ignoring the other components of garnet by treating the atomic fraction as $Fe^{2+}/(Fe^{2+}+Mg^{2+})$ only, permits an estimate of a minimum temperature. This is seen in the results of the Perchuk and Lavrent'eva (1983) calibration, 1, in Table 3.2. Perchuk and Lavrent'eva (1983) formulated their thermometer using the Fe-Mg atomic fractions so it is an inherent part of their calibration. Using an atomic fraction based on all the components yields temperatures that are 10 to 15°C higher.

Estimates obtained from both rim and core compositions are given. Some workers believe that core temperatures represent peak metamorphic temperatures. However, this is only valid if the zoning observed is a true reflection of the changing pressure -

Table 3.2
Garnet - Cordierite Geothermometry

		K(D)	1.	2.	3.
9D	c	7.06	733	771	736
	r		658	682	663
23C	c	6.91	685	714	689
	r		665	672	669
24B	r	8.23	617	634	620
44	r	7.32	648	670	653
135B	c	8.00	752	793	753
	r		624	643	628
182A	c	6.27	701	735	704
	r		694	724	696
239B		7.67	635	656	639
Range	c		752	793	753
			685	714	689
	r		694	724	669
			617	634	620
av.#			649	668	652

1. - Perchuk and Lavrent'eva (1983)
2. - Thompson (1976)
3. - Holdaway and Lee (1977)

* - all temperature estimates in °C

temperature regime. Garnet, being a very refractory phase, may well retain its initial core composition. Unfortunately the same is not necessarily true of cordierite. The observed core compositions of cordierite in the Tsu Lake rocks show only a slight variation from rim compositions. There is also the analytical problem of obtaining true core compositions from a thin-section; only extremes of composition would indicate core concentrations. In reality it would be necessary to obtain numerous profiles of many grains of the phase of interest, before one could be reasonably sure of having seen a slice through the core. Therefore, although the core estimates are higher than the rim estimates, it is unlikely that peak metamorphic temperatures are indicated.

The rim temperatures exhibit some scatter, a maximum of 90°C, Table 3.2; this is within the error of the calibrations. The results of the Holdaway and Lee (1978) and Perchuk and Lavrent'eva (1983) geothermometers yield temperature estimates within a few degrees of one another, indicating excellent agreement between natural and experimental calibrations. The estimates of the Thompson (1976) calibration are higher only by a maximum of 40°C.

The agreement between the three calibrations, the limited range of temperatures and the $Fe^{2+}/(Fe^{2+}+Mg^{2+})$ distribution (given earlier) suggests equilibrium conditions. The temperature estimates are reasonable for hornblende granulites (Winkler, 1974). Unfortunately no comparison of the garnet-cordierite temperatures could be made between the Tsu Lake and the Deskenetlata Lake samples. The cordierite in the one sample from Deskenetlata Lake which contained the appropriate assemblage, was extensively altered to pinite, thus not permiting the determination of an accurate cordierite composition.

Orthopyroxene-Clinopyroxene

The intercrystalline reaction, on which the pyroxene geothermometer is based, involves the transfer of Mg and Ca between ortho- and clinopyroxene. It is not, strictly speaking, an exchange reaction of the same type as the other geothermometers previously discussed. Rather it is a transfer reaction involving the mutual solubility of two structurally similar phases (enstatite and diopside). Thus the transfer reactions are:

1. $\underset{opx}{Mg_2Si_2O_6} = \underset{cpx}{Mg_2Si_2O_6}$

2. $\underset{\text{opx}}{CaMgSi_2O_6} = \underset{\text{cpx}}{CaMgSi_2O_6}$

These govern the shape of the solvus.

However, Fe is inevitably involved in what may be classified as a true exchange reaction:

3. $\underset{\text{en}}{MgSiO_3} + \underset{\text{hed}}{CaFeSi_2O_6} = \underset{\text{fs}}{FeSiO_3} + \underset{\text{diop}}{CaMgSi_2O_6}$

As well there is the possibility of a Mg and Fe intracrystalline exchange between the similar sized M_1 and M_2 sites of both pyroxenes.

4. $Fe\text{-}M_1 + Mg\text{-}M_2 = Mg\text{-}M_1 + Fe\text{-}M_2$

The presence of the reactions (3) and (4) seriously complicates the use and calibration of a geothermometer based on the diopside-enstatite miscibility gap.

Calibrations of the two-pyroxene geothermometer are formulated on the enthalpy and entropy changes for reaction (1). The approaches used for the calibration are wide and varied. The two most common calibrations to date are those of Wood and Banno (1973) and Wells (1977). Wood and Banno (1973) used the experimental data of Davis and Boyd (1970) on the diopside-enstatite miscibility gap at 30 kb pressure for the temperature range of 900 - 1300°C. A linear relationship was obtained between temperature and $\ln[a(Mg_2Si_2O_6\text{-cpx})/a(Mg_2Si_2O_6\text{-opx}]$. Wells' (1977) calibration, used the same approach as Wood and Banno (1973), but incorporated more recent experimental data. The only difference between the two calibrations appears to be in lower ΔH and ΔS values for the Wells' thermometer.

There are a number of problems associated with such a formulation. Bohlen and Essene (1979) showed that the relationship between lnK(D) and 1/T was a curve rather than a straight line. This causes overestimates of the temperature. Lindsley (1983) noted that their large ΔH (both calibrations) for reaction (1) appears to be in error. Thus the assumptions made by Wood and Banno (1973) and Wells (1977), in deriving the activities for the $Mg_2Si_2O_6$ component of the clino- and orthopyroxene, are invalid. They had simplified the ordering between the intracrystalline sites to an ideal solid solution model. Wells (1977) conceded that the large ΔS obtained for his calibration implied the inadequacy of the simple ideal model. However, he noted that his model was consistent with the experimental data. It has been suggested that the exchanges of Fe, Mg and Ca take place only on the M_2 site. The Mg:Fe ratio in the M_1 sites of clino- and orthopyroxene remains constant with increasing temperature (Kretz, 1982). The Ca content of the pyroxenes changes with temperature (as temperature increases there is less Ca in clinopyroxene and more in orthopyroxene). This would imply that the simple ideal model is completely inadequate. Additional factors that were ignored in the calibrations are the effects of pressure on the reaction and the effect of the Al content on the solubility of $Mg_2Si_2O_6$ in clinopyroxene.

Other authors have based their calibrations on more realistic assessments of the activities involved, or have avoided the problems involved with the calculation of the activities by constructing isotherms on the pyroxene quadrilateral. By this method only the pyroxene compositions need to be projected onto the quadrilateral.

Saxena (1976) used a thermodynamic approach which considered:

i. a model accounting for the nonideality of the Fe-Mg solid solution on the sites in orthopyroxene;

ii. a solid solution model accounting for the influence of Ca on the Fe-Mg distribution on the M_2 site.

In other words, a regular solution model is necessary to describe the behaviour on each site of a pyroxene. The data of Ross and Huebner (1975) was used to constrain the dependence of lnK(D) on temperature, the site occupancy of clinopyroxene and that of orthopyroxene on temperature. The method requires successive iterations for each of the temperature dependent factors until equations relating lnK(D), a(opx) and a(cpx) are matched to a particular temperature. A more detailed explanation of Saxena's procedure can be found in appendix 2. Saxena (1976) noted that the formulation is approximate because some of the Margules parameters used in the solution model, at the time were not well known; however relative temperatures should be correct. Pressure was not taken into account, hence only pyroxenes formed under the same pressure should be compared. Similarly the effect of non-quadrilateral pyroxene components on the system is unknown so reliable temperatures will only be given when there is a negligible concentration of these components.

Both natural and experimental data were utilised by Kretz (1982) in his calibration. The experimental data of Lindsley and Dixon (1976) were used to find the linear dependence of the enstatite component on temperature. The natural data were used to find the influence of the $Fe^{2+}/(Fe^{2+}+Mg)$ ratio of the clinopyroxene on this relationship. In addition Kretz (1982) evaluated the temperature dependence of the Fe:Mg exchange, reaction (3). The calibration of the two reactions, exchange and transfer, permit an evaluation of the relative kinetics of each. Significant differences in temperatures would suggest that the reactions have approached equilibrium at different rates. Kretz avoided the need for site occupancy data by assuming activities are equivalent to mole fractions. The effect of this assumption is not as crucial as with the Wood and Banno (1973) geothermometer; the calibration using natural data has helped to smooth out any major inaccuracies caused by this assumption.

The Lindsley (1983) calibration combined new experimental data on the Ca-Fe-Mg pyroxene system for a pressure range of 1 atm to 15 kb and for temperatures between 800 - 1200°C, with calculated phase equilibria. From this data Lindsley constructed isotherms on the pyroxene quadrilateral. Temperatures are estimated graphically by projecting compositions onto the quadrilateral. The method of projection is purely empirical; hence it may be inaccurate because of complexities introduced by ordering on the M_1 and M_2 sites, or by the influence of other components on the system such as Al which appears to have an effect (Lindsley, 1983). Lindsley tested his calibration on a number of data sets and noted that for metamorphic rocks there was little consistency with estimated temperatures of other geothermometers. Data was scattered for rocks that should have been equilibrated at the same temperature.

Saxena (1983) attempted to reevaluate his own calibration of 1976. The attempt was to emphasize possible inter- and intracrystalline relationships and the difficulties these introduce in pyroxene geothermometry. The main problems appear in the analytical difficulty of measuring small but critical concentrations in the pyroxene phases accurately and in the possibility of disequilibrium in the measured phases. The small values of ΔH and ΔS for reaction (1) imply the estimated temperatures are very sensitive to small errors in the calculated activities and hence, to errors in the measured compositions. Thus the method of calculation of site occupancies is very important. The rate of the reactions occurring between the pyroxenes will determine whether the temperatures obtained are representative of equilibrium. Ca transfers at a slower rate than the Fe-Mg exchange

(Saxena, 1983); therefore temperatures estimated using all three elements may not necessarily imply a "blocking temperature" closest to the peak metamorphic temperature. Saxena suggested the pyroxene thermometer would be more useful in the study of reaction kinetics of a rock system rather than the pressure-temperature conditions under which it was formed.

Application.

Five of the calibrations discussed, were tested on the Tsu Lake samples. The data, except for the estimates of the Lindsley (1983) calibration, are presented in Table 3.3. Estimates of the ferric iron content were obtained by charge balance calculations; in some cases an assumption of a zero ferric iron concentration was necessary to achieve ideal stoichiometry. The temperature estimates are based on both limiting cases, all iron in the divalent state and maximum estimated ferric iron.

The calibrations of Wood and Banno (1973) and Wells (1977) appear to be relatively insensitive to the ferric iron content of the pyroxenes, at the worst causing a 20°C increase in the temperature estimate. The Saxena (1976) geothermometer, on the other hand, appears to have a variable sensitivity. The effect of estimating the ferric content is to cause a decrease in the calculated temperatures relative to those obtained by assuming all Fe^{2+}, the opposite effect to that observed for the Wood and Banno (1973) calibration. The magnitude of the difference can vary from 5 °C to as much as 100 °C. The Kretz (1982) calibration is affected by the ferric iron content in much the same way as the Saxena (1976) calibration, although it is not as sensitive.

There is considerable variation in the estimated temperatures of the Wood and Banno (1973) and Wells (1977) geothermometers, outside the range of error allowable in the calibrations. Some of the temperatures are much higher than might be reasonably expected for hornblende granulites. They are also higher than the temperatures obtained for the Adirondack granulites using the same calibrations (Bohlen and Essene, 1979). The observed assemblages suggest the Tsu Lake area was metamorphosed at lower temperatures than the Adirondack granulites.

One possible explanation for the unreasonably high temperatures could be the ideal M_1-M_2 site occupancy model. A comparison of site occupancies calculated by the Wood

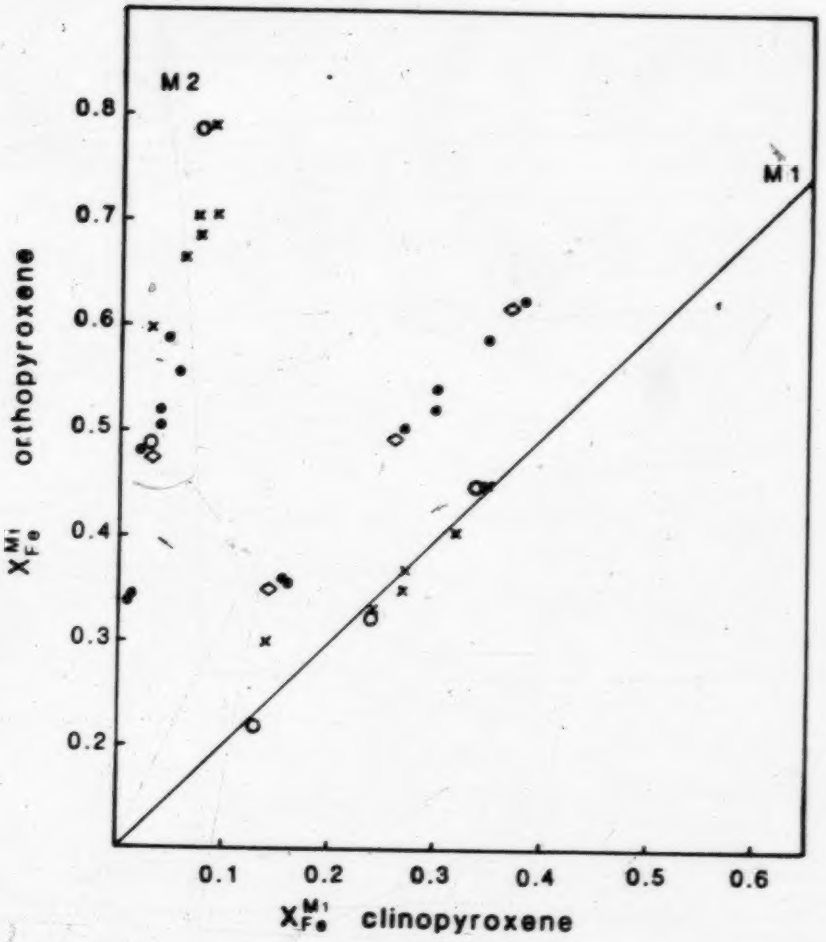

Fig. 3.4. Calculated site occupancies of orthopyroxene and clinopyroxene. The diagram shows the distribution between XFe-opx-M_1 and XFe-cpx-M_1 (along the line labelled M_1, and between XFe-opx-M_2 and XFe-cpx-M_2 (area labelled M_2). Symbols: Fe^{2+} maximum estimate (Saxena method) (diagonal crosses), Fe^{3+} maximum estimate (Saxena method) (open circles); Fe^{2+} maximum estimate (Wood and Banno method) (closed circles); Fe^{3+} maximum estimate (Wood and Banno method) (open diamonds).

Table 3.3
Orthopyroxene - Clinopyroxene Geothermometry

	1.	2.	3.	4.	5.
1B	956	955		785	852
7C	881	935	840	851	819
141B	842 850	868 878	810 800	793 769	783 762
160	814 822	862 874	795 790	783 756	760 765
183D	878	937	850	776	810
186A	871	939	830	858	822
200A	872 888	845 864	885 770	687 680	752 721
Range	956 814	955 845	885 795	858 687	852 752
Av.	873	905	835	790	800
Range	956 812	955 864	850 770	858 680	852 721
Av.	878	911	813	782	793

1. - Wood and Banno (1973)
2. - Wells (1977)
3. - Saxena (1976)
4. - Kretz (1981) (1)
5 - Kretz (1981) (2)

All temperature estimates are in °C

For any one sample, if two rows of data are given, the first is calculated with all Fe in the divalent state, while the second is calculated with an estimated Fe^{3+} content and Banno (1973) method and the Saxena (1976) method is shown in Fig 3.4. The calculated site occupancies of the Saxena (1976) model conform to the pattern observed for measured natural pyroxenes (Kretz, 1981). The Wood and Banno data, however, departs from this pattern significantly. Using their method the amount of Fe^{2+} is overestimated in the M_1 site and underestimated in the M_2 site.

It could be expected that the Saxena (1976) geothermometer would yield more realistic temperature estimates than the Wood and Banno (1973) and Wells (1977) calibrations. While the temperatures are lower by about 50 °C, unfortunately there is considerable scatter. The temperatures are still inordinately high for hornblende-bearing granulites, although, conceivably this may be explained away by Saxena's (1976) approximate calibration. The scattered data probably lie just outside the error limits of the calibration.

It is more likely, however, that the results reflect the sensitivity of the geothermometer to small errors in the concentration and/or the effects of reaction kinetics.

Elements present in low concentrations are the most probable sources of error; Ca and Mn being the most likely candidates in pyroxenes. Intrasample variations in composition are not severe. The average temperature estimate for any particular sample has an error of 20 to 30°C. There appears to be an intersample correlation between the calculated activity of Mg in clinopyroxene and orthopyroxene and the Ca concentration in orthopyroxene. However, limited data makes this difficult to assess accurately. The same correlation is not observed between temperature and X(Ca) in orthopyroxene which suggests that the scattered results are caused by small errors in the Ca determination.

The calibrations of Kretz (1982) permit an assessment of the kinetics of the transfer and exchange reactions. There is moderate agreement between the two sets of results for most of the data, suggesting that the reactions have occurred at the same rate. The actual values, though, are not much lower than the Saxena (1976) estimates. Nor is there any reduction in the ranges of values calculated.

The absolute estimates of temperature are difficult to explain. There appears to have been attainment of equilibrium of Fe and Mg between the two pyroxene phases. The discrepancy between garnet-cordierite results and those obtained by the two pyroxene method is puzzling. It is not merely one of the pyroxene calibrations that gives these results, otherwise it could be suggested that the calibration in question was seriously in error. Nor does it appear to be a problem pertinent to the Tsu Lake data alone. With all the calibrations discussed there has been a consistent discrepancy in the calculated pyroxene temperatures of all metamorphic rocks. It has been suggested there are some ordering effects / exsolution in metamorphic pyroxenes which do not permit a comparison between them and the experimental data of rapidly quenched, non-ordered igneous pyroxenes (Lindsley, 1983).

Pyroxene-Ilmenite

Little is known about the thermodynamics of the Fe - Mg exchange between pyroxene and ilmenite. The reactions which describe the relationship are:

i. $\underset{\text{gei}}{MgTiO_3} + \underset{\text{fs}}{FeSiO_3} = \underset{\text{ilm}}{FeTiO_3} + \underset{\text{en}}{MgSiO_3}$

ii. $\underset{\text{gei}}{MgTiO_3} + \underset{\text{hed}}{CaFeSiO_3} = \underset{\text{ilm}}{FeTiO_3} + \underset{\text{diop}}{CaMgSiO_3}$

The equilibrium constants are defined in appendix 2.

Anderson *et al*. (1972) attempted calibrations of those two reactions using natural data and temperature - estimates from the magnetite-ilmenite geothermometer. Their attempts were not very successful mainly as a result of the assumptions in their calibration. Ilmenite comprises a solid solution field of $FeTiO_3$, $MgTiO_3$ and Fe_2O_3 which was treated as ideal. Later it was shown to be non-ideal (Bishop, 1980). Some inaccuracies were probably encountered in the magnetite - ilmenite geothermometer with the treatment of additional components.

Bishop (1980) investigated the thermodynamics of the reactions (i) and (ii) experimentally. Synthetic end-member starting materials were run in the temperature range of 800 to 1500 °C at pressures of 13 and 36 kb. Reversals were obtained for most of the runs. Deviations from ideal conditions for the relationship lnK(D) versus 1 / T (both reactions) suggested non-ideality of the $MgTiO_3$ - $FeTiO_3$ solid solution. A regular solution model was calculated from the data and applied to both calibrations. The ΔG(R) of the solid solution was assumed to be independent of temperature. The orthopyroxene solid solution was treated as ideal in the temperature range of the experiments as were the

Fe_2O_3 and the $FeTiO_3$ solid solutions.

Extrapolation of the geothermometers to phases formed below 1100 °C will probably result in complications. It is believed that the assumptions used above are not valid at lower temperatures. Other problems result because of the difficulties in analysing very small concentrations of Mg in ilmenite, which is critical for metamorphic ilmenites. The influence of additional components, such as Mn, to the pyroxene and ilmenite solid solutions, has been ignored.

Application.

Results of the application of both the orthopyroxene - ilmenite and clinopyroxene - ilmenite geothermometers are given in Table 3.4. The ferric iron content of the ilmenite was calculated by the method outlined in the appendix 1. Averaging was applied in the same manner as with the other geothermometers.

The results are somewhat scattered. Sample 141B appears to give anomalous results. The Mg content in the ilmenite of in this sample is unusually high. If this sample is excluded the range of values extends about 150°C for both geothermometers. There is about 100°C disagreement between the two calibrations. It should be noted that the temperatures for the clinopyroxene - ilmenite calibration are within the same range as those calculated for the two-pyroxene thermometer.

Several possible causes exist for these results. Firstly the ilmenite may not be a primary granulite facies phase. Magnetite readily exsolves ilmenite by oxidation as it cools down below granulite facies temperatures. Bohlen and Essene (1977) have noted the occurrence of exsolved ilmenite in the Adirondack granulites. The textures in the Tsu Lake rocks suggest that some of the ilmenite is secondary. Where ilmenite is the only opaque phase present its origin is uncertain. The temperatures obtained from the magnetite - ilmenite geothermometer indicate a reequilibration of the FeO - Fe_2O_3 - TiO_2 system or the presence of secondary "exsolved" ilmenite. It is not certain what would be the effect of resetting this system on the $MgTiO_3$ - $FeTiO_3$ system of a primary ilmenite.

Secondly there is the question of Fe - Mg ordering/exsolution effects in metamorphic pyroxenes. The temperature difference of the two reactions may be merely a result of the inadequate calibration of one or both of the geothermometers. Or it may

Table 3.4
Pyroxene - Ilmenite Geothermometry

	lnK(D1)	lnK(D2)	Opx	Cpx
8B	4.40		741	
8E	4.45		734	
22D		4.85		939
22L	4.65		700	
55C		5.07		839
56A	4.77		683	
141B	3.14	3.72	1012	1152
160	4.22	4.81	772	842
182A	4.64		704	
186A	4.24	4.73	768	867
231	4.50		722	

All temperature estimates are in °C
ln(KD1) - distribution coefficient for the opx-ilm equilibrium
lnK(D2) - distribution coefficient for the cpx-ilm equilibrium

yield information on the kinetics of the clino- and orthopyroxene reactions. It is significant that clinopyroxenes showed visible exsolution textures while this feature was not apparent in orthopyroxenes.

Thirdly there is the problem of additional components in all three phases. Mn is present in substantial amounts in ilmenite and in lesser concentrations in ortho- and clinopyroxenes. Minor amounts of V are present in ilmenite; and Ca, Na and Al are present in orthopyroxene. Their effect on the equilibrium conditions of the end-member reactions is unknown.

It is not certain whether the questions raised here can be resolved using the available data. A more definitive answer to the ortho-, clinopyroxene question perhaps could be achieved with resort to Mossbauer spectroscopy to obtain information on the site occupancies in pyroxenes. As more experimentation is conducted on the $MgTiO_3$ - $FeTiO_3$ system corrections for minor element influences could be made. The main conclusion is that the estimates from the clinopyroxene - ilmenite reaction do not represent granulite facies temperatures, while those of the orthopyroxene - ilmenite reaction are reasonable.

Magnetite-Ilmenite

The experimental studies of Buddington and Lindsley (1964) established a calibration of the compositional dependence of the solid solutions of coexisting magnetite and ilmenite on temperature and oxygen fugacity. Magnetite consists of a solid solution between Fe_3O_4 and Fe_2TiO_4 (ulvospinel). Only minor % $FeTiO_3$ is soluble in this series at geologic temperatures. At the time of formation of a magnetite all the TiO_2 present, should be accommodated solely in within the ulvospinel component. With a decrease in temperature from this time the TiO_2 in a magnetite is retained only if the cooling is sufficiently rapid or reducing conditions exist. Otherwise the excess TiO_2 is "exsolved" by oxidising Fe_2TiO_4 to $FeTiO_3$.

Reactions involving magnetite and ilmenite which are related to temperature and pressure are:

i. $6Fe_2TiO_4 + O_2 = 2Fe_3O_4 + 6FeTiO_3$

ii. $FeTiO_3 + Fe_3O_4 = Fe_2O_3 + Fe_2TiO_4$

iii. $4Fe_3O_4 + O_2 = 6Fe_2O_3$

The first two of these equations have been considered in the compositional isopleths of Buddington and Lindsley (1964) and Spencer and Lindsley (1981) whereas Powell and Powell (1977) give separate calibrations for each.

The hydrothermal experiments on synthetic Fe-Ti oxides of Buddington and Lindsley (1964) provided the basis for the construction of their oxygen fugacity-temperature-composition diagram. The intersections of the compositional curves of the magnetite and ilmenite solid solutions provide the estimates of temperature and fO_2.

The calibration suffers from a number of limitations. The curves were constructed from a restricted composition range and involved extrapolation to temperatures and oxygen fugacities outside the range of the experiments. The use of synthetic end-member materials did not allow the influence of minor elements to be assessed. Natural Fe-Ti oxides containing minor elements must be normalised to end-member components before application to the calibration.

The Spencer and Lindsley (1981) calibration incorporated new experimental data obtained from a wider temperature, oxygen fugacity and compositional range. The application of a solution model to the system resolved some of the problems encountered with the Buddington and Lindsley (1964) calibration. Normalisation procedures must still be applied. The Powell and Powell (1977) thermodynamic approach was found by Spencer and Lindsley (1981) to be useful only for a limited range of temperatures and oxygen fugacities.

The necessity of interpreting metamorphic magnetite - ilmenite textures places limitations on the application of the geothermometer-oxygen barometer. Bohlen and Essene (1977) assumed that the primary premetamorphic magnetite in their samples was free of exsolved ilmenite. They devised a procedure whereby the exsolved ilmenite, now present, could be reintegrated to derive the original composition of the metamorphic magnetite. Application of this procedure to the Adirondack orthogneissic granulites yielded temperatures in the range of 620 - 800°C, reasonable conditions for the area.

According to Buddington and Lindsley (1964) a primary igneous magnetite containing "exsolved" ilmenite could be equilibrated with independent ilmenite grains during metamorphism. This would probably involve partial resorption of the exsolved ilmenite lamellae. The question arises as to whether total resorption would result. The answer to this question is dependent on the kinetics of the resorption reaction. In hydrothermal experiments synthetic Fe-Ti oxides react rapidly (1 - 2 hours at 1000 °C, Buddington and Lindsley, 1964), hence it could be expected that total resorption would take place during metamorphism. However, under natural conditions the exsolved ilmenite lamellae would not necessarily be in contact with a fluid phase. The change in oxygen fugacity would take place through an interface of magnetite.

Even assuming that total resorption does take place the validity of the reintegration procedure used by Bohlen and Essene (1977) must be examined. Bowles (1977) noted that several generations of exsolved ilmenite within a single magnetite grain, represented the various stages in the cooling history of the rock. Reintegration techniques must encompass all the stages of ilmenite exsolution to be sure of obtaining the homogeneous magnetite composition. The Bohlen and Essene (1977) technique utilised only magnetites with homogeneous ilmenite lamellae, although the textures reported suggested more than one generation of ilmenite exsolution. The stage of the cooling process that their temperatures represent, is unknown.

Oliver (1978) showed that the cooling history of a granulite facies terrain could be established by applying the magnetite - ilmenite geothermometer to complex intergrowths of exsolved ilmenite in magnetite. The complexity of the exsolution textures of ilmenite in magnetite was shown to decrease with decreasing temperature.

Application.

The reintegration technique used by Bohlen and Essene (1977) or Bowles (1977) was not attempted in this study. The textural relations observed in and between the oxide phases are too complex to allow adequate interpretation. Magnetite contains exsolved ilmenite in two principal forms; (i) as thin lamellae and (ii) granular blebs of ilmenite at the grain boundaries. Ilmenite other than the exsolved variety occurs adjacent to magnetite. Frequently this variety contains blebs of exsolved magnetite and rutile. Hercynite is present in rocks of appropriate composition with exsolved magnetite and corundum associated with the rims.

Ilmenite-magnetite pairs representing the most homogeneous grains i.e., devoid of "proper exsolution" rather than "oxidation exsolution" features, were tested with the

Spencer and Lindsley (1981) calibration. Undoubtedly some of the ilmenites selected were exsolved ilmenite granules. The temperatures obtained in this way will give an estimate of the temperature when Ti migration effectively ceased.

The temperatures obtained were in the range of 520 - 590°C, averaging 550 °C. The results are not presented here and they are useful only in their implications for the temperature estimates of other geothermometers. Any estimates below 590°C clearly do not record peak metamorphic temperatures. Such is the case with the garnet - biotite estimates; a further indication of the disequilibrium of that system.

Any attempt to evaluate the magnetite-ilmenite system of a metamorphic rock for consistency should involve a procedure similar to that used by Bowles (1977) or Oliver (1978). It is suspected though, that the reintegration of all the textural patterns would be considerably more difficult in a metaigneous than an igneous rock.

Two Feldspar

The occurrence of coexisting plagioclase and alkali feldspar in several samples could be considered suitable for the application of the two feldspar geothermometer. In practice however, the method is less than ideal. The plagioclase feldspars are coarsely antiperthitic. Application of the geothermometer would require reintegration techniques similar to those outlined by Bohlen and Essene (1977) and Whitney and Stormer (1977). There is also the problem of whether the feldspar pairs are in equilibrium with each other.

The two feldspar thermometer is based on the solubility of albite in plagioclase and alkali feldspar. Several calibrations have appeared since Barth (1951) first proposed the system for use as a geothermometer. Not all of the calibrations available are based on sound thermodynamic premises. Brown and Parsons (1981) outline in detail the failings of some . Their arguments are summarised below.

According to Brown and Parsons (1981) both Stormer (1975) and Powell and Powell (1977) treat the feldspar solid solutions as a double binary system. The effect of the orthoclase component on the mole fraction of albite in plagioclase and the effect of the anorthite content on the mole fraction of albite in alkali feldspar are ignored. Treatment of parts of the system as binary when the components are part of a ternary system is invalid. There is also no experimental basis for the construction of such thermometer. The binary Margules parameters necessary for that are insufficiently known. The correct formulation of the feldspar thermometer would require a knowledge of the ternary Margules parameters, which at present, are still unknown.

Most of the experimental data used for the calibration are for feldspars with complete Al-Si framework disorder. However natural feldspars, especially those formed during slow cooling conditions, are likely to exhibit finally some degree of ordering. It is not known whether the initial formation of a feldspar crystal would involve an ordered or disordered state. Nor is the structural state known at the time when equilibrium was reached. Whitney and Stormer (1977) proposed a modification to the Stormer (1975) calibration which accounted for the structural state of the feldspars. Their justification for this was based on the differences observed in the experimental thermodynamic data for ordered and disordered feldspars. There is some disagreement as to whether the observed differences have a physical basis.

Finally there is the problem of attainment of equilibrium. Thermometers based on graphical or numerical procedures do not provide a criterion for testing for this. However, Brown and Parsons (1981) outline several areas where feldspars could be tested for equilibrium.

In view of the preceding discussion the feldspar pairs (involving antiperthic plagioclase) were subjected to the criteria of Brown and Parsons (1981). It appears that peak metamorphic equilibrium was never reached or, if it was that it has not been retained. It is doubtful that reintegration of exsolved alkali feldspar in plagioclase would accomplish an equilibrium pair. Low temperatures are suggested by the structural state of the alkali feldspar (microcline) and the very low anorthite content of the same. The structural state of the K-feldspar also implies that the area has undergone slow cooling.

Geobarometry

The most useful geobarometer is one which involves the partitioning of components between different phases. At least three phases are usually involved in the reaction, with the components of interest being exchanged between two of the phases. The volume change of the reaction critically determines the pressure dependency on the K(D) but such reactions are usually temperature dependent as well.

The assemblage grnt-cord-sill-qtz is present in the Tsu Lake rocks and permits the use of the grnt-cord geobarometer. Another assemblage which could have been used, is based on the exchange of Al between orthopyroxene and garnet (Newton, 1983). Unfortunately the assemblage is rare at Tsu Lake and a polished thin-section of a sample containing this assemblage was not available.

Garnet-Cordierite Geobarometer

The reaction:

cordierite = garnet + sillimanite + quartz

forms the basis for a geobarometer. Because both garnet and cordierite are dominantly solid-solution series of Fe^{2+} and Mg the geobarometer is governed by the end-member reactions:

i. $1/2Mg_2Al_4Si_5O_{18} = 1/3Mg_3Al_2Si_3O_{12} + 2/3Al_2SiO_5 + 4/5SiO_2$ (metastable)

ii. $1/2Fe_2Al_4Si_5O_{18} = 1/3Fe_3Al_2Si_3O_{12} + 2/3Al_2SiO_5 + 4/5SiO_2$.

The problems which affect the calibration of the garnet-cordierite geothermometer are inherently worse in the geobarometer. The conflicting data, both experimental and derived, may be summarised as follows:

a. negative dP/dT slopes for both reactions, i.e., K(D) increasing with temperature (Hensen and Green, 1971; Weisbrod, 1973; Holdaway and Lee, 1977; Thompson, 1976);

b. positive dP/dT slopes for both reactions (Hutcheon *et al.*, 1974); Martignole and Sisi, 1981; Aranovich and Podlesskii, 1983);

c. a positive slope for reaction (i) and a negative slope for reaction (ii) (Newton and Wood, 1979).

In evaluating the conflicting data consideration must be given to the sources of the data. For case (a) experiments were used to evaluate hydrous conditions of reaction (ii) only; reaction (i) being derived from theoretical considerations of reaction (ii). Newton and Wood (1979) calculated the dP/dT slope of reaction (i) from measured thermodynamic data. Reaction (ii) was derived from the experimental data of Weisbrod (1973) using the Newton and Wood (1979) hydration theory; hence the same sign of the dP/dT slope for reaction (ii) as in case (a). The postulated dP/dT slopes of reactions (i) and (ii) were derived, in the case of Martignole and Sisi (1981), from the metastable Mg anhydrous reaction using the available thermodynamic data and the Martignole and Sisi (1981) hydration theory. Derivation of the Fe end member reaction was achieved from reaction (i) following the theoretical considerations advocated by Thompson (1976). With Aranovich and Podlesskii (1983) the calibrations were obtained from experimental data.

The largest inconsistency lies in the orientation of reaction (ii). Aranovich and Podlesskii (1983) suggested that the experiments performed for reaction (ii) by all the authors of case (a), were insufficient to support the interpretation that was achieved. The presence of hercynite inclusions in the starting materials may have resulted in a distortion of the equilibrium conditions. Martignole and Sisi (1981) offered an alternate explanation: insufficient experimental time for the attainment of hydration equilibrium.

If reaction (i) is derived from this data (case (a)) then it too will assume the same sign for the slope dP/dT. This would account for the discrepancy of a negative dP/dT slope for the metastable reaction (i) with observed data on the breakdown of the stable hydrous Mg cordierite (Lonker, 1981).

The size of the slope of the Mg end-member reaction differs between case (b) and case (c). However conflicts between the hydration models used, account for this. Newton and Wood (1979) consider H_2O to be in solid solution with cordierite. However, the exact H_2O content of the fully hydrous end member is unknown and has been arbitarily assigned a value for use in their calculations. Martignole and Sisi (1981) showed that the hydration experimental results depart significantly from a solid solution model. They suggested the results fit better a model of chemical and physical equilibrium between hydrous cordierite and H_2O vapour similar to the H_2O adsorption behaviour of zeolites. Both models are based on the hydration data of Mirwald and Schreyer (1977).

The experimental data collected by Aranovich and Podlesskii (1983) most closely resemble the theoretical models of Martignole and Sisi (1981). However, the hydration model used by the former authors, like Newton and Wood (1979), assumed ideal solution between wet and dry cordierite end members. A compilation of all available hydration data was used by them to determine the dependency of the hydration state on temperature and pressure.

Application.

Application of the Martignole and Sisi (1981) geobarometer requires the knowledge of the water content of cordierite. For an analysis obtained using the microprobe this presents a problem. Only a rough estimate can be expected from an indirect determination by difference of the oxides from 100 weight percent. The estimate is naturally dependent on the accuracy of the analysis.

With cordierite there is less chance of error than with a hydrous phase which contains an unknown ferric/ferrous ratio, such as biotite. However, the real danger of this approach is the assumption that all the H_2O by difference is due to H_2O. Volatile or other components undetectable by electron microprobe analysis may also be present, for example, CO_2.

Martignole and Nantel (1982) used a semiquantitative estimate of the fluid content, based on electron microprobe data. Very crude estimates of the fluid composition were obtained from optical data. Armbruster and Bloss (1980) found that the 2V and optical sign of cordierite was related to the composition of the channel fluids. CO_2-rich cordierite is optically positive; H_2O-rich cordierite is optically negative with a small 2V and anhydrous cordierite has a 2V close to 90°.

Estimates of the H_2O content were obtained for all the cordierite-bearing samples, although only three contained the appropriate assemblages for garnet-cordierite geobarometry. The analytical error in the fluid content for averaged analyses of each sample, ranged from 0.12 to 0.45 weight percent. The errors noted for Martignole and Nantel (1982) analyses, were more than double this, 0.5 to 0.9 weight percent. The calculated values for nH_2O are given in Table 3.5. For the samples containing the appropriate assemblage the average nH_2O is 0.82.

Estimates of the total pressure were obtained from the nH_2O - Mg-cord - Mg-grnt isopleth diagram in Martignole and Sisi (1981). The total pressure, averaged, is about 5.7 kb, Table 3.5, when an nH_2O of 0.8 is assumed. No attempt was made to estimate the fH_2O because of the inherently large errors involved in this calculation. From the same diagram the temperature may also be estimated. An average of 700 °C for the grnt-cord-sill-qtz assemblage was obtained, which is slightly higher than the temperatures calculated from the Fe-Mg grnt-cord geothermometer. If a much lower nH_2O is assumed then pressures of

Table 3.5
Garnet - Cordierite Geobarometry

	$n(H_2O)$	1.		2.		3.	
44	0.96	5.3	700	4.5	720	4.5	675
135B	0.93	5.8	700	4.5	700	4.0	680
239B	0.56	5.8	700	4.5	700	4.0	680

1. - Martignole and Sisi (1981) for $n(H_2O)=0.8$
2. - Martignole and Sisi (1981) for $n(H_2O)=0.5$
3. - Aranovich and Podlesski (1983)

Pressure values are all in kbar.
Temperature estimates are all in °C.

4.5 kb and temperatures of 700 °C, are obtained.

Pressure and temperature estimates were obtained from a similar Mg-cord - Mg-grnt isopleth diagram of Aranovich and Podlesskii (1983). For this diagram P(total) is assumed to equal PH_2O. From this calibration the pressures were about 4.0 to 4.2 kb, and the temperatures were around 650 to 700 °C, Table 3.5.

The Aranovich and Podlesskii (1983) geothermo-barometer yields temperatures that are in close agreement with the temperatures obtained for the Fe-Mg exchange grnt-cord goethermometer. It suggests that perhaps the pressure estimates from this calibration are more realistic than the pressures obtained from the 0.8 nH_2O Martignole and Sisi (1983) calibration. However, this depends on the accuracy of the grnt-cord geothermometer. The pressures calculated by assuming a lower nH_2O are more in accordance with the Aranovich and Podlesskii (1983) calibration, which suggests that perhaps the fluid composition of the cordierite channel fluids is not 100 percent H_2O. Both pressure calibrations are subject to large errors, because the cordierite and garnet isopleths intersect at small angles.

Conclusions

There is a discrepancy of 150 °C in the temperatures estimated for the Tsu Lake basic assemblage, Tables 3.3 and 3.5, and the Tsu Lake pelitic assemblage, Tables 3.1 and 3.2, if the temperatures calculated from the various calibrations of the relevant geothermometers, are assumed to be correct. From earlier discussions, it would appear that the geothermometers involving one, or both of the pyroxene phases record temperatures that are inconsistent with other mineral thermometers.

Petrographical and field observations suggest that both the pelitic and basic lithologies have experienced the same phase of metamorphism. The stability regions of the mineral reactions discussed in the first part of this chapter, suggest that the basic and the pelitic assemblages can only have crystallised at the same temperatures if $P(H_2O < P(tot)$. Estimates of pressures from the pelitic assemblages support this statement; temperatures calculated from the grnt - cord - sill - qtz geothermometer-geobarometer agree only with temperatures calculated from the Fe-Mg grnt - cord geothermometer if $P(H_2O)$ is assumed less than P(tot). Also the temperatures implied by the presence of the amphibole breakdown reaction, are inconsistent with the opx-cpx geothermometry.

The best estimate for the temperature of metamorphism in the Tsu Lake area is 700±50°C. Pressure is estimated at 4.5±0.5 kb. Estimates of the pressure-temperature conditions at Deskenatlata Lake are difficult to achieve, primarily because of the lack of data. A reasonable estimate of temperature would be 600 to 650 °C; based on the pelitic assemblage and the absence of a hornblende breakdown reaction.

CHAPTER 4

GEOCHEMISTRY

Two topics are addressed in this chapter:

a. the nature of the large ion lithophile (LIL) element patterns in the Tsu Lake granulites;

b. the rare earth element (REE)[2] characteristics of a low pressure granulite facies terrain as exemplified by the Tsu Lake granulites.

Both topics are concerned with problems that are related to granulite facies metamorphism in general, rather than specific problems pertinent to the Tsu Lake area alone.

Fifty five samples were selected for geochemical analysis. The samples are believed to represent the range of lithologies found at Tsu Lake. Major and minor elements which were determined are: Si, Al, Fe^{3+}, Fe^{2+}, Mn, Mg, Ca, Na, K, Ti, H_2O, P, CO_2 and S. The following trace elements were determined: Pb, Yb, La, Ba, Nb, Zr, Y, Sr, Rb, Cu, Ni, Cr, Co, V, U, Th, Mo, B, and Be. Details on the analytical technique may be found in appendix 1.

The classification of the lithologies into metaigneous and metasedimentary groups was first attempted by use of discriminant function of Shaw (1972). The suitability of the discriminant function as a means of distinguishing the rock origins in the Tsu Lake area was tested on a number of samples which are known to have an igneous origin. Several samples of the dykes which intrude the Tsu Lake granulites had been analysed for this purpose. The metagabbroic unit was also used as a test case. The discriminant function for these samples indicated sedimentary protoliths. Thus it would appear that the discriminant function is not a reliable indicator of sedimentary and igneous protolithologies. It may be that the discriminant function of Shaw (1972) is unreliable for distinguishing the origins of rocks of basic compositions. However, van de Kamp *et al*. (1976) reached a similar conclusion to that suggested here, regarding the use of the discriminant function of Shaw (1972) on rocks of granodioritic composition.

---

[2] The term rare earth element/elements is used to denote any one of the elements in the group of lanthanides from La to Lu. Sometimes the element Y has been included in this group, although this is not the case in this thesis.

The discrimination diagrams of Leake (1969) and van de Kamp *et al*. (1976), which utilise Niggli numbers, have been tested on unmetamorphosed sedimentary and granitic rocks. The trends seen in the chemical variations between mg - Si, Zr - Si and mg - Cr or Ni, appear to be more reliable indicators of sedimentary and igneous origins. The data on the Tsu Lake samples were tested for significant trends between the components listed above, and were classified as metaigneous or metasedimentary accordingly. These classifications are not altogether conclusive because of the small number of samples which were analysed. Statistical tests could not be applied to each data group for this reason. The data have been presented in appendix 3 under the appropriate group classifications. A third group, the granitic lithologies, was defined on the basis of field associations. These rocks are believed to be the partial melts of pelitic units.

An indication of the compositional variation within the metaigneous and metasedimentary groups, is given in Tables 4.1 and 4.2. Two of the metaigneous samples 200A, and 1B, show very unusual compositions in comparison with other samples. The Al_2O_3 content of these two samples is very low and the MgO content is very high. High concentrations of Ni and Cr are also observed. The compositions suggest perhaps the rocks were originally olivine cumulates. However, the igneous classification of these two samples could be questioned on the basis of their field associations and their LIL element characteristics. Bostock (1982) suggested that some of the amphibolites were derived from iron formations. The metasedimentary samples show the range in compositions from restite to migmatite and quartzofeldspathic rocks.

Significance of LIL element patterns in granulites

Many observations have been made on the apparent depletion of the LIL elements, K, Rb, Cs, and two heat producing elements Th and U, in rocks of granulite facies grade (Lambert and Heier, 1968; Heier, 1973; Sighinolfi, 1969; 1971; Lewis and Spooner, 1973; Field and Clough, 1976; Collerson and Fryer, 1978; Allen, 1979; Barbey and Cuney, 1982; additional references have been cited by these authors). High K/Rb ratios occur because of the fractionation of K relative to Rb. In contrast other LIL elements, Ba

Table 4.1
Whole Rock Geochemical Analyses: Metaigneous Lithologies

Sample no.	200A	1B	GAB	186A	130	178
SiO_2	48.4	50.9	47.7	50.4	58.6	62.7
Al_2O_3	6.2	7.7	16.4	15.3	16.8	17.2
Fe_2O_3	2.6	2.3	1.7	1.1	2.1	2.2
FeO	10.1	6.2	7.0	9.1	5.1	3.5
MgO	1.2	18.4	11.0	7.21	3.70	2.37
CaO	3.96	9.40	11.5	9.49	5.85	5.03
Na_2O	nd	1.1	0.6	2.0	1.2	3.0
K_2O	1.59	1.91	0.58	1.10	1.88	2.03
TiO_2	0.65	1.13	0.22	0.66	0.85	0.78
MnO	0.20	0.14	0.18	0.25	0.12	0.11
S	0.45	0.31	0.03	0.24	0.19	0.11
P_2O_5	0.06	0.49	nd	0.15	0.38	0.22
H_2O	4.8		2.7	1.5	1.4	1.1
CO_2	nd		0.1	nd	0.1	0.1
V	130	140	170	180	150	110
Cr	2200	977	460	160	39	23
Ni	1000	308	210	88	32	14
Cu	130	103	60	89	92	14
Co	220	64	57	42	23	20
Rb	115	146	290	31	93	122
Sr	36	412	130	260	580	770
Ba	65	922	43	340	870	1600
Zr	44	155	134	61	140	198
Nb	2	8	9	3	8	12
Y	38	23	35	40	39	43
Pb	11	16	45	22	28	26
U	0	3	0	6	0	0
Th	0	15	3	6	8	22

trace elements concentrations are given in ppm

Table 4.2
Whole Rock Geochemical Analyses: Metasedimentary Lithologies

Sample no.	23C	142C	23B	59	83A	215	54A
SiO_2	38.4	48.1	54.1	55.1	60.3	67.7	74.0
Al_2O_3	25.5	18.5	17.5	22.9	23.8	15.2	14.2
Fe_2O_3	6.2	6.4	3.6	2.3	nd	4.8	nd
FeO	15.9	10.1	11.1	8.5	0.6	4.0	0.3
MgO	5.71	6.47	3.90	3.04	0.28	1.89	0.13
CaO	0.36	1.77	3.21	1.30	5.53	0.14	0.48
Na_2O	nd	0.7	1.2	0.9	5.5	nd	2.1
K_2O	1.15	2.99	1.32	3.44	2.33	2.22	8.05
TiO_2	2.57	1.77	0.94	1.00	0.05	0.98	0.07
MnO	0.62	0.2	0.56	0.18	0.03	0.08	0.01
S	0.12	0.03	0.04	0.09	0.01	0.04	nd
P_2O_5	0.01	0.03	0.03	0.03	0.04	0.02	0.13
H_2O	2.4	1.8	1.4	1.2	0.7	2.0	0.4
CO_2	0.1	0.2	0.1	0.1	0.1	nd	nd
V	410	260	130	160	34	96	18
Cr	41	460	210	190	17	140	nd
Ni	180	140	60	85	10	56	nd
Cu	25	5.6	18	23	18	16	5.7
Co	50	51	30	35	nd	24	12
Rb	89	168	73	189	29	118	432
Sr	37	250	310	250	79	42	240
Ba	730	1500	550	1300	330	650	780
Zr	762	376	452	226	46	279	7
Nb	30	14	6	15	2	10	2
Y	83	28	110	70	29	26	29
Pb	13	27	23	34	45	12	62
U	9	0	3	0	7	0	31
Th	14	12	21	13	18	17	6

trace elements concentrations are given in ppm

and Sr, have normal to enriched abundances relative to concentrations in amphibolite facies terrains. These geochemical features were thought to be characteristic of medium to high-pressure granulites (Lambert and Heier, 1968), with geobarometric data indicating depths of formation of 35 to 50 km for depleted granulites, and 25 to 35 km for undepleted granulites (Condie *et al.*, 1982).

There are, however, a number of reports indicating a lack of the LIL element depletion characteristics. Sometimes the presence of variations in the characteristic LIL element patterns for granulite facies terrains are reported. U in particular, may show variable behaviour (Gray, 1977; Dostal and Capedri, 1978; Barbey and Cuney, 1982). Some examples of areas where the characteristic LIL element features are not shown are:

i. the intermediate-pressure granulite facies terrain of Mt. Aloysius, Tomlinson Range, Australia, (Gray, 1977);

ii. the high-pressure granulite facies terrain of Stary Gieraltow, East Sudetes, Poland, (Tarney and Windley, 1977);

iii. the intermediate-pressure granulite facies terrain of the Arunta Block, central Australia, (Allen, 1979);

iv. the intermediate to high-pressure Lapland Granulite belt (Barbey and Cuney, 1982);

v. the intermediate to high-pressure granulites of the Arendal-Tromoy region, southern Norway (Field *et al.*, 1980);

vi. the high-pressure granulites of Madras, India (Weaver, 1980).

Examples of LIL depletion in amphibolites facies terrains have been reported by Field and Clough (1976), Lambert (1976), Moorbath (1969, 1976).

Early theories on the mechanisms of LIL element depletions have been summarised by Tarney (1976):

i. the depletion is a Precambrian process caused by mantle degassing which provides fluids for the transport of the LIL elements (Tarney *et al.*, 1972; Sheraton *et al.*, 1972);

ii. granulites are the mafic to intermediate restites which remain after a melt enriched in the LIL elements is removed (Fyfe, 1973);

iii. the anhydrous assemblages which develop in high-pressure granulites cannot accommodate the LIL elements and these are removed by metamorphic fluids (Heier, 1973; Tarney, 1976);

iv. depletion is a primary feature (Holland and Lambert, 1975);

Clearly none of these theories can adequately explain why there should be variable depletions in the LIL elements, such as in those areas cited above. Nor do they explain why depletion processes are apparently independent of metamorphic grade. More recent theories, some comprising combinations of those hypotheses cited above, postulate that LIL element depletion processes are controlled by:

i. the composition of the host rock, and the mineral-fluid or mineral-melt-fluid equilibria (Rollinson and Windley, 1980; Barbey and Cuney, 1982);

ii. metasomatism postdating the granulite facies event (Allen, 1979).

The interest in the possibility of the metamorphic fluid as a fractionating agent for the LIL elements has stemmed from studies of fluid inclusion compositions in granulite facies rocks. The fluid phase appears to be composed of mixtures of H_2O, CO_2, halogens and perhaps S-bearing species (Collerson and Fryer, 1978; and references therein). As the LIL elements, K, Rb, Cs, are all capable of forming soluble halides, a fluid enriched in the halogens could conceivably remove these elements. U forms the soluble complex ionic species, UO_2^{2+}, and $[(UO_2)(CO_3)_2]^{2-}$ (Collerson and Fryer, 1978). Th forms soluble chlorides and sulphates in acidic solutions and hydroxides in basic solutions.

The strongest argument against a fluid phase as a LIL depleting agent is based on the quantitative aspects of the hypotheses above. The concentration of the halogens in the metamorphic fluid is uncertain and therefore may not be high enough to remove sufficient quantities of the LIL elements to cause an observable depletion. Estimates of the amount of fluid required to bring about a LIL depletion suggest the actual volume of fluid is small (Rollinson and Windley, 1980) and such fluid could be derived from dehydration reactions. Such estimates are tentative, however, because of the lack of information on mineral/fluid partition coefficients for the LIL elements.

Some evidence was found, which supports the fluid phase transport hypothesis (Dostal and Capedri, 1978). U distribution in both amphibolites and granulites from the Valle Strona area, Italy was examined by fission track methods. Dostal and Capedri (1978) observed that in the amphibolite facies rocks the bulk of the U resides in the accessory phases, sphene, rutile, apatite, and zircon, and a minor amount of U is associated with fractures or the margins of the hydrous minerals, biotite and hornblende. In the granulites U was found only in the accessory minerals. The conclusion reached was that the depletion of U in the granulites was due to the leaching of U from fractures and grain boundaries by migrating fluids.

Evidence against hypotheses which contend that the LIL depletion characteristics are a primary feature is found in the K/Rb ratio trends of depleted granulite terrains. For igneous rocks the K/Rb ratio increases with an increasing amount of K. Shaw (1968) established a "main trend" which defines the K and Rb fractionation of igneous rocks. Similar K/Rb versus K trends have been noted for depleted granulite facies terrains although the variation is different from that observed for igneous rocks (Field and Clough, 1976). The divergence from an igneous fractionation trend has been interpreted to reflect a chemical differentiation process unrelated to igneous processes or the original LIL element characteristics. The K-Rb fractionation trends are dissimilar for the different granulite facies terrains. Barbey and Cuney (1982) applied a statistical analysis to the K-Rb data from sedimentary, metasedimentary and metaigneous rocks and noted that the K/Rb trends are dependent on the mineralogy of the rock type.

Tsu Lake LIL element characteristics

For the purpose of data presentation the Tsu Lake granulites have been divided into the three groups mentioned earlier: that is metaigneous, metasedimentary and granitic lithologies. The metasedimentary group includes both migmatite and restite samples. The relationships between: K-Rb, K-Sr, K-Ba, Rb-Sr, Ba-Rb and Ba-Sr, are shown in Fig. 4.1 to Fig.4.6.

The range of the K/Rb ratios shown by the metasediments is from 98 to 667, Fig. 4.1. Some of the extreme K/Rb values are for restite samples where K and Rb have both been depleted relative to the original pelitic sediment. This is seen more clearly in the actual K (0.95 - 6.8 wt.%) and Rb (28 - 440 ppm) values and by a comparison with average values of sedimentary rocks. The "average" shale has 4 wt. % and 174 ppm of K and Rb respectively, resulting in a K/Rb ratio of 230 (Barbey and Cuney, 1982). Greywackes display more variable K and Rb concentrations because their compositions are strongly dependent on the source rocks of the detrital material. Average values of K (1.9 wt. %) and Rb (79 ppm) have been quoted (Barbey and Cuney, 1982).

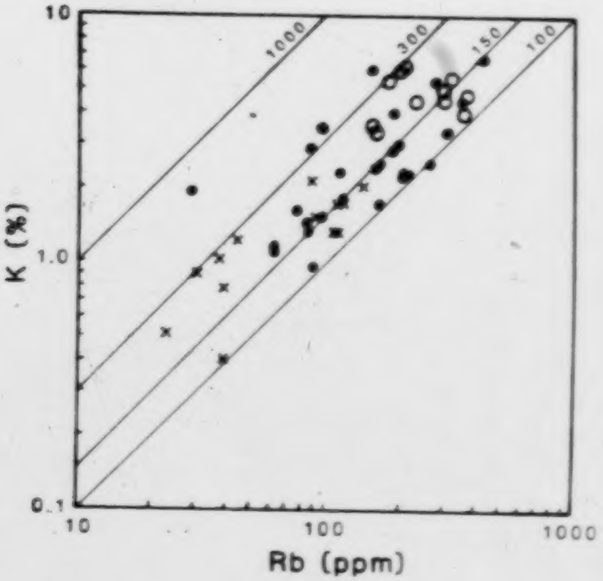

Fig. 4.1. Relationship between K (wt. %) and Rb (ppm) for the Tsu Lake samples. Symbols: metasediments (closed circles), metaigneous rocks (crosses), granitic rocks (open circles).

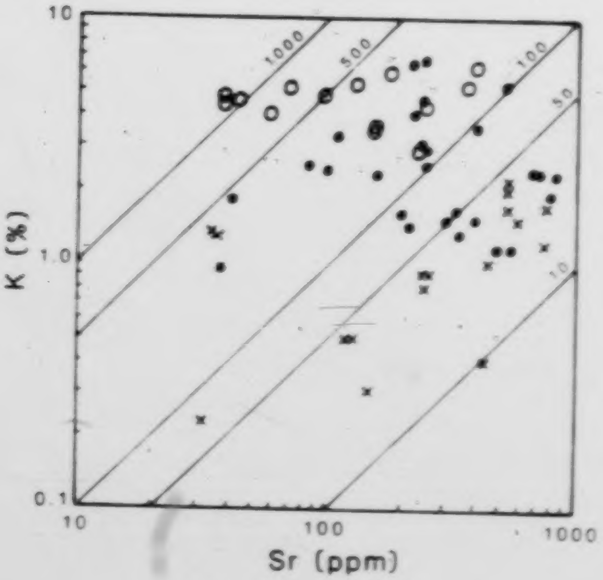

Fig 4.2. Relationship between K (wt. %) and Sr (ppm) for the Tsu Lake samples. Symbols: metasediments (closed circles), metaigneous rocks (crosses), granitic rocks (open circles).

Except for several extreme values most of the metasedimentary K/Rb ratios fall within the range of "normal" values, K/Rb < 300, i.e., there is no evidence of depletion.

The metaigneous rocks have K/Rb ratios that lie between 100 and 300 which is within the limits of what is accepted as undepleted. The concentrations of Rb (11 - 290 ppm) and K (0.4 - 2 wt. %) are much lower than those of the metasediments and merely reflect the rock type.

The granitic rocks also display a restricted range of K/Rb ratios, 114 to 300. The narrow range of K/Rb ratios reflects the same mode of formation of these rocks. In contrast to the metaigneous rocks or the restite samples, the high K concentrations (3.4 - 6.4 wt. %) and the Rb concentrations (160 - 370 ppm) of the granitic rocks indicate the strong fractionation of these elements into the melt phase.

The most significant feature of the relationship between K and Sr, Fig. 4.2, is the division of the data into three groups, corresponding to the three main lithologic types. The majority of metaigneous samples have K/Sr ratios which are less than 50. One sample which shows an extreme value of 373, is of dubious igneous origin. The metasediments show a much wider range of K/Sr ratios (22 - 498) although the data are scattered and do not define a linear trend. The granitic samples display the most extreme range of K/Sr values (164 - 1288) and show a trend of increasing Sr with almost constant K.

Depleted granulite terrains exhibit average K/Sr ratios of about 15 (Allen, 1979). Higher values are expected for undepleted terrains or those which have experienced metasomatism. The enriched K/Sr ratios of the Tsu Lake granulites are partially explained by the individual K and Sr values of each lithologic group. Of the three units the granitic lithologies display the most restricted range of K, and Sr (38 - 400 ppm) values. The range of Sr values for both the metasediments and the metaigneous samples is much wider than is found for the unmetamorphosed equivalents (see Barbey and Cuney, 1982, for references), suggesting that Sr has been enriched in these rocks.

The K/Ba ratios show similar patterns for each lithologic group as shown by K-Sr, Fig. 4.3. Again the granitic rocks show the most extreme range of K/Ba ratios (24 - 1482). The metaigneous rocks have the lowest K/Ba ratios (9 - 40). The metasediments have a wider range of K/Ba ratios (13 - 106) than the metaigneous rocks, although this range reflects the extreme values of only a few samples. The average K/Ba ratio is only

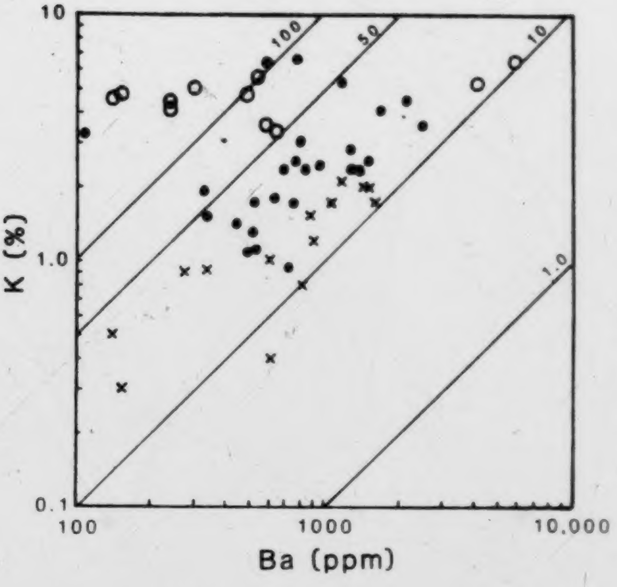

Fig. 4.3. Relationship between K (wt. %) and Ba (ppm) for the Tsu Lake samples. Symbols: metasediments (closed circles), metaigneous rocks (crosses), granitic rocks (open circles).

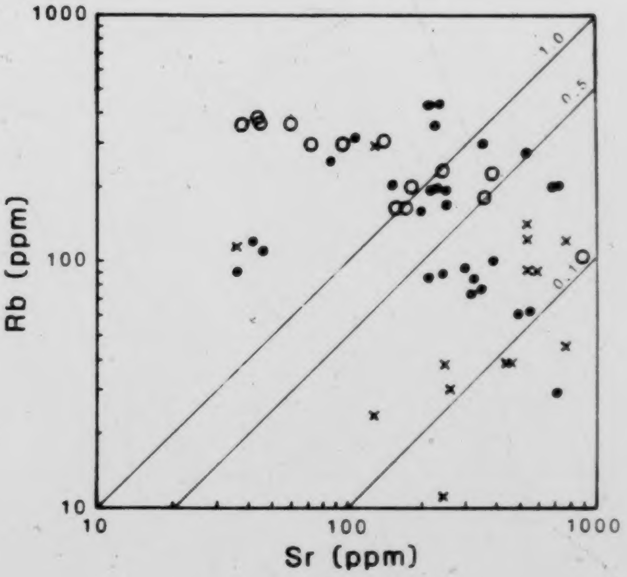

Fig. 4.4. Relationship between Rb (ppm) and Sr (ppm) for the Tsu Lake samples. Symbols: metasediments (closed circles), metaigneous rocks (crosses), granitic rocks (open circles).

slightly higher than the average of the metaigneous rocks.

K/Ba ratios of 10 are expected for depleted granulite terrains; undepleted terrains have K/Ba ratios of 25 to 50. As with K/Sr ratios and the Sr concentrations, the Ba concentrations for each group are indicative of the K/Ba ratios; granitic rocks have the smallest range of Ba values, 140 - 580 ppm, metasediments have Ba contents in the range, 110 - 2500 ppm, and the metaigneous rocks have Ba contents of 140 - 1500 ppm.

The relationships between Rb-Sr, Fig. 4.4, Ba-Rb, Fig. 4.5, and Ba-Sr, Fig. 4.6, reinforce the group trends noted between K and Rb, Sr and Ba. The coherent geochemical behaviour of Sr and Ba, in this instance, is shown in the relationships between Ba-Rb and Rb-Sr. The granitic rocks have the most extreme ranges of Rb/Sr (0.5 - 9.4) and Ba/Rb (0.2 - 27) ratios. The Ba/Rb ratios for the metasediments and the metaigneous samples range from 1.45 to 26, and 0.2 to 26 respectively. For Rb/Sr the metasediments show ratios ranging from 0.12 to 2.95, and the metaigneous rocks have ratios of 0.05 to 3.2. Depleted terrains normally have Ba/Rb ratios between 60 and 100 and Rb/Sr values of 0.02. The Ba/Rb ratios for all the units of the Tsu Lake granulites suggest undepleted characteristics. The Rb/Sr ratios, however, tend to be more enriched than is usual for an undepleted terrain.

Both the granitic units and the metaigneous samples show more regular distributions between Ba-Rb, Ba-Sr and Rb-Sr than do the metasediments. This is particularily evident in the Ba-Sr relationships where there is almost a constant Ba/Sr ratio for the granitic samples, 4, and the metaigneous rocks, 1. The scattered data for the metasediments, Fig. 4.6, are probably a reflection of the variety of rock types this lithologic group encompasses, i.e., restites and migmatitic samples.

In summary, the Tsu Lake granulites show LIL element patterns that are not consistent with those seen in depleted terrains. Allen (1979) reported similar features for the Utralanama Block in central Australia. In those granulites the average K/Rb and Ba/Rb ratios are indicative of undepleted terrains, while the K/Sr and Rb/Sr ratios are unusually high and the K/Ba ratio suggests depletion. Allen suggested that the anomalous geochemical features were caused by a metasomatic event after an initial granulite facies event.The metasomatism restored some of the LIL depletions caused by the earlier metamorphic event. He also suggested that the K/Ba ratio may be more indicative of the

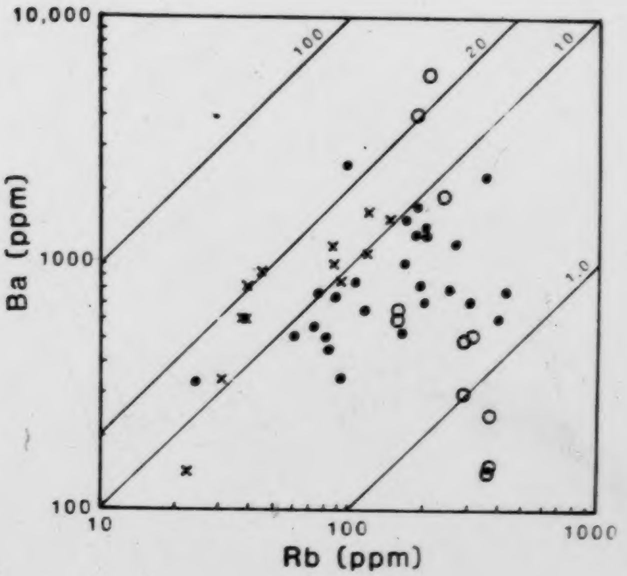

Fig. 4.5. Relationship between Ba (ppm) and Rb (ppm) for the Tsu Lake samples. Symbols: metasediments (closed circles), metaigneous rocks (crosses), granitic rocks (open circles).

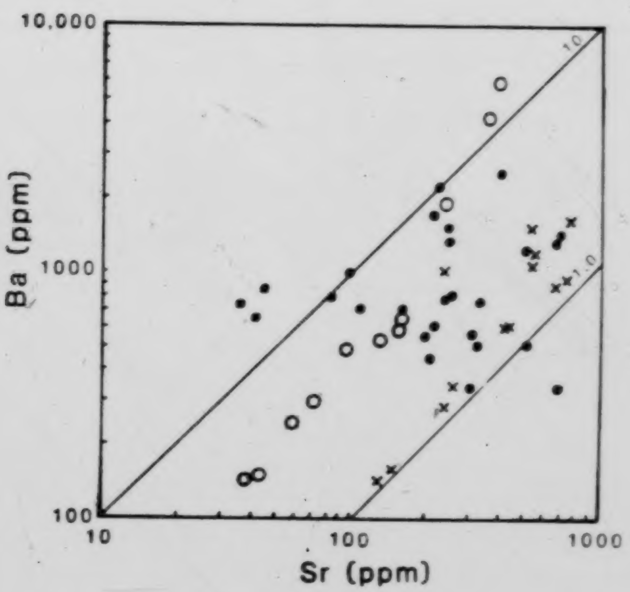

Fig 4.6. Relationship between Ba (ppm) and Sr (ppm) for the Tsu Lake samples. Symbols: metasediments (closed circles), metaigneous rocks (crosses), granitic rocks (open circles).

original granulite facies depletion than the K/Rb ratio since it is apparently unmodified by metasomatism.

If Allen's premise is correct then the K/Ba ratios of the Tsu Lake granulites suggest the area has undepleted LIL characteristics. The K/Rb ratios indicate the same feature, that is an undepleted LIL geochemsitry. It is noteworthy that the ratios of the LIL pairs which involve Sr are enriched. Such a feature is suggestive of Sr depletion or K enrichment. However, as was noted earlier, the Sr concentrations of the metasediments and the metaigneous rocks suggest the rocks have been enriched in Sr. This can only imply that metasomatism has caused an enrichment in K relative to Sr.

Studies of the geochemistry of the NW Churchill Province indicate that large scale metasomatism has occurred in the Tsu Lake area. Burwash and Krupicka (1969) postulated that K and Rb had been enriched by metasomatism in the Athabasca mobile belt, of which the Tsu Lake area is a part. Later studies (Burwash and Krupicka, 1970; Burwash *et al.*, 1973; Burwash and Culbert, 1976) showed that CaO, MgO, Na_2O, Sr and some trace elements have been depleted in this area. A more recent detailed study by Goff *et al.* (in prep.) of the composition of the shield in NE Alberta, also part of the Athabasca mobile belt, confirmed the geochemical features noted by Burwash and Krupicka (1969). Relative to the Canadian shield and the average continental crust, the NE Albertan shield is enriched in K and Rb, and possibly Ba, and depleted in Sr. Estimated average ratios for the various LIL elements for the NE Albertan shield (Goff *et al.*, in prep.) are: K/Rb - 205, K/Sr - 148, K/Ba - 41, Ba/Rb - 4.99, Rb/Sr - 0.72, and Ba/Sr - 3.59. The anomalous behaviour of Sr in samples of this study relative to the regional trends may merely reflect localised metasomatism.

However, not all of the LIL element geochemical features of the Tsu Lake granulites can be explained by metasomatic processes. The trends shown by the Ba-Rb and Ba-Sr variations of the granitic and metasedimentary samples are very similar to those observed for the restite and melt components of some low pressure granulites from S. Africa (McCarthy, 1976). During partial melting Ba and Sr were retained in the residue while Rb was fractionated into the melt. This behaviour supports the proposed derivation of the Tsu Lake granitic lithologies by partial melting of the pelitic units.

REE Geochemistry

The use of the REE as a petrogenetic tool for metamorphic studies, is restricted to a characterisation of either (i) the original protolithic material; or (ii) the prevailing metamorphic conditions. Generally the REE are considered to be immobile, on a rock unit scale, for all grades of metamorphism, i.e., they behave isochemically. Local redistribution between the new metamorphic minerals within the rock system is to be expected as the precursor phases break down. Studies of areas where there are prograding metamorphic sequences, have not reported any significant changes in the REE whole rock chemistry. Examples of these include: greenschist - amphibolite facies boundary (Cullers *et al.*, 1974); amphibolite - granulite facies boundary (Green *et al.*, 1972; Field *et al.*, 1980).

However, there are several cases recorded of mobile REE behaviour. Most of those involve a type of metamorphism where large volumes of fluid pass through the rock system. Frey *et al.* (1974) reported changes in the REE content of altered ocean floor basalts, that were attributed to the breakdown of REE enriched glasses. A study of eastern Icelandic lava flows showed variations in the LREE (Wood *et al.*, 1976), probably as a result of the zeolitisation, or the breakdown of interstitial, LREE enriched glass. Similarly, Hellman *et al.* (1979) reported several modes of lanthanide variation for volcanics which had undergone burial metamorphism; enrichment, depletion and selective REE mobility. Variably metamorphosed (amphibolite facies) dolerite dykes showed LREE depletion relative to unaltered dykes of the same age (Weaver and Tarney, 1981). They believed that the degree of mobility is controlled by the availablity of a fluid phase for element transfer.

With granulite facies metamorphism there is also the possibility of REE mobility, despite the generally anhydrous nature of the rocks and hence paucity of a H_2O-rich fluid phase. The previous section discussed the depletion of the LIL elements in granulite facies rocks. It is also believed that the HREE are depleted (Pride and Muecke, 1980). Possible depletion mechanisms have already been discussed.

The problem with assessing the mobility versus immobility question, is in finding adequate tests which enable the detection of changes in the REE chemistry. One approach is to compare unmetamorphosed samples to metamorphosed ones, essentially the method used by Weaver and Tarney (1981) and Muecke *et al.* (1979). However, the chances of finding unmetamorphosed, original material in a high grade metamorphic terrain, are somewhat remote. A second approach, the most commonly employed, is to compare the REE compositions of the metamorphic samples to the probable protolithic material. Naturally, misinterpretations may arise from this method as a result of assumptions concerning the compositional nature of the original material. .

The approach used here differs little from that discussed above. The objectives were to determine how the Tsu Lake rocks, as an example of an undepleted (LIL elements) granulite facies terrain, compared to rocks of similar composition from depleted granulite terrains. Secondly, mineral REE compositions were examined in an attempt to evaluate their usefulness petrogenetically.

Little is known about mineral REE patterns from metamorphic rocks. It is possible that mineral REE patterns would reveal more about the "alteration", i.e., depletion processes affecting them, than would the whole rock REE compositions. The most extensive study to date is that of Pride and Muecke (1981) on the Scourian granulite facies minerals. They attempted to prove that the HREE depletion observed in the whole rocks is accounted for in the mineral patterns. Their results provide a very useful comparison for this study.

Whole Rock REE Geochemistry

Sample Selection

Samples were chosen to fulfill several criteria:

i. similar assemblages / compositions for comparison with other areas;

ii. representatives of the range of compositions seen at Tsu Lake (including both metaigneous and metasedimentary lithologies);

iii. igneous lithologies which may or may not be related to the metamorphic lithologies.

These criteria resulted in the selection of six groups of samples: two groups of metamorphic basic composition, two groups of metamorphic pelitic to restite compositions, one group of granites and one group of dolerites.

The basic samples were divided into two groups according to the amount of hornblende present. The first group consists of the lithologies designated group 1 and 3 in Chapter 2; while the second group consists of the group 2 lithologies. A sample of the metagabbroic unit was among those included in the second group. The objective in selecting these two sample groups was to evaluate the influence of hornblende on the whole rock pattern. Hence the assemblages of the first two groups are:

i. opx-plag±cpx,hbl,biot

ii. hbl-opx-plag±cpx,biot.

The pelitic to restite samples were divided into two groups primarily on the basis of composition. One group, the most felsic, consists of rocks which are migmatitic in appearance. The samples in this group were selected to ensure that relative degrees of migmatisation were represented. The assemblage

iii. grnt-biot-sill-plag±cord

appears to be the restite portion of the migmatite. Included in the group is one sample which has a high concentration of monazite. It is uncertain where this sample fits, in terms of mineralogy, in the classification scheme. However, because its appearance suggested some degree of migmatisation, it was included for analysis.

The second of the pelitic groups was based on the assemblage

iv. grnt-biot-plag.

Samples in this group, although having a common mineral assemblage, were thought to have been derived in two different ways. Field associations suggest that one type is the liquid fraction, or pegmatite portion of a partial melt. The other type appears to be derived from metamorphism of quartzo-feldspathic sediments. Garnet-cordierite gneisses associated with the second type, possibly as a restite product of them, were included in this group.

Three types of granitic rocks are exposed in the Tsu Lake area: the Slave Granite, the Megacrystic Granite and the Granodiorite from Deskenatlata Lake. All three were analysed to check for relationships to the Tsu Lake metasedimentary units.

The dolerite dykes which intrude the megacrystic granite and the Tsu Lake gneiss, are thought to be part of the Sparrow dyke swarm. They are younger than the granulite facies metamorphism and hence, provide a comparison with the basic units and the metagabbro.

A total of 21 rock samples were analysed. Where possible this included at least two samples from each group, or subgroup as a test of the compositional variability within each group. Exceptions to this are from the garnet-biotite assemblages. The major element compositions of all the phases present in the selected rock samples, were available.

The REE were determined by instrumental neutron activation analysis (INAA). The procedure is described in detail in appendix 1. The results for several standard rock materials are presented there. All the analytical results for the samples are to be found in appendix 3.

Results

Basic Rocks

All three samples of group 1 and 3 (hornblende poor) show similar REE patterns, Fig. 4.7. There is only a slight enrichment in the LREE, with the Ce(N)/Yb(N) ratio ranging from 1.8 to 3.3. Eu does not show significantly anomalous behaviour. Patterns for 186A and 141B are very similar which is consistent with their mineralogies. It also indicates that these rocks are probably representative of all rocks of their type in the area.

The total REE contents are low, but are comparable to rocks of similar composition from elsewhere. The field of Lewisian basic granulites (Weaver and Tarney, 1980), shown in Fig. 4.7, encompasses the range of compositions of the Tsu Lake group 1 and 3 samples. Relative to the Tsu Lake rocks, the REE pattern of the average Scourian basic rock (Pride and Muecke, 1980), also part of the Lewisian complex, is much flatter and displays a prominent negative Eu anomaly.

The samples in group 2 display two distinct types of REE patterns, which correspond to the differences in their mineralogies, Fig. 4.8. The amphibolites bearing only one pyroxene (opx), samples 56A and GAB, show relatively flat patterns. The Ce(N)/Yb(N) ratio suggests the same degree of fractionation as the rocks of group 1. Sample 56A also contains approximately the same total REE amount. Sample GAB differs only in having a very low total REE concentration. However, this is to be expected of a rock of gabbroic parentage. Sample GAB is the only sample for which an igneous origin is unequivocal.

The two pyroxene amphibolites, samples 1B and 183D, display REE patterns which are markedly different from any of the basic rocks so far discussed. The degree of

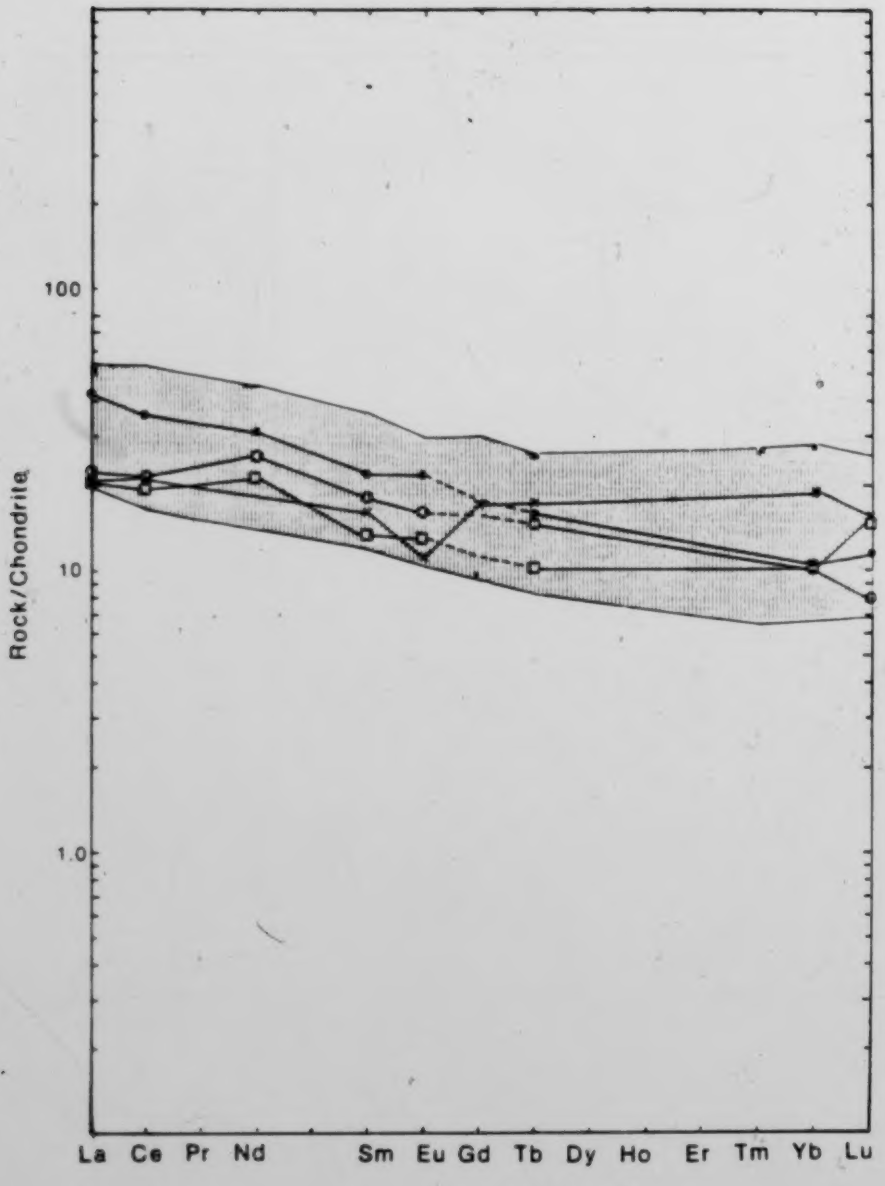

Fig. 4.7. Chondrite normalised REE patterns of the Tsu Lake group 1 basic rocks compared to the REE patterns of the Lewisian basic granulites and the average Scourian basic granulites. Symbols: 141B (open circles), 186A (closed circles), 22L (open squares), Scourian basic granulites (crosses), Lewisian granulites (vertical lines). Chondrite normalising values are taken from Evensen *et al*. (1978).

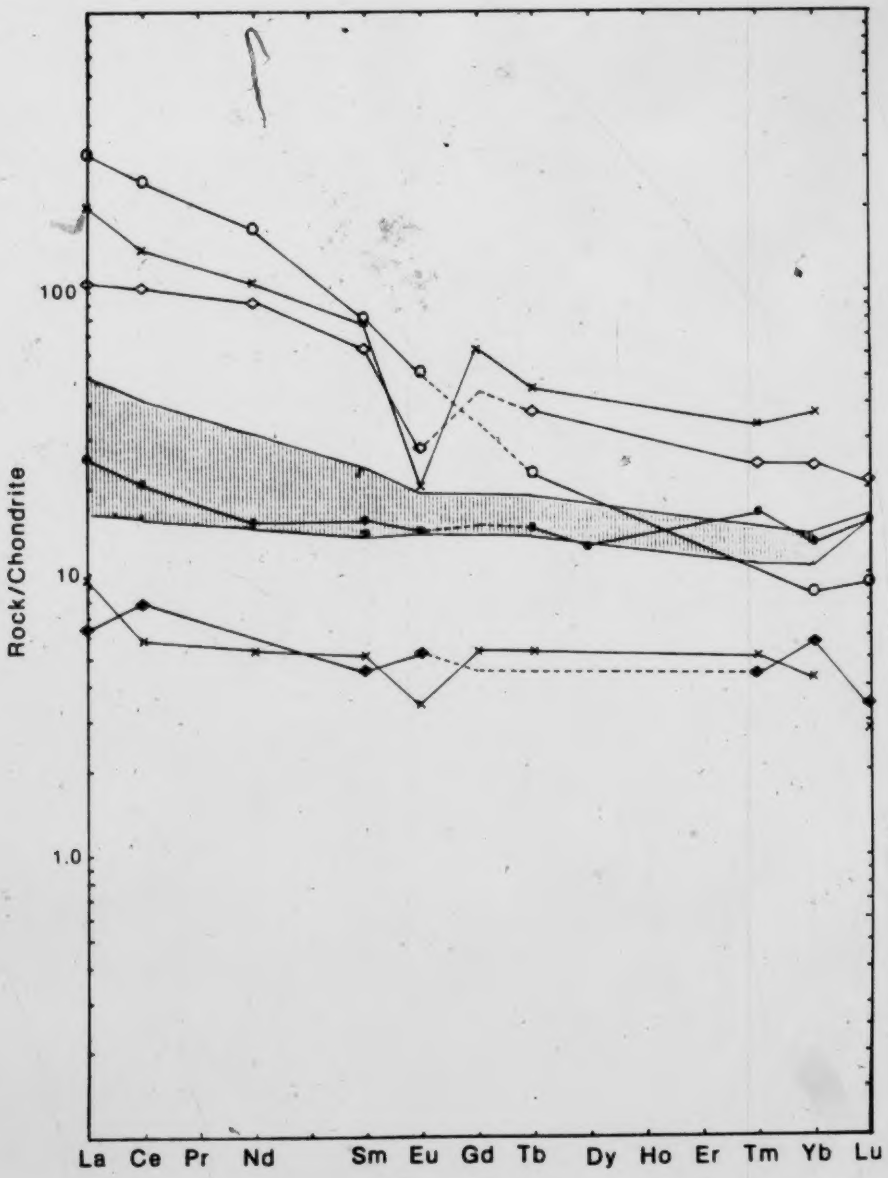

Fig. 4.8. Chondrite normalised REE patterns of the Tsu Lake group 2 basic granulites compared to the REE patterns of the Madras basic granulites and the field of Archean tholeiites. Symbols: 1B (open circles), 183D (open diamonds), 56A (closed circles), GAB (closed diamonds), Madras granulites (crosses). Archean tholeiites (vertical lines). References for the published data are given in the text.

fractionation is much greater, with the Ce(N) / Yb(N) ratio being in the range 4 to 24, and the total REE contents are higher. Only two rocks are represented here and they show dissimilar degrees of fractionation. It is conceivable that a much wider range of REE compositions could be expected from rocks of this type. It should be noted that the igneous origin of one of these two samples is questionable, as was discussed earlier.

However, such REE enriched basic rocks are not altogether rare. REE patterns comparable to one of the two pyroxene amphibolites, sample 183D, are found in the basic granulites from Madras (Weaver, 1980). The high REE concentrations are a reflection of the original parental material. The most REE enriched Madras samples represent the most fractionated ones, i.e., there is a correlation between the total REE concentration and Ce(N) / Yb(N). The Madras suite of samples is believed to represent a series of cogenetic liquids which separated by fractional crystallisation from a tholeiitic magma. Two ultramafic samples in the Madras suite probably represent cumulates of the same magma. Another example of enriched metamorphic basic rocks is found in the granulite facies gneisses of the Lofoten-Vesteralen area (Iden, 1981).

If both groups 1 and 2 are compared to the Madras suite then it is seen that the REE patterns are not alike. Hence, the possibility arises that the Tsu Lake basic rocks represent a cogenetic suite. But inspection of the concentration of the incompatible elements for some of the rocks, suggests that such a situtation is unlikely. The incompatible elements are not always enriched in the most fractionated samples.

Poor correlations were found between the REE and U and Hf concentrations, for all the basic rocks, thus suggesting that perhaps an accessory phase controls the REE abundances in these samples. U and Hf can be present in both apatite and zircon. However the correlations for the LREE and U or Hf are positive, and for the HREE and U or Hf, they are negative. This indicates that apatite, not zircon, is the more likely phase responsible for these variations.

REE concentrations and fractionation patterns for modern igneous suites are found to be comparable to the metamorphic suites of Madras, Lofoten and Tsu Lake. Saunders (1983) compiled data for a number of ocean island alkali basalt suites. The data listed for the alkali basalts of Iceland show the same type of fractionation patterns as the metamorphic suites. In general continental tholeiites have lower REE concentrations and

Ce(N) / Yb(N) ratios than alkali basalts (Cullers and Graf, 1983). They also tend not to have Eu anomalies, a feature which is prominent in the alkali basalt suites. The REE concentrations and fractionation patterns of the Tsu Lake basic rocks are closer to those of modern continental tholeiites than modern alkali basalts.

The Tsu Lake samples have also been compared to the REE patterns of Archean tholeiites (Condie, 1976). Both the depleted Archean tholeiites (DAT) and the enriched Archean tholeiites (EAT) are shown in Fig. 4.8. The Archean tholeiite REE patterns are less fractionated and less enriched than those of the two pyroxene amphibolites but are similar to the group 1 samples. Only averaged values of the REE concentrations for the Archean EAT and DAT units were available, hence it is impossible to estimate whether the Tsu Lake amphibolite REE values are unusual for early Proterozoic / late Archean basic rocks.

Despite the differences in the absolute REE abundances between rocks of groups 1 and 2 and the Scourian basic granulites, it is not thought that the lower average values of the Scourian samples are indicative of REE depletion. When Pride and Muecke (1980) speak of REE depletion they are referring to the composition of the terrain as a whole rather than a particular rock type. The section of the Madras terrain studied by Weaver (1980) showed variable depletions in the LIL elements that were attributed to metasomatic / metamorphic processes, yet the basic rocks are enriched in the REE. A similar situation exists for the Lofoten-Vesteralen terrain. These factors suggest that the REE abundances for the Tsu Lake rocks are indicative of protolithic concentrations.

The REE patterns of the Tsu Lake basic rocks do not show any inconsistencies in the REE concentrations like those shown in the Strangways sapphirine granulites (Windrim *et al.*, 1984). REE mobility is believed to have taken place in the Strangways granulites, prior to or during metamorphism. The total REE concentrations of such rocks do not show any correlation with the degree of REE fractionation. Prominent negative Eu anomalies characterise their REE patterns, even in the rocks with low total REE concentrations, a highly unusual feature. The lack of these characteristics in the Tsu Lake basic rocks supports the above suggestion, that the REE patterns of these samples are representive the premetamorphic REE patterns.

Dolerites

The REE patterns of the two dolerite dyke samples are shown in Fig. 4.9. They are characterised by moderate total REE contents and average Ce(N) / Yb(N) ratios of 2. The most noticeable feature of their REE patterns is the depletion of Lu and the slight enrichment of La relative to the rest of the REE. The group 1 and 2 metabasic samples do not show this feature. Because the overall fractionation patterns for the igneous and metabasic samples are dissimilar this confirms the supposition that the dykes found at Tsu Lake are not related to the metabasic samples. It also tends to suggest that there is a considerable age difference between the generation of the igneous protoliths of the metabasic samples and the dykes. The absence of any geochemical relationships between the two groups supports this. The REE values, except for Lu, of the dolerite dykes fall within the range of values expected for continental tholeiites.

Pelitic Rocks I

The REE patterns for two samples with the grnt - biot - plag assemblage, are shown in Fig. 4.10. The REE pattern of the North American Shale Composite (NASC) (Haskin and Paster, 1979), the assumed composition of a pelitic sediment in North America, is shown in the same diagram for reference purposes. Sample 23B is believed to be the precursor material of sample 23C, which has a restite assemblage. Sample 183B differs from 23B in having a larger proportion of accessory phases, the presence of 943 ppm of Zr and 0.42 wt. % P_2O_5 is indicative of the high modal amounts of zircon and apatite respectively. The field associations of 183B suggest it is a biotite-rich pegmatite phase, perhaps associated with the partial melting of other sediments.

The REE patterns confirm the different mode of origin for samples 23B and 183B. Sample 23B is characterised by higher total REE contents, relative to 183B, a low Ce(N) / Yb(N) ratio and a prominent negative Eu anomaly. The MREE are depleted relative to the light and heavy REE resulting overall in a concave-up pattern. Sample 183B shows low total REE, a high Ce(N) / Yb(N) ratio and a prominent positive Eu anomaly.

Samples 23B and 183B appear to have almost complimentary REE chemistry. Examples of this pair of REE patterns have been observed by other authors (Dostal, 1975; Dostal and Capedri, 1979; Price and Taylor, 1977). In all cases cited, the REE patterns were derived by the partial melting of a pelitic sediment; the residuum or melanocratic

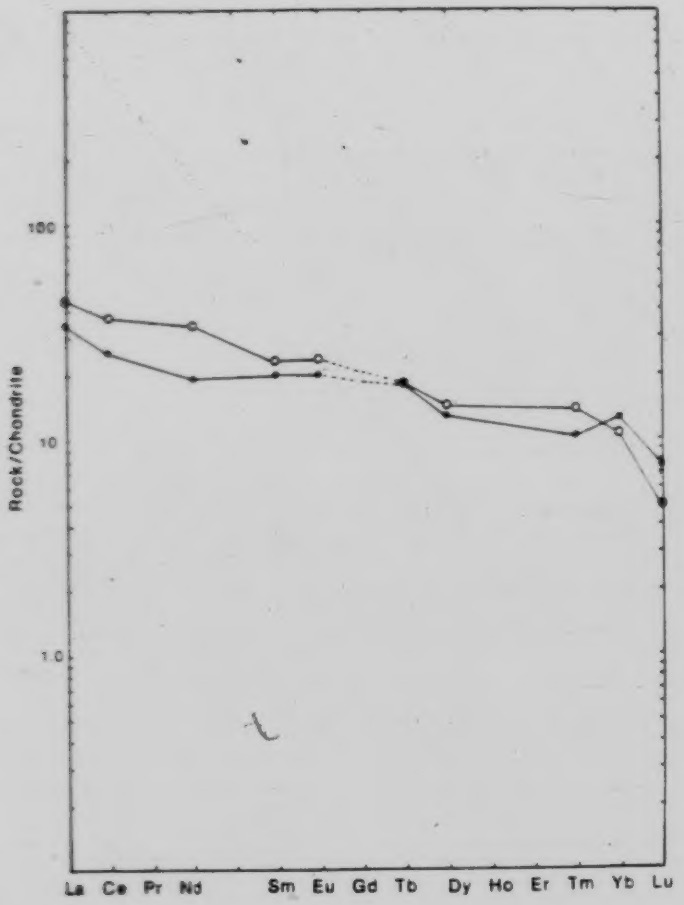

Fig 4.9. Chondrite normalised REE patterns of the Tsu Lake dolerites.
Symbols: 145B (closed circles), 166D (open circles).

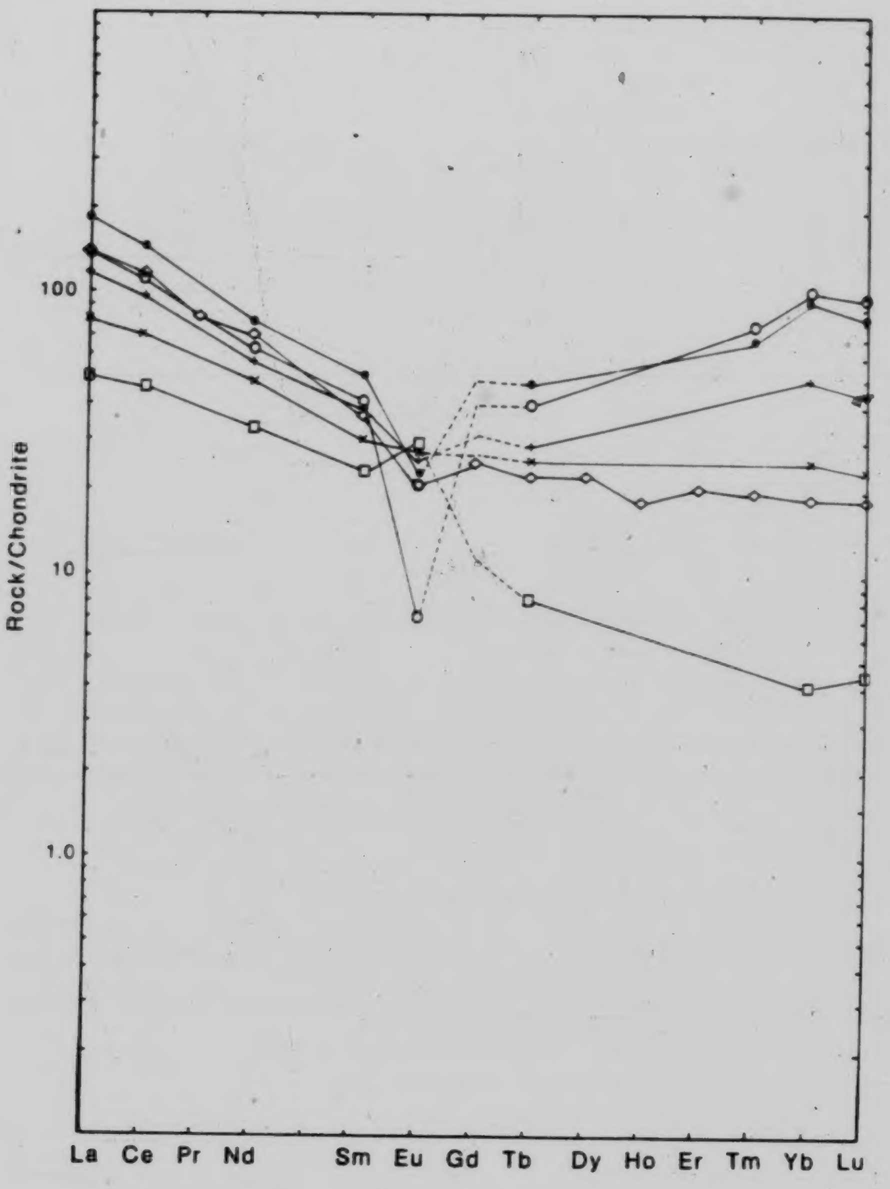

Fig. 4.10. Chondrite normalised REE patterns of the Tsu Lake group 4 and group 5 pelitic / restite samples compared to the NASC and to the theoretical REE patterns of the original unmelted pelites. Symbols. 23B (closed circles), 23C (open circles), 183B (open squares), NASC (open diamonds), composite of 50% melt-50% restite (diagonal crosses), composite of 75% melt-25% restite (vertical crosses). NASC REE values are taken from Haskin and Paster (1979).

portion of the migmatite has higher REE contents, the melt fraction or leucocratic portion has the lower REE cotents.

Attempts were made to calculate the composition of the original unmelted pelitic material by mixing in varying proportions, the REE compositions of the restite and partial melt materials. The REE patterns for mixes of 50% melt, 50% restite and 75% melt, 25% restite are shown in Fig. 4.10. Clearly they do not match the expected composition of a pelitic sediment, that of the NASC. Evaluation of the major element composition of these two rocks shows that fraction assumed to be the partial melt, sample 183B, does not have a composition consistent with a minimum melt. This conclusion is supported by the mineralogy of the rock. The high concentrations of the accessory phases, apatite and zircon, have evidently exerted a strong control on the REE composition of this sample. Possibly the influx of a hydrothermal solution, associated with the general partial melting in the area, has caused the high concentrations of accessory phases, and resultant REE compositions.

The REE pattern of 23B, consistent with that of a residuum, contradicts its suggested origin which was discussed earlier in chapter 2. It appears that 23B itself has been partially melted, and that sample 23C, the garnet-cordierite gneiss associated with 23B, represents an advanced stage in the partial melting sequence.

The major element chemistry of 23C is consistent with a derivation by partial melting from 23B. The REE pattern of 23C is very similar to that of 23B. The total REE content is slightly lower but the degree of fractionation is about the same. The most significant difference is in the larger negative Eu anomaly for 23C. This implies that feldspar fractionation has been important during partial melting of 23B. It is expected that the size of the Eu anomaly will increase if the felsic phases are removed selectively from the restite material.

The lack of any substantial differences in the total REE concentrations between 23B and 23C, with the exception of Eu, implies that the REE are preferentially retained in the restite material. However, the HREE in 23C are slightly higher than in 23B, implying that the partition coefficient for the HREE is greater than 1, i.e., the HREE are partitioned into the restite, not the melt phase. Field observations suggest that only a small proportion (less than 25%) of the felsic material has been removed from the precursor material of

23C. However major element chemistry implies that at least 50% of 23B must have been melted to produce 23C, if a minimum melt composition was extracted.

McCarthy and Kable (1978) report a suite of partially melted rocks where the LREE were partitioned into the melt phase and the HREE and Eu were retained in the restite material. They conclude that the REE chemistry of the restite and melt materials was controlled by the melting of a minor phase enriched in REE, not apatite or zircon.

Pelitic Rocks II

The samples in these group 6, lithologies differ from the pelitic and restite samples discussed above, in that most of the felsic portion of the rock has been retained with the restite material. Geochemical analyses of these samples include both mafic and felsic portions.

Samples 135B, 216 and 44 contain decreasing amounts of felsic material in the order listed. This classification is based on petrographic observations. Sample 290A is unusual, in terms of its mineralogy, and consists of bands of cord - spin - monaz. separated by bands of quartz and feldspar. Despite the unusual assemblage it is thought to have undergone considerable migmatisation. All samples are banded in appearance although this is most prevalent in sample 44.

The REE patterns of these four samples are shown in Fig. 4.11, along the NASC pattern for comparison. Sample 135B has a REE pattern very similar to that of the NASC. The other samples deviate from a NASC REE composition in both the LREE and the HREE. All samples display a negative Eu anomaly. There is an apparent correlation between the total REE content and the degree of Ce(N)/Yb(N) fractionation. The Ce(N)/Yb(N) ratios increase with increasing total REE content, from sample 135B through to 290A.

If the observation on the amounts of the felsic fractions remaining with the rock are correct, then the REE patterns of the samples suggest that the LREE are preferentially retained in the restite portion of a partial melt relative to the HREE, the opposite of that observed for the group 1 pelitic and restite samples, and by McCarthy and Kable (1978). Monazite appears to be the only REE phase in the restite portion of these migmatites. It was observed to increase in modal abundance from 135B to 290A. Presumedly its formation in these rocks is necessary because of the absence of other suitable LREE-bearing phases. Geochemical data concurs with the petrographical observation.

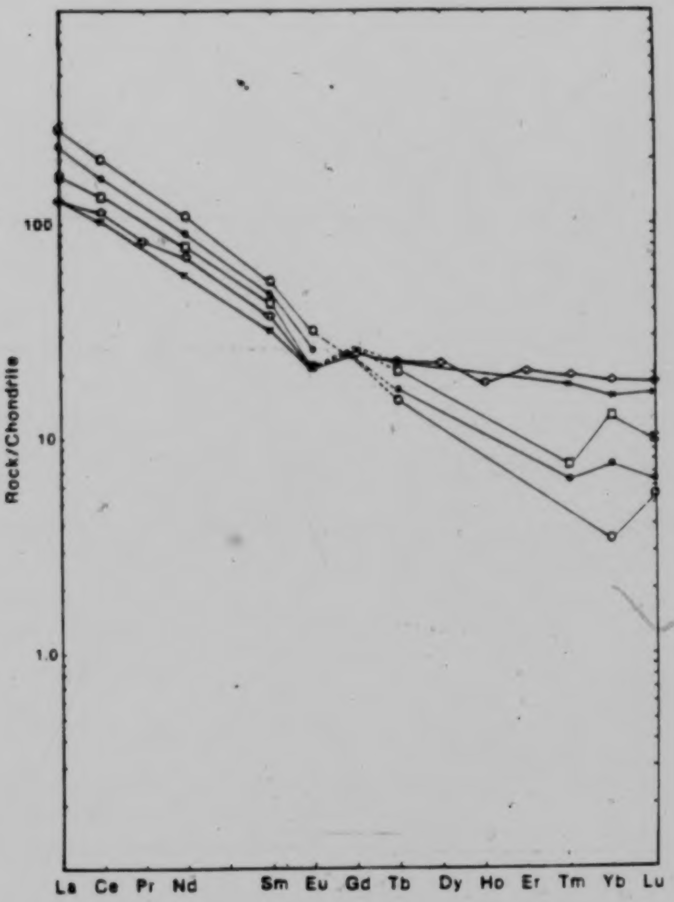

Fig. 4.11. Chondrite normalised REE patterns of the Tsu Lake group 6 pelitic/migmatitic samples compared to the NASC. Symbols 135B (crosses), 216 (open squares), 44 (closed circles), 290A (open circles), NASC (open diamonds).

There is a positive correlation between La and Th, and a negative correlation between Lu and Th for this group of samples. As monazite is the only phase in these samples which can contain Th in significant amounts, the observed correlation corresponds to a change in the modal abundance of this phase. Although garnet is present in some restite materials it is strongly HREE selective and hence cannot accommodate significant amounts of the LREE in its structure. The difference in the REE partitioning behaviour found between this group of migmatites and the restite materials discussed above, is difficult to explain. Mineralogical observations suggest that there is a compositional difference in the protolithologies of these two groups which affected their relative degrees of partial melting. Whether this difference is sufficient to cause differences in the REE partitioning behaviour is unknown.

Granites

The characteristics of granitic REE patterns have been documented by Haskin *et al.* (1968) who note that the REE content and the extent of Eu depletion in granitic materials increases with increasing SiO_2 content. However Bowden and Whitley (1974) believe the Eu depletion is related to the molar (K+Na)/Al ratio of the granite. Apparent contradictions to these generalisations for granitic rocks were found by Emmermann *et al.* (1975). The reverse of the relationship reported between the total REE content and the SiO_2 (Haskin *et al.*, 1968) was observed. No correlation between the size of the Eu anomaly and the molar (K+Na)/Al was found. Overall there is no correlation between the composition of the granite and its REE pattern. For the suite of granitic rocks studied by Emmermann *et al.* (1975) a correlation between the age of the granite and the type of REE pattern was observed. The differences in the REE patterns were produced by two processes: (a) progressive anatexis, and (b) magmatic differentiation.

The REE patterns of the samples from the three different granitic/ granodioritic units in the Tsu Lake area are displayed in Fig. 4.12. All units are characterised by unique REE patterns.

The Slave Granite, samples 92 and 122, have REE patterns which are the most similar to the granite composite of Haskin *et al.* (1968). The two samples of the megacrystic granite, 40A and 233A, have large differences in REE concentrations. Only half of the REE pattern for sample 40A is shown because the rest of the REE

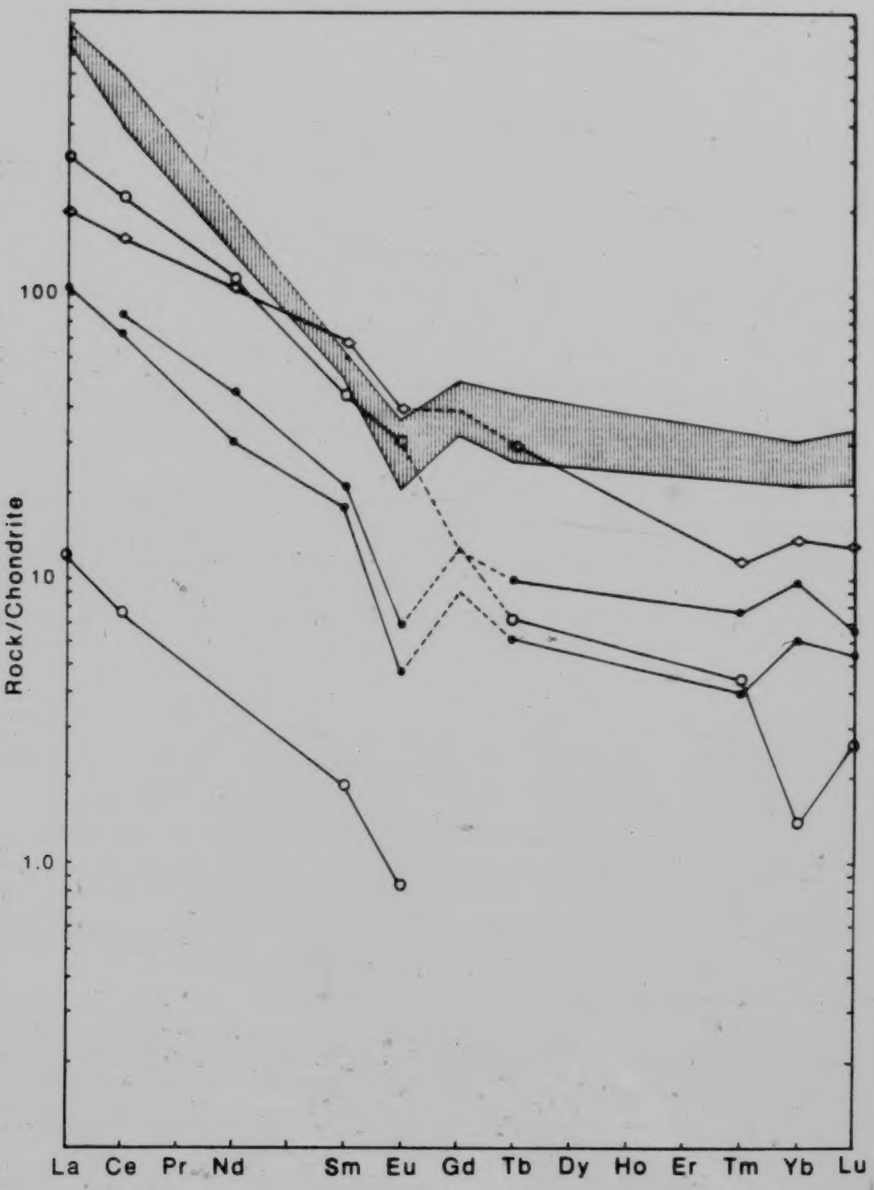

Fig. 4.12. Chondrite normalised REE patterns of the Slave Granite, the megacrystic granite, and the biotite granodiorite compared to the granite composite of Haskin *et al*. (1968). Symbols: Slave Granite (closed circles), megacrystic granite (open circles), biotite granodiorite (open diamonds), granite composite (vertical lines).

concentrations were below the detection limits of the analytical technique. It appears as if the same type of REE fractionation pattern could be present in both these samples from a comparison of their LREE contents. The absence of a Eu anomaly is significant in the megacrystic granite. The granodiorite sample, D4A, from Deskenatlata Lake is the most enriched in the REE of the three granitic units. It has slightly higher Ce(N)/Yb(N) ratio and a slightly smaller negative Eu anomaly than the Slave Granite.

The absence of a Eu anomaly in the megacrystic unit would suggest that it is older than the Slave Granite, if both have been generated by anatectic melting. Note that this is only relevant if it is assumed that the REE characteristics of the suite of samples studied by Emmermann *et al.* (1975) are applicable to this area. It is felt that there is insufficient data to reach a positive conclusion on the significance of the absence of a Eu anomaly in the megacrystic unit.

Mineral REE Geochemistry

The purpose of determining the REE concentrations of mineral phases in the Tsu Lake granulite facies rocks was twofold

i. to determine the relationship between the whole REE compositions and the mineral REE compositions

ii. to examine the problem of REE mobility in granulite facies terrains, in terms of the REE compositions of the mineral phases, by comparing an undepleted (in the REE and LIL elements) terrain, Tsu Lake, with a terrain, the Scourian complex (Pride and Muecke, 1980), which is reported to be depleted in these elements.

The study is restricted to the basic rocks which do not appear to have suffered metamorphic alteration of their protolithic REE concentrations. Two additional sets of minerals were studied because of the high concentrations of accessory phases present. It was desirable to see what effect, if any, the accessory phases have on the REE compositions of the other coexisting phases. As a test of compositional extremes two sets of minerals from similar rocks were analysed.

In the following discussion on the REE compositions of the Tsu Lake granulites facies minerals, comparisons will be made with igneous minerals as well as with those from the Scourian granulite facies terrain.

Mineral Selectivity for the REE

It is pertinent here to consider the chemical properties of the REE as these properties control REE behaviour. The elements from La (atomic number 57) to Lu (atomic number 71) have very similar chemical properties which are a result of their electronic configurations. The REE group is characterised by the sequential addition of a 4f electron. Because the 4f electrons are well shielded by outer electron shells, $5s^2$ and $5p^6$, they do not participate directly in bonding or chemical interactions, e.g., ligand field effects. Therefore, the REE can be expected to have the same valence states, there are a few exceptions. The 3+ oxidation state is the most stable valency and corresponds to the loss of the $6s^2$ electrons and a 4f or 5d electron. Under geological conditions Eu can also exist in the 2+ state, and Ce in the 4+ state. Hence the reason for the presence of Eu and Ce anomalies in rocks and minerals is the result of the variable valence for these two elements.

An important feature of the REE chemistry which partially controls the fractionation pattern of the REE in minerals, is known as the lanthanide contraction. The addition of non-bonding 4f electrons causes a decrease in ionic radius with an increase in the nuclear charge. The largest difference in ionic radius is found between La and Ce, and the decrease in the size of the ionic radius from La to Gd is greater than from Gd to Lu.

The ionic radii of the REE are larger than most of the major elements of geological materials. In the 3+ state they are similar in size to Ca^{2+}, Y^{3+}, Th^{4+}, U^{4+}, Mn^{2+} and Zr^{2+}. However, the ionic radius is also a function of the coordination number and valence state and the REE exhibit a wide range of ionic radii for the various coordination numbers (Shannon, 1976).

The substitution of the REE into minerals is controlled by:

i. ionic radius, charge and coordination number,

ii. temperature and pressure conditions,

iii. oxygen fugacity, which controls the valence for elements with variable valence states,

iv. compositional dependence, (Henderson, 1983).

The influence of the coordination number effect is seen in the REE selectivity of sphene and apatite. The REE replace Ca in both these minerals but sphene has an affinity for the HREE while apatite is LREE selective (Khomyakov, 1963). In general the degree of selectivity for the LREE, MREE or HREE decreases as the REE content in the mineral decreases.

Thus, it can be expected that the major rock-forming minerals which usually contain low amounts of the REE, will not show significant degrees of REE fractionation, but may show wide variations in the actual shape of the REE pattern (Clark, 1983). For many of the common minerals the REE distribution in a particular phase does not show any variation in shape despite a range of major element compositions for that phase. This is because the size of the crystallographic site into which the REE substitute is not dependent on composition (Gromet and Silver, 1983). Feldspars are one example of a phase where the REE pattern does not change shape significantly. For other minerals the size of the crystallographic site is sensitive to compositional variations. The difference in the size of the M_2 site in orthopyroxenes and clinopyroxenes is an example of this.

Accessory phases, such as apatite, zircon, sphene, monazite and allanite, show large degrees of REE fractionation. There is a tendency for the REE-rich phases to be sensitive to changes in the composition of the rock. Hence they have a greater potential than the major minerals for recording alteration effects, e.g., metamorphic or metasomatic effects, although the extent to which they can record REE depletion during metamorphism is limited. Large changes to the whole rock REE patterns would be required before such changes would be noticeable in the mineral REE patterns.

Results

Orthopyroxene

The REE distribution patterns for the orthopyroxene samples are displayed in Fig. 4.13. The distributions are concave-up with maximum concentrations of the LREE and the HREE. A negative Eu anomaly is present in three of the samples with Eu/Eu*[1] ranging from 0.31 to 0.52. The orthopyroxene without the Eu anomaly, sample 141B, appears to be a special case. Plagioclase from this rock also does not show a significant Eu anomaly.

The total REE abundances of the Tsu Lake orthopyroxenes are the lowest of all the major mineral phases present. There would appear to be a positive correlation between

---

[1] Eu/Eu* is defined as the ratio of the measured Eu concentration to the Eu concentration obtained by interpolation between Sm and Gd to Tb.

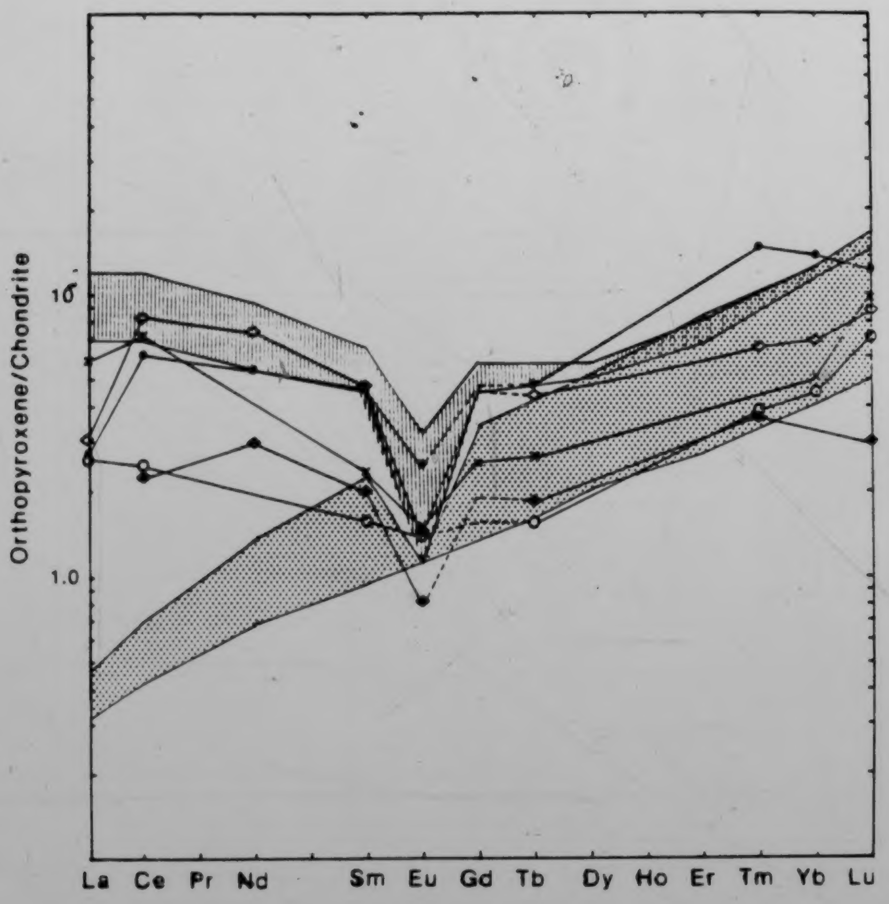

Fig. 4.13. Chondrite normalised REE patterns of the Tsu Lake orthopyroxenes compared to orthopyroxenes from other rocks types. Symbols: 141B-opx (open circles), 186A-opx (closed circles), 183D-opx (open diamonds), GAb-opx (closed diamonds), Scourian opx (crosses), dacitic opx (vertical lines), basaltic opx (dots). References for published data are: Schnetzler and Philpotts (1970); Nagasawa and Schnetzler (1971); Pride and Muecke (1981).

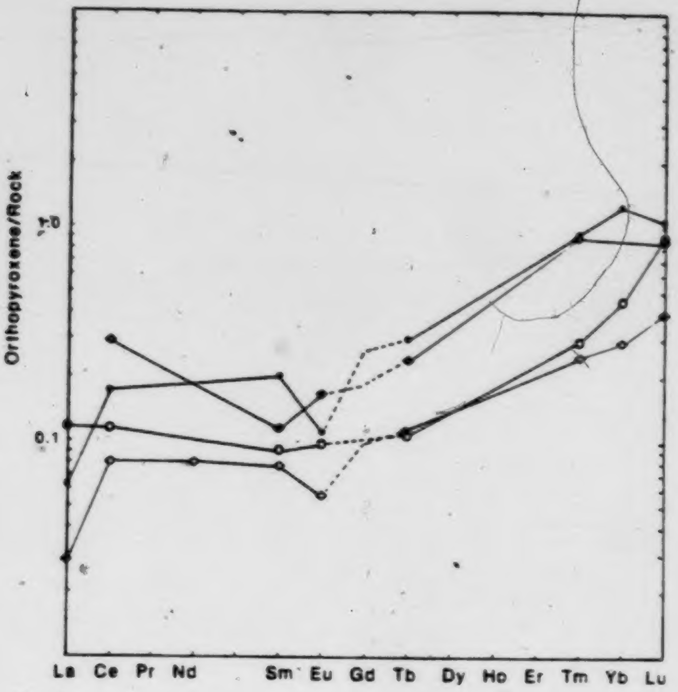

Fig. 4.14. REE distribution coefficients for the partitioning of the REE between the orthopyroxene and the bulk rock. Symbols as in Fig. 4.13.

the total REE content and the concentration of Fe in the orthopyroxene. An examination of the REE distribution between the orthopyroxene and the whole rock, Fig. 4.14, reveals that the correlation could be real.

The high REE concentrations in 183D-opx are a reflection of the REE-enriched nature of the whole rock. The two group 1 samples, 141B and 186A, contain orthopyroxenes which have different REE partition coefficients to the group 2 samples, GAB-opx and 183D-opx. It is difficult to say how much these partition coefficients are dependent on the whole rock major element compositions but limited data suggests there could be a relationship. The most Mg-rich rocks have the lowest orthopyroxene/rock REE partition coefficients.

The REE distribution patterns in Fig. 4.14 merely show the fraction of the REE partitioned into orthopyroxene relative to the total amount of the REE present in the rock. The fractional contribution of the REE concentration in orthopyroxene to the whole rock pattern could not be assessed because of the lack of data on the modal abundances of each phase in the rock.

With the exception of orthopyroxene 141B the REE patterns are very similar in shape. A comparison with REE data of orthopyroxenes from igneous rocks, Fig. 4.13, shows that the REE amounts of two of the Tsu Lake orthopyroxenes lie within the range of values expected for dacites. The REE distribution patterns for orthopyroxenes from basalts are distinctly different; they show selective HREE enrichment. The average REE pattern for orthopyroxenes from the Scourian rocks lies between the extremes of the REE values for the Tsu Lake orthopyroxenes.

Pride and Muecke (1981) noted the presence of Ce anomalies in the orthopyroxenes of their study. It could be argued, however, that La is depleted relative to the rest of the REE. The same type of La depletion/Ce enrichment is seen in the Tsu Lake orthopyroxenes. Pride and Muecke (1981) attributed the anomalous Ce values to an analytical error, which is due to a spectral interference between Fe and Ce (see appendix 1 for discussion of errors in the INAA technique). It is acknowledged that the problem to which they referred is serious with their analytical conditions. However, the Fe - Ce spectral interference is adequately resolved under the analytical conditions used in this study. Therefore it is concluded that La, not Ce, shows anomalous behaviour, i.e., depletion. Possibly the analytical error in Ce has accentuated relatively the La depletion in the Scourian orthopyroxenes.

The variation in the REE fractionation patterns can be partially explained by a consideration of the crystallographic sites available for REE substitution and consideration of experimental results on REE partitioning. Orthopyroxene should be HREE selective. The only suitable cations the REE can substitute for are Mg^{2+} and Fe^{2+} in 6-fold coordination. As the ionic radius of Lu is closest in size to those of Mg^{2+} and Fe^{2+} for this coordination number, there should be a progressive decrease in the concentration of each REE from Lu through to La (Matsui *et al*. 1977). Evidence of the difficulty the REE have in substituting into the orthopyroxene structure, is seen in the experimental studies of Morris (1975). In these experiments Gd^{3+} was observed to substitute directly for Ca in the M_2 site of clinopyroxenes. In pure Mg clinoenstatite Gd^{3+} appeared not to be occupying a crystallographic site in the mineral; instead it formed local clusters within the lattice. Only orthopyroxenes from basalts show a HREE-enriched distribution pattern. However, it must be remembered that orthopyroxenes in the more acidic volcanic rocks are richer in Ca than those in basalts. The subcalcic clinopyroxene, pigeonite, may form instead of orthopyroxene. The shift in composition of the orthopyroxene may be sufficient to cause a change in the REE partitioning characteristics of this phase in igneous rocks, although this is unlikely. Explanation of the REE patterns of the granulitic orthopyroxenes is difficult.

Perhaps the discrepancy between the natural data and theoretical predictions can be explained by the dependence of the REE distribution coefficients on temperature. Orthopyroxenes from basalts are formed at higher temperatures than orthopyroxenes from dacites or granulite facies rocks. The lower temperature of formation for the orthopyroxenes with the MREE depleted patterns may be a cause of the departure of the REE substitutions from the theoretical HREE-enriched trend. The similarity in the REE patterns for orthopyroxenes from dacites and the two different granulite facies terrains may be merely a function of the similarities in the temperature of formation of the orthopyroxenes.

It could be argued that the difference in REE patterns for orthopyroxenes from different igneous suites is a function of the composition of the melt. Watson (1976) demonstrated experimentally that a basic melt is enriched in the REE relative to an acidic melt. An increase in the mineral / melt REE distribution coefficient could be expected as the silica content of a magma increases. Examination of the relationship between the REE content in orthopyroxene and that in the rock, for samples in this study, Fig. 4.14, shows that there is a dependence of the mineral REE partition coefficient on the whole rock concentration.

There is little experimental data on opx / melt REE partition coefficients to confirm or refute either of the two suggestions above. Irving (1978) summarised the available data for subcalcic pyroxenes which imply that the partition coefficient is slightly temperature dependent. Data for grnt / melt partition coefficients suggests that the composition of the melt has a stronger control over the resultant REE pattern of garnet than either the temperature of formation or the composition of the garnet (Nicholls and Harris, 1980). The same control on the REE partitioning into orthopyroxene by the melt composition can be expected, as it is the instability of the REE in the acidic melt structure that is responsible for the observed partitioning behaviour.

However, arguments on the relationship between the REE distribution pattern of the mineral and the melt composition for igneous systems, are not strictly applicable to metamorphic rocks. The partition of the REE into a metamorphic mineral is dependent on the nature and abundance of other phases present, as well as the total REE content of the rock.

Clinopyroxene

The REE distributions for the clinopyroxene samples show concave-down patterns mainly with a maximum enrichment in Nd and Sm, Fig. 4.15. 183D-cpx is an exception, showing an overall LREE-enriched pattern. For 141B-cpx and 186A-cpx the Ce(N) / Yb(N) ratios are 1.57 and 1.49 respectively; while 183D-cpx has a Ce(N) / Yb(N) ratio of 6.7. All the clinopyroxenes of this study show negative Eu anomalies with a range of Eu / Eu* values from 0.24 to 0.6. Philpotts (1970) found a correlation between the Fe^{2+} content of the clinopyroxene and the size of the Eu anomaly; the most Fe-rich clinopyroxenes had larger Eu anomalies than the Mg-rich clinopyroxenes. The same correlation is noted for the Tsu Lake clinopyroxenes, although the actual compositional difference between the clinopyroxenes is small.

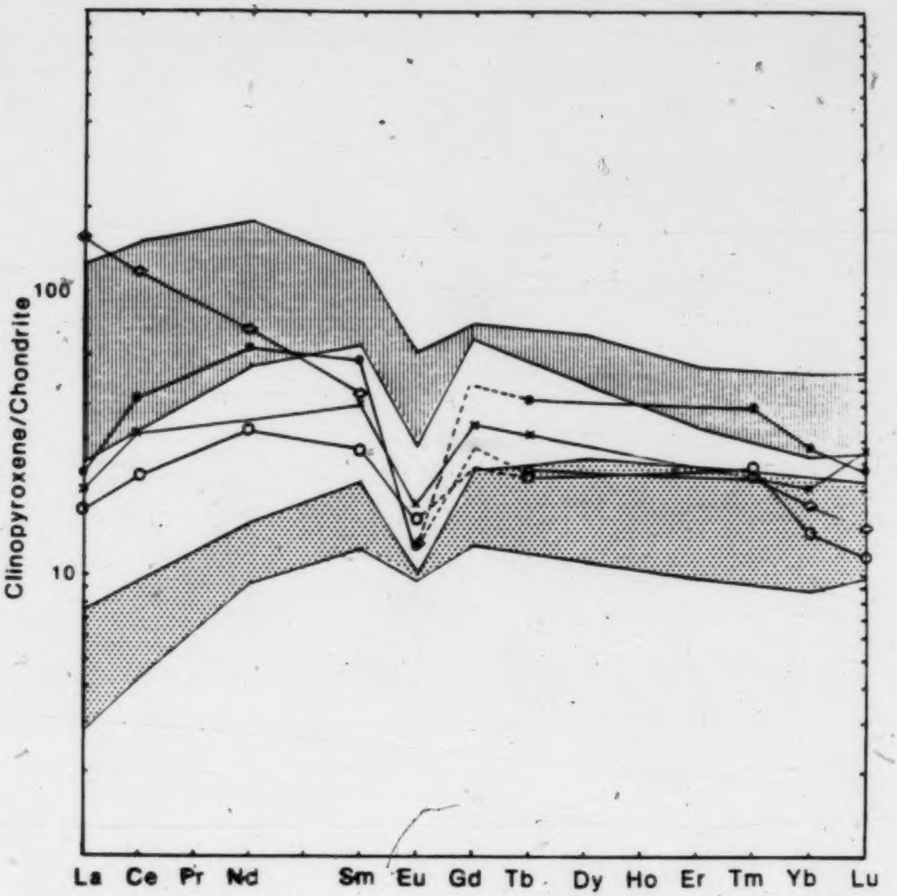

Fig. 4.15. Chondrite normalised REE patterns of the Tsu Lake clinopyroxenes compared to the clinopyroxenes from other rock types. Symbols: 141B-cpx (open circles), 186A-cpx (closed circles), 183D-cpx (open diamonds), Scourian cpx (crosses), dacitic cpx (vertical lines), andesitic cpx (dots). References for the published data are the same as those listed for Fig. 4.13.

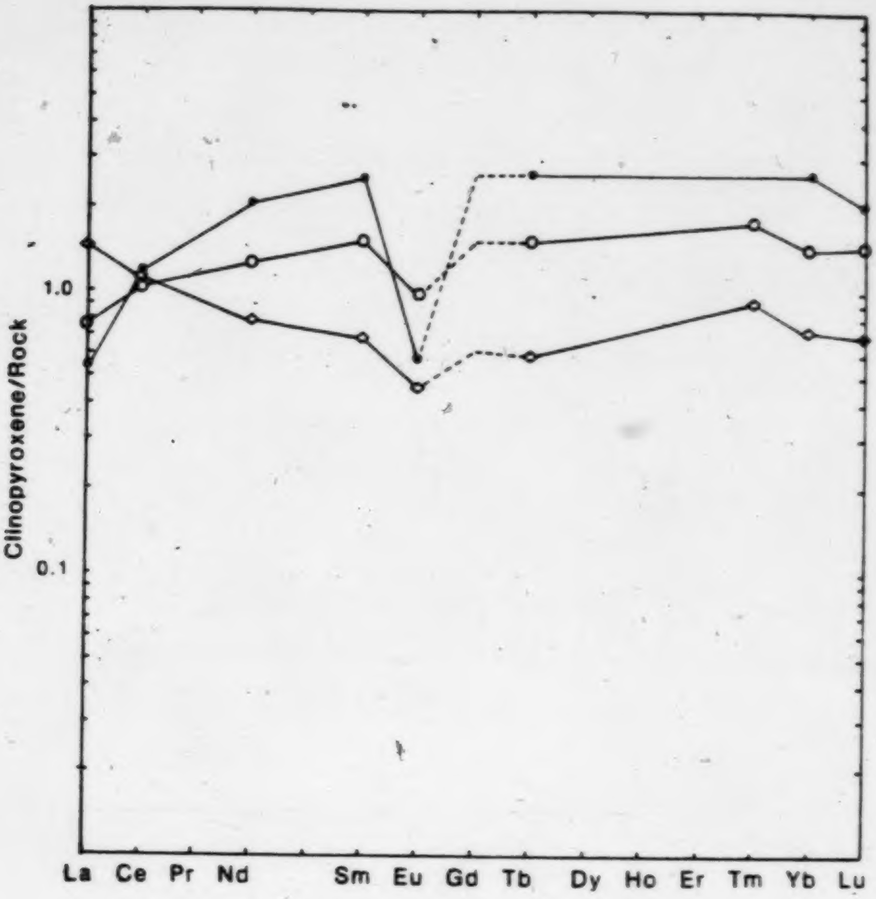

Fig. 4.16. REE distribution coefficients for the partitioning of the REE between clinopyroxene and the bulk rock. Symbols as in Fig. 4.15.

The whole rock composition appears to have influenced the relative abundances of the REE in the clinopyroxenes of this study, Fig. 4.16. A lack of data on all of the whole rock compositions prevents firm confirmation of this, but such rock compositional differences are also inferred from the compositional differences of the mineral phases.

Clinopyroxenes from 186A and 141B have very similar REE patterns to those for clinopyroxenes from dacites although absolute abundances are slightly lower. The REE patterns for clinopyroxenes from andesites and basalts are different with distributions ranging from MREE or HREE-enriched to slightly LREE-enriched. As with the orthopyroxene REE patterns the Scourian clinopyroxenes have REE distributions which lie between the extremes of the data for the Tsu Lake clinopyroxenes.

Crystallo-chemical considerations indicate that the REE should substitute preferentially for the larger Ca^{2+} cation in the M_2 site which has 8-fold coordination, rather than Mg or Fe^{2+} in the M_1 site with 6-fold coordination. This implies that there should be a maximum enrichment in Pr which is closest in size to the Ca^{2+} cation in 8-fold coordination. Andesitic and basaltic clinopyroxenes are frequently subcalcic, pigeonite. Hence it can be expected that the smaller HREE would substitute into the clinopyroxene structure more readily than the larger LREE. However, this argument cannot explain the difference in the REE patterns between andesitic and dacitic clinopyroxenes because pigeonite can also occur in dacites.

It would appear that the size of the M_2 site is slightly smaller than the ionic radius of Ca^{2+} would suggest. (Matsui*et al.*, 1977). With a decrease in size of the M_2 site, there is an increasing distortion in the 8-fold symmetry of the site. (Cameron and Papike, 1980; Nicholls and Harris 1980). The amount of distortion of this site will determine which of the REE will be enriched.

It is thought that temperature has a stronger control over REE substitution into clinopyroxenes than the composition of the phase itself. This could explain the similarity between the granulite facies clinopyroxenes and dacitic clinopyroxenes. The control of the REE partitioning into minerals by the composition of the melt may be more important in igneous systems, however, than in metamorphic rocks. Like the orthopyroxene, the REE distribution distribution patterns of granulitic clinopyroxenes are slightly dependent of the total REE concentration of the rock, Fig. 4.15.

Hornblende

Large differences in the total REE abundances are apparent for the Tsu Lake hornblendes, Fig. 4.17. These differences are the result of differences in the whole rock REE abundances, Fig. 4.18. The REE values of the rocks reflect the concentrations in the original protolithic materials. The total REE abundances of the whole rocks of this study have contributed to the LREE-enriched patterns of the hornblendes.

Fractionation patterns of the REE for the hornblendes vary from LREE-enriched, 141B-hbl and 183D-hbl, to a flat unfractionated REE pattern, GAB-hbl, Fig. 4.16. Negative Eu anomalies, with Eu/Eu* ranging from 0.41 to 0.85, are present in all three hornblendes. The two most REE enriched hornblendes show fractionation patterns very similar to the average REE pattern of the Scourian hornblendes. The REE patterns for the granulitic hornblendes, both areas, are more enriched in the LREE relative to the MREE, than the dacitic hornblendes which tend to have a maximum enrichment in the MREE. Only the metagabbroic hornblende, GAB-hbl, has REE concentrations similar to those expected for an andesitic hornblende, although the actual degree of fractionation is different.

The M_4 site in the amphibole structure is the most suitable site which will accept the REE; the A site is too big even for the largest of the REE. For calcic amphiboles the coordination number of the M_4 site closely approximates 8-fold symmetry (Hawthorne, 1983). The distortion of this site is less than that of the analogous M_2 site in clinopyroxenes because it is usually completely filled by Ca and Na. Occasionally Fe or Mn can occupy this site but not to the same degree as in clinopyroxene.

The predicted maximum enrichment in Pr is closely approached in the REE patterns of most of the granulitic hornblendes. Only the igneous hornblendes depart from the theoretical REE fractionation pattern. This deviation could be partly the result of the control of the melt composition on REE fractionation in igneous systems. Temperature of formation and composition of the hornblende may be controlling factors in REE partitioning. It is difficult to assess which one of these factors is dominant in controlling the REE distribution into metamorphic hornblendes.

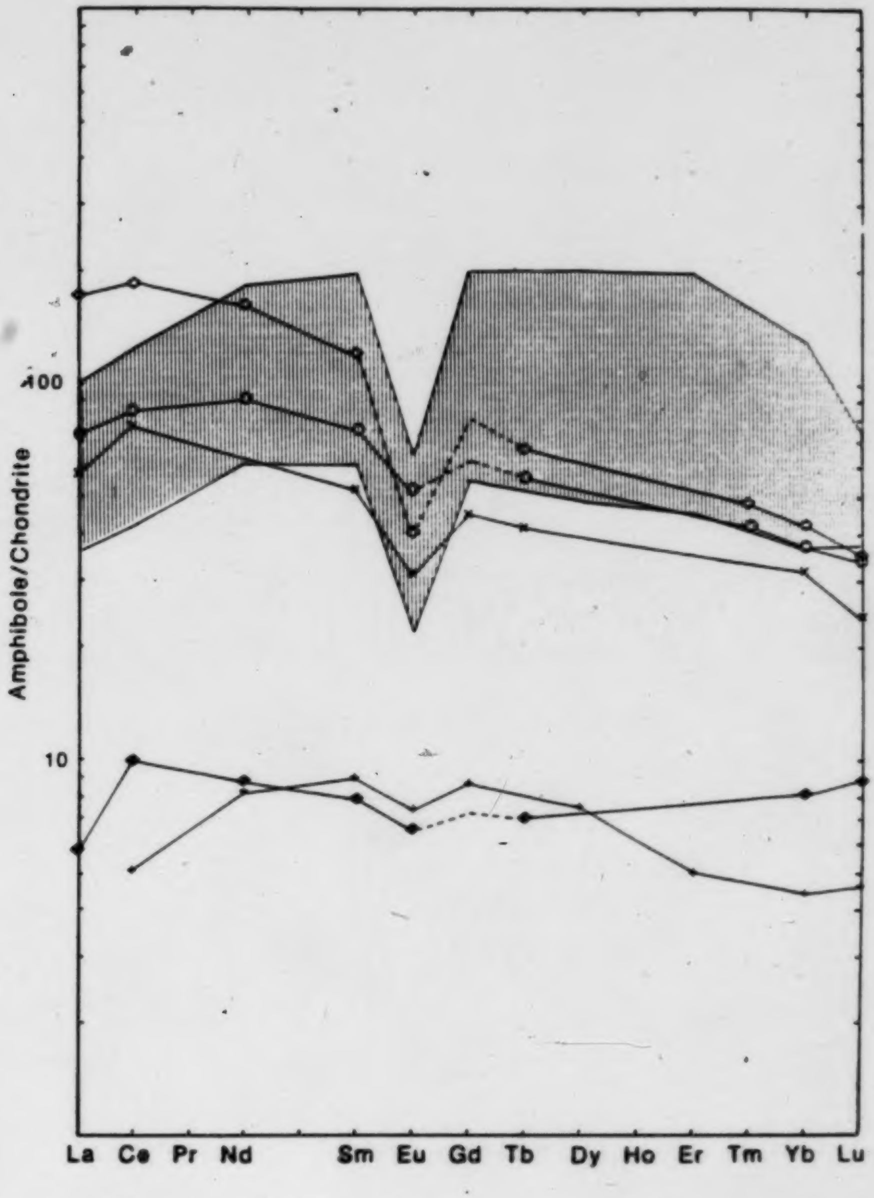

Fig. 4.17. Chondrite normalised REE patterns of the Tsu Lake hornblendes compared to hornblendes from other rock types. Symbols: 141B-hbl (open circles), 183D-hbl (open diamonds), GAB-hbl (closed diamonds), Scourian hbl (diagonal crosses), dacitic hbl (vertical lines), andesitic hbl (vertical crosses). References for the published data are the same as those listed for Fig. 4.13.

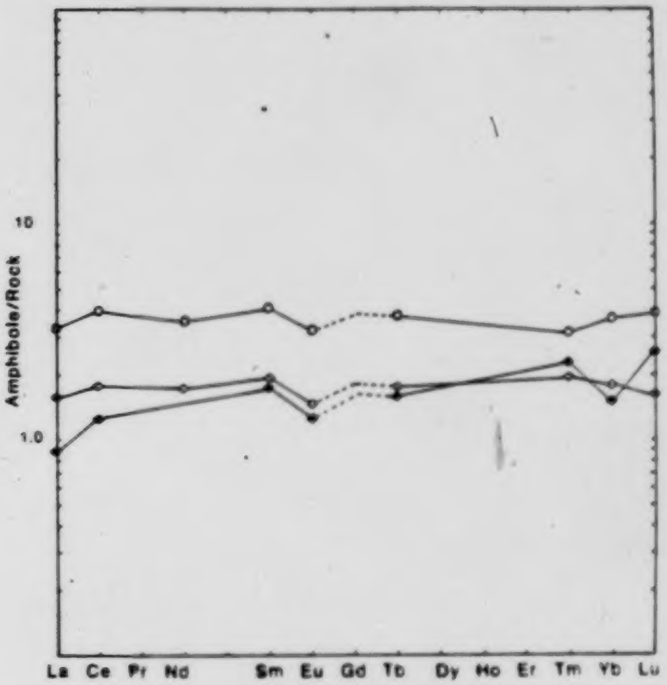

Fig 4.18. REE distribution ccoefficients for the partitioning of the REE between the hornblende and the bulk rock. Symbols as in Fig. 4.17.

Plagioclase

All of the plagioclases show LREE-enriched fractionation patterns and positive Eu anomalies, Fig. 4.19. This sample group includes two plagioclases from pelitic lithologies, 290A-plag and 183B-plag. There is little relative variation in the total REE concentration of the plagioclase, except for GAB-plag. There is a wide variation in the size of the Eu anomaly; Eu/Eu* varying from 1.28 to 30.

The plagioclase REE fractionation patterns quite strongly reflect the concentration of the REE in the rock, Fig. 4.20. Three distinct types of plag/rock REE patterns, corresponding to the different lithologic groups, 1, 2 and 6, are apparent. The different REE patterns for group 1 and 2 lithologies are significant. None of the minerals so far discussed, have REE fractionation patterns so dependent on whole rock composition.

Chondrite normalised REE patterns of plagioclase, in general, do not show uniquely defined patterns indicative of a particular rock type. There is a considerable overlap in the REE composition ranges of plagioclases from igneous rocks, although andesitic plagioclases tend to show flatter REE fractionation patterns than dacitic or rhyolitic plagioclases. The Tsu Lake granulitic plagioclases have REE concentrations that are greater than dacitic plagioclases although the degree of fractionation is similar. Scourian granulitic plagioclases have REE patterns that are comparable in both abundance and fractionation, to the dacitic plagioclases.

Assessment of the crystallo-chemical control on the partition of the REE into plagioclase is difficult because of the complexity of the feldspar structure. The coordination number of the site which accommodates the large cations Ca, Na and K, is variable. K usually has an irregular 9-fold coordination. The size of the site decreases with the smaller cations so that with Na, 7-fold coordination prevails. Even with 7-fold coordination the site in the plagioclase structure is much larger than the ionic radius of La, the largest REE. Therefore LREE-enriched patterns in plagioclase with a maximum enrichment in La, are predicted, and also observed.

The larger Eu^{2+} cation is more readily accommodated in the feldspar structure than the trivalent REE; hence the presence of a positive Eu anomaly in this phase. It has been suggested that the size of the Eu anomaly is dependent on the composition of the feldspar (Schnetzler and Philpotts, 1970); no correlation between these two factors was observed

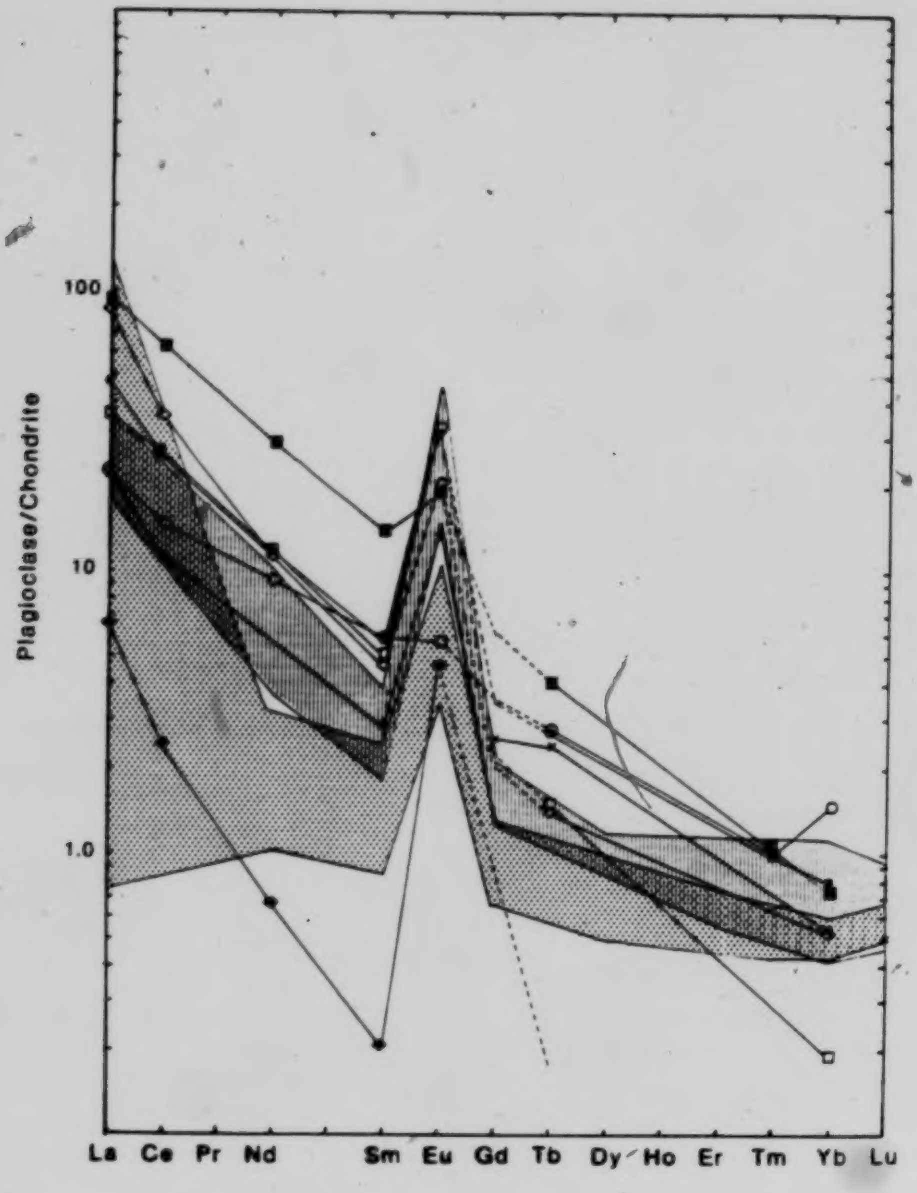

Fig. 4.19. Chondrite normalised REE patterns of the Tsu Lake plagioclases compared to plagioclases from other rock types. Symbols: 141B-plag (open circles), 186A-plag (closed circles), 183D-plag (open diamonds), GAB-plag (closed diamonds), 183B-plag (open squares), 290A-plag (closed squares), Scourian plag (crosses), dacitic plag (vertical lines), andesitic plag (dots). References for the published data are the same as those listed for Fig. 4.13.

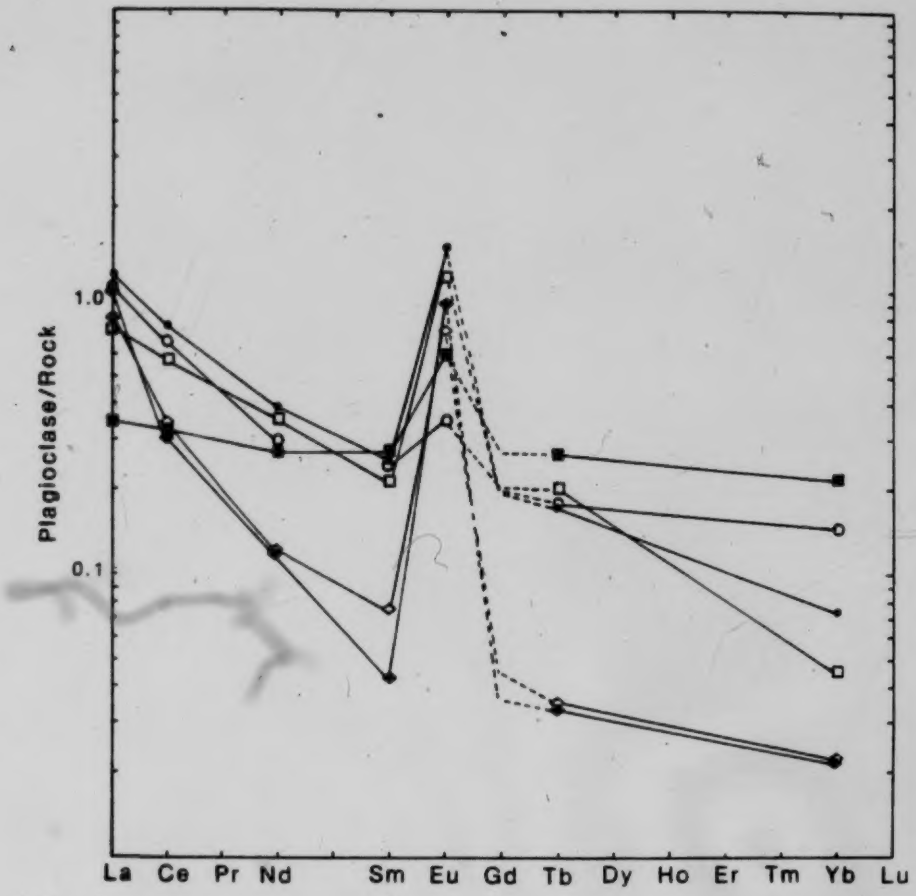

Fig. 4.20. REE distribution coefficients for the partitioning of the REE between the plagioclase and the bulk rock. Symbols as in Fig. 4.19.

for the Tsu Lake plagioclases. Similarly, no correlation was reported for the Scourian granulitic plagioclases (Pride and Muecke, 1981). The variation in the size of the Eu anomaly could be due to temperature and oxygen fugacity conditions which exert a strong control over the partitioning of Eu^{2+} into plagioclase (Drake and Weill, 1975).

Experimental studies on the plag/melt systems suggest that the REE distribution coefficient is not strongly dependent on temperature (Drake and Weill, 1975). This, perhaps, accounts for the lack of any major variations in the REE patterns of plagioclases from different igneous rocks.

Apatite

The REE contents of the apatites show a wide variation in the total REE concentrations, Fig. 4.21. A comparison of the REE content of the apatite versus that of the rock, Fig. 4.22, shows that the relative total REE concentrations of the apatite are a function of the total REE content of the rock. All the apatites from the basic rocks, 183D-apat, 186A-apat, and GAB-apat, show the same REE partition coefficient. A most significant feature of Figs. 4.21 and 4.22, is the difference in the degree of fractionation and the total REE abundances between the apatite from the pelitic rock and those from the basic rocks. This feature suggests there is a strong whole rock compositional control on the nature of the REE distributions in apatites.

The apatite from the basic samples all show LREE-enriched fractionation patterns with negative Eu anomalies. The size of the Eu anomaly is about the same for all three samples; the maximum variation in Eu/Eu* is from 0.31 to 0.4. Sample 183B-apat from pelitic rock displays a concave-down shaped REE fractionation pattern with a maximum enrichment in Nd. The Eu anomaly for this sample is much larger than those in the basic rocks with a Eu/Eu* of 0.15.

The REE patterns of the Tsu Lake apatites have been compared to those of apatites from granitic and dacitic rocks, and some gneisses. Unfortunately no data were available on the REE concentrations of the accessory phases of the Scourian granulites. Only the pelitic apatite, 183B-apat, is comparable to the dacitic REE patterns, although the pelitic apatite is less enriched in the HREE. Two of the apatites from the basic rocks fall within the range of REE values expected for gneissic rocks.

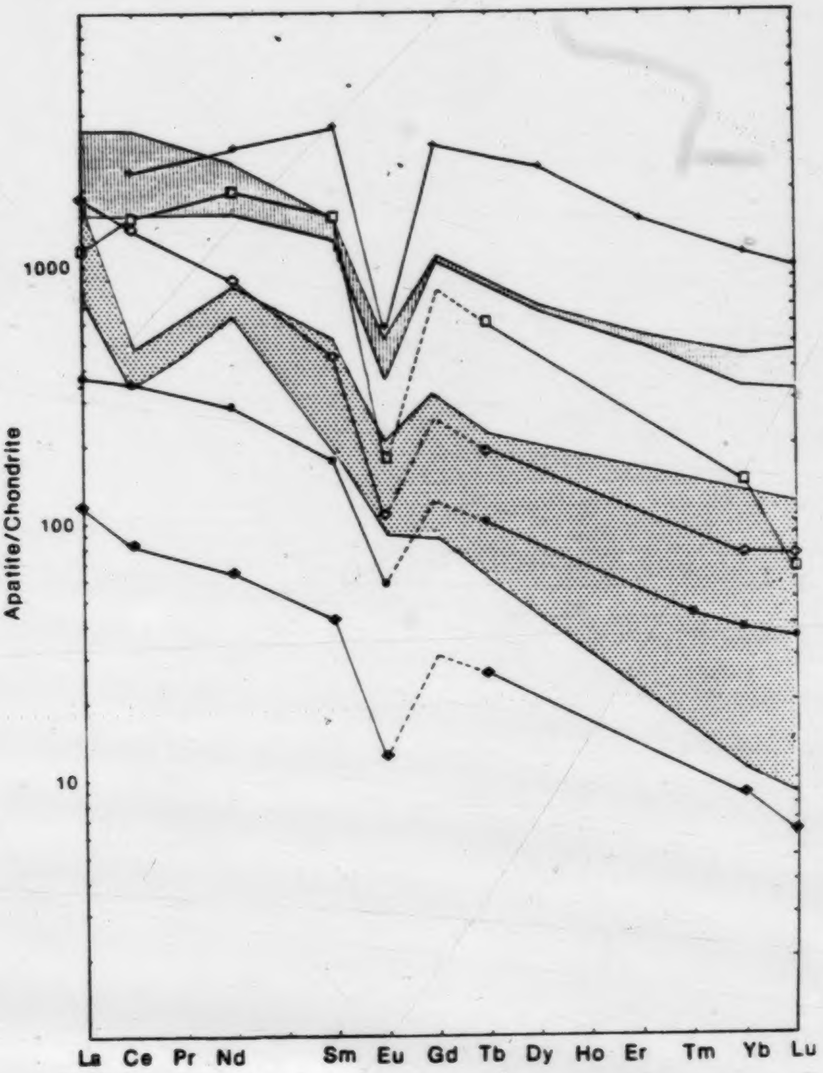

Fig. 4.21.Chondrite normalised REE patterns of the Tsu Lake apatites compared to apatites from other rock types. Symbols: 186A-apat (closed circles), 183D-apat (open diamonds), GAB-apat (closed diamonds), 183B-apat (open squares), dacitic apat (vertical lines), granitic apat (crosses), gneissic apat (dots). References for the published data are: Nagasawa (1970); Puchelt and Emmermann (1976).

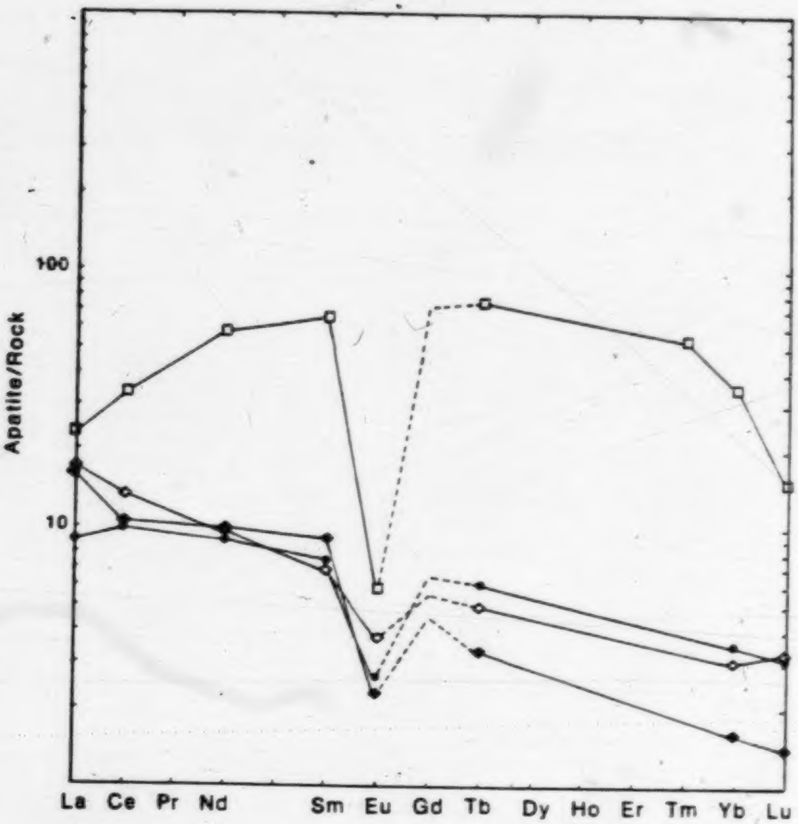

Fig. 4.22. REE distribution coefficients for the partitioning of the REE between the apatite and the bulk rock. Symbols as in Fig. 4.21.

The lack of any similarity in the REE patterns of the dacitic apatites and the apatites from the Tsu Lake basic rocks is significant. It supports the contention that the similarity between the REE patterns of major minerals in these two different rocks types is merely fortuitous and implies that there could be a temperature control on the REE distributions.

Fleischer and Altschuler (1969) report a compositional dependence on the REE distribution in apatites from igneous rocks, similar to that seen for the Tsu Lake apatites. Those apatites from the most silica-rich rocks are more enriched in the HREE than the those from mafic rocks.

The REE replace Ca in the apatite structure in two crystallographically different sites; one with 7-fold coordination and the other with 9-fold coordination (Henderson, 1980). Therefore it can be expected that maximum enrichment in Ce(N) or Pr(N) will be present. The difference in REE selectivity between apatites from acidic and basic rocks is presumably related to whole rock compositional control. It does not appear to be the result of differences in the total REE concentrations which can affect the REE selectivity of a mineral (Khomyakov, 1963).

Zircon

The modal abundance of zircon in the basic rocks is very low, hence it was not possible to separate out sufficient quantities of zircon in these samples for analysis. Only one zircon sample, 183B-zir, from a pelitic rock, was considered in this study. Its chondrite normalised REE pattern is shown in Fig. 4.23. The abundances of La and Ce have been corrected for U fission product interferences. Nd could not be quantified because of a large spectral interference from Hf. Sample 183B-zir has a REE pattern characterised by HREE enrichment and small anomalies in both Ce and Eu. The extent to which the HREE are partitioned into zircon relative to other phases is seen in the zircon/rock REE patterns, Fig. 4.24.

Zircon REE patterns are quite variable, in terms of their LREE concentrations, and may be dependent on the composition of the whole rock (Haskin and Paster, 1979; Murali *et al.*, 1983). Assessment of the effects of bulk compositions is difficult, however, because the refractory nature of zircon could conceivably allow it to survive more than one cycle of magmatism without significant changes in the REE contents. REE patterns of zircons from metamorphic rocks are particularily difficult to interpret because they are

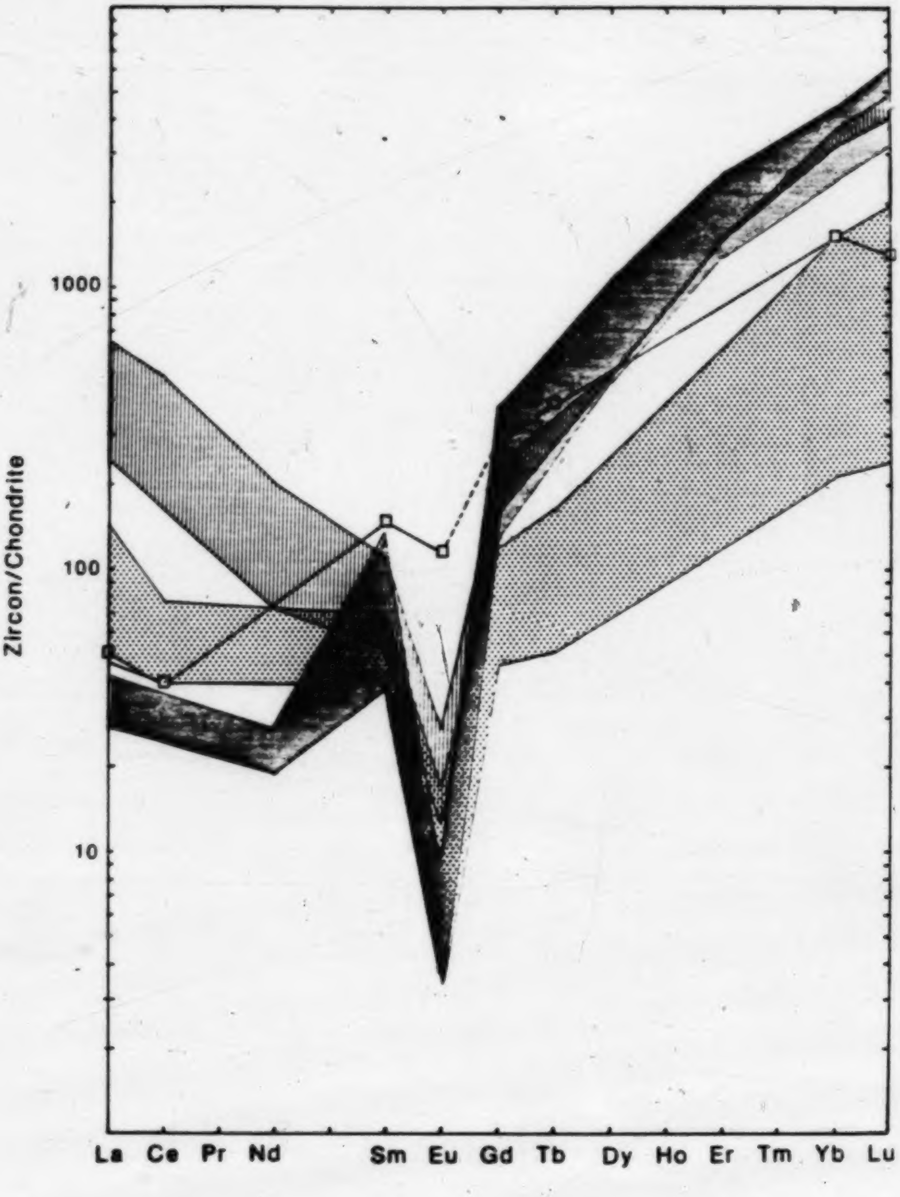

Fig 4.23. Chondrite normalised REE patterns of a Tsu Lake zricon compared to zircons from other rock types. Symbols: 183B-zir (open squares), dacitic zir (vertical lines), charnockitic zir (large dots), granitic zir (small dots). References for the published data are: Nagasawa (1970); Murali *et al*. (1983).

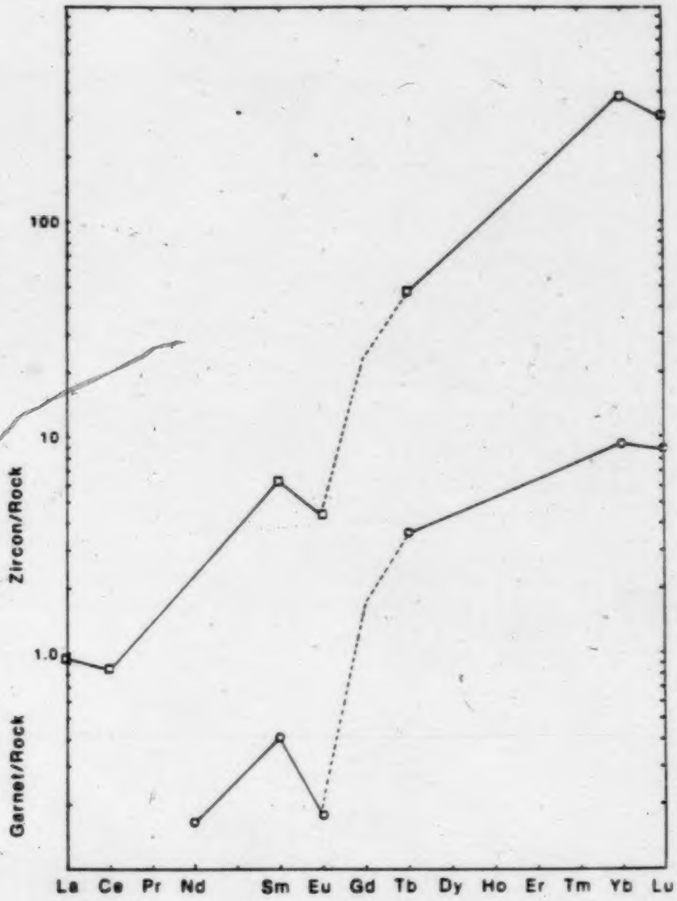

Fig. 4.24. REE distribution coefficients for the partitioning of the REE between (a) zircon and the bulk rock, and (b) garnet and the bulk rock. Symbols: 183-zir (open squares), 183B-grnt (open circles).

likely to have been inherited from precursor igneous materials.

Murali *et al*. (1983) recorded three different types of zircon REE patterns: (a) moderately HREE-enriched patterns with negative or positive Ce anomalies and negative Eu anomalies; (b) HREE-enriched patterns with negative Eu anomalies; (c) variably HREE-enriched with no anomalies. Sample 183B-zir has REE characteristics of the type (a) of Murali *et al*. (1983). Its REE pattern shows little similarity to the REE patterns of zircons from granites or dacites. The small negative Eu anomaly for this sample is noteworthy. Zircon in this rock is believed to be of a primary metamorphic origin. The high modal abundance of this phase in the rock, along with the high concentration of apatite, does not indicate an inherited igneous phase.

Garnet

As garnet does not occur in the Tsu Lake basic rocks only one garnet from a pelitic rock, 183B, could be analysed. The chondrite normalised REE pattern of 183B-grnt shown in Fig. 4.25, and the grnt/rock REE pattern is shown in Fig. 4.24. The distribution of the REE in the garnet does not appear to have been affected by the total REE concentration in the rock. The garnet exhibits a HREE-enriched fractionation pattern with a prominent negative Eu anomaly. There is little fractionation amongst the HREE but the LREE are differentiated with respect to one another.

Consideration of the crystallo-chemical factors suggests that the REE patterns of garnets should be HREE-enriched. The REE substitute for the divalent cations, Ca, Mg, Fe, in 8-fold coordinated sites. In Fe or Mg-rich garnets the structure most easily acccepts the HREE. As the amount of Ca increases the substitution of the LREE is favoured. The experimental studies of Nicholls and Harris (1980) demonstrate the expected correlation between the LREE concentration and the Ca content of the garnet.

The Tsu Lake garnet has a REE pattern very similar to the average REE pattern of the Scourian garnets with the exception of the Eu anomaly. Neither of the REE patterns of the garnets from the two granulite facies areas show any similarity to the REE patterns of the dacitic garnets.

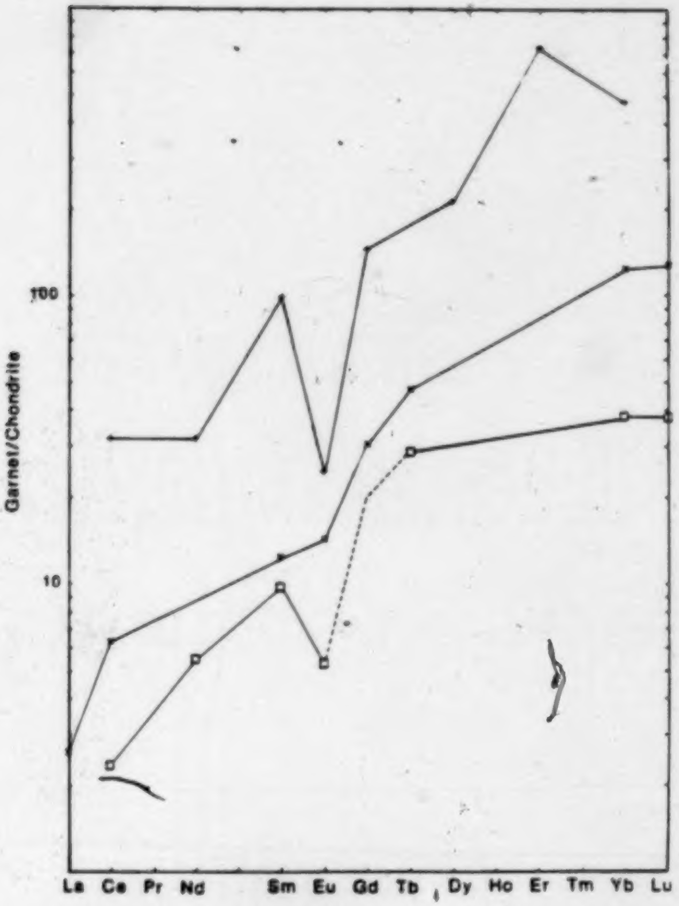

Fig. 4.25. Chondrite normalised REE patterns of a Tsu Lake garnet compared to garnets from other rock types. Symbols: 183B-grnt (open squares), Scourian grnt (diagonal crosses), dacitic grnt (vertical crosses). References for the published data are: Nagasawa and Schnetzler (1971); Pride and Muecke (1981).

Mineral / Mineral Pairs

The partitioning of the REE between two phases in the Tsu Lake granulite facies minerals was examined and compared to the same mineral pairs from igneous pairs. Figs. 4.26 to 4.34 show the REE relationships between the mineral pairs: opx / plag, cpx / plag, opx / cpx, hbl / plag, opx / hbl, cpx / hbl, opx / apat, cpx / apat, and hbl / apat.

The Tsu Lake opx / plag pairs display a range of REE distribution coefficients, Fig. 4.26, although the degree of REE fractionation is about the same in all three pairs. The REE distribution coefficients overlap with the values shown by the basaltic and andesitic opx / plag pairs. In contrast the REE partitioning into dacitic orthopyroxenes relative to dacitic plagioclases is much higher than the partitioning between the same Tsu Lake minerals. The Scourian REE distribution coefficients for this mineral pair are distinctly different for the LREE than any of the mineral pairs of the rock units discussed so far.

The REE distribution coefficients for the Tsu Lake cpx / plag pairs show values that are similar to those shown by cpx / plag pairs from andesitic and basaltic rocks, Fig. 4.27. Scourian cpx / plag REE distribution coefficients are similar to dacitic cpx / plag values for the LREE but have smaller values for the HREE.

REE fractionation between clinopyroxene and orthopyroxene for two of the Tsu Lake pairs is very similar to that shown by the Scourian cpx / opx pair, Fig. 4.28. Reitan and Roelandts (1973) note the same type of partitioning for cpx / opx pairs from the mafic granulites of Lofoten-Vesteralen. Partitioning of the REE between the cpx / opx pairs from dacites differs from the relationship seen in the granulitic pairs by the absence of a Eu anomaly. This feature may be only indicative of different oxygen fugacity conditions. The cpx / opx pair from 183D has a REE distribution coefficient comparable to that expected for an andesitic / basaltic cpx / opx pair. The difference in the REE partitioning relationships of the cpx / opx pair between 183D and the other two Tsu Lake samples is significant. It suggests that 183D-hbl has had an important influence over the partitioning of the REE into the pyroxenes of that rock.

For the hbl / plag pairs the REE distribution coefficients of the Tsu Lake samples do not differ appreciably from the values expected for dacitic or Scourian granulitic hbl / plag pairs, Fig. 4.29. In contrast to this the REE distribution coefficients for the hbl / plag pairs from andesites are much lower and do not show Eu anomalies.

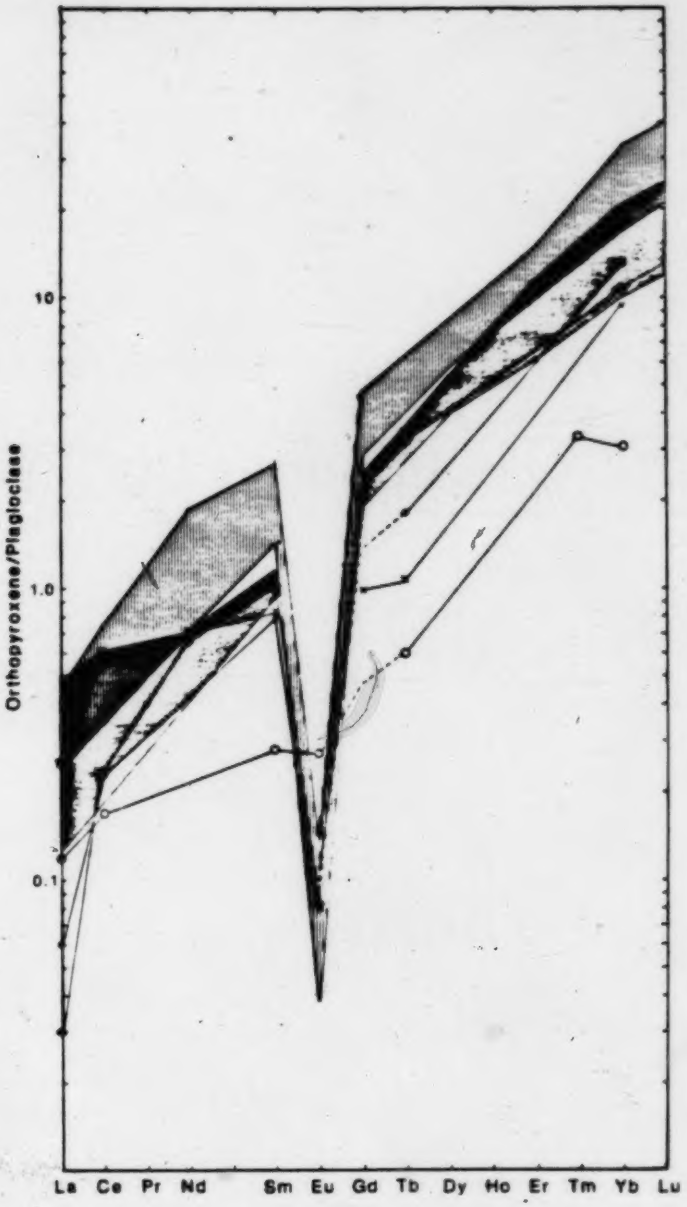

Fig. 4.26. REE distribution coefficients for coexisting orthopyroxene - plagioclase pairs. Symbols: 141B opx-plag (open circles), 186A opx-plag (closed circles), 183D opx-plag (open diamonds), Scourian opx-plag (diagonal crosses), dacitic opx-plag (vertical lines), andesitic opx-plag (small dots).

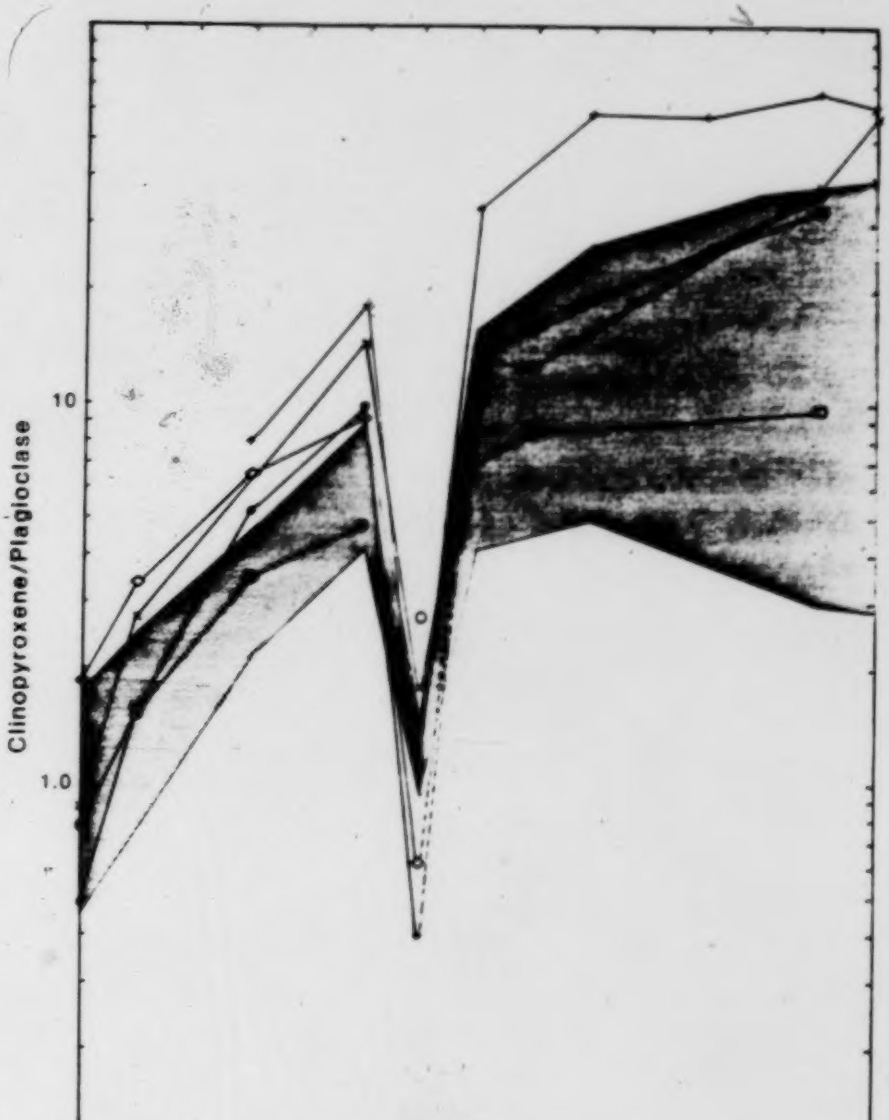

Fig. 4.27. REE distribution coefficients for coexisting clinopyroxene - plagioclase pairs. Symbols: 141B cpx-plag (open circles), 186A cpx-plag (closed circles), 183D cpx-plag (open diamonds), Scourian cpx-plag (diagonal crosses), dacitic cpx-plag (vertical crosses), andesitic cpx-plag (small dots).

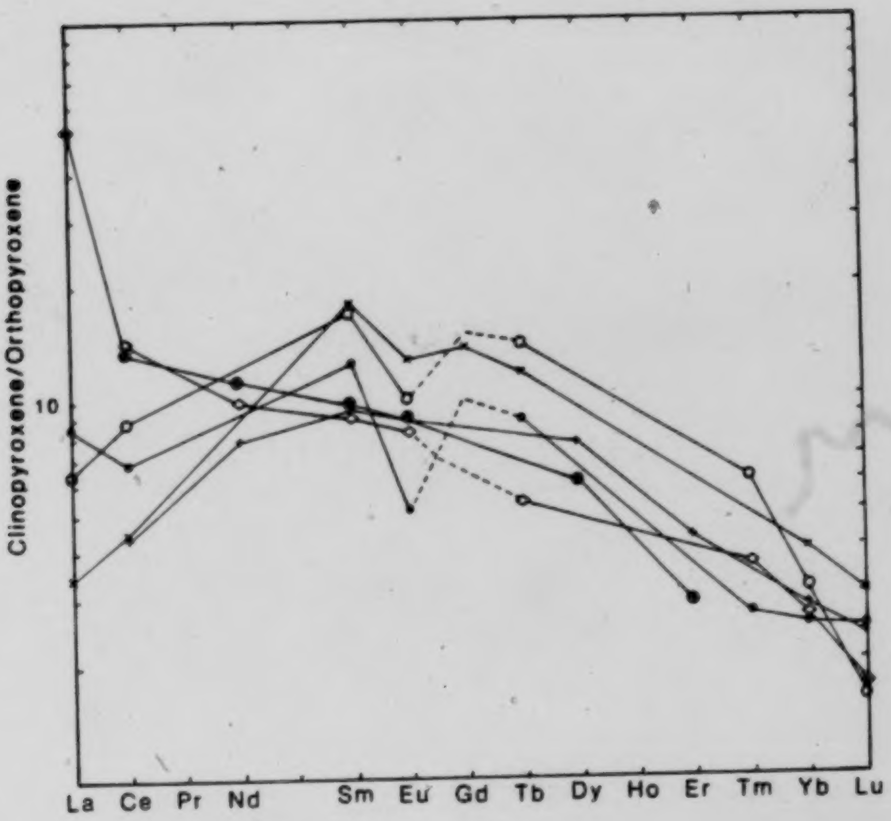

Fig. 4.28. REE distribution coefficients for coexisting clinopyroxene - orthopyroxene pairs. Symbols: 141B cpx-opx (open circles), 186A cpx-opx (closed circles), 183D cpx-opx (open diamonds), Scourian cpx-opx (diagonal crosses), dacitic cpx-opx (vertical crosses), andesitic cpx-opx (crosses within circles).

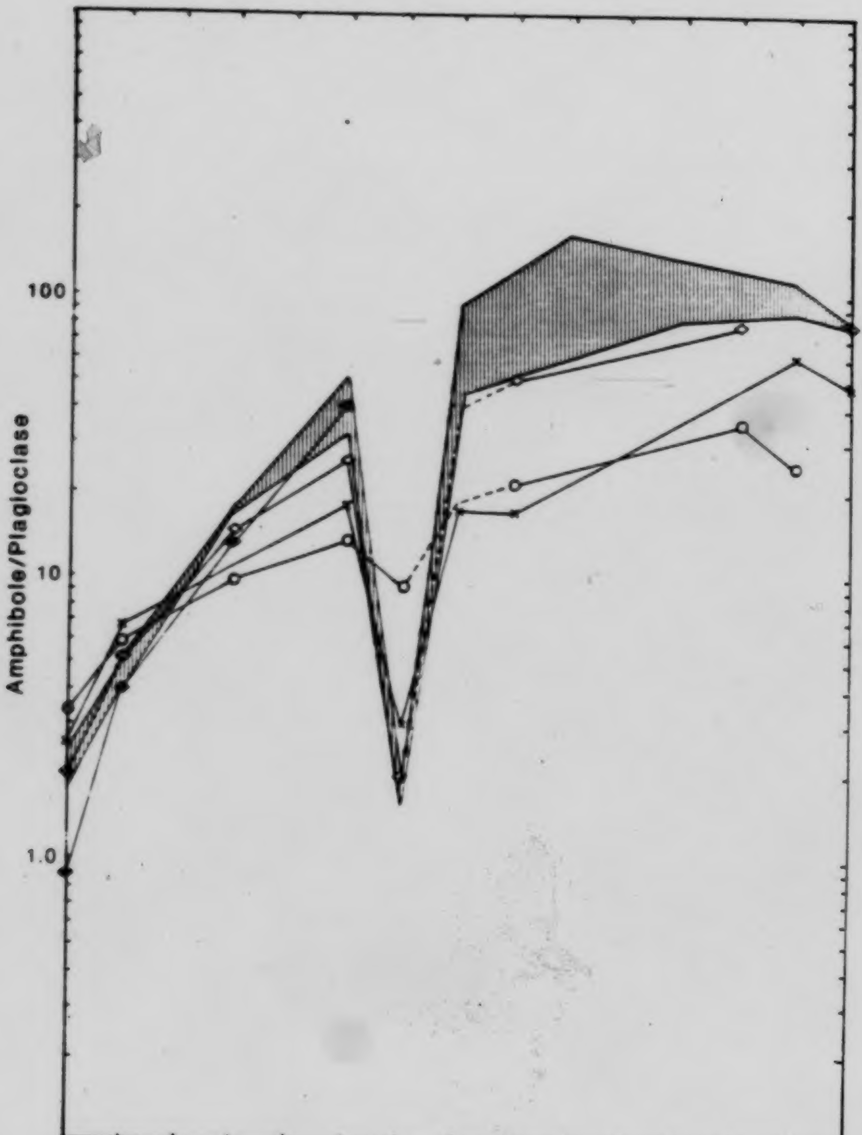

Fig. 4.29. REE distribution coefficients for coexisting hornblende - plagioclase pairs. Symbols: 141B hbl-plag (open circles), 183D hbl-plag (open diamonds), GAB hbl-plag (closed diamonds), Scourian hbl-plag (crosses), dacitic hbl-plag (vertical lines).

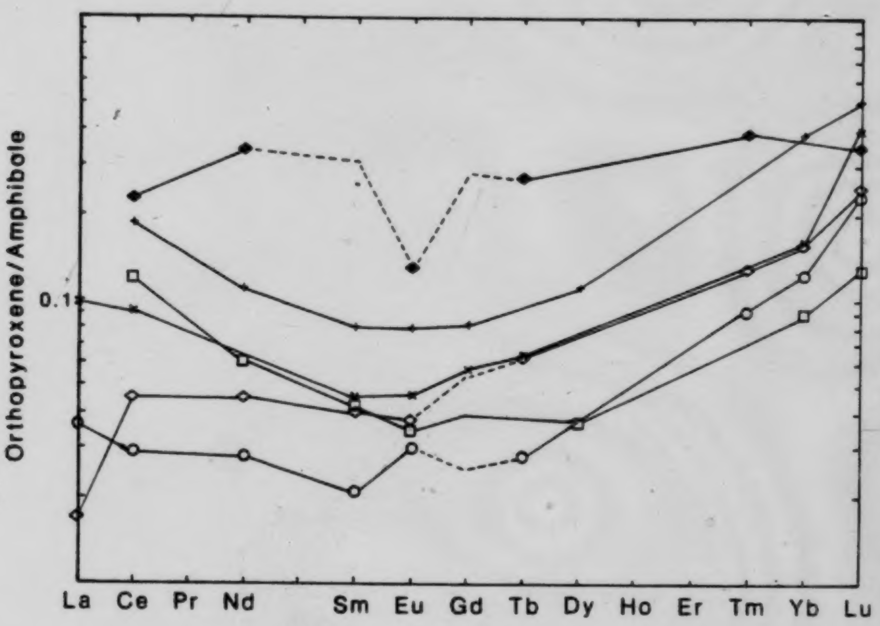

Fig. 4.30. REE distribution coefficients for coexisting orthopyroxene - hornblende pairs. Symbols: 141B opx-hbl (open circles), 183D opx-hbl (open diamonds), GAB opx-hbl (closed diamonds), Scourian opx-hbl (diagonal crosses), dacitic opx-hbl (vertical crosses), andesitic opx-hbl (open squares).

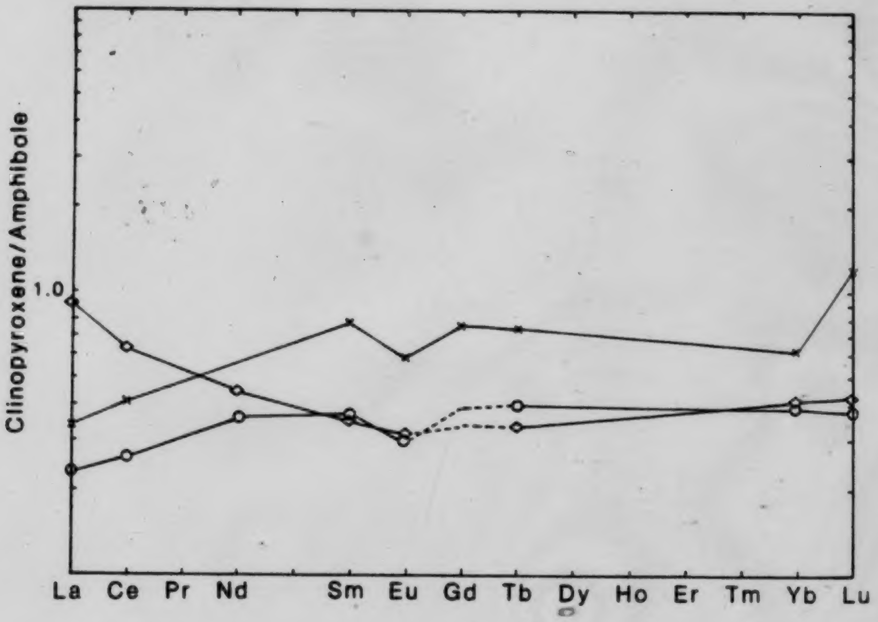

Fig.4.31. REE distribution coefficients for coexisting clinopyroxene - hornblende pairs. Symbols: 141B cpx-hbl (open circles), 183D cpx-hbl (open diamonds), Scourian cpx-hbl (diagonal crosses).

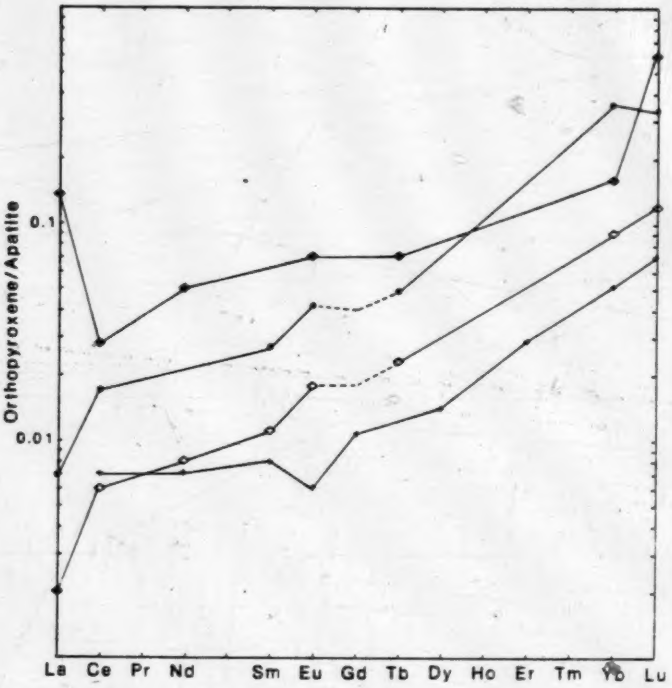

Fig. 4.32. REE distributions coefficients for coexisting oprthopyroxene - apatite pairs. Symbols: 183D opx-apat (open diamonds), GAB opx-apat (closed diamonds), 186A opx-apat (closed circles), dacitic opx-apat (vertical crosses).

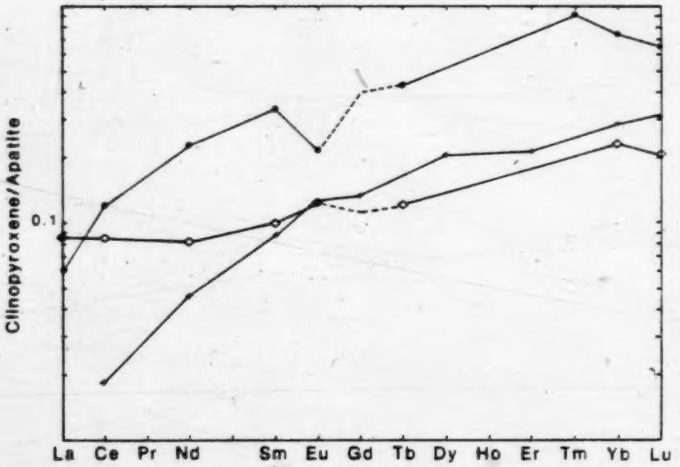

Fig. 4.33. REE distributions coefficients for coexisting clinopyroxene - apatite pairs. Symbols: 186A cpx-apat (closed circles), 183D cpx-apat (open diamonds), dacitic cpx-apat (vertical crosses).

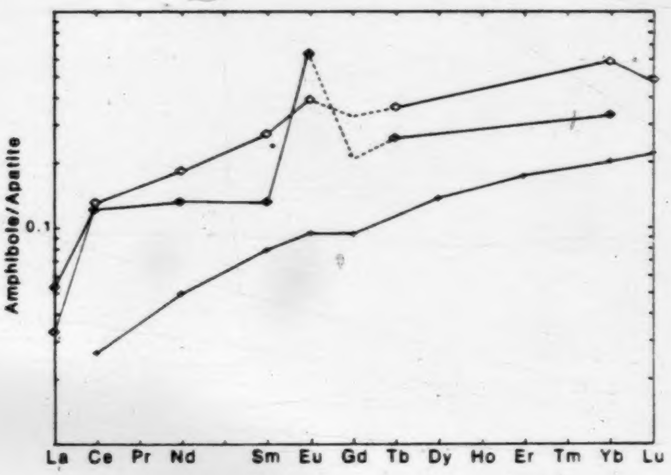

Fig. 4.34. REE distribution coefficients for coexisting hornblende - apatite pairs. Symbols: 183D hbl-apat (open diamonds), GAB hbl-apat (closed diamonds), dacitic hbl-apat (vertical crosses).

The Tsu Lake opx/hbl REE distribution coefficients show values that reflect the assemblage with which the mineral pair is associated, Fig. 4.30. Except for GAB-opx/hbl the Tsu Lake samples have similar distribution coefficients to dacitic opx/hbl pairs and to the Scourian data.

The REE distribution coefficients for the cpx/hbl pairs of the Tsu Lake rocks are very similar, Fig. 4.31. This contrasts with that seen for the opx/hbl pairs. It implies that hornblende exerts a stronger control over the partitioning of the REE into orthopyroxene than it does with clinopyroxene. Similar conclusions regarding the role of hornblende in the REE partitioning relations between minerals in the Tsu Lake rocks were inferred from the nature of the partitioning between orthopyroxene and clinopyroxene.

For the minerals, orthopyroxene, clinopyroxene and hornblende, relative to apatite, the REE distribution coefficients are higher than the values for the same mineral pairs from dacitic rocks, Figs. 4.32 to 4.34. This is merely a reflection of the higher total REE concentrations of the dacitic apatites compared to apatites from basic granulites.

Conclusions

The similarity between the REE patterns of the Scourian granulite facies minerals and those from dacitic rocks, has been interpreted to mean that the granulite facies minerals have been in equilibrium with a graniodioritic melt (Pride and Muecke, 1981). This interpretation is based on the following assumptions:

i. the geochemical characteristics of the Scourian complex are consistent with a model whereby the gneisses represent the residuum left after partial melting of a precursor greywacke material (Pride and Muecke, 1980);

ii. the assumptions used in the model are applicable to this area, i.e., the equation of Shaw (1970) for equilibrium partial melting, mineral/melt distribution coefficients for rhyolitic rocks from Arth and Hanson (1975), and trace element concentrations of a greywacke parent material, are all valid (Pride and Muecke, 1980);

iii. the similarity between the REE patterns of the Scourian granulite facies minerals and minerals from dacitic rocks is not fortuitous (Pride and Muecke, 1981).

The last assumption, regarding the REE patterns of the minerals, relies heavily on the appropriateness of the two preceding assumptions. The validity of the first assumption has been challenged elsewhere (Weaver and Tarney, 1981) . On the basis of the data presented in this study the validity of the third assumption can be challenged here.

The geochemical characteristics of the Tsu Lake granulites are not the same as those shown by the Scourian granulites. There is no depletion of the LIL elements, a feature which is frequently characteristic of medium to high-pressure granulites. The mineralogy of the Tsu Lake granulites suggests low pressure metamorphic conditions, hence the geochemistry of these rocks is not considered to be unusual. The partial melting theory necessary to explain the geochemical features of the Scourian granulites is not required to explain the geochemistry of the Tsu Lake granulites. Some of the Tsu Lake gneisses, notably the pelitic units, have experienced partial melting but the basic rocks, which were used in the study of mineral REE patterns, are believed to be unaffected by this event.

The REE patterns of the Tsu Lake granulite facies basic rocks are not consistent with the REE patterns predicted from crystallochemical considerations. The deviations from the theoretical trends are likely to be the result of temperature and compositional controls on the REE partitioning relations. Of the major mineral phases the orthopyroxenes, clinopyroxenes and hornblendes of the Tsu Lake rocks show REE patterns that resemble those shown by the same phases of dacitic rocks, in terms of relative degrees of REE fractionation. The similarity is accentuated by the large differences observed in the REE fractionation patterns of dacitic and andesitic/basaltic minerals. Absolute abundances of the REE are not always the same. The Scourian orthopyroxene, clinopyroxene and hornblende REE patterns compare more closely to the data from the same phases of the Tsu Lake rocks, in both absolute and relative REE abundances, than do the data from the dacitic minerals.

The REE patterns for the Tsu Lake plagioclases seem to reflect the rock type/assemblage although the patterns are similar to the REE patterns of both the Scourian and dacitic plagioclases. The most significant departure from dacite-like REE characteristics is with the Tsu Lake apatites. The REE patterns for this phase resemble those shown by the other gneisses but are quite dissimilar to dacitic apatites in terms of the degree of REE fractionation and absolute REE abundances.

The REE partitioning between two mineral phases is a little more difficult to interpret because the differences in the distribution coefficients for mineral pairs from different rock types are not as pronounced as they are with the chondrite-normalised REE abundances. Only the hbl/plag distribution coefficients of the Tsu Lake rocks can be said to be similar to that of the same dacitic mineral pair. The rest of the mineral pairs have REE distribution coefficients comparable to andesitic/basaltic mineral pairs, where that data is available for comparison. In all cases the distribution coefficients of the Scourian mineral pairs are very similar to those obtained from the Tsu Lake data.

A comparison of the REE data for the Tsu Lake, Scourian and dacitic minerals suggests that the similarity of the chondrite-normalised REE patterns of metamorphic minerals to igneous minerals is fortuitous. It is tentatively suggested that the similarity could be the result of a temperature effect, although there is no experimental evidence to support this claim. Mahood and Hildreth (1983), from a study of rhyolitic minerals, concluded that a temperature dependence of the crystal/melt REE partitioning relations is small for rhyolitic samples and such an effect is swamped by the melt compositional effect. While this may be true for igneous systems the same is not necessarily true for metamorphic rocks which have not been in equilibrium with a melt.

The similarity of the REE data for the Tsu Lake rocks and the Scourian rocks suggests that the same control on the REE partitioning relations has been operational in both areas. Whatever model is used to explain the geochemical characteristics of the Scourian complex, cannot be used to explain the REE data. The lack of the same geochemical characteristics in the Tsu Lake gneisses precludes this. Temperature has been suggested as a suitable control of the REE partitioning relations in granulite facies rocks as the pressure-temperature conditions of the two areas concerned, although quite different in terms of pressure, appear to have experienced relatively similar temperatures, i.e., the temperature difference between these two areas is less than the temperature difference between the liquidus temperatures of rhyolitic and basic melts. The type of phases which are present, presumably also control the REE partitioning. However it is dominantly the temperature and the whole rock composition which control the nature of the metamorphic assemblage; hence temperature can be considered to be the strongest control.

CHAPTER 5

CONCLUSIONS

Mineralogy

The mineral assemblages of both the pelitic and basic rocks from the Tsu Lake area indicate the attainment of granulite facies conditions. The pelitic samples show evidence of partial melting while the basic samples appear to have been unaffected. In contrast the Deskenatlata Lake assemblages are typical of amphibolite facies grade metamorphism. Assessment of the nature of the metamorphism is based on compositional data for the minerals as well as the presence of diagnostic assemblages. Compositions of the minerals of the Tsu Lake rocks are consistent with those commonly found in granulite facies rocks and are quite distinct from the equivalent Deskenatlata Lake mineral compositions.

Both amphiboles and biotites of Tsu Lake show the increased amount of Ti substitution that is associated with high grade metamorphism. The same phases in the Deskenatlata Lake rocks have conspicuously lower Ti concentrations. The type of substitution reactions in biotite are slightly different to those observed in other granulite facies terrains. This suggests that either the nature of the granulite facies conditions at Tsu Lake, or the presence of later metamorphic overprints, is responsible for the observed compositional effects in biotites. The latter explanation is preferred because of the presence of other metamorphic overprint effects.

The pyroxenes show compositional effects that appear to be related too the reactions which formed these minerals. The preference of Mg or Fe^{2+} for the tschermakite substitution in orthopyroxene is apparently affected by the presence of clinopyroxene and / or biotite.

The compositions of the garnets reflect their mode of formation; either as a restite phase in a partially melted rock or as a primary metamorphic phase. The presence of zoning in garnets does not necessarily imply a preservation of the original granulite facies compositions. It is most likely the result of a retrograde metamorphic event, since any original zoning should have been obliterated by the high temperatures. The cordierites, like the garnets, also show compositions that reflect their mode of formation.

The absence of any miscibility gap in the compositional range of the Tsu Lake plagioclases is consistent with granulite facies conditions. The Deskenatlata Lake plagioclases encompass a range of compositions that are not restricted by a miscibility gap. The lack of this compositional gap in the Deskenatlata Lake plagioclases implies that the predicted miscibility gap of Spear (1980) occurs at lower temperatures than he suggested.

The oxide phases, ilmenite and magnetite, have both suffered post granulite facies alteration in the form of oxidation-exsolution. The magnetites are distinguished by significant concentrations of V, a feature which is believed to be characteristic of granulite facies metamorphism. Hercynite compositions reflect their formation by different mineral reactions.

There is little petrographical evidence of lower grade metamorphic overprints in the Tsu Lake rocks. The occurrence of prehnite associated with biotite in the intermediate to basic rocks is perhaps the strongest evidence for the existence of another metamorphic event. Other minerals show exsolution features, eg., ilmenite, magnetite, hercynite, feldspars and clinopyroxene. These features could be considered to result from a retrograde metamorphic event associated with the uplift of the area which had been subjected to the granulite facies metamorphism. Similarly the presence of sphenitisation features implies the occurrence of a low grade metamorphic event.

Compositional data on the granulite facies minerals also indicates regular partitioning relations between most of major mineral pairs. The implications of these results are that the granulite facies event is relatively unaffected by the later overprints. The order of preference for Fe over Mg partitioning into the Tsu Lake minerals is in accordance with that predicted by Eugster and Ilton (1983) for granulite facies conditions, with the exception of biotite. The mineral most affected by metamorphic overprinting is biotite.

A review of several of geothermometers and geobarometers indicates there are a number of serious problems associated with some of the commonly used calibrations. The orthopyroxene - clinopyroxene geothermometer would seem to be inappropriate for application to metamorphic systems. Some inexplicable problems, possibly related to ordering/exsolution features of metamorphic pyroxenes, hamper the use of this geothermometer. Similar problems are encountered with the clinopyroxene - ilmenite geothermometer.

The use of reintegration techniques in the application of the ilmenite - magnetite geothermometer is questioned. A literature review of exsolution features of magnetite and ilmenite from slowly cooled systems, i.e., igneous plutons and granulite facies rocks, suggests that the textures which result are complex. Simple reintegration procedures, such as those used by Bohlen and Essene (1977) are probably inadequate to resolve these complex exsolution textures.

The thermodynamic validity of the two feldspar geothermometer has been questioned by other authors. Its use was avoided here because of the uncertainty surrounding its applicability.

The inability to model accurately the influence of the other garnet components on the Fe - Mg system restricts the usefulness of the garnet geothermometers. The garnet - biotite geothermometer is also affected by the unknown influences of the Al and Ti components in biotite. However, the extreme range of the temperature estimates obtained from the garnet - biotite geothermometer for the Tsu Lake rocks is believed, in this case, to result also from the retrograde metamorphism which disturbed the Fe - Mg system in biotite.

Use of the garnet - cordierite geobarometer is restricted by conflicts in the cordierite hydration theories. These conflicts influence the thermodynamic modelling of the geobarometer. Additionally uncertainties in the H_2O concentrations from indirect determinations by electron microprobe analysis could lead to large errors in the estimated pressures.

Estimates of the pressure - temperature conditions at Tsu Lake were, therefore, based mainly on the stability fields of critical mineral assemblages rather than on geothermometer temperature estimates. The stability of hornblende in the basic granulites and the melting - dehydration reactions of Thompson and Tracy (1979) for pelitic rocks were used as the pressure - temperature constraints. Temperatures of 680 - 750 °C are suggested by the pelitic assemblages for the Tsu Lake area. Garnet - cordierite temperature estimates fall within these limits. Estimates based on the breakdown in the stability of hornblende suggest temperatures of about 700 °C.

Pressure was more difficult to constrain than temperature. Because temperatures estimated from the grnt - cord - sill - qtz geothermo-geobarometer agree with the temperature estimates from pelitic and basic assemblages, it is suggested that the pressure estimates from this calibration are reasonable. Therefore pressure is constrained at 4.5 ±0.5 kb with $P(H_2O)<P(tot)$.

For Deskenatlata Lake the temperatures are estimated at 600 - 650 °C based on the absence of a hornblende breakdown reaction and on the presence of sphene. Pressure could not be estimated because of the lack of suitable assemblages. Much higher fO_2 conditions at Deskenatlata Lake than at Tsu Lake are implied because of the occurrence of sphene and magnetite. These observations agree with those of Bostock (1982).

The estimates of the pressure - temperature conditions of the granulite facies event at Tsu Lake differ markedly from the estimates suggested by Nielsen *et al.* (1981) for the Archean metamorpic event in NE Alberta. The estimates for Tsu Lake are more in accordance with the estimates for the Aphebian amphibolite facies event. Because granulite facies assemblages, not amphibolite facies assemblages, are found at Tsu Lake, it is unlikely that the Aphebian metamorphic event has been described for this area. The discrepancy between the two estimates, this research and that of Nielsen *et al.* (1981), is probably a reflection of the different interpretations of the mineralogical data.

The metamorphic event which is recorded at Deskenatlata Lake is more likely to be the Aphebian amphibolite facies event rather than a lower grade Archean event such as that described by Fraser (1978). This interpretation is based on the occurrence of a major structural feature between Tsu Lake and Deskenatlata Lake, the Deskenatlata Lake fault zone.

The presence and mode of occurrence of prehnite in rocks of both the Tsu Lake and the Deskenatlata Lake areas suggests that this phase may have been produced by a single metamorphic event. From the stability field of this phase it is suggested that prehnite developed during the Aphebian greenschist facies metamorphic event.

Geochemistry

A review of the current literature on LIL element patterns in granulite facies terrains suggests that intermediate to high pressure granulites do not always show the characteristic depleted LIL element patterns. The influence of the composition of the fluid phase has been cited as one factor in determining the LIL element fractionation patterns of a rock system, while the composition of the original rock is also important. Metasomatism may obscure original metamorphic depletion patterns. The variation in K/Rb with respect to the K content in granulitic rocks has often been attributed to igneous fractionation processes. The same variation may be caused by variations in the mineralogy of the rock.

The Tsu Lake granulites show LIL element patterns that are undepleted with respect to the LIL characteristics of some granulite facies terrains. However, they do show the effects of the metasomatic event which affected the Athabasca mobile belt.

The REE patterns of metamorphic basic rocks do not reveal much information about the metamorphic events which have affected them. Evidence for the mobility of the REE during such an event is sparse. A lack of a correlation between the total REE concentrations and the degree of REE fractionation, such as that observed in the Strangways granulites, is one indication of a disturbance to the REE system.

The Tsu Lake basic rocks do not show any evidence of REE mobility. However, the pelitic rocks show features which indicate the REE have been fractionated between the melt and restite portions of these partially melted rocks.

One study of metamorphic minerals cites the similarity between the REE patterns of the metamorphic minerals and those of dacitic minerals as evidence for the generation of the metamorphic rocks in equilibrium with a granodioritic melt. The REE patterns of the Tsu Lake granulite facies minerals also show some similarities to dacitic mineral patterns. However, there are important differences, especially in the partitioning relations between the major minerals and the REE patterns of the accessory phases. The similarity to the dacitic minerals may be fortuitous, and possibly related to temperature control of the REE fractionations.

REFERENCES

Abbey, S. 1983. Studies in 'standard samples' of silicate rocks and minerals . GSC Paper 83-15

Allen, A.R., 1979. Metasomatism of a depleted granulite facies terrain in the Arunta block, Central Australia. I. Geochemical evidence. Contrib. Mineral. Petrol. *71,* 85 - 98.

Anderson, A.T., Braziunas, T.F., Jacoby, J., and Smith, J.V., 1972. Thermal and mechanical history of breccias 14306, 14063, 14270 and 14321. In: Proc. Third Lunar Sci. Conf., Geochim. Cosmochim. Acta Suppl. *3,* v1, 819 - 835.

Anderson, D.E. and Olimpio, J.C., 1977. Progressive homogenization of metamorphic garnets, South Morar, Scotland: evidence for volume diffusion. Can. Mineral. *15,* 205 - 216.

Apps, M.J., 1978. Development of INAA. In: Univ. of Alberta SLOWPOKE Facility Ann. Rept. p11.

Aranovich, L.Ya. and Podlesski, K.K., 1983. The cordierite - garnet - sillimanite - quartz equilibrium: experiments and applications. In: Kinetics and equilibrium in mineral reactions. (ed,S.K. Saxena) Springer - Verlag New York. p 173 - 198.

Armbruster, T.H. and Bloss, F.D., 1980. Effects of channel H_2O and CO_2 in cordierite. Fortschr. Mineral., *58,* 7 - 9.

Barbey, P. and Cuney, M., 1982. K, Rb, Sr, Ba, U and Th geochemistry of the Lapland Granulites (Fennoscandia). LILE fractionation controlling factors. Contrib. Mineral. Petrol., *81,* 304 - 316.

Barth, T.F.W., 1951. The feldspar geologic thermometer. Nor. Geol. Tidsskr., *42,* 330 - 339.

Bergerioux, C.; Kennedy,G. and Zikovsky,L. 1979. Use of the semi-absolute method in neutron activation analysis. Jour. Radioanal. Chem., *50,* 229 - 234.

Bishop, F.C., 1980. The distribution of Fe^{2+} and Mg between coexisting ilmenite and pyroxene with applications to geothermometry. Am. Jour. Sci., *280,* 46 - 77.

Bohlen, S.R. and Essene, E.J., 1977. Feldspar and oxide thermometry of granulites in the Adirondack Highlands. Contrib. Mineral. Petrol., *62,* 153 - 169.

Bohlen, S.R. and Essene, E.J., 1979. A critical evaluation of two-pyroxene thermometry in Adirondack granulites. Lithos *12,* 335 - 345.

Bohlen, S.R., Peacor, D.R. and Essene, E.J., 1980. Crystal chemistry of a metamorphic biotite and its significance in water barometry. Am. Mineral., *65,* 55 - 62.

Bohlen, S.R., Wall, V.J. and Boettcher, A.L., 1983. Geobarometry in granulites. In: Kinetics and equilibrium in mineral reactions. (ed. S.K. Saxena). Springer - Verlag New York. p 141 - 171.

Bostock, H.H., 1980. Reconnaissance geology of the Fort Smith - Hill Island Lake area, Northwest Territories. In: Current Research, Part A, Geol. Surv. Can. Paper *80 - 1A,* 153 - 155.

Bostock, H.H., 1981. A granite diapir of batholithic dimensions at the west margin of the Churchill Province. In: Current Research, Part B, Geol. Surv. Can. Paper *81 - 1B,* 73 - 82.

Bostock, H.H., 1982. Geology of the Fort Smith map area, District of Mackenzie, Northwest Territories . In: Geol. Surv. Can. Publ. Open File *859.*

Bowden,P., and Whitley, J.E., 1974. Rare earth patterns in peralkaline and associated granites. Lithos *7,* 15 - 21.

Bowles, J.F.W., 1977. A method of tracing the temperature and oxygen-fugacity histories of complex magnetite-ilmenite grains. Mineral. Mag., *41,* 103 - 109.

Brown, W.L. and Parsons, I., 1981. Towards a more practical two-feldspar geothermometer. Contrib. Mineral. Petrol., *76,* 369 - 377.

Bucher-Nurminen, K. and Droop, G., 1983. The metamorphic evolution of garnet - cordierite - sillimanite gneisses of Gruf - Complex, Eastern Pennine Alps. Contrib. Mineral. Petrol., *84,* 215 - 227.

Buddington, A.F. and Lindsley, D.H., 1964. Iron-titanium oxide minerals and synthetic equivalents. Jour. of Petrol., *5,* 310 - 357.

Burwash, R.A. and Krupicka, J., 1969. Cratonic reactivation in the Precambrian basement of western Canada. I. Deformation and chemistry. Can. J. Earth Sci. *6,* 1381 - 1404.

Burwash, R.A. and Krupicka, J., 1970. Cratonic reactivation in the Precambrian basement of western Canada. Part II. Metasomatism and isostasy. Can. Jour. Earth Sci., *7,* 1275 - 1294.

Burwash, R.A., Krupicka, J. and Culbert, R.R., 1973. Cratonic rectivation in the Precambrian basement of western Canada. III. Crustal evolution. Can. Jour. Earth Sci., *10,* 283 - 291.

Burwash, R.A. and Culbert, R.R., 1976. Multivariate geochemical and mineral patterns in the Precambrian basement of Western Canada. Can. Jour. Earth Sci., *13,* 1 - 18.

Cameron, M. and Papike, J.J., 1980. Crystal chemistry of silicate pyroxenes. Chapter 2 in: Reviews in mineralogy; v7, Pyroxenes. (ed. C.T. Prewitt)

Carmicheal, D.M., 1974. Mineral equilibria in mafic granulites. Can. Mineral., *12,* 429 - 430.

Cawthorn, R.G. and Collerson, K.D., 1974. The recalculation of pyroxene end-member parameters and the estimation of ferrous and ferric iron content from electron microprobe analyses. Am. Mineral., *59,* 1203 - 1208.

Charboneau, B.W., 1980. The Fort Smith radioactive belt, Northwest Territories In: Current Research, Part C. Geol. Surv. Can., Paper *80-1C,* 45 - 57.

Clark, A.M., 1983. REE mineralogy. In: Developments in Geochemistry 2; Rare Earth Element Geochemistry. (ed. P. Henderson) Elsevier.

Collerson, K.D. and Fryer, B.J., 1978. The role of fluids in the formation and subsequent development of early continental crust. Contrib. Mineral. Petrol., *67,* 151 - 167.

Condie, K.C., 1976. Trace element geochemistry of Archean greenstone. Earth Sci. Rev., *12,* 393 - 417.

Condie, K.C., Allen, P. and Narayana, B.L., 1982. Geochemistry of the Archean low- to high-grade transition zone, southern India. Contrib. Mineral. Petrol., *81,* 157 - 167.

Cullers, R.L., Medaris, L.G. and Haskin, L.A., 1970. Gadolinium distribution between aqueous and silicate phases. Science *169,* 580.

Cullers, R.L., Yeh, L.-T., Chauduri, S. and Guidotti, C.V., 1974. Rare earth elements in Silurian pelitic schists from N.W. Maine. Geochim. Cosmochim. Acta, *38,* 389 - 400.

Cullers, R.L. and Graf, J.L., 1983. Rare earth elements in igneous rocks of the continental crust: intermediate and silicic rocks - ore petrogenesis. In: Developments in Geochemsistry 2; Rare Earth Element Geochemistry. (ed P. Henderson). Elsevier. p 275 - 316.

Currie, K.L., 1971. The reaction 3 cordierite = 2 garnet + 4 sillimanite + 5 quartz as a geological thermometer in the Opinicon Lake region, Ontario. Contrib. Mineral. Petrol., *33,* 215 - 226.

Currie, K.L., 1974. A note on the calibration of the garnet - cordierite geothermometer and geobarometer. Contrib. Mineral. Petrol., *44,* 35 - 44.

Currie, L.A. 1968. Limits for qualitative detection and quantitative determination: application to radiochemistry. Anal. Chem. *40,* 586 - 593.

Dahl, O., 1969. Irregular distribution of iron and magnesium among coexisitng biotite and garnet. Lithos *2,* 311 - 322.

Dallmeyer, R.D., 1974(a). Metamorphic history of the northeastern Reading Prong, New York and northern New Jersey. Jour. of Petrol., *15,* 325 - 360.

Dallmeyer, R.D., 1974(b). The role of crystal structure in controlling the partitioning of Mg and Fe^{2+} between coexisting garnet and biotite. Am. Mineral., *59,* 201 - 203.

Davidson, A., 1972. The Churchill Province. Geol. Assoc. Can. Spec. Paper *11,* 381 - 433.

Davidson, L.R., 1968. Variation in ferrous iron - magnesium distribution coefficients of metamorphic pyroxenes from Quairading, Western Australia. Contrib. Mineral. Petrol., *19,* 239 - 259.

Deer, W.A., Howie, R.A. and Zussman J., 1978. Rock-forming minerals, vol 2A, Single-chain silicates. 2nd Ed. Longman, London.

Deer W.A., Howie, R.A. and Zussman, J., 1982. Rock-forming minerals, vol 1A, Orthosilicates. 2nd Ed. Longman, London and New York.

de Waard, D., 1965. The occurrence of garnet in the granulite-facies terrane of the Adirondack Highlands. Jour. of Petrol., *6,* 165 - 191.

Dostal, J., 1975. The origin of garnet - cordierite - sillimanite bearing rocks from Chandos Township, Ontario. Contrib. Mineral. Petrol., *49,* 163 - 175.

Dostal, J. and Capedri, S., 1978. Uranium in metamorphic rocks. Contrib. Mineral. Petrol., *66,* 409 - 414.

Dostal, J. and Capedri, S., 1979. Rare earth elements in high-grade metamorphic rocks from the Western Alps. Lithos *12,* 41 - 49.

Drake, M.J. and Weill, D.F., 1975. Partition of Sr, Ba, Ca, Y, Eu^{2+}, Eu^{3+} and other REE between plagioclase feldspar and magmatic liquid - experimental study. Geochim. Cosmochim. Acta, *39,* 689 - 712.

Dymek, R.F., 1983. Titanium, aluminum and interlayer cation substitutions in biotite from high-grade gneisses, West Greenland. Am. Mineral., *68,* 880 - 899.

Emmermann, R., Daieva, L., and Schneider, J., 1975. Petrologic significance of rare earths distribution in granites. Contrib. Mineral. Petrol., *52,* 267 - 283.

Eugster, H.P. and Ilton, E.S., 1983. Mg-Fe fractionation in metamorphic environments. In: Kinetics and equilibrium in mineral reactions. (ed. S.K. Saxena), Springer - Verlag, New York. p 115 - 140.

Evans, H.T., Appleman, D.E., Handwerker, D.S., 1963. The least squares refinement of crystal unit cell with powder diffraction data by an automatic computing method. (abstr.) Program Ann. Meet. Am. Cryst. Assoc., March 28, 1963. Cambridge, Mass., 42 - 43.

Evensen, N.M., Hamilton, P.J., and O'Nions, R.K., 1978. Rare-earth abundances in chondritic meteorites. Geochim. Cosmochim. Acta, *42,* 1199 - 1212.

Ferry, J.M. and Spear, F.S., 1978. Experimental calibration of the partitioning of Fe and Mg between biotite and garnet. Contrib. Mineral. Petrol., *66,* 113 - 117.

Field, D. and Clough, P.W.L., 1976. K/Rb ratios and metasomatism in metabasites from a Precambrian amphibolite-granulite transition zone. Jour. Geol. Soc. Lond., *132,* 277 - 288.

Field, D.; Drury, S.A., and Cooper, D.C., 1980. Rare-earth and LIL element fractionation in high-grade charnockitic gneisses, south Norway. Lithos *13,* 281 - 289.

Fleischer, R.M. and Altschuler, Z.S., 1969. The relationship of the rare-earth composition of minerals to geological environment. Geochim. Cosmochim. Acta, *33,* 725 - 732.

Fraser, J.A., 1978. Metamorphism in the Churchill Province, District of Mackenzie. In: Metamorphism in the Canadian Shield, Geol. Surv. Can., Paper *78 - 10,* 195 - 202.

Frey, F.A., Bryan, W.B. and Thompson, G., 1974. Atlantic ocean floor: geochemistry and petrology of basalts from Legs 2 and 3 of the Deep Sea Drilling Project. J. Geophys. Res. *79,* 5507 - 5527.

Froese, E., 1978. The graphical representation of mineral assemblages in biotite-bearing granulites. In: Current Research, Part A, Geol. Surv. Can. Paper *78A.*

Fyfe, W.S., 1973. The granulite facies and the Archean crust. Phil. Trans. Roy. Soc. Lond. *A273,* 457 - 461.

Ganguly, J. and Saxena, S.K., 1984. Mixing properties of aluminosilicate garnets: constraints from natural and experimental data, and applications to geothermo-barometry. Am. Mineral., *69,* 88 - 97.

Ghent, E.D. and Stout, M.Z., 1984. TiO_2 activity in metamorphosed pelitic and basic rocks: principles and application to metamorphism in southeastern Canadian Cordillera. Contrib. Mineral. Petrol., *86,* 248 - 255.

Gladney, E.S.; Burns, C.E. and Roelandts, I. 1983. 1982 compilation of elemental concentrations in eleven United States Geological Survey rock standards. Geostandards Newsletter *VII,* no.1 April 1983.

Glassley, W.E. and Sorenson, K., 1980. Constant P(s) - T amphibolite to granulite facies transition in Agto (West Greenland) metadolerites: implications and applications. Jour. of Petrol., *21,* 69 - 105.

Godfrey, J.D. and Langenberg, C.W., 1978. Metamorphism in the Canadian Shield of northeastern Alberta. In: Metamorphism in the Canadian Shield, Geol. Surv. Can., Paper *78 - 10,* 129 - 138.

Goff, S.P., Godfrey, J.D., and Holland, J.G.R., 1985. The petrology and geochemistry of the Canadian shield of northeastern Alberta. Alberta Research Bulletin. *(in prep).*

Goldman, D.S. and Albee, A.L., 1977. Correlation of Mg/Fe partitioning between garnet and biotite with $^{18}O/^{16}O$ partitioning between quartz and magnetite. Am. Jour. Sci., *277,* 750 - 767.

Grant, J.A., 1973. Phase equilibria in high-grade metamorphism and partial melting in pelitic rocks. Am. Jour. Sci., *273,* 289 - 317.

Gray, C.M., 1977. The geochemistry of central Australian granulites in relation to chemical and isotopic effects of granulite facies metamorphism. Contrib. Mineral. Petrol., *65,* 79 - 89.

Green, T.H., Brunfelt, A.O. and Heier, K.S., 1972. Rare-earth element distribution and K/Rb ratios in granulites, mangerites and anorthosites, Lofoten-Vesteraalen, Norway. Geochim. Cosmochim. Acta, *36,* 241 - 257.

Greenwood, H.J., 1975. Thermodynamically valid projections of extensive phase relationships. Am. Mineral., *60,* 1 - 8.

Greenwood, H.J., 1976. Metamorphism at moderate temperatures and pressures. In: Evolution of the crystalline rocks. (eds. D.K. Bailey and R. Macdonald). Academic Press Inc. (Lond) Ltd. p 187 - 269.

Grew, E.S., 1980. Sillimanite and ilmenite from high-grade metamorphic rocks of Antarctica and other areas. Jour. of Petrol., *21,* 39 - 68.

Grew, E.S., 1981. Granulite facies metamorphism at Molodezhnaya station, East Antarctica. Jour. of Petrol., *22,* 297 - 336.

Gromet, L.P. and Silver, L.T., 1983. Rare earth element distributions among minerals in a granodiorite and their petrogenetic implications. Geochim. Cosmochim. Acta, *47,* 925 - 939.

Gryntakis, E.M. and Kim, J.I. 1978. A compilation of resonance integrals. Part II. Z = 53 - 100 (Iodine-Fermium). Jour. Radioanal. Chem., *47,* 181 - 278.

Gunter, A.E., 1977. Water in synthetic cordierite and its significance in the experimental reaction: aluminous-biotite + sillimanite + quartz = iron-cordierite + sanidine + water. Geol. Assoc. Annual Meeting (Abstr.)*2,* 22.

Haggerty, S.E., 1976. Opaque mineral oxides in terrestrial igneous rocks. Chapter 8 in: Reviews in Mineralogy; Oxide Minerals. (ed D. Rumble)

Hansen, B., 1981. The transition from pyroxene granulite facies to garnet clinopyroxene granulite facies. Experiments in the system CaO - MgO - Al_2O_3 - SiO_2. Contrib. Mineral. Petrol., *76,* 234 - 242.

Harris, N.B.W., 1976. The significance of garnet and cordierite from the Sioux Lookout region of the English River Gneiss Belt, northern Ontario. Contrib. Mineral. Petrol., *55,* 91 - 104.

Haskin, L.A., Haskin, M.A., Frey, F.A. and Wildeman, T.R., 1968. Relative and absolute terrestrial abundances of the rare earths. In: Origin and distribution of the elements. (ed. L.H. Ahrens) Pergammon Press, Oxford, p889 - 912.

Haskin, L.A. and Paster, T.P., 1979. Geochemistry and mineralogy of the rare earths. In: Handbook on the physics and chemistry of the rare earths, chapter 21. (eds. K.A. Gshneider, Jr., and L. Eyring). North - Holland Publishing Co.

Hawthorne, F. C., 1983. The crystal chemistry of the amphiboles. Can. Mineral. *21,* 173 - 480.

Heier, K.S., 1973. Geochemistry of granulite facies rocks and problems of their origin. Phil. Roy. Soc. Lond. *A273,* 429 - 442.

Hellman, P.R., Smith, R.E. and Henderson, P., 1979. The mobility of the rare earth elements: evidence and implications from selected terrains affected by burial metamorphism. Contrib. Mineral. Petrol. *71,* 23 - 44.

Helz, R.T., 1973. Phase relations of basalts in their melting range at $P(H_2O)$ - 5kb as a function of oxygen fugacity. Part I, mafic phases. Jour. of Petrol., *14,* 249 - 302.

Henderson, P., 1980. Rare earth element partition between sphene, apatite and other coexisting minerals of the Kangerdlugssuaq Intrusion, E. Greenland. Contrib. Mineral. Petrol., *72,* 81 - 85.

Henderson, P., 1983. General geochemical properties and abundances of the rare earth elements. In: Developments in Geochemistry, 2; Rare Earth Element Geochemistry. (ed P. Henderson). Elsevier. p 1 - 31.

Henry, J., 1974. Garnet - cordierite gneisses near the Egersund-Ogna anorthositic intrusion, southwestern Norway. Lithos *7,* 207 - 216.

Hensen, B.J., 1977. Theoretical phase relations involving cordierite and garnet in the system MgO - FeO - Al_2O_3 - SiO_2. Contrib. Mineral. Petrol., *33,* 195 - 214.

Hensen, B.J., 1971. Cordierite - garnet bearing assemblages as geothermometers and barometers in granulite facies terranes. Tectonophys., *43,* 73 - 88.

Hensen, B.J. and Green, D.H., 1971. Experimental study of the stability of cordierite and garnet in pelitic compositions at high pressures and temperatures. I. Compositions with excess alumino-silicate. Contrib. Mineral. Petrol., *33,* 309 - 330.

Hensen, B.J. and Green, D.H., 1973. Experimental study of the stability of cordierite and garnet in pelitic compositions at high pressures and temperatures. III. Synthesis of experimental data and geological application. Contrib. Mineral. Petrol., *38,* 151 - 166.

Hertogen, J. and Gijbels, R. 1971. Instrumental neutron activation analysis of rocks with a low energy photon detector. Anal. Chim. Acta, *56,* 61 - 82.

Hoede, D. and Das, H.A. 1981. Accuracy and precision of instrumental neutron activation analysis based on gamma-spectrometry with a planar intrinsic Ge detector. J. Radioanal. Chem. *62,* 171 - 186.

Holdaway, M.J., 1971. Stability of andalusite and the aluminum silicate phase diagram. Am. Jour. Sci., *271,* 97 - 131.

Holdaway, M.J. and Lee, S.M., 1977. Fe-Mg cordierite stability in high grade pelitic rocks based on experimental, theoretical and natural observations. Contrib. Mineral. Petrol., *63,* 175 - 198.

Holland, J.G.R. and Lambert, R. St.J., 1975. The chemistry and origin of the Lewisian gneisses of the Scottish mainland: the Scourie and Inver assemblages and sub-crustal accretion. Precamb. Res., *2,* 161 - 188.

Hollister, L.S., 1966. Garnet zoning: an interpretation based on the Rayleigh fractionation model. Science *154,* 1647 - 1651.

Hollister, L.S., 1977. The reaction forming cordierite from garnet, the Khtada Lake metamorphic complex, British Columbia. Can. Mineral., *15,* 217 - 229.

Howie, R.A., 1955. The geochemistry of the charnockite series of Madras, India. Trans. Roy. Soc. Edin., *62,* 725 - 768.

Hutcheon, I., Froese, E. and Gordon, T.M., 1974. The assemblage quartz - sillimanite - garnet - cordierite as an indicator of metamorphic conditions in the Daly Bay Complex, N.W.T. Contrib. Mineral. Petrol., *44,* 29 - 34.

Iden, I.K., 1981. Geochemistry of Precambrian basal gneisses in Lofoten - Vesteralen, Northern Norway. Precamb. Res., *14,* 135 - 166.

Irving, A.J., 1978. A review of experimental studies of crystal/liquid trace element partitioning. Geochim. Cosmochim. Acta, *42,* 743 - 770.

Jacobs, J.W.; Korotev, R.L.; Blanchard, D.P. and Haskin, L.A. 1977. A well tested procedure for instrumental neutron activation analysis of silicate rocks and minerals. Jour. Radioanal. Chem. *40*, 93 - 114.

Jen, L.S. and Kretz, R. 1981. Mineral chemistry of some mafic granulites from the Adirondack region. Can. Mineral., *19*, 479 - 491.

Kay, S.M., 1983. Metamorphism in the Aleutian Arc: the Finger Bay pluton, Adak, Alaska. Can. Mineral., *21* 665 - 681.

Kennedy, G. and Fowler, A. 1983. Interference from uranium in neutron activation analysis of rare earths in silicate rocks. J. Rad. Chem. *78*, 165 - 169.

Khomyakov, A.P., 1963. Relation between content and composition of the rare earths in minerals. Geochemistry, p 125 - 133.

Kretz, R., 1981. Site-occupancy interpretation of the distribution of Mg and Fe between orthopyroxene and clinopyroxene in metamorphic rocks. Can. Mineral., *19*, 493 - 500.

Kretz, R., 1982. Transfer and exchange equilibria in a portion of the pyroxene quadrilateral as deduced from natural and experimental data. Geochim. Cosmochim. Acta, *46*, 411 - 421.

Kretz, R. and Jen, L.S., 1978. Effect of temperature on the distribution of Mg and Fe^{2+} between calcic pyroxene and hornblende. Can. Mineral., *16*, 533 - 537.

Kuniyoshi, S. and Liou, J.G., 1976. Contact metamorphism of the Karmutsen Volcanics, Vancouver Island, British Columbia. Jour. of Petrol., *17*, 73 - 99.

Lambert, I.B. and Heier, K.S., 1968. Geochemical investigations of deep -seated rocks in the Australian Shield. Lithos *1* 30 - 53.

Lambert, R. St.J., 1976. Archean thermal regimes, crustal and upper mantle temperatures and a progressive evolutionary model for the earth. In: The early history of the earth. (ed. B.F. Windley). Wiley, London. p 363 - 373.

Leake, B.E., 1965. The relationship between composition of calciferous amphibole and grade of metamorphism. In: Controls of Metamorphism (eds. W.S. Pitcher and G.W. Flinn). p 299 - 318.

Leake, B.E., 1969. The discrimination of ortho- and paracharnockitic rocks, anorthosites and amphibolites. Indian Mineral., *10*, 89 104.

Leake, B.E., 1978. Nomenclature of amphiboles. Can. Mineral., *16*, 501 - 520.

Lederer, C.M. and Shirley, V.S. (Ed) 1978. Table of Isotopes, 7th Ed. John Wiley & Sons.

Lewis, J.D., and Spooner, C.M., 1973. K/Rb ratios in Precambrian granulite terranes.

Geochim. Cosmochim. Acta, *37,* 1111 - 1118.

Lindsley, D.H., 1983. Pyroxene thermometry. Am. Mineral., *68,* 477 - 493.

Lindsley, D.H. and Dixon, S.A., 1976. Diopside - enstatite equilibria at 850°C - 1400°C, 5 - 35kb. Am. Jour. Sci., *276,* 1285 - 1301.

Liou, J.G., 1971. Synthesis and stability relations of prehnite, $Ca_2Al_2Si_3O_{10}(OH)_2$. Am. Mineral., *56,* 507 - 531.

Lonker, S.W., 1981. The P-T-X relations of the cordierite - garnet - sillimanite - quartz equilibrium. Am. Jour. Sci., *281,* 1056 - 1090.

Loomis, T.P., 1975. Reaction of zoning of garnet. Contrib. Mineral. Petrol., *52,* 285 - 305.

Mahood, G. and Hildreth, W., 1983. Large partition coefficients for trace elements in high-silica rhyolites. Geochim. Cosmochim. Acta, *47,* 11 - 30.

Manna, S.S. and Sen, S.K., 1974. Origin of garnet in basic granulites around Saltora, W. Bengal, India. Contrib. Mineral. Petrol., *44,* 195 - 218.

Martignole, J. and Nantel, S., 1982. Geothermobarometry of cordierite bearing metapelites near the Morin anorthosite complex, Grenville Province, Quebec. Can. Mineral., *20,* 307 - 318.

Martignole, J. and Sisi, J.C., 1981. Cordierite - garnet - H_2O equilibrium: a geological thermometer, barometer and water fugacity indicator. Contrib. Mineral. Petrol., *77,* 38 - 46.

Matsui, Y., Onuma, N., Nagasawa, H., Higuchi, H. and Banno, S., 1977. Crystal structure control in trace element partition between crystal and magma. Bull. Soc. Fr. Mineral. Cristallogr., *100,* 315 - 324.

McCarthy, T.S., 1976. Chemical interrelationships in a low-pressure granulite terrain in Namaqualand, South Africa, and their bearing on granite genesis and the composition of the lower crust. Geochim. Cosmochim. Acta, *40,* 1057 - 1068.

McCarthy, T.S. and Kable, E.J.D., 1978. On the behaviour of rare - earth elements during partial melting of granitic rock. Chem. Geol., *22,* 21 - 29.

Mirwald, P.W. and Schreyer, W., 1977. Die stabile und metastabile Abbaureaktion von Mg-cordierit in Talk, Disthen und Quartz und ihre Abhangigkeit vom Gleichgewichtswassergehalt des Cordierits. Forschr. Mineral., *55,* 95 - 97.

Mirwald, P.W., Maresch, W.V. and Schreyer, W., 1979. Der Wassergehalt von Mg-cordierit zwsichen 500° and 800° sowie 0.5 und 11 kbar. Fortschr.

Mineral., *57,* 101 - 102.

Moore, A.C., 1976. Intergrowth of prehnite and biotite. Mineral. Mag., *40,* 526 - 529.

Moorbath, S., 1976. Age and isotopic constraints for the evolution of the Archean crust. In: The early history of the earth. (ed. B.F. Windley). p 351 - 360.

Moorbath, S., Welke, H. and Gale, N.H., 1969. The significance of Pb isotopic studies in ancient high-grade metamorphic basement complexes, as exemplified by the Lewisian rocks of N.W. Scotland. Earth Planet. Sci. Lett., *6,* 245 - 269.

Morris, R.V., 1975. Electron-paramagnetic resonance study of site preferences of Gd^{3+} and Eu^{2+} in polycrystalline silicate and aluminate minerals. Geochim. Cosmochim. Acta, *39,* 621 - 634.

Morris, R.V. and Haskin, L.A., 1974. EPR measurement of the effect of glass composition on the oxidation states of europium. Geochim. Cosmochim. Acta *38,* 1435 - 1445.

Muecke, G.K., Pride, C. and Sarkar, P., 1979. Rare-earth element geochemistry of regional metamorphic rocks. In: Origin and distribution of the elements: Physics and chemistry of the earth.(ed. L.H.Ahrens), v11. Pergammon Press, Oxford.p 449 - 464.

Murali, A.V., Parthasarathy, R., Mahadevan, T.M., and Sankar Das, M., 1983. Trace element characteristics, REE patterns and partition coefficients of zircons from different geological environments - A case study on Indian zircons. Geochim. Cosmochim. Acta, *47,* 2047 - 2052.

Nagasawa, H., 1970. Rare earth concentrations in zircons and apatites nd their host dacites and granites. Earth Planet. Sci. Lett., *9,* 359 - 364.

Nagasawa, H. and Schnetzler, C.C., 1971. Partitioning of rare earth, alkali and alkaline earth elements between phenocrysts and acidic igneous magma. Geochim. Cosmochim. Acta, *35,* 953 - 968.

Newton, R.C., 1983. Geobarometry of high-grade metamorphic rocks. Am. Jour. Sci., *283A,* 1 - 28.

Newton, R.C. and Wood, B.J., 1979. Thermodynamics of water in cordierite and some petrologic consequences of cordierite as a hydrous phase. Contrib. Mineral. Petrol., *68,* 391 - 405.

Nicholls, I.A. and Harris, K.L., 1980. Experimental rare earth element partition coefficients for garnet, clinopyroxene and amphibole coexisting with andesitic and basaltic liquids. Geochim. Cosmochim. Acta, *44,* 287 - 308.

Nielsen, P.A., Langenberg, C.W., Baadsgaard, H. and Godfrey, J.D., 1981. Precambrian metamorphic conditions and crustal evolution, northeastern Alberta, Canada.

Precamb. Res., *16*, 171 - 193.

Oliver, G.J.H., 1978. Ilmenite - magnetite geothermometry and oxygen barometry in granulite and amphibolite facies gneisses from Doubtful Sound. Fiordland, New Zealand. Lithos *11*, 147 - 153.

Perchuk, L.L. and Lavrent'eva, I.V., 1983. Experimental investigation of exchange equilibria in the system cordierite - garnet - biotite. In: Kinetics and equilibrium in mineral reactions. (ed. S.K. Saxena) Springer - Verlag, New York. p 199 - 239.

Phillips, I.R. and Rickwood, P.C., 1975. The biotite - prehnite association. Lithos *8*, 275 - 281.

Philpotts, J.A., 1970. Redox estimation from a calculation of Eu^{2+} and Eu^{3+} concentrations in natural phases. Earth Plan. Sci. Lett. *9*, 257.

Powell, M. and Powell, R., 1977. Plagioclase - alkali feldspar geothermometry revisited. Mineral. Mag., *41*, 253 - 256.

Price, R.C. and Taylor, S.R., 1977. The rare earth element geochemistry of granite, gneiss and migmatite from the western metamorphic belt of south-eastern Australia. Contrib. Mineral. Petrol., *62*, 249 - 263.

Pride, C. and Muecke, G.K., 1980. Rare earth element geochemistry of the Scourian Complex, N.W. Scotland - evidence for the granite - granulite link. Contrib. Mineral. Petrol., *73*, 403 - 412.

Pride, C. and Muecke, G.K., 1981. Rare earth element distributions among coexisting granulite facies minerals, Scourian Complex, N.W. Scotland. Contrib. Mineral. Petrol. *76*, 463 - 471.

Puchelt, H. and Emmermann, R. 1976. Bearing of rare earth patterns of apatites from igneous and metamorphic rocks. Earth Planet. Sci. Lett., *31*, 279 - 286.

Reinhardt, E.W., 1968. Phase relations in cordierite-bearing gneisses from the Gananoque area, Ontario. Can. Jour. Earth Sci., *5*, 455 - 482.

Reinhardt, E.W., 1969. Geology of the Precambrian rocks of Thubun Lakes map area in relationship to the MacDonald fault system, District of Mackenzie. Geol. Surv. Can. Paper *69 -21*.

Reitan, P.H. and Roedlandts, I., 1973. Rare earth element partitioning coexisting metamorphic pyroxenes. Geol. Soc. Am. Abstr., *5*, 778 - 779.

Ribbe, P.H., 1975. Exsolution textures in ternary and plagioclase feldspars; interference colours. Chapter 10 in: Reviews in mineralogy; vol 2, Feldspar Mineralogy. (ed. P.H. Ribbe).

Ribbe, P.H., 1980. Aluminum silicate polymorphs and mullite. Chapter 8 in: Reviews in Mineralogy, v5, Orthosilicates.(ed. P.H. Ribbe).

Richardson, S.M., 1974. Cation exchange reactions and metamorphism of high-grade pelites in central Massachusetts. Geol. Soc. Am. Program with Abstracts, *6*, 1059.

Rollinson, H.R. and Windley, B.F., 1980. Selective elemental depletion during metamorphism of Archean granulites, Scourie, NW Scotland. Contrib. Mineral. Petrol., *72*, 257 - 263.

Ross, M. and Huebner, J.S., 1975. A pyroxene geothermometer based on composition - temperature relationships of naturally occuring orthopyroxene, pigeonite and augite. (Abstr.) International Symposium Geotherm. Geobarom. Penn. State Univ.

Rumble, D. III., 1976. Oxide minerals in metamorphic rocks. Chapter 3 in: Reviews in mineralogy; Oxide Minerals. (ed D. Rumble).

Rumble, D.III., 1978. Mineralogy, petrology and oxygen isotope geochemistry of the Clough Formation, Black Mountain, western New Hamphsire, U.S.A. Jour. of Petrol., *19*, 317 - 340.

Rumble, D. III, Ferry, J.M. Hoering, T.C. and Boucot, A.J., 1982. Fluid flow during metamorphism at the Beaver Brook fossil locality, New Hampshire. Am. Jour. Sci., *282*, 886 - 919.

Rutherford, M.J., 1973. The phase relations of aluminous iron biotites in the system $KAlSi_3O_8$ - $KAlSiO_4$ Al_2O_3 - Fe - O - H. Jour. Petrol., *14*, 159 - 180.

Saunders, A.D., 1983. The rare earth element characteristics of igneous rocks from the ocean basins. In: Developments in Geochemistry 2; Rare Earth Element Geochemistry. (ed P. Henderson). Elsevier.

Savage, D. and Sills, J.D., 1980. High pressure metamorphism in the Scourian of NW Scotland: evidence from garnet granulites. Contrib. Mineral. Petrol., *74*, 153 - 163.

Saxena, S.K., 1976. Two-pyroxene geothermometer: a model with an approximate solution. Am. Mineral., *61*, 643 - 652.

Saxena, S.K., 1983. Problems of two-pyroxene geothermometry. Earth Planet. Sci. Lett., *65*, 382 - 388.

Schnetzler, C.C. and Philpotts, J.A., 1970. Partition coefficients of rare-earth elements between igneous matrix and rock-forming mineral phenocrysts. II. Geochim. Cosmochim. Acta, *34*, 331 - 340.

Schreyer, W. 1976. Experimental metamorphic petrology at low pressures and high temperatures. In: Evolution of the crystalline rocks. (eds D.K. Bailey and R. Macdonald) Acad. Press Inc (Lond) Ltd.

Sen, S.K., 1970. Magnesium - iron compositional variance in hornblende pyroxene granulites. Contrib. Mineral. Petrol., *29,* 76 - 88.

Sen, S.K., 1973. Compositional relations among hornblende and pyroxenes in basic granulites and an application to the origin of garnets. Contrib. Mineral. Petrol., *38,* 299 - 306.

Sen, S.K. and Sobhen, R., 1971. Breakdown reactions for natural hornblendes in granulite facies. N. Jb. Mineral. Abh., *114,* 301 - 319.

Sen, S.K. and Sobhen, R., 1971. Hornblende - pyroxene granulites: a study from the type charnockite area. N. Jb. Mineral. Abh., *115,* 291 - 314.

Shannon, R.D., 1976. Revised effective ionic radii and systematic studies of interatomic distances in halides and chalcogenides. Acta Crystallogr. Sect. A, *32,* 751 - 767.

Shaw, D.M., 1968. A review of K - Rb fractionation trends by covariance analysis. Geochim. Cosmochim., *32,* 573 - 601.

Shaw, D.M., 1970. Trace element fractionation during anatexis. Geochim. Cosmochim. Acta, *34,* 237 - 243.

Shaw, D.M., 1972. The origin of the Apsley gneiss, Ontario. Can. Jour. Earth Sci., *9,* 18 - 35.

Sheraton, J.W., Skinnner, A.C., Tarney, J., 1973. The geochemistry of the Scourian gneisses of the Assynt district. In: The early Precambrian of Scotland and related rocks of Greenland. (eds. R.G. Park and J. Tarney). Univ. of Birmingham Press.

Sighinolfi, G.P., 1969. K-Rb ratios in high grade metamorphism: a confirmation of the hypothesis of a continual crustal evolution. Contrib. Mineral. Petrol., *21,* 346 - 356.

Sighinolfi, G.P., 1971. Investigations into deep crustal levels: fractionating effects and geochemical trends related to high-grade metamorphsim. Geochim. Cosmochim. Acta, *35,* 1005 - 1021.

Sighinolfi, G.P. and Gorgoni, C., 1978. Chemical evolution of high-grade metamorphic rocks - anatexis and remotion of material from granulite terrains. Chem. Geol., *22,* 157 - 176.

Smith, D.G.W., Gold, C.M., Tomlinson, D.A., and Wynne, D.A., 1981. EDATA2: A Fortran IV programme for processing energy and / or wavelength dispersive data from microbeam instruments to give quantitative compositional results. (2nd printing

1981). Department of Geology, Univ. of Alberta.

Spear, F.S., 1977. Evidence for a miscibility gap in plagioclase felspar in the composition range An[illegible] - An[illegible]. Carnegie Inst. Wash. Year Book, *76,* 619 - 621.

Spear, F.S., 1980. NaSi - CaAl exchange equilibrium between plagioclase and amphibole. An empircal model. Contrib. Mineral. Petrol., *72,* 33 - 41.

Spear, F.S., 1981. An experimental study of hornblende stability and compositional variability in amphibolite. Am. Jour. Sci., *281,* 697 - 734.

Spencer, K.J. and Lindsley, D.H., 1981. A solution model for coexisting iron-titanium oxides. Am. Mineral., *66,* 1189 - 1201.

Stephenson, N.C.N., 1979. Coexisting garnets and biotites from Precambrian gneisses of the south coast of Western Australia. Lithos *12,* 73 - 87.

Stormer, J.C.(Jr), 1975. A practical two feldspar geothermometer. Am. Mineral., *60,* 667 - 674.

Tarney, J., Skinner, A.C., and Sheraton, J.W., 1972. A geochemical comparison of major Archean gneiss units from northwest Scotland and East Greenland. Report 24th Int. Geol. Congress, Montreal, 1, 162 - 174.

Tarney, J., 1976. Geochemistry of Archean high-grade gneisses, with implications as to the origin and evolution of the Precambrian crust. In: The early history of the earth. (ed. B.F. Windley). Wiley & Sons, London.

Tarney, J. and Windley, B.F., 1977. Chemistry, thermal gradients and evolution of the lower continental crust. Jour. Geol. Soc. Lond., *143,* 153

Thompson, A.B., 1976. Mineral reactions in pelitic rocks: II. Calculation of some P-T-X(Fe-Mg) phase relations. Am. Jour. Sci., *276,* 425 - 454.

Thompson, A.B. and Tracy, R.J., 1979. Model systems for anatexis of pelitic rocks. II. Facies series melting reactions in the system CaO - $KAlO_2$ - $NaAlO_2$ - Al_2O_3 - SiO_2 - H_2O. Contrib. Mineral. Petrol., *70,* 429 - 438.

Thompson, A.B., 1982. Dehydration melting of pelitic rocks and the generation of H_2O undersaturated granitic liquids. Am. Jour. Sci., *282,* 1567 - 1595.

Thompson, J.B. Jr., 1957. The graphical analysis of mineral assemblages in pelitic schists. Am. Mineral., *42,* 842 - 859.

Tulloch, A.J., 1979. Secondary Ca - Al silicates as low-grade alteration products of granitoid biotite. Contrib. Mineral. Petrol., *69,* 105 - 117.

van de Kamp, P.C., Leake, B.E. and Senior, A., 1976. The petrography and geochemistry of some Californian arkoses with application to identifying gneisses of metasedimentary origin. Jour. of Geol., *84,* 195 - 212.

Watson, E.B., 1976. Two-liquid partition coefficients: experimental data and geochemical implications. Contrib. Mineral. Petrol., *56,* 119 - 134.

Weaver, B.L., 1980. Rare-earth element geochemistry of Madras granulites. Contrib. Mineral. Petrol., *71,* 271 - 279.

Weaver, B.L. and Tarney, J., 1980. Rare-earth geochemistry of Lewisian granulite facies gneisses, northwest Scotland: implications for the petrogenesis of the Archean lower continental crust. Earth Planet. Sci. Lett., *51,* 279 - 296.

Weaver, B.L. and Tarney, J., 1981. Lewisian gneiss geochemistry and Archean crustal development models. Earth Planet. Sc. Lett., *55,* 171 - 180.

Weaver, B.L. and Tarney, J., 1981. Chemical changes during dyke metamorphism in high-grade basement terrains. Nature *289,* 47 - 49.

Weill, D. and Drake, M., 1973. Europium anomaly in plagioclase feldspar - experimental results and semiquantitative models. Science *180,* 1059 - 1060.

Weisbrod, A., 1973. Cordierite - garnet equilibrium in the systen Fe - Mn - Al - Si - O - H. Carnegie Inst. Wash. Year Book, *72,* 515 - 518.

Weisbrod, A. 1973. Refinements of the equilibrium conditions of the reaction Fe cordierite - almandine - quartz - sillimanite (+ H_2O). Carnegie Inst. Wash. Year Book, *72,* 518 - 521.

Wells, P.R.A., 1977. Pyroxene thermometry in simple and complex systems. Contrib. Mineral. Petrol., *62,* 129 - 139.

Whitney, J.A. and Stormer, J.C., 1977. The distribution of $NaAlSi_3O_8$ between coexisting microcline and plagioclase and its effect on geothermometric calculations. Am. Mineral., *62,* 687 - 691.

Windrim, D.P., McCulloch, M.T., Chappell, B.W. and Cameron, W.E., 1984. Nd isotopic systematics and chemsitry of Central Australian sapphirine granulites: an example of rare earth element mobility. Earth Planet. Sci. Lett., *70,* 27 - 39.

Winkler, H.G.F., 1974. Petrogenesis of metamorphic rocks. Springer, Berlin-Heidelberg-New York, 320pp.

Wood, B.J., 1973. Fe^{2+} - Mg^{2+} partition between coexisting cordierite and garnet. A discussion of experimental data. Contrib. Mineral. Petrol., *40,* 253 - 258.

Wood, B.J. and Banno, S., 1973. Garnet-orthopyroxene and orthopyroxene

-clinopyroxene relationships in simple and complex systems. Contrib. Mineral. Petrol., *42*, 109 - 124.

Wood, B.J. and Fraser, D.G., 1977. Elementary thermodynamics for geologists. Oxford Univ. Press.

Wood, D.A., Gibson, I.L. and Thompson, R.N., 1976. Elemental mobility during zeolite facies metamorphism of the Tertiary basalts of eastern Iceland. Contrib. Mineral. Petrol. *55*, 241 - 254.

Woodsworth, G.J., 1977. Homogenisation of zoned garnets from pelitic schists. Can. Mineral., *15*, 230 - 242.

APPENDIX 1

ELECTRON MICROPROBE ANALYSIS

All major and minor elements in minerals were determined by the electron microprobe energy dispersive analysis (EDA) technique. An ARL SEMQ microprobe fitted with an ORTEC energy dispersive spectrometer was used to collect the data. An operating voltage of 15 kV, an average probe current of 4 nA and a counting time of 240 s were maintained for all analytical runs.

The stability of the instrument during an analytical run was monitored in the following ways:

i. a calibration standard, willemite, was run at the beginning and the end of each analytical session;

ii. a Faraday cage measurement, which is used to record the ratio of the probe current to the aperture current, was taken immediately before any standards were analysed, immediately after analysing them, and at the end of the session before the final calibration standard. If the electron beam was observed to be unstable during the analysis of the samples then additional Faraday cage readings were taken after the filament had been resaturated.

The purpose of the calibration standard was to monitor instrumental drift in the energy dispersive detector system, such as changes in the gain of the amplifier with time. However, it may also be used to monitor large changes in the probe current with time by noting the variation in the total number of counts full spectrum obtained over a specified length of time.

The electron beam was normally rastered over an area of 6.5 by 6.5 um for both the standard and sample materials. As the position of the scanning coils is above the lower aperture in the SEMQ instrument, it is essential that the size of the rastered area is kept constant for all materials analysed. A change in the size of the raster may cause a change in the probe:aperture current ratio as part of the electron beam may be deflected to the sides of the lower aperture rather than through it. Exceptions to this were for those samples whose size was much smaller than the size of the rastered beam, e.g., exsolved K-feldpsar in antiperthite. In such situations a point beam was used.

For hydrous phases the position of the rastered beam was shifted every 30 s to prevent the loss of volatiles, and hence a change in the composition of the area being analysed. The feldspars were treated in a similar manner to prevent the migration of the lighter elements, Na and K.

Table A.1. shows the standards which were normally used for the elements listed. Hydrous mineral standards, e.g., kaersutite, were avoided because of the potential damage which may occur / have occurred to such materials. The main exception to the standard - element list above is with garnet samples. All elements for this mineral, except for Mn and Fe, were run against a garnet standard. Fe had to be taken from a hematite standard because an almandine standard was not available to the analyst.

All data were processed using the Fortran IV program EDATA2 (Smith *et al.*, 1981), which employs ZAF corrections. The program corrects also for probe current drift, instrumental drift, escape peak generations, electronic noise, peak:background stripping and the overlapping of analytical lines. Dead time corrections are not necessary because these are accounted for electronically. Corrections are made, however, for counting losses associated with the electronic pulse pile-up rejection.

Estimates of the 'error' in an elemental concentration obtained by electron microprobe analysis are difficult to make because many of the factors which are needed for an accurate assessment of the error are unknown. For example, the uncertainty associated with the concentration of the element in a standard is usually unknown. The uncertainty in the ZAF correction factors is unknown and can only be approximated. An estimate of the 'error' can be obtained from an analysis of uncertainty in the counting statistics, although this will only give an indication of the minimum uncertainty. This was attempted here by estimating the detection limits for each of the major elements in a variety of different minerals, Table A.2. None of the detection limits for the minor elements could be calculated as the data on the peak:background ratios are only given in the data output from EDATA2 for the major elements. The equation used for estimating the detection limit at the 90% confidence level is:

$L(D) = 2.71 + 4.65 \quad B$ where B is the total background counts (Currie, 1968).

This equation is normally used for activation analysis data but is also applicable here.

With the exception of the hydrous phases, all analyses presented in the data tables which follow, have been recalculated to 100 wt. %, although the totals before recalculation are indicated. H_2O was calculated by assuming it to be the difference

Table A.1
Electron microprobe standards

element	type	concentration	name / locality
Na	albite	8.597%	Clevelandite
Mg	diopside	11.233%	Wakefield
Al	sanidine	9.930%	Hohenfels
Si	sanidine	30.23%	Hohenfels
Cl	default		
K	sanidine	10.05%	Hohehfels
Ca	diopside	18.39%	Wakefield
Ti	rutile	59.95%	
V	default		
Cr	default		
Mn	willemite	3.733%	
Fe	hematite	69.86%	
Zn	willemite	53.716%	
Mg	garnet	11.163%	Kakanui
Al	garnet	12.560%	Kakanui
Si	garnet	19.380%	Kakanui
Ca	garnet	3.695%	Kakanui

Table A.2
Statistical Detection Limits for EDA

	opx	cpx	hbl	biot	grnt	plag
Na						0.10
Mg	0.06	0.06	0.06	0.06	0.06	
Al			0.05	0.05	0.05	0.04
Si	0.04	0.04	0.04	0.04	0.05	0.04
K			0.05	0.05		
Ca	0.05	0.05	0.04		0.10	0.04
Ti			0.06	0.09		
Mn	0.07				0.18	
Fe	0.07	0.08	0.08	0.10	0.11	

All values in weight percent of the element
Note these detection limits are only applicable for the conditions detailed in the text, e.g., counting times, accelerating voltage, probe/aperture current ratio, and to the minerals which were analysed.

between the total sum of the oxides and 100%. Such a calculation is tentative and includes in its value all the error associated with the analysis as well as the concentrations of any other undetectable elements. For micas and amphiboles the H_2O content includes potential F concentrations. For cordierites the H_2O content includes an amount of unknown CO_2 and possibly NH_3 as well. Unknown ferrous/ferric ratios contribute significantly to the error associated with the H_2O concentrations. The assumption of the presence of H_2O instead of O will have a small effect on the size of the ZAF corrections. The analyses of hydrous minerals in this study were processed while assuming all iron to be present as the ferrous ion. This will result in an estimate of a maximum H_2O content.

Because it was necessary to have some indication of the probable ferrous/ferric ratio in the minerals used as geothermometers, estimates of this ratio were calculated from charge balance considerations. There is no facility in the program EDATA2 for estimating the ferrous/ferric ratio, the ratio must be known before the data are processed. This problem was tackled in the following manner. All data for which ferrous/ferric ratio estimates were required, were processed initially by EDATA2 assuming the ferric iron content as zero. Once the weight percents of the elements were known then the ferrous/ferric ratio was estimated by a program written for this purpose. The actual calculations of the ferrous/ferric ratio done by this method are probably not very accurate because the weight percent of each element as calculated by EDATA2, changes slightly as the ferrous/ferric ratio changes (the ZAF corrections are dependent on the average atomic weight of the sample, which in turn, is dependent on the oxidation ratio). Strictly speaking, after ferrous/ferric ratio has been calculated by stoichiometric estimates, the data should be reprocessed by EDATA2 using the new, estimated oxidation ratio. This last step was not undertaken in this study.

Because of the uncertainty in the actual ferric and ferrous iron contents the data have been presented in appendix 3 in two ways. Firstly, the total iron concentration as all ferrous iron is given as the oxide value. Secondly, the estimated ferrous - ferric iron contents are given in the structural formulae.

Details of the method of calculating the ferrous/ferric ratio for various mineral species are given below.

Pyroxenes.

The structural formula is based on 6 oxygens. Site assignments are:

Al(IV) = 2.00 - Si

Al(VI) = Al(tot) - Al(IV).

Cations in the octahedral site are summed. If the total is less than 2, then no ferric iron is present. If the total is greater than 2, then a small amount of the total iron is converted to ferric iron and the structural formula is recalculated. This procedure continues iteratively until convergence to 2 is achieved.

Amphiboles.

The structural formula is based on 23 oxygens. The data is not recalculated to 100 %, i.e., the formula is calculated on an anhydrous basis. Site assignments are:

Al(IV) = 8.00 - Si

Al(VI) = Al(tot) - Si

Procedure one: all divalent and trivalent cations in the octahedral sites are summed. Note this excludes Na and K. If the total is greater than 15 then some iron is converted to ferric iron as in the manner described for the pyroxenes, until convergence to 15 is achieved. This will result in the calculation of a maximum ferric iron content. Procedure two allows the calculation of a minimum ferric iron content. The divalent and trivalent octahedral cations, excluding Ca, are normalised to 13.

Ilmenite.

The structural formula is based on 3 oxygens. The ferric iron is estimated by summing the cations and normalising to 2.

Magnetite.

The structural formula is based on 4 oxygens.The weight percents of the elements are calculated by initially assuming a ratio of 2:1 for ferric:ferrous iron. Adjustments to this ratio are made by assigning sufficient Fe^{2+} or Fe^{3+} to balance the other trivalent and divalent cations present, and then dividing the remaining total Fe between ferrous and ferric in the ratio of 1:2 ferrous:ferric.

WHOLE ROCK GEOCHEMICAL ANALYSES

All major, minor and trace element analyses of the whole rocks listed in the appendix 3 were determined at the geochemical laboratories of the Geological Survey of Canada in Ottawa. The major and minor elements: Si, Ti, Al, Fe(tot), Mn, Mg, Ca, Na, K, P, were determined by XRF analysis on fused glass discs. The discs were prepared by fusing 1 g of the sample in a mixture of 5 g of $Li_2B_4O_7$ and 0.3 g of LiF. Matrix corrections were applied by employing alpha factors. The estimated detection limits and standard deviations are given below. H_2O(total) FeO, CO_2 and S were determined by rapid chemical means. The trace elements: Ba, Be, Co, Cr, Cu, La, Ni, Sr, V, Y and Yb were determined by spectrochemical methods, while Nb, Pb, Rb, Sr, Th, U, Y and Zr were determined by XRF on pressed powdered pellets.

Table A.3.
Statistical detection limits for whole rock geochemical analyses.

	detection limit (%)	standard deviation
SiO_2	0.40	0.53
TiO_2	0.02	0.02
Al_2O_3	0.40	0.40
Fe_2O_3	0.10	0.10
FeO	0.03	
MnO	0.01	0.01
MgO	0.10	0.14
CaO	0.10	0.15
Na_2O	0.50	0.50
K_2O	0.05	0.16
H_2O	0.05	
CO_2	0.05	
P_2O_5	0.02	0.02
S	0.02	

INSTRUMENTAL NEUTRON ACTIVATION ANALYSIS

Sample Preparation

Crushing

The method by which the samples are prepared for INAA can be critical in determining the quality of the final results. Certain methods of crushing the sample can add contaminants which will increase the background radiation of the sample and hence raise the detection limits for all elements being determined. Contamination by elements which activate readily, eg., W and Co, should be avoided. The contaminants in some cases may produce radioisotopes which interfere spectrally with the radioisotopes of interest. The overlap of the ^{187}W 72 keV gamma-ray onto the 70 gamma-ray of ^{153}Sm is one such example.

A tungsten carbide swing mill, the most common crushing device used for pulverising rock samples, will add both W and Co to the sample. Some of the ceramic plates from a disc grinder have been reported to contaminate a sample with Co (Jacobs *et al.*, 1977).

Since a certain amount of contamination could not be avoided during crushing, the contamination was minimised by using the following procedure. The sample, which had all weathered surfaces removed from it, was crushed initially in a jaw crusher in order to produce suitable size fragments for the next step. Splitting of the sample into portions for various geochemical procedures was undertaken at this stage. A riffle splitter, such as that used by sedimentologists, was used to achieve a split. A disc grinder equipped with mullite plates, was subsequently used to bring the particle size down to about 1 - 2 mm. Samples of which REE analyses of the bulk rock were required, were crushed to a finer grain size in an agate swing mill. Samples which were to be used for mineral separations were crushed to a finer grain size in the disc grinder. This procedure could not be avoided as swing mill crushing has a tendency to overgrind the sample, and this is not desirable in mineral separations.

Mineral Separations

Because accessory phases were being studied in this research project it was necessary to use a Wilfley table to achieve a preconcentration of the heavy minerals. Heavy liquid techniques and magnetic separations (using a Franz 130 isodynamic separator) were employed to separate each mineral fraction from the Wilfley table concentrates. Final purification was achieved by hand picking under a binocular microscope. All mineral separates were carefully washed in acetone to remove any of the heavy liquids which may have adhered to the grain surfaces. Mineral samples were ground finally by hand in an agate or borazon mortar.

Pelletisation

The planar low energy photon detector (LEPD) which was used to count each sample is sensitive to changes in the sample geometry and relative sample-detector positions. Experiments were conducted to assess the effect of this on the precision of the analysis. The results of these experiments will discussed in the next section. In an attempt to minimise the error due to small changes in the sample density and dimensions a method of controlling the geometry of the sample was devised. This involved pellisation of the sample so that a uniform thickness and hence density, for different samples is achieved.

It proved impossible to compress a pure powdered sample so that the pellet would hold its shape without deterioration or attrition of material. Therefore it was necessary to add a binder to ensure adequate cohesion of the material. Cellulose was found to be suitable as a binder. A pellet of cellulose was prepared, irradiated and counted in the same manner as the samples to check for any impurities contained within the cellulose or contaminants picked up from the sample compression dies. No significant amounts of the elements being determined, nor any interferring elements, were detected.

The pellets were prepared in the following manner. An aliquot of approximately 0.2 g of the sample and 0.05 g of cellulose were each weighed separately then mixed together by hand. The mixture was compressed into a pellet of 1 cm diameter and 0.2 cm thickness at a pressure of 2000 p.s.i. (143 kg cm^{-2}). Loss of material during this procedure was calculated by reweighing the pellet. A thin film of Mylar (such as that sometimes used in the preparation of XRF samples) was placed over one face of the pellet and a rim and backing of some additional cellulose was provided. A final compression at 12000 p.s.i. (857 kg cm^{-2}) bound the three materials together into a pellet of 1.5 cm diameter and 0.15 cm thickness. Actual sample thickness is on the order of 0.1 cm. When prepared in this way the sample is completely enclosed in cellulose and Mylar and thus offers little opportunity for intersample contaminations. In the cases where it is necessary to use smaller sample amounts it is possible to maintain the usual pellet volume by diluting with cellulose; although, of course, this will alter the sample density.

Semi-absolute Technique

The REE and U, Th, Hf, and Ta were determined by INAA using the semi-absolute technique. All samples were irradiated in the SLOWPOKE II reactor at the University of Alberta, and were counted on a low energy photon detector (LEPD) which had a planar geometry.

The mass of an element in a sample is related to the activity of one of its radioisotopes by the following equation:

$$m = \frac{N \; M \lambda}{N(av) \theta P_{\gamma} \; A \epsilon_{\gamma} GDC} \qquad (1)$$

where

2 m - mass of the element of interest
N - net area of the photopeak of interest
M - atomic weight of the element of interest
λ - decay constant of the activated isotope
$N(av)$ - Avogadros number
θ - isotopic abundance of the isotope of interest
P_{γ} - gamma-ray emission probability
ϵ_{γ} - gamma-ray detection efficiency
G - $1 - \exp(-\lambda t_a)$
D - $\exp(-\lambda t_d)$
C - $1 - \exp(-\lambda t_c)$
t_a - activation time
t_d - decay time
t_c - counting time
A - saturated activity per target atom = $\sigma(eff)\phi$
$\sigma(eff)$ - effective cross-section
ϕ - total flux

Parameters λ, P_{γ}, θ and M must be obtained from published data. Sometimes these parameters are inaccurately known. Sources of nuclear data used in this study are: Gryntakis and Kim (1978) and Lederer and Shirley (1978). Parameter A is dependent on the characteristics of the reactor or neutron source used. Parameters ϵ_{γ} and N are dependent on the characteristics of the detector system. In particular ϵ_γ is dependent on the active volume and geometry of the detector. The LEPD has the largest efficiency of detection in the low energy range. Gamma-rays of greater energy than 400 keV are not efficiently detected by this spectrometer. N is dependent on the resolution of the counting system. The characteristics of the preamplifier and the amplifier are as important as those of the detector itself in determining this parameter.

The semi-absolute technique (Bergerioux *et al.*, 1979) involves the experimental derivation of the reactor and detector system parameters. These parameters can then be used in equation (1). The technique is suitable only if the neutron energy spectrum and flux is stable with respect to time. It was on the basis of the exceptional stability of the SLOWPOKE II reactor, the type which is installed at the University of Alberta, that the semi-absolute technique was designed. Once the experimental parameters are known, then samples can be analysed without the necessity of analysing standards or flux monitors. The experimental parameters can only be applied to samples irradiated and counted under exactly the same conditions as the standards which were used to determine these values, i.e., time of irradiation, level of flux, and the same counting positions with respect to the detector.

In establishing the experimental reactor and detector parameters a number of areas had to be investigated. These included:

i. selection a suitable irradiation - decay - counting scheme;

ii. identification of potential sources of error associated with the use of a planar detector;

iii. the nature of interferences.

Irradiation - Decay - Counting

Nuclear data for the REE and several other elements suitable for analysis by low energy gamma-ray spectrometry may be found in Lederer and Shirley (1978). On the basis of the half lives, the REE and the other elements may be split into three groups. Of these elements only Pr may not be detected using the planar LEPD since it only emits one gamma-ray of 1576 keV in energy. Hence:

i. $T_{1/2}$< 10 hours - ^{155}Sm, ^{165}Dy, ^{165}Dy^{m}, ^{152}Eu^{m}, ^{171}Er, ^{149}Nd, ^{176}Lu^{m}, ^{239}U, ^{233}Th;

ii. 10 hours < $T_{1/2}$ < 10 days - ^{140}La, ^{143}Ce ^{153}Sm, ^{166}Ho, ^{175}Yb, ^{177}Lu, ^{239}Np

iii. 10 days < T½ - ^{141}Ce, ^{147}Nd, ^{152}Eu, ^{154}Eu, ^{153}Gd, ^{160}Tb, ^{170}Tm, ^{181}Hf, ^{233}Pa, ^{182}Ta, ^{131}Ba.

Since most of the elements of interest are in groups 2 and 3, only one irradiation scheme was used. Dy was not determined. Samples were irradiated for 2 hours at 1×10^{12} $ncm^{-2}s^{-1}$.

Counting was undertaken after a 7 day decay time for ^{140}La, ^{153}Sm, ^{166}Ho, ^{239}Np and ^{175}Yb, and involved a 4 hour counting period. It was discovered that ^{166}Ho could not be detected using this scheme. Counting after a shorter decay interval would not suffice for determining this element as the background radiation was still too high after a 7 day period. An 18 day decay interval and a 10 hour count time were used in the determination of the rest of the elements; ^{141}Ce, ^{147}Nd, ^{152}Eu, ^{153}Gd, ^{160}Tb, ^{170}Tm, ^{169}Yb, ^{177}Lu, ^{181}Hf, ^{182}Ta, ^{233}Pa.

- Detection System

The LEPD used in this project was a PHYGE (passivated hyperpure germanium) planar detector, APTEC Model PS5010-A31P. The detector is operated at a negative bias of 1500 V. It has an active area of 500 mm^2 and a sensitive depth of 10 mm. The window consists of 0.125 mm thickness of Be and is sited 5 - 7 mm from the detector. The energy resolution for this part of the system is 0.35 keV FWHM for Fe Kα (6.4 keV) X-rays and 0.58 keV FWHM for 122 keV (^{57}Co) (manufacturer's specifications). Signals were processed by an APTEC preamplifier, Model SP103, a Canberra Model 2010 amplifier and an Nuclear Data 575 ADC (analog to digital converter). The amplifier was operated with a positive unipolar input/output, a shaping time of 4 us and the baseline restorer set in the asymmetrical medium mode. The gain on the amplifier was set to process incoming pulses equivalent to gamma-rays of up to 450 keV in energy.

The ADC was operated at a conversion gain of 4096 channels. This gave approximately 0.10 keV per channel which is more than the minimum 5 channels per FWHM required for an accurate Gaussian peak fit during data processing (Hertogen and Gijbels, 1971).

As is the case with most solid state detectors it is possible to have escape peaks generated. These are due to the fluorescence of the detector material by gamma-rays and subsequent escape of X-rays generated. In the case of Ge, escape peaks are lower in energy by approximately 10 keV than the associated photopeaks from which they were generated. For a planar detector of similar active volume to the one used in this study, the escape peak size was found to be unimportant at high energies, becoming important only below 50 keV (Hertogen and Gijbels, 1971). No escape peaks were recognised in any of the spectra collected during this study, hence the escape peak effect has been ignored.

Sources of Error

The small volume of the planar detector is sensitive to changes in the geometry of the sample and its position with respect to the detector, (Hertogen and Gijbels, 1971; Hoede and Das, 1971; Potts and Hussey, 1983). In particular the detection efficiency may change drastically with perpendicular distance from the detector; the effect being most noticeable at close geometries. Sample geometry may be a critical factor in the positioning of the sample as the relative centre of gravity of it may move with respect to the detector in the same counting position. Lateral distance from the detector axis may be another source of error.

These potential sources were tackled in two ways. One, the method of controlling the dimensions of the sample by pelletisation, has already been discussed. Two, the variation in the counting statistics due to changes in the lateral position of the sample with respect to the detector axis, was investigated. The activity from a liquid source of a ^{152}Eu standard was counted in different positions laterally from the vertical axis of the detector. The results of these experiments showed that errors due to lateral differences of up to 2 mm in sample positions, can be neglected.

Self Absorption

In the detection of low energy gamma-rays a problem may arise which is unimportant with higher energy gamma-rays; that of the absorption of the low energy gamma-rays by the sample matrix. A series of experiments were conducted to assess the importance of this problem in the samples analysed in this study. Absorbers were made of various minerals of differing densities, such as those minerals of interest in this study. The absorbers were placed between a source of radiation, in this case a ^{152}Eu standard, and the detector. The reduction in transmission of the gamma-rays due to absorption by the mineral materials, could thus be measured. It was found that self absorption by the sample matrix is not likely to be a problem with the sample sizes used in this project for those gamma-rays of greater than 50 keV in energy.

Interferences

There are two types of interferences which may occur with gamma-ray spectrometry:

i. spectral

ii. nuclear.

Spectral interferences result when the energy of a gamma-ray from one radionuclide overlaps with the energy of another produced from a different nuclide. Nuclear interferences are the result of different nuclear reactions producing the same radionuclide. The nuclear interferences which are important to this project are the result of the fissioning of U. Fission products of U include: ^{141}Ce, ^{143}Ce, ^{147}Nd, and ^{139}Ba which decays to ^{140}La. Both types of interferences can be corrected in the same manner.

It is possible to use an empirical correction method for interferences. Measurement of the amount of the interferring nuclide present, allows a correction to be made to the photopeak of interest. This requires that the relative intensities of the gamma-rays from the interferring nuclide to be known to a reasonable degree of accuracy and that at least one major gamma-ray of this nuclide is free from interferences.

For the purpose of determining relative gamma-ray intensities standards containing known amounts of the elements of interest were prepared. Powdered quartz was used a base in order to provide a similar matrix to the samples. The quartz was spiked with solutions (Aldrich AAS standards) containing known concentrations of the relevant elements.

Because there are several interferences amongst the REE themselves it was pertinent to determine the relative intensities of the REE radionuclides. To avoid gamma-ray interferences the REE were split into two groups: (i) La, Ce, Nd, Eu, Gd, Tb, Ho, Tm, Lu and (ii) Ce, Sm, Dy and Yb. Separate standards of U and Th were prepared. The U standard contained U of natural isotopic composition (pers. comm. M.J.M. Duke). The amount of the REE produced by the fissioning of U were found to be similar to the amounts reported by Kennedy and Fowler (1983) for U fissioned in a SLOWPOKE reactor.

Determination of the Semi-absolute Experimental Parameters

US Geological Survey (USGS) rock standards were used to derive the reactor and detector parameters discussed earlier. Five of the USGS standards which had well characterised REE concentrations were used: BCR-1 (basalt), AGV-1 (andesite), GSP-1 (granodiorite), G-2 (granite) and W-1 (diabase). Values for La, Sm and U were calculated from the 7 day count only. Ho and Er could not be quantified in this study. The rest of the REE and other elements were calculated from the 18 day counts as the background counts at this time were lower, and the peak:background ratios were lower than those at the 7 day count, and hence gave better counting statistics.

As a check on the validity of the experimental parameters the data from the standards were processed as if from samples. The concentrations of the REE and U, Th, Hf and Ta in these standards as determined by the method under discussion are given in Table A.4. They are compared to the recommended concentration values from Gladney *et al.* (1983).

The error in the experimentally derived reactor and detector parameters has been estimated by accounting for the error in:

i. the recommended concentration of the element of interest in the standard,
ii. weight of the sample,
iii. the absolute detection efficiency,
iv. the counting statistics (peak - background calculations),
v. the calculation of the "interference factors" for corrections.

The error associated with the determination of each element in a sample is calculated by accounting for the factors listed above as well as the error associated with the experimental parameters.

Data Processing

All spectra were processed initially for photopeak areas and peak centroid energies by a program called PREP11 (Apps, 1979). The program indicates the energy, peak and background areas, percent one sigma error in the peak area, FWHM and accuracy of Gaussian fit for multiplet peaks. A Fortran 77 program was written to handle subsequent calculation of elemental concentrations from information on the photopeak

Table A 4.
Experimentally derived values for 5 U.S.G.S. rock standards compared to the recommended values.

	W-1	BCR-1	AGV-1	GSP-1	G-2
La	11.6±0.4	26±2	38±3	181±10	87±3
lit	11±1	25.00±0.08	38±3	183±13	86±5
Ce	23.9±0.5	54.0±1.6	69±2	417±5	154±3
lit	23±2	53.7±0.8	66±6	406±20	159±11
Nd	14±1	29±2	34±2	205±3	48±2
lit	15±3	28.7±0.6	34±5	190±17	53±8
Sm	3.37±0.05	6.8±0.1	5.8±0.1	26.2±0.9	7.3±0.2
lit	3.5±0.3	6.6±0.2	5.9±0.5	27±3	7.2±0.6
Eu	1.09±0.02	1.98±0.04	1.58±0.04	2.17±0.04	1.37±0.03
lit	1.11±0.09	1.96±0.05	1.66±0.11	2.4±0.2	1.4±0.1
Tb	0.66±0.03	1.06±0.01	0.77±0.07	1.13±0.03	0.41±0.06
lit	0.65±0.07	1.05±0.09	0.7±0.1	1.4±0.1	0.48±0.07
Tm	0.43±0.02	0.5±0.1	0.11±0.06	0.16±0.06	0.19±0.09
lit	0.34±0.07	0.59±0.04	0.32±0.05	0.5±0.1	0.17±0.07
Yb	2.31±0.02	3.4±0.1	1.79±0.09	1.74±0.05	0.60±0.07
lit	2.1±0.2	3.39±0.08	1.7±0.2	1.7±0.4	0.8±0.1
Lu	0.34±0.03	0.51±0.03	0.30±0.04	0.26±0.03	0.13±0.02
lit	0.34±0.04	0.51±0.03	0.28±0.03	0.22±0.05	0.11±0.02
Hf	2.51±0.02	4.91±0.05	5.1±0.2	15.1±0.6	7.8±0.3
lit	2.6±0.3	4.9±0.3	5.1±0.4	15±1	7.9±0.7
U	0.58±0.05	1.76±0.04	1.9±0.1	2.8±0.4	2.0±0.1
lit	0.57±0.07	1.7±0.2	1.9±0.3	2.2±0.3	2.0±0.2
Th	2.3±0.2	6.1±0.3	6.1±0.3	108±3	24.0±0.7
lit	2.4±0.4	6.0±0.6	6.5±0.4	105±5	25±2
Ta	0.49±0.03	0.81±0.05	0.89±0.06	0.91±0.06	0.87±0.05
lit	0.50±0.07	0.79±0.09	0.9±0.1	0.9±0.1	0.8±0.1

lit - literature (recommended) values from Gladney *et al.* 1983.
nm - not measured

areas, mass of the sample, activation, decay and counting times. The program will calculate the amount of any interferences where necessary.

APPENDIX 2

NUMERICAL EXPRESSIONS OF GEOTHERMOMETERS

Garnet - Biotite

Ferry and Spear (1978)

The basic equation is:

$H - T \quad S + P \quad V + 3RT\ln K(D) = 0$

$\ln K(D) = (X_{py})(X_{ann}) / (X_{alm})(X_{phl})$

where $X_{py} = Mg / (Mg + Fe^{2+} + Ca + Mn)$ of garnet.

similarly for Xalm which the Fe atomic fraction of garnet.

and where $X_{ann} = Fe^{2+} / (Fe^{2+} + Mg + Ti + Al)$ of biotite.

similarly for Xphl which is the Mg atomic fraction of biotite.

The experimentally determined values are:

H = 12454 cal.

S = 4.662 eu.

V = 0.057 cal / bar.

Therefore:

$12454 - 4.662T(^{\circ}K) + 0.057P(bars) + 3RT\ln K(D) = 0.$

and rearranging.

$12454 + 0.057P / -3R\ln K(D) + 4.662 = T(^{\circ}K).$

Thompson (1976)

The definition of the basic equation is the same as that defined for the Ferry and Spear calibration above.

$\ln K(D) = (X_{alm})(X_{phl}) / (X_{py})(X_{ann})$ (Note that lnK(D) is the inverse of that for Ferry and Spear (1978))

H = 5444.39

S = -3.100

V = -0.0465

Substituting into equation (1):

$5444.39 - 0.0465P / -R\ln K(D) + 3.1 = T(^{\circ}K)$

Holdaway and Lee (1977)

The definition of the basic equation and the distribution coefficient is the same as that given for the Ferry and Spear calibration above.

H = 6150 cal

S = 3.93 cal / deg

V = 0.0246 cal / bar

Therefore:

6150 + 0.0246P / -3RlnK(D) + 3.93 = T(°K)

Perchuk and Lavrent eva (1983)

The definition for the basic equation is the same as that for the Ferry and Spear calibration above and the definition for the distribution coefficient is the same as that given for the Thompson calibration above.

H = 7843.7 cal

S = 5.699 cal / deg

V = 0.0246 cal / bar

Substituting into equation (1):

7843.7 + 0.0246P - 6000) / RlnK(D) + 5.699 = T(°K)

Ganguly and Saxena (1984)

The definition for the distribution coefficient is the same as that given for the Thompson calibration above. The main difference to the Ferry and Spear (1978) calibration is with the definition of the mole fractions of garnet. The term incorporating the mixing properites of garnet with that of the distribution coefficient is defined as K(a) where;

K(a) = [(Xalm)(Xphl) / (Xpy)(Xann)] [(alm)(phl) / (py)(ann)]

Therefore, the expression relating K(a) and K(D) is:

RTlnK(a) = RTlnK(D) - [W(Fe-Mg)(XFe -XMg) + (WMgK - WFeK)] - [WFeMg(XMg - XFe)

+ (WFe - WMg)X]

Since Ferry and Spear (1978) used alm$_{90}$py$_{10}$ in their experiments then Xalm = 0.9 and Xpy = 0.1, so WFeMg(XFe - XMg) = 0.8 WFeMg. The rest of the expression for lnK(a) is zero because no other components were present in the garnets used in the experiments.

Therefore:

$$\ln K(a) = \frac{2089 + 9.56P(kb) - 0.8WFeMg}{T} - 0.782$$

and so:

$$T = \frac{2089 + 9.59P(kb) + [B(WFeMg) + WCaXCa + WMnXMn]/R}{\ln K(D)' + 0.782}$$

where $B = (XFe - XMg) - 0.8$

Garnet - Cordierite

Thompson (1976)

The basic equation which was used for the garnet - biotite geothermometer is applicable here.

Hence:

$H = 5415.18$

$S = -1.781$

$V = -0.0308$

Therefore:

$T = 5415.18 - 0.0308P / -R\ln K(D) - 1.781$

Holdaway and Lee (1977)

The definition for the basic equation and the distribution coefficient are the same as described for the garnet - biotite geothermometer of Holdaway and Lee (1977).

Hence:

$H = 6150$ cal

$S = 2.69$

$V = 0.0303$

Therefore:

$T(^\circ K) = 6150 - 0.0303P / -R\ln K(D) + 2.69$

Perchuk and Lavrent'eva

The definition for the basic equation and the distribution coefficient are the same as described for the garnet - biotite geothermometer of Perchuk and Lavrent'eva (1983).

Hence:

$H = 3020$ cal

$S = 1.287$ cal/deg

$V = 0.018$ cal/bar

Therefore:

$T(^{\circ}K) = 3020 - 0.018P / \ln K(D) + 1.287$

Orthopyroxene - Clinopyroxene

Wood and Banno (1973)

The definition of the basic equation is:

$H - T \quad S + P \quad V + RT \ln K(D) = 0$

where $K(D) = (aMg_2Si_2O_6\text{-cpx}) / (aMg_2Si_2O_6\text{-opx})$

and

$aMg_2Si_2O_6(\text{opx or cpx}) = [Mg / Mg+Ca+Fe^{2+}+Mn+Na]_2 \, . \, [Mg / Mg+Fe^{2+}+Fe^{3+}Al+Ti+Cr]_1$

Temperature estimates are derived from the equation:

$T(^{\circ}K) = -10202 / \ln K(D) - 7.65XFe\text{-opx} + 3.88(XFe\text{-opx})^2 - 4.6$

Wells (1977)

The definition of the basic equation and the distribution coefficient is the same as that given for Wood and Banno above.

The temperature equation is:

$T(^{\circ}K) = 7341 / 3.355 + 2.44XFe\text{-opx} - \ln K(D)$

Saxena (1976)

The mole fraction $XMg\text{-cpx} = Mg / Mg+Fe+Ca$

The temperature is calculated in the following steps:

1. Assume a temperature of metamorphism.
2. Apply the temperature estimate to the following equation in order to calculate $XFe\text{-opx-}M_1$, hence:

$$-4479 + 1948 \quad 10^3/T = RT.\ln[XFe\text{-opx-}M_1 (1 - 2XFe\text{-opx} + XFe\text{-opx-}M_1) / (2XFe\text{-opx} - XFe\text{-opx-}M_1)(1 - XFe\text{-opx-}M_1)] + AMg\text{-}Fe\text{-}M_1(1 - 2XFe\text{-opx-}M_1) - AMg\text{-}Fe\text{-}m_2(1 - 2(2XFe\text{-opx} - XFe\text{-opx-}M_1) \qquad (1)$$

3. Calculate aMg-opx from the following equation using the site occupancy data from equation (1):

aMg-opx = [(1 - XFe-M_1-opx)exp(AMg-Fe-M_1 / RT(XFe-M_1-opx)^2).((1 - 2XCa-opx - 2XFe-opx + XFe-M_1-opx)).exp(AFe-Mg-M_2 / RT(2XFe-opx - XFe-M_1-opx).(2XFe-opx - XFe-M_1-opx + 2XCa-opx) + 2AMg-Ca-M_2 / RT.XCa-opx(2XFe-opx - XFe-M_1-opx + 2XCa-opx) - 2AFe-Ca-M_2 / RTXCa-opx(2Fe-opx - XFe-M_1-opx)] (2)

4.Calculate XCa-M_2-cpx, Mg-M_2-cpx, and aMg-cpx from the following equations:

RTlnK(D) = -28456 + 65596(10^3 / T) - 54737(10^3 / T)^2 + 15259(10^3 / T)^3 (3)

Mg-M_2-cpx = exp[WMg-Fe-M_2 / RT(1 - XMg-M_2-cpx)XFe-M_2-cpx + WMg-Ca-M_2 / RT(1 - XMg-M_2-cpx)XCa-M_2-cpx - WFe-Ca / RT- (1 - XCa-M_2-cpx + XMg-M_2-cpx)XCa-M_2-cpx] (4)

RTlnK(D) = RTln[(1 - 2XMg-cpx + XMg-M_2-cpx)XMg-M_2-cpx / (2XMg-cpx - XMg-M_2-cpx)(1 - 2XCa-cpx - XMg-M_2-cpx)] + 2XCa-cpx(WMg-Ca-M_2 - WFe-Ca-M_2) + [WMg-Fe(1 - 2XCa-cpx - XMg-M_2-cpx)(1 - XMg-M_2-cpx)] - WMgFe[XMg-M_2-cpx(2XCa-cpx + XMg-M_2-cpx)] (5)

then substitute XMg-M_2-cpx, Mg-M_2-cpx and XMg-M_1-cpx into:

XMg-M_1-cpx = 2(XMg-cpx - XMg-M_2-cpx) (6)

and

RTlnXMg-M_1-cpx.XMg-M_2-cpx. Mg-M_2-cpx = RTlnaMg-opx. (7)

$WMg\text{-}Ca\text{-}M_1 = 6531$

$WFe\text{-}Ca\text{-}M_2 = 5200$

$WMg\text{-}Fe\text{-}M_2 = 5218 - 16807(10^3/T) + 14280(10^3/T)^2$

$AFe\text{-}Mg\text{-}M_2 = 2458 \quad 10^3/T - 1.261$

$AMg\text{-}Ca\text{-}M_2 = 7184$

$AFe\text{-}Ca = 5000$

$AMg\text{-}Fe\text{-}M_1 = 3525 \quad 10^3/T - 1667$

If the two sides of equation (7) do not converge then another temperature must be selected and the equations recalculated until convergence is achieved.

Kretz (1982)

The temperature equation of the first reaction is defined as:

$<1080\ ^\circ C\ T(^\circ K) = 1000/(0.054 + 0.608X\text{-}cpx - 0.304\ln(1 - 2[Ca]))$

where

$X = Fe^{2+}/(Fe^{2+}+Mg)$

and

$[Ca] = Ca/(Ca+Mg+Fe^{2+})$

The second temperature is defined by:

$T(^\circ K) = 1130/(\ln K(D) + 0.505)$

where

$K(D) = (XFe\text{-}opx)(XMg\text{-}cpx)/(XMg\text{-}opx)(XFe\text{-}cpx)$

Pyroxene - Ilmenite

Bishop (1980)

The temperature equation for the orthopyroxene - ilmenite reaction is:

$T(^\circ K) = 1646 + 1634[Fe^{2+}/(Fe^{2+} + Mg)](Il) + 0.024P/\ln K(D)$

where

$K(D) = (XMg\text{-}opx)(XFe\text{-}ilm)/(XFe\text{-}opx)(XMg\text{-}ilm).$

The temperature equation for the clinopyroxene - ilmenite reaction is:

$T(^\circ K) = 748 + 2745[Mg/(Mg+Fe^{2+})](Cpx) + 817[2(Fe^{2+}/(Fe^{2+}+Mg))(Ilm)] + 0.0106P/\ln K(D)$

where

$K(D) = (XMg\text{-}cpx)(XFe\text{-}ilm)/(XFe\text{-}cpx)(XMg\text{-}ilm).$

APPENDIX 3

Table I
Amphibole Analyses

Sample no	1B	7C	22D	22G
SiO_2	48.46	49.09	41.79	42.00
Al_2O_3	7.66	9.16	13.85	12.19
TiO_2	1.38	1.78	1.32	0.93
FeO*	6.96	13.86	11.30	18.48
MnO	0.04	0.14	0.31	0.37
MgO	18.28	13.13	13.45	9.85
CaO	11.93	12.50	12.23	11.22
Na_2O	1.49	1.20	1.26	1.58
K_2O	0.94	1.15	1.22	1.43
V_2O_3	0.13	nd	0.04	nd
Cr_2O_3	0.40	nd	0.04	nd
Cl	nd	0.10	0.10	0.10
H_2O	2.33	0.93	3.14	1.87
Total@	100.00	100.00	100.00	100.00

Structural formula on the basis of 23 oxygens

Si	6.909	6.833	6.717	6.692	6.134	6.096	6.320	6.235
Al(IV)	1.092	1.167	1.284	1.308	1.866	1.904	1.681	1.765
Al(VI)	0.197	0.107	0.290	0.260	0.531	0.478	0.482	0.368
Ti	0.148	0.147	0.195	0.195	0.145	0.145	0.106	0.104
Fe^{3+}	nd	0.084	nd	0.047	0.079	0.102	0.057	0.112
Fe^{2+}	0.831	0.738	1.690	1.637	1.309	1.277	2.270	2.184
Mn	0.005	0.005	0.018	0.018	0.038	0.038	0.047	0.046
Mg	3.889	3.846	2.854	2.844	2.945	2.927	2.212	2.183
Ca	1.824	1.804	1.953	1.946	1.926	1.914	1.812	1.787
Na	0.412	0.407	0.339	0.338	0.358	0.355	0.462	0.456
K	0.171	0.169	0.213	0.212	0.228	0.226	0.275	0.271
V	0.015	0.015	nd	nd	0.004	0.004	nd	nd
Cr	0.045	0.044	nd	nd	0.005	0.005	nd	nd
Sum#	14.953	12.986	15.000	13.000	14.983	12.976	14.985	12.997

* - all Fe in the oxide is calculated as Fe^{2+}

@ - H_2O is calculated as the difference between the total sum of the oxides and 100%

# - data given for the structural formulae represent two methods of estimating the Fe^{3+} content.

The first column gives an estimate of the maximum Fe^{3+} by adding the cations exclusive of Na and K and normalising to 15.

The second column estimates the minimum Fe^{3+} by adding the cations exclusive of Ca, Na and K, and normalising to 13.

Table I. (continued)

Sample no.	55C		56A		1418		160	
SiO_2	47.04		45.38		44.69		43.61	
Al_2O_3	7.31		9.03		9.09		9.95	
TiO_2	1.03		1.36		1.72		1.77	
FeO*	12.58		12.88		12.98		17.06	
MnO	0.16		0.14		nd		0.14	
MgO	14.88		13.87		13.55		10.56	
CaO	11.67		11.08		11.78		11.27	
Na_2O	1.49		1.44		1.39		1.56	
K_2O	0.69		0.86		1.33		1.28	
V_2O_5	nd		0.18		0.29		0.27	
Cr_2O_3	0.26		0.05		0.48		nd	
Cl	nd		0.03		nd		0.06	
H_2O	2.91		3.63		2.70		2.47	
Total@	100.00		100.00		100.00		100.00	
Structural formula on the basis of 23 oxygens								
Si	6.15	6.830	7.537	7.537	6.630	6.567	6.574	6.511
Al(IV)	1.085	1.170	0.464	0.464	1.370	1.433	1.426	1.489
Al(VI)	0.181	0.081	nd	nd	0.219	0.141	0.343	0.263
Ti	0.114	0.112	0.170	0.170	0.192	0.190	0.202	0.200
Fe^{3+}	0.024	0.094	nd	nd	nd	0.079	nd	0.080
Fe^{2+}	1.524	1.435	1.790	1.790	1.612	1.577	2.153	2.052
Mn	0.019	0.019	nd	0.020	nd	nd	0.018	0.018
Mg	3.263	3.223	3.437	3.437	2.998	2.970	2.375	2.352
Ca	1.841	1.819	1.973	1.973	1.874	1.857	1.823	1.806
Na	0.424	0.419	0.463	0.463	0.401	0.397	0.456	0.452
K	0.129	0.128	0.183	0.183	0.250	0.248	0.245	0.243
V	nd	nd	0.006	0.006	0.035	0.035	0.033	0.033
Cr	0.301	0.030	nd	nd	0.057	0.056	nd	nd
Sum#	14.996	12.994	14.938	12.965	14.987	12.988	14.946	12.996

* - all Fe in the oxide is calculated as Fe^{2+}

@ - H_2O is calculated as the difference between the total sum of the oxides and 100%

# - data given for the structural formulae represent two methods of estimating the Fe^{3+} content.

The first column gives an estimate of the maximum Fe^{3+} by adding the cations exclusive of Na and K and normalising to 15.

The second column estimates the minimum Fe^{3+} by adding the cations exclusive of Ca, Na and K, and normalising to 13.

Table I. (continued)

Sample no.	183D	231	GAB	D1B
SiO_2	44.59	45.94	48.82	50.58
Al_2O_3	9.23	9.55	7.91	5.64
TiO_2	2.00	1.45	0.40	0.39
FeO*	14.17	12.79	10.19	8.79
MnO	0.14	0.15	0.14	0.22
MgO	12.42	14.13	6.39	16.93
CaO	11.06	11.11	11.02	11.85
Na_2O	1.06	1.57	0.80	0.72
K_2O	1.16	0.95	0.33	0.53
V_2O_5	0.08	0.22	0.09	0.18
Cr_2O_3	nd	0.15	0.22	0.25
Cl	nd	0.08	nd	0.07
H_2O	4.10	1.944	3.68	3.86
Total(m)	100.00	100.00	100.00	100.00

Structural formula on the basis of 23 oxygens

	183D		231		GAB		D1B	
Si	6.706	6.615	6.707	6.589	7.064	6.896	7.318	7.250
Al(IV)	1.294	1.385	1.293	1.411	0.937	1.104	0.683	0.750
Al(VI)	0.343	0.230	0.352	0.204	0.413	0.213	0.279	0.202
Ti	0.226	0.223	0.160	0.157	0.044	0.043	0.043	0.042
Fe^{3+}	nd	0.096	nd	0.108	0.031	0.129	nd	0.077
Fe^{2+}	1.784	1.663	1.562	1.426	1.202	1.075	1.064	0.977
Mn	0.018	0.018	0.018	0.018	0.018	0.018	0.027	0.027
Mg	2.787	2.750	3.078	3.023	3.538	3.454	3.654	3.620
Ca	1.784	1.760	1.740	1.709	1.711	1.670	1.840	1.823
Na	0.310	0.306	0.446	0.438	0.224	0.219	0.203	0.201
K	0.222	0.219	0.177	0.174	0.061	0.059	0.098	0.097
V	0.010	0.010	0.026	.025	0.011	0.011	0.023	0.022
Cr	nd	nd	0.017	0.017	0.025	0.025	0.028	0.028
Sum#	14.952	12.990	14.952	12.979	14.992	12.966	14.957	12.996

* - all Fe in the oxide is calculated as Fe^{2+}

(m) - H_2O is calculated as the difference between the total sum of the oxides and 100%

# - data given for the structural formulae represent two methods of estimating the Fe^{3+} content.

The first column gives an estimate of the maximum Fe^{3+} by adding the cations exclusive of Na and K, and normalising to 15.

The second column estimates the minimum Fe^{3+} by adding the cations exclusive of Ca, Na and K, and normalising to 13.

Table I. (continued)

Sample no.	D10A	D10B	D12B	D21B
SiO_2	49.79	53.19	47.94	44.04
Al_2O_3	6.69	3.57	6.80	10.08
TiO_2	0.22	nd	0.47	1.10
FeO*	10.92	8.73	18.57	15.67
MnO	0.29	0.23	0.67	0.60
MgO	15.53	18.00	11.20	11.55
CaO	11.98	12.71	10.85	10.81
Na_2O	0.67	0.54	1.06	1.33
K_2O	0.66	0.16	0.38	0.84
V_2O_3	0.09	nd	0.07	0.10
Cr_2O_3	0.03	nd	nd	0.04
Cl	0.03	nd	nd	0.03
H_2O	3.09	2.88	2.00	3.81
Total@	100.00	100.00	100.00	100.00

Structural formula on the basis of 23 oxygens

Si	7.222	7.142	7.568	7.530	7.131	6.985	6.648	6.517
Al(IV)	0.778	0.858	0.432	0.470	0.869	1.015	1.352	1.484
Al(VI)	0.366	0.274	0.167	0.126	0.325	0.154	0.442	0.275
Ti	0.024	0.024	nd	nd	0.053	0.052	0.125	0.123
Fe^{3+}	nd	0.085	0.023	0.061	nd	0.118	0.024	0.120
Fe^{2+}	1.326	1.226	1.016	0.973	2.311	2.146	1.955	1.821
Mn	0.035	0.035	0.028	0.028	0.084	0.082	0.077	0.075
Mg	3.361	3.324	3.820	3.801	2.486	2.435	2.602	2.550
Ca	1.864	1.844	1.940	1.931	1.732	1.696	1.750	1.716
Na	0.189	0.187	0.149	0.148	0.305	0.299	0.390	0.382
K	0.123	0.121	.028	0.028	0.071	0.070	0.162	0.159
V	0.011	0.011	nd	nd	0.008	0.008	0.012	0.012
Cr	0.003	0.003	nd	nd	nd	nd	0.005	0.005
Sum#	14.991	12.981	14.984	12.989	14.998	12.994	14.994	12.981

* - all Fe in the oxide is calculated as Fe^{2+}

@ - H_2O is calculated as the difference between the total sum of the oxides and 100%

# - data given for the structural formulae represent two methods of estimating the Fe^{3+} content.

The first column gives an estimate of the maximum Fe^{3+} by adding the cations exclusive of Na and K and normalising to 15.

The second column estimates the minimum Fe^{3+} by adding the cations exclusive of Ca, Na and K, and normalising to 13.

Table II.
Orthopyroxene Analyses

Sample no.	1B	5A	7C	8B	8E	9F	13B	22L
SiO_2	54.52	50.86	51.99	48.96	48.60	49.15	49.56	52.84
Al_2O_3	0.83	1.99	0.96	2.94	4.47	3.79	1.40	0.78
TiO_2	nd	nd	nd	nd	nd	nd	0.03	nd
FeO*	16.61	26.73	26.09	30.61	30.25	28.70	32.75	23.76
MnO	0.45	0.62	0.66	1.05	0.64	0.63	0.97	0.38
MgO	27.03	19.55	19.54	16.02	15.96	17.62	14.62	21.76
CaO	0.57	0.26	0.76	0.18	0.09	0.11	0.45	0.46
Na_2O	nd	nd	nd	nd	nd	nd	nd	nd
K_2O	nd	nd	nd	nd	nd	nd	nd	0.10
Cr_2O_3	nd	nd	nd	nd	nd	nd	nd	nd
Total@	100.55	99.86	100.54	100.25	99.37	98.97	99.21	99.51
Structural formula on the basis of 6 oxygens								
Si	1.964	1.927	1.971	1.899	1.875	1.879	1.948	1.975
Al(IV)	0.031	0.073	0.029	0.101	0.145	0.121	0.052	0.025
Al(VI)	0.005	0.0.16	0.014	0.033	0.079	0.050	0.013	0.009
Ti	nd	nd	nd	nd	nd	nd	0.001	nd
Fe^{3+}#	0.006	0.012	-	0.015	0.010	0.014	0.009	0.004
Fe^{2+}	0.496	0.835	0.828	0.979	0.966	0.904	1.068	0.739
Mn	0.014	0.020	0.021	0.035	0.021	0.020	0.032	0.012
Mg	1.457	1.105	1.105	0.927	0.919	1.005	0.857	1.213
Ca	0.022	0.011	0.031	0.008	0.004	0.005	0.019	0.018
Na	nd	nd	nd	nd	nd	nd	nd	nd
K	nd	nd	nd	nd	nd	nd	nd	0.005
Cr	nd	nd	nd	nd	nd	nd	nd	nd
Sum	1.999	1.999	1.999	1.996	1.999	1.998	1.999	1.999

* - all FeO represents total Fe calculated as Fe^{2+}

# - Fe in the structural formula has been divided into estimates of Fe^{3+} and Fe^{2+}

@ - Total represents the total sum of the oxides before recalculation to 100 %

Table II. (continued)

Sample no.	56A	141B	142A	160	182A	183D	186A	189A
SiO_2	52.60	51.95	47.87	50.75	48.30	52.02	51.421	48.70
Al_2O_3	0.945	0.96	5.71	0.68	5.92	0.59	0.572	3.88
TiO_2	nd	0.03	0.04	nd	nd	nd	nd	nd
FeO*	23.77	25.00	28.87	31.21	27.06	26.96	29.06	29.55
MnO	0.68	0.46	0.43	0.77	0.59	0.81	0.72	0.54
MgO	21.28	20.74	16.78	15.42	18.06	18.84	17.32	17.00
CaO	0.63	0.60	0.11	0.98	0.04	0.76	0.91	0.17
Na_2O	nd	0.21	0.18	0.18	nd	nd	nd	0.17
K_2O	0.09	nd	nd	nd	nd	nd	nd	nd
Cr_2O_3	nd	0.04	nd	nd	nd	nd	nd	nd
Total@	98.15	99.35	99.81	99.24	99.32	98.97	99.18	100.27
Structural formula on the basis of 6 oxygens								
Si	1.973	1.951	1.827	1.976	1.832	1.982	1.980	1.866
Al(IV)	0.027	0.049	0.173	0.024	0.168	0.018	0.02	0.134
Al(VI)	0.015	-	0.084	0.007	0.097	0.009	0.006	0.041
Ti	nd	-	0.001	nd	nd	nd	nd	nd
Fe^{3+}#	nd	0.008	0.019	0.006	0.014	nd	nd	0.019
Fe^{2+}	0.746	0.772	0.903	1.011	0.845	0.860	0.936	0.929
Mn	0.022	0.015	0.014	0.025	0.019	0.026	0.023	0.017
Mg	1.191	1.162	0.956	0.896	1.022	1.071	0.995	0.972
Ca	0.025	0.024	0.005	0.041	0.002	0.031	0.038	0.007
Na	nd	0.015	0.013	0.014	nd	nd	nd	0.013
K	0.004	nd	nd	nd	nd	nd	nd	nd
Cr	nd	0.001	nd	nd	nd	nd	nd	nd
Sum	1.998	1.998	1.995	1.999	1.998	1.996	1.998	1.997

* - all FeO represents total Fe calculated as Fe^{2+}

# - Fe in the structural formula has been divided into estimates of Fe^{3+} and Fe^{2+}

@ - Total represents the total sum of the oxides before recalculation to 100 %

Table II. (continued)

Sample no.	200A	231	GAB	D12B
SiO_2	53.78	52.42	53.33	53.57
Al_2O_3	1.15	1.15	1.03	0.76
TiO_2	nd	nd	nd	nd
FeO*	16.91	23.35	20.90	27.89
MnO	0.28	0.67	0.53	1.94
MgO	26.80	21.42	23.66	14.45
CaO	0.59	0.59	0.56	1.07
Na_2O	0.27	0.17	nd	0.32
K_2O	nd	0.17	nd	nd
Cr_2O_3	0.21	nd	nd	nd
Total@	99.95	99.37	98.99	98.24
Structural formula on the basis of 6 oxygens				
Si	1.940	1.958	1.968	2.051
Al(IV)	0.060	0.042	0.032	nd
Al(VI)	nd	0.009	0.013	0.085
Ti	nd	nd	nd	nd
Fe^{3+}#	0.046	0.012	0.002	nd
Fe^{2+}	0.495	0.718	0.644	0.894
Mn	0.009	0.021	0.017	0.063
Mg	1.443	1.194	1.303	0.825
Ca	0.023	0.024	0.022	0.044
Na	0.019	0.012	nd	0.024
K	nd	nd	nd	nd
Cr	0.006	nd	nd	nd
Sum	1.999	1.997	2.000	1.935

* - all FeO represents total Fe calculated as Fe^{2+}

# - Fe in the structural formula has been divided into estimates of Fe^{3+} and Fe^{2+}

@ - Total represents the total sum of the oxides before recalculation to 100 %

Table III.
Clinopyroxene Analyses

Sample no.	1B	7C(rim)	7C(core)	22D	22G	55C	141B
SiO_2	53.73	52.45	52.32	51.70	50.60	51.92	52.46
Al_2O_3	1.22	1.54	1.46	2.45	2.33	1.28	1.45
TiO_2	0.15	0.16	0.21	0.33	nd	nd	nd
FeO*	5.69	10.75	11.24	6.85	13.81	11.00	9.52
MnO	0.14	0.28	0.24	0.46	0.66	0.34	0.16
MgO	16.24	13.28	13.41	14.58	12.46	13.14	13.78
CaO	22.60	21.55	21.01	23.52	20.16	21.90	22.08
Na_2O	nd	nd	0.11	nd	nd	0.29	0.38
K_2O	0.02	nd	nd	nd	nd	nd	nd
Cr_2O_3	0.23	nd	nd	nd	nd	0.14	0.16
Total##	99.93	99.81	100.11	100.16	100.17	99.96	98.76
Structural formula on the basis of 6 oxygens							
Si	1.970	1.964	1.962	1.914	1.942	1.946	1.953
Al	0.030	0.036	0.038	0.086	0.085	0.054	0.047
Al	0.023	0.032	0.027	0.021	0.018	0.003	0.017
Ti	0.004	0.005	0.006	0.009	nd	nd	nd
Fe^{3+} #	nd	nd	nd	0.012	0.014	0.014	0.012
Fe^{2+}	0.175	0.337	0.353	0.200	0.423	0.331	0.285
Mn	0.004	0.009	0.008	0.015	0.021	0.011	0.006
Mg	0.888	0.742	0.751	0.805	0.704	0.735	0.766
Ca	0.889	0.866	0.846	0.934	0.818	0.881	0.882
Na	nd	nd	0.008	nd	nd	0.021	0.028
K	0.001	nd	nd	nd	nd	nd	nd
Cr	0.007	nd	nd	nd	nd	0.004	0.005
Sum	1.991	1.991	1.997	1.996	1.998	1.999	1.999

* - all FeO represents total Fe calculated as Fe^{2+}

# - Fe in the structural formula has been divided into estimates of Fe^{3+} and Fe^{2+}

## - Total represents the total sum of the oxides before recalculation to 100%

Table III. (continued)

Sample no.	160	183D	186A	200A	D10B	D10D
SiO_2	51.67	52.73	52.11	53.28	53.68	53.11
Al_2O_3	1.19	1.20	1.12	1.25	0.68	1.22
TiO_2	nd	0.08	0.11	nd	nd	nd
FeO*	13.34	10.68	12.59	5.42	5.43	5.31
MnO	0.33	0.29	0.25	0.03	0.25	0.12
MgO	11.60	13.23	12.30	16.05	15.09	15.18
CaO	21.34	21.58	21.03	23.28	24.65	24.96
Na_2O	0.34	nd	nd	0.33	0.18	nd
K_2O	0.07	nd	nd	nd	nd	nd
Cr_2O_3	0.12	0.08	0.25	0.36	nd	nd
Total@	100.09	98.84	99.07	99.93	99.99	99.86
Structural formula on the basis of 6 oxygens						
Si	1.956	1.975	1.969	1.950	1.977	1.958
Al(IV)	0.045	0.025	0.031	0.050	0.023	0.042
Al(VI)	0.009	0.028	0.019	0.004	0.007	0.011
Ti	nd	0.002	0.003	nd	nd	nd
Fe^{3+}#	0.014	nd	nd	0.014	0.008	0.008
Fe^{2+}	0.408	0.335	0.398	0.152	0.160	0.156
Mn	0.011	0.009	0.008	0.001	0.008	0.004
Mg	0.655	0.740	0.693	0.876	0.830	0.835
Ca	0.867	0.867	0.853	0.914	0.974	0.987
Na	0.025	nd	nd	0.023	0.013	nd
K	0.004	nd	nd	nd	nd	nd
Cr	0.004	0.003	0.007	0.010	nd	nd
Sum	1.995	1.987	1.989	1.996	1.999	2.000

* - all FeO represents total Fe calculated as Fe^{2+}

- Fe in the structural formula has been divided into estimates of Fe^{3+} and Fe^{2+}

@ - Total represents the total sum of the oxides before recalculation to 100%

Table IV.
Biotite Analyses

Sample no.	1B	5A	5E	7C	8B	8E	9D
SiO_2	39.82	37.49	36.51	38.81	35.69	36.49	32.85
Al_2O_3	13.12	14.24	15.97	13.64	15.06	15.75	18.77
TiO_2	4.80	4.17	3.58	4.90	4.21	4.24	2.51
FeO*	8.60	14.00	18.68	14.90	21.41	17.26	22.99
MnO	0.04	nd	nd	nd	nd	nd	nd
MgO	19.71	15.85	10.83	15.80	10.34	12.56	7.53
CaO	nd	nd	nd	0.11	nd	nd	nd
Na_2O	nd	nd	nd	nd	0.32	nd	nd
K_2O	9.20	8.83	9.40	9.07	8.90	9.53	7.47
V_2O_3	0.15	0.24	nd	nd	nd	nd	0.05
Cr_2O_3	0.33	nd	nd	nd	nd	nd	nd
Cl	0.03	0.09	0.07	0.12	nd	nd	nd
H_2O	4.22	5.12	4.94	2.67	4.15	3.99	7.81
Total@	100.00	100.00	100.00	100.00	100.00	100.00	100.00
Structural formula on the basis of 22 oxygens							
Si	5.713	5.576	5.554	5.644	5.458	5.474	5.231
Al(IV)	2.287	2.424	2.447	2.356	2.542	2.527	2.769
Al(VI)		0.074	2.864	0.017	0.173	0.259	0.754
Ti	0.519	0.468	0.410	0.537	0.485	0.479	0.301
Fe^{2+}	1.032	1.742	2.378	1.813	2.739	2.167	3.063
Mn	0.005	nd	nd	nd	nd	nd	nd
Mg	4.220	3.516	2.458	3.430	2.358	2.811	1.789
Ca	nd	nd	nd	0.018	nd	nd	nd
Na	nd	nd	nd	nd	0.095	nd	nd
K	1.685	1.677	1.825	1.683	1.738	1.825	1.519
V	0.017	0.028	nd	nd	nd	nd	nd
Cr	0.033	nd	nd	nd	nd	nd	nd
Sum	15.449	15.506	15.489	15.465	15.588	15.541	15.433

* - all Fe is calculated as Fe^{2+}

@ - H_2O is calculated as the difference between the sum of the oxides and 100%

Table IV. (continued)

Sample no.	9F	13B	13D	22G	22L	23B	23C
SiO_2	37.78	35.00	34.50	35.11	37.39	36.30	35.81
Al_2O_3	14.77	14.31	14.35	15.41	14.54	14.69	16.65
TiO_2	2.77	6.57	7.14	2.78	5.09	6.02	4.17
FeO*	14.88	21.45	23.41	20.43	13.70	17.48	18.07
MnO	nd	nd	nd	0.17	nd	nd	nd
MgO	15.91	9.38	7.56	12.42	15.00	12.66	11.58
CaO	nd	nd	nd	nd	nd	nd	nd
Na_2O	nd	nd	0.24	nd	nd	nd	0.42
K_2O	8.86	8.92	9.00	8.40	9.56	9.40	8.79
V_2O_3	0.10	0.15	0.13	0.08	0.33	0.10	0.22
Cr_2O_3	0.1	nd	nd	nd	0.27	nd	nd
Cl	nd	0.18	0.17	0.12	0.12	0.33	0.12
H_2O	4.56	3.94	3.58	5.10	3.99	3.04	4.21
Total@	100.00	100.00	100.00	100.00	100.00	100.00	100.00
	Structural formula on the basis of 22 oxygens						
Si	5.616	5.377	5.334	5.398	5.521	5.412	5.298
Al(IV)	2.384	2.623	2.667	2.602	2.479	2.583	2.611
Al(VI)	0.204	nd	nd	0.193	0.052	0.001	0.343
Ti	0.310	0.761	0.831	0.322	0.567	0.676	0.472
Fe^{2+}	1.851	2.758	3.029	2.628	1.692	2.182	2.275
Mn	nd	nd	nd	0.022	nd	nd	nd
Mg	3.529	2.150	1.745	2.849	3.304	2.818	2.599
Ca	nd	nd	nd	nd	nd	nd	nd
Na	nd	nd	0.071	nd	nd	nd	0.124
K	1.682	1.750	1.777	1.650	1.803	1.790	1.688
V	nd	0.019	0.016	0.01	0.039	0.013	0.026
Cr	0.012	nd	nd	nd	0.031	nd	nd
Sum	15.588	15.406	15.418	15.674	15.488	15.479	15.528

* - all Fe is calculated as Fe^{2+}

@ - H_2O is calculated as the difference between the sum of the oxides and 100%

Table IV. (continued)

Sample no.	24B	44	54A	56A	87	135B	142A
SiO_2	36.98	37.75	36.73	37.72	36.80	34.78	36.29
Al_2O_3	17.75	15.40	15.82	13.94	15.32	18.16	14.89
TiO_2	2.02	3.33	3.30	4.36	3.48	3.18	5.67
FeO*	16.94	16.09	20.90	11.70	15.90	22.48	16.57
MnO	nd	nd	0.13	nd	nd	nd	nd
MgO	12.18	13.20	10.26	16.76	13.77	8.24	12.78
CaO	nd	nd	nd	nd	nd	nd	nd
Na_2O	nd	nd	nd	0.15	0.29	nd	0.16
K_2O	8.66	9.31	9.50	9.13	9.34	9.20	9.46
V_2O_3	nd	nd	0.11	0.18	nd	0.16	0.19
Cr_2O_3	nd	nd	nd	nd	nd	0.04	0.05
Cl	nd	0.04	nd	0.07	0.09	0.10	0.07
H_2O	5.47	4.74	3.30	6.02	4.91	3.69	3.86
Total@	100.00	100.00	100.00	100.00	100.00	100.00	100.00
Structural formula on the basis of 22 oxygens							
Si	5.555	5.648	5.547	5.614	5.537	5.319	5.430
Al(IV)	2.445	2.352	2.454	2.386	2.463	2.682	2.570
Al(VI)	0.699	0.365	0.363	0.061	0.255	0.592	0.057
Ti	0.228	0.375	0.376	0.489	0.394	0.366	0.640
Fe^{2+}	2.129	2.01	2.640	1.455	2.002	2.876	2.074
Mn	nd	nd	0.017	nd	nd	nd	nd
Mg	2.730	2.95	2.312	3.723	3.092	1.880	2.854
Ca	nd	nd	nd	nd	nd	nd	nd
Na	nd	nd	nd	0.044	0.086	nd	0.046
K	1.661	1.779	1.831	1.735	1.794	1.796	1.807
V	nd	nd	0.013	0.021	nd	nd	0.022
Cr	nd	nd	nd	nd	nd	nd	0.006
Sum	15.447		15.550	15.527	15.623	15.535	15.504

* - all Fe is calculated as Fe^{2+}

@ - H_2O is calculated as the difference between the sum of the oxides and 100%

Table IV. (continued)

Sample no.	160	182A	183B	186A	189A	200A	215A
SiO_2	36.15	36.41	36.00	35.91	35.72	37.79	37.86
Al_2O_3	13.74	15.21	16.19	13.72	15.16	13.96	15.55
TiO_2	5.48	5.76	3.00	5.89	5.29	2.84	3.09
FeO*	19.90	15.39	17.89	20.02	18.60	10.94	14.48
MnO	0.07	nd	nd	0.12	nd	0.07	nd
MgO	10.76	13.26	12.95	10.86	11.64	18.78	13.67
CaO	nd	nd	nd	nd	nd	nd	nd
Na_2O	0.23	nd	0.26	nd	0.24	0.24	0.26
K_2O	9.14	9.28	9.51	8.72	9.30	9.25	9.12
V_2O_3	0.28	nd	0.08	0.31	0.14	nd	nd
Cr_2O_3	nd	nd	nd	0.25	nd	0.92	nd
Cl	0.02	0.08	nd	0.06	nd	nd	nd
H_2O	4.20	4.57	3.98	4.30	3.83	5.15	3.93
Total$^{(a)}$	100.00	100.00	100.00	100.00	100.00	100.00	100.00
Structural formula on the basis of 22 oxygens							
Si	5.515	5.443	5.422	5.470	5.395	5.573	5.616
Al(IV)	2.485	2.557	2.578	2.530	2.605	2.427	2.384
Al(VI)	nd	0.124	0.298	nd	0.095	nd	0.336
Ti	0.629	0.649	0.341	0.676	0.602	0.316	0.346
Fe_2^+	2.541	1.925	2.255	2.552	~~2.351~~	1.350	2.045
Mn	0.010	nd	nd	0.015	nd	0.008	nd
Mg	2.450	2.958	2.911	2.468	2.623	4.134	3.025
Ca	nd	nd	nd	nd	nd	nd	nd
Na	0.068	nd	0.076	nd	0.071	0.067	0.075
K	1.781	1.771	1.829	1.696	1.794	1.742	1.726
V	0.035	nd	0.010	0.038	0.017	nd	nd
Cr	nd	nd	nd	0.031	nd	0.107	nd
Sum	15.501	15.428	15.719	15.410	15.552	15.723	15.552

* - all Fe is calculated as Fe^{2+}

(a) - H_2O is calculated as the difference between the sum of the oxides and 100%

Table IV. (continued)

Sample no.	216	231	239B	290B	D1B
SiO_2	37.99	38.14	37.43	33.50	38.09
Al_2O_3	16.44	14.39	14.83	17.74	15.06
TiO_2	3.28	4.17	4.58	2.35	2.35
FeO*	13.62	12.04	15.35	18.97	11.80
MnO	nd	nd	nd	nd	0.07
MgO	14.88	16.67	13.58	12.61	16.51
CaO	nd	nd	0.075	nd	0.05
Na_2O	0.24	0.19	nd	0.29	0.22
K_2O	9.34	9.32	9.24	6.83	9.20
V_2O_3	nd	0.18	nd	nd	0.10
Cr_2O_3	nd	nd	nd	nd	0.16
Cl	0.07	0.03	0.13	0.12	0.09
H_2O	40.08	4.69	4.12	7.63	6.30
Total**	100.00	100.00	100.00	100.00	100.00
	Structural formula on the basis of 22 oxygens				
Si	5.574	5.602	5.565	5.212	5.679
Al(IV)	2.426	2.398	2.436	2.788	2.321
Al(VI)	0.417	0.094	0.165	0.465	0.328
Ti	0.362	0.462	0.513	0.275	0.264
Fe^{2+}	1.672	1.479	1.909	2.470	1.473
Mn	nd	nd	nd	nd	0.008
Mg	3.257	3.697	3.012	2.927	3.673
Ca	nd	nd	0.119	nd	0.007
Na	0.068	0.055	nd	0.086	0.063
K	1.748	1.747	1.754	1.357	1.752
V	nd	0.021	nd	nd	0.012
Cr	nd	nd	nd	nd	0.019
Sum	15.524	15.555	15.473	15.581	15.598

* - all Fe is calculated as Fe^{2+}

** - H_2O is calculated as the difference between the sum of the oxides and 100%

Table IV. (continued)

Sample no.	D10A	D12B	D14C	D21B	D11
SiO_2	37.14	36.48	36.46	37.10	34.03
Al_2O_3	15.38	15.06	18.63	14.42	19.16
TiO_2	1.92	3.09	1.92	3.96	3.95
FeO*	13.86	21.67	14.98	15.87	22.59
MnO	0.14	0.26	0.13	0.21	nd
MgO	16.76	10.48	12.96	13.66	6.42
CaO	nd	nd	nd	nd	nd
Na_2O	nd	0.34	0.22	0.27	nd
K_2O	8.14	9.15	9.63	9.09	8.95
V_2O_3	nd	nd	0.14	0.15	nd
Cr_2O_3	nd	nd	nd	nd	nd
Cl	0.08	nd	0.09	nd	0.08
H_2O	6.42	3.42	4.86	5.27	
Total@	100.00	100.00	100.00	100.00	100.00
Structural formula on the basis of 22 oxygens					
Si	5.579	5.550	5.446	5.593	5.263
Al(IV)	2.421	2.450	2.555	2.407	2.737
Al(VI)	0.302	0.252	0.727	0.157	0.755
Ti	0.218	0.354	0.216	0.450	0.461
Fe^{2+}	1.742	2.759	1.873	2.002	2.922
Mn	0.018	0.033	0.016	0.027	nd
Mg	3.755	2.378	2.886	3.072	1.481
Ca	nd	nd	nd	nd	nd
Na	nd	0.102	0.063	0.080	nd
K	1.561	1.778	1.836	1.749	1.767
V	nd	nd	0.002	0.018	nd
Cr	nd	nd	nd	nd	nd
Sum	15.596	15.657	15.619	15.555	15.386

* - all Fe is calculated as Fe^{2+}

@ - H_2O is calculated as the difference between the sum of the oxides and 100%

Table V.
Garnet Analyses

Sample no.	8B(rim)	8B(core)	8E(rim)	8E(core)	9D(rim)	9D(core)	13D(rim)	13D(core)
SiO_2	37.32	37.44	37.44	37.77	37.14	37.48	36.83	37.25
Al_2O_3	21.87	21.94	21.67	21.80	21.66	21.80	21.49	21.65
TiO_2	nd	nd	nd	nd	nd	nd	nd	nd
FeO*	30.58	30.16	32.41	30.91	33.76	32.33	34.88	32.78
MnO	3.12	3.01	1.53	1.57	2.00	1.91	1.47	2.00
MgO	5.13	5.64	5.51	6.63	4.54	5.55	2.86	4.19
CaO	1.99	1.82	1.45	1.33	0.91	0.93	2.47	2.13
Na_2O	nd	nd	nd	nd	nd	nd	nd	nd
K_2O	nd	nd	nd	nd	nd	nd	nd	nd
Total#	101.26	101.56	102.76	102.72	101.45	100.90	101.66	101.07
Structural formula on the basis of 12 oxygens								
Si	2.955	2.955	2.964	2.966	2.962	2.965	2.962	2.972
Al(IV)	0.045	0.045	0.036	0.034	0.038	0.035	0.038	0.028
Al(VI)	1.997	1.996	1.986	1.984	1.998	1.998	1.999	2.008
Fe^{2+}	2.026	1.992	2.147	2.031	2.252	2.140	2.347	2.187
Mn	0.210	0.201	0.102	0.104	0.135	0.128	0.100	0.135
Mg	0.606	0.664	0.650	0.776	0.540	0.656	0.343	0.498
Ca	0.169	0.154	0.123	0.112	0.078	0.079	0.213	0.182
Na	nd	nd	nd	nd	nd	nd	nd	nd
K	nd	nd	nd	nd	nd	nd	nd	nd
Sum	5.007	5.007	5.008	5.008	5.003	5.001	5.002	5.010
End-member proportions								
Pyr	0.201	0.220	0.215	0.257	0.180	0.218	0.114	0.166
Alm	0.673	0.713	0.710	0.677	0.750	0.713	0.782	0.728
Gross	0.056	0.051	0.041	0.037	0.026	0.026	0.071	0.061
Spess	0.070	0.067	0.034	0.035	0.045	0.043	0.033	0.045

* - all Fe is calculated as Fe^{2+}

# - Total represents the total sum of the oxides before recalculation to 100%

Table V. (continued)

Sample no.	23C(rim)	23C(core)	24B(rim)	54A(rim)	54A(core)	87	135B(rim)	135B(core)
SiO_2	37.06	37.28	36.96	36.97	37.14	36.96	36.96	37.31
Al_2O_3	21.69	21.66	21.84	21.47	21.71	21.66	21.60	21.90
TiO_2	nd	nd	nd	nd	nd	nd	nd	nd
FeO*	33.78	33.11	34.14	33.56	32.59	35.54	36.49	34.61
MnO	1.28	1.23	1.86	2.40	2.35	1.01	0.91	0.71
MgO	5.29	5.85	4.37	4.15	4.92	3.70	3.19	4.58
CaO	0.90	0.87	0.83	1.45	1.28	1.12	0.85	0.89
Na_2O	nd	nd	nd	nd	nd	nd	nd	nd
K_2O	nd	nd	nd	nd	nd	nd	nd	nd
Total#	101.43	101.41	101.47	103.49	103.93	100.97	102.00	102.13
Structural formula on the basis of 12 oxygens								
Si	2.947	2.953	2.950	2.958	2.954	2.961	2.969	2.966
Al(IV)	0.053	0.047	0.050	0.042	0.046	0.039	0.031	0.034
Al(VI)	1.980	1.976	2.006	1.983	1.990	2.008	2.014	2.020
Fe^{2+}	2.248	2.195	2.280	2.246	2.169	2.383	2.459	2.302
Mn	0.086	0.083	0.126	0.163	0.158	0.069	0.062	0.048
Mg	0.628	0.691	0.521	0.495	0.584	0.443	0.382	0.543
Ca	0.077	0.074	0.071	0.124	0.110	0.096	0.074	0.076
Sum	5.019	5.018	5.004	5.012	5.011	4.998	4.991	4.990
End-member proportions								
Pyr	0.207	0.227	0.174	0.164	0.193	0.148	0.128	0.183
Alm	0.740	0.723	0.761	0.742	0.718	0.797	0.826	0.775
Gross	0.025	0.024	0.024	0.041	0.036	0.032	0.025	0.026
Spess	0.028	0.027	0.042	0.054	0.052	0.023	0.021	0.016

* - all Fe is calculated as Fe^{2+}

# - Total represents the total sum of the oxides before recalculation to 100%

Table V. (continued)

Sample no.	182A(rim)	182A(core)	183B(rim)	183B(core)	239B	44	D11
SiO_2	38.11	38.08	36.98	37.67	36.97	37.14	37.04
Al_2O_3	22.19	22.28	21.45	21.72	21.91	21.88	21.71
TiO_2	nd	nd	nd	nd	nd	nd	nd
FeO*	29.08	28.83	34.09	32.89	34.48	32.62	34.49
MnO	1.89	1.93	1.33	1.28	2.91	3.72	2.77
MgO	7.57	7.73	4.65	5.30	3.08	3.83	3.01
CaO	1.17	1.17	1.51	1.45	0.65	0.78	0.98
Na_2O	nd	nd	nd	nd	nd	nd	nd
K_2O	nd	nd	nd	nd	nd	nd	nd
Total#	101.27	101.43	101.98	101.59	101.67	101.32	101.41
Structural formula on the basis of 12 oxygens							
Si	2.966	2.961	2.952	2.961	2.967	2.967	2.974
Al(IV)	0.034	0.039	0.048	0.039	0.033	0.033	0.026
Al(VI)	2.003	2.004	1.971	1.991	2.040	2.028	2.030
Fe^{2+}	1.894	1.876	2.277	2.181	2.316	2.181	2.317
Mn	0.124	0.127	0.090	0.086	0.198	0.252	0.188
Mg	0.880	0.897	0.553	0.626	0.369	0.457	.361
Ca	0.097	0.097	0.129	0.123	0.056	0.067	0.084
Sum	4.998	5.001	5.021	5.006	4.978	4.985	4.980
End-member proportions							
Pyr	0.294	0.299	0.182	0.208	0.125	0.155	0.122
Alm	0.631	0.625	0.747	0.723	0.788	0.738	0.786
Gross	0.033	0.032	0.042	0.041	0.019	0.023	0.029
Spess	0.042	0.042	0.030	0.029	0.067	0.085	0.064

* - all Fe is calculated as Fe^{2+}

# - Total represents the total sum of the oxides before recalculation to 100%

Table VI.
Plagioclase Analyses

	1B	5A	5E	7C	8B	8E	9D	9F
SiO_2	55.31	47.63	56.18	54.05	58.54	60.18	60.89	56.55
Al_2O_3	28.10	33.49	27.68	29.06	26.18	24.99	24.27	27.45
FeO	0.13	0.11	nd	0.36	0.09	nd	nd	0.13
CaO	10.53	16.62	9.68	11.11	8.00	6.76	6.08	9.61
Na_2O	5.74	2.03	5.85	4.99	6.92	7.69	8.26	6.15
K_2O	0.19	0.13	0.61	0.26	0.28	0.34	0.21	0.10
BaO	nd	nd	nd	nd	nd	nd	nd	nd
Total@	101.15	99.71	99.53	99.36	100.19	99.28	100.16	99.44
Structural formula on the basis of 8 oxygens								
Si	2.493	2.181	2.525	2.444	2.614	2.640	2.712	2.535
Al(IV)	1.493	1.809	1.467	1.549	1.378	1.292	1.275	1.454
Fe^{2+}	0.005	0.004	nd	0.014	0.00	nd	nd	0.005
Ca	0.510	0.817	0.467	0.539	0.383	0.251	0.291	0.462
Na	0.502	0.180	0.511	0.438	0.600	0.503	0.714	0.535
K	0.008	0.007	0.035	0.015	0.016	0.016	0.012	0.006
Ba	nd	nd	nd	nd	nd	nd	nd	nd
Sum	5.002	4.999	5.004	4.994	4.702	5.003	4.998	4.991

@ - Total represent the total sum of the oxides before recalculation to 100%

Table VI. (continued)

Sample no. @	13D	22L	23B	44	54A	56A	87A	135B
SiO_2	56.85	57.84	58.79	67.65	60.24	48.91	60.69	57.96
Al_2O_3	27.21	26.53	25.78	19.54	24.92	32.53	24.69	26.02
FeO	0.14	nd	nd	0.28	nd	0.13	nd	1.09
CaO	9.50	8.67	8.07	0.35	6.61	15.59	6.38	6.05
Na_2O	6.03	6.45	6.81	10.89	7.75	2.44	7.85	8.31
K_2O	0.28	0.51	0.42	0.91	0.43	0.31	0.30	0.10
BaO	nd	nd	nd	0.33	nd	nd	nd	nd
Total	99.44	99.15	100.05	99.53	100.78	98.53	99.63	102.08
Structural formula on the basis of 8 oxygens								
Si	2.549	2.589	2.628	2.976	2.682	2.237	2.698	2.609
Al(IV)	1.439	1.401	1.359	1.012	1.308	1.754	1.294	1.381
Fe^{2+}	0.005	nd	nd	0.010	nd	0.005	nd	0.041
Ca	0.457	0.416	0.387	0.016	0.315	0.765	0.304	0.292
Na	0.525	0.561	0.591	0.929	0.669	0.216	0.677	0.726
K	0.016	0.029	0.024	0.051	0.025	0.018	0.017	0.006
Sum	4.991	4.995	4.989	4.996	5.001	4.994	4.991	5.056
End member proportions								
An	0.458	0.414	0.386	0.016	0.313	0.765	0.305	0.285
Ab	0.526	0.557	0.590	0.932	0.663	0.216	0.678	0.709
Or	0.016	0.029	0.023	0.052	0.025	0.018	0.017	0.006

@ - Total represent the total sum of the oxides before recalculation to 100%
nd - not detected

Table VI. (continued)

Sample no.	135B	141B	142A	160	182A	183B	183D	186A
SiO_2	66.57	46.22	57.57	48.35	57.99	58.49	53.93	56.96
Al_2O_3	19.48	34.04	26.86	32.64	26.43	26.28	29.60	26.77
FeO	nd	0.14	0.08	0.23	nd	nd	0.30	0.12
CaO	0.34	17.79	8.87	15.96	8.34	7.96	12.02	9.02
Na_2O	11.46	1.39	6.23	2.51	6.77	6.82	3.84	6.41
K_2O	1.95	0.14	0.40	0.28	0.43	0.30	0.27	0.59
BaO	0.20	0.12	nd	nd	nd	0.05	nd	nd
Total	99.61	100.32	99.20	99.48	99.16	100.01		99.66
Structural formula on the basis of 8 oxygens								
Si	2.952	2.131	2.576	2.216	2.595	2.613	2.431	2.562
Al(IV)	1.019	0.1851	1.418	1.764	1.395	1.385	1.573	1.420
Fe^{2+}	nd	0.005	0.003	0.009	nd	nd	0.011	0.005
Ca	0.016	0.880	0.426	0.785	0.401	0.382	0.581	0.435
Na	0.986	0.124	0.541	0.223	0.588	0.591	0.336	0.560
K	0.110	0.008	0.023	0.016	0.024	0.017	0.015	0.034
Sum	5.001	5.001	4.986	5.013	5.003	4.988	4.948	5.014
End member proportions								
An	0.014	0.869	0.430	0.766	0.395	0.386	0.623	0.423
Ab	0.887	0.123	0.547	0.218	0.581	0.597	0.361	0.544
Or	0.099	0.008	0.023	0.016	0.024	0.017	0.016	0.033

@ - Total represent the total sum of the oxides before recalculation to 100%
nd - not detected

Table VI. (continued)

Sample no.	189A	231	290B	GAB	DJB
SiO_2	58.09	49.08	58.30	46.89	57.05
Al_2O_3	26.50	32.21	26.31	33.93	26.97
FeO	0.07	0.31	0.21	0.05	0.09
CaO	8.44	15.03	7.99	17.29	8.90
Na_2O	6.51	2.89	6.40	1.72	6.10
K_2O	0.38	0.36	0.82	0.08	0.60
BaO	nd	0.12	nd	nd	0.14
Total	99.42	100.93	98.72	99.23	98.68
Structural formula on the basis of 8 oxygens					
Si	2.597	2.245	2.610	2.152	2.565
Al	1.397	1.739	1.385	1.836	1.430
Fe^{2+}	0.003	0.012	0.008	0.002	0.003
Ca	0.405	0.738	0.384	0.852	0.429
Na	0.565	0.257	0.556	0.154	0.532
K	0.022	0.021	0.047	0.005	0.034
Sum	4.987	5.013	4.989	5.000	4.993
End member proportions					
An	0.408	0.726	0.389	0.843	0.431
Ab	0.570	0.253	0.564	0.152	0.534
Or	0.022	0.021	0.047	0.005	0.035

@ - Total represent the total sum of the oxides before recalculation to 100%

nd - not detected

Table VI. (continued)

Sample no.	D10A	D12B	D14C	D21B
SiO_2	54.86	59.71	57.44	57.11
Al_2O_3	28.50	25.12	26.39	27.01
FeO	0.17	0.15	nd	0.14
CaO	10.89	6.77	8.21	9.02
Na_2O	5.04	7.49	7.16	6.11
K_2O	0.49	0.70	0.70	0.51
BaO	0.05	0.08	nd	0.11
Total@	100.28	100.28	100.64	98.02
Structural formula on the basis of 8 oxygens				
Si	2.474	2.666	2.582	2.563
Al	1.516	1.322	1.398	1.429
Fe^{2+}	0.006	0.006	nd	0.005
Na	0.527	0.324	0.396	0.434
K	0.441	0.649	0.625	0.532
Sum	4.993	5.007	5.041	4.993
End member proportions				
An	0.529	0.320	0.373	0.436
Ab	0.443	0.641	0.589	0.535
Or	0.028	0.040	0.038	0.029

@ - Total represent the total sum of the oxides before recalculation to 100%
nd - not detected

Table VII.
K-feldspar Analyses

Sample no.	5E(a)	5E(m)	8E(a)	13D	44(m)	135B(m)	135B(p)	182A(a)
SiO_2	65.13	64.16	64.66	64.76	65.02	64.94	64.80	64.36
Al_2O_3	18.65	18.77	18.64	19.23	18.72	18.94	18.91	18.82
FeO	nd	nd	nd	nd	nd	nd	nd	nd
CaO	0.09	nd	nd	0.51	nd	0.10	0.07	nd
Na_2O	0.47	0.84	0.96	1.23	1.19	1.10	1.06	0.70
K_2O	15.24	15.16	15.39	13.89	14.54	14.25	14.47	15.12
BaO	0.43	0.62	0.45	1.38	0.54	0.55	0.59	0.99
Total	100.02	100.25	100.46	99.48	99.07	101.01	101.03	99.12
Structural formula on the basis of 8 oxygens								
Si	3.001	2.981	2.983	2.961	2.988	2.985	2.983	2.976
Al	1.013	1.021	1.014	1.037	1.015	1.026	1.026	1.026
Ca	0.004	nd	nd	0.025	nd	0.005	0.004	nd
Na	0.042	0.075	0.077	0.109	0.106	0.098	0.095	0.063
K	0.895	0.893	0.906	0.811	0.853	0.836	0.850	0.893
Ba	0.008	0.011	0.008	0.025	0.010	0.010	0.011	0.018
Sum	4.963	4.980	4.989	4.968	4.972	4.960	4.969	4.976
End member proportions								
An	0.005	nd	nd	0.027	nd	0.005	0.004	nd
Ab	0.044	0.078	0.079	0.116	0.110	0.105	0.100	0.066
Or	0.951	0.922	0.922	0.858	0.890	0.890	0.896	0.934

* - Total represent the total sum of the oxides before recalculation to 100%
nd - not detected
(a) - exsolved phase in antiperthite
(m) - microcline
(p) - host perthite phase

Table VII. (continued)

Sample no.	182A(m)	189A(a)	239B(m)	D1B	D10D	D14C
SiO_2	64.82	64.05	64.69	65.01	64.66	63.94
Al_2O_3	18.96	18.92	19.13	18.70	18.56	18.89
FeO	nd	nd	nd	nd	nd	nd
CaO	nd	nd	nd	nd	0.06	nd
Na_2O	1.34	0.57	2.46	0.59	0.23	0.76
K_2O	14.05	14.90	12.98	14.73	16.17	15.01
BaO	0.83	1.56	0.64	0.98	0.29	1.40
Total	99.33	100.13	101.85	100.05	100.20	100.96
	Structural formula on the basis of 8 oxygens					
Si	2.985	2.970	2.967	2.994	2.988	2.967
Al	1.029	1.035	1.035	1.015	1.011	1.034
Ca	nd	nd	nd	nd	0.003	nd
Na	0.119	0.052	0.219	0.052	0.021	0.068
K	0.825	0.882	0.760	0.866	0.954	0.889
Ba	0.015	0.028	0.012	0.018	0.005	0.026
Sum	4.978	4.967	4.993	4.945	4.982	4.983
	End member proportions					
An	nd	nd	nd	nd	0.003	nd
Ab	0.126	0.055	0.223	0.058	0.021	0.071
Or	0.874	0.945	0.777	0.943	0.976	0.929

@ - Total represent the total sum of the oxides before recalculation to 100%
nd - not detected
(a) - exsolved phase in antiperthite
(m) - microcline
(p) - host perthite phase

Table VIII.
Cordierite Analyses

Sample no.	9D	23C	24B	44	135B	182A
SiO_2	48.10	48.25	48.14	47.87	47.24	48.51
Al_2O_3	32.52	32.67	32.65	32.42	32.55	32.79
FeO*	8.56	7.63	7.84	8.35	10.34	6.00
MnO	0.20	nd	0.13	0.37	0.03	0.11
MgO	8.14	8.67	8.26	7.20	7.19	9.80
CaO	nd	nd	nd	nd	nd	nd
Na_2O	nd	0.51	nd	nd	nd	nd
K_2O	nd	0.07	nd	0.29	nd	0.18
Cl	0.04	0.10	0.11	0.20	0.07	0.19
H_2O	2.45	2.01	2.90	2.70	2.67	2.45
Total@	100.00	100.00	100.00	100.00	100.00	100.00
Structural formula on the basis 18 oxygens						
Si	4.993	4.981	5.001	5.028	4.952	4.990
Al	3.981	3.976	4.000	4.016	4.024	3.977
Fe^{2+}	0.743	0.659	0.681	0.734	0.907	0.516
Mn	0.018	nd	0.011	0.033	0.003	0.009
Mg	1.260	1.335	1.280	1.129	1.125	1.504
Sum	10.993	11.061	10.974	10.939	11.011	10.997

* - all Fe is calculated as Fe^{2+}

@ - H_2O is calculated as the difference between the sum of the oxides and 100%

Table VIII. (continued)

	210B	215A	216	239B	290B	D11
SiO_2	47.87	48.77	48.55	47.99	48.03	42.30
Al_2O_3	33.06	33.71	33.48	32.66	32.69	33.51
FeO*	10.21	7.10	6.27	9.83	7.17	5.03
MnO	0.17	0.28	0.40	0.41	0.15	nd
MgO	7.21	8.76	9.18	6.71	8.70	2.13
CaO	nd	nd	nd	nd	nd	0.45
Na_2O	0.20	0.41	0.30	0.32	nd	nd
K_2O	nd	nd	0.21	0.32	0.29	3.42
Cl	0.09	0.18	0.20	0.19	0.24	0.16
H_2O	0.83	0.63	1.43	1.63	2.64	11.57
Total**	100.00	100.00	100.00	100.00	100.00	100.00
Structural formula on the basis 18 oxygens						
Si	4.955	4.970	4.970	4.991	4.991	4.939
Al	4.035	4.050	4.041	4.005	4.005	4.615
Fe^{2+}	0.884	0.605	0.537	0.855	0.623	0.491
Mn	0.015	0.024	0.035	0.037	0.013	nd
Mg	1.114	1.331	1.402	1.041	1.349	0.372
Sum	11.002	10.980	10.985	11.035	10.982	10.983

* - all Fe is calculated as Fe^{2+}

** - H_2O is calculated as the difference between the sum of the oxides and 100%

Table IX.
Sillimanite Analyses

Sample no.	135B	210B	215A	216	239B	D11
SiO_2	36.79	36.55	36.71	36.34	36.12	36.76
Al_2O_3	62.18	61.99	61.65	61.81	62.08	62.07
Fe_2O_3*	0.94	1.27	1.31	1.48	1.50	0.76
Total@	99.10	100.91	101.43	100.37	100.86	99.04
Structural formula on the basis of 5 oxygens						
Si	0.995	0.991	0.997	0.988	0.982	0.997
Al	1.983	1.982	1.974	1.982	1.990	1.984
Fe^{3+}	0.019	0.026	0.027	0.030	0.031	0.016
Sum	2.997	2.999	2.997	2.999	3.002	2.997

* - all Fe is represented as Fe^{3+}

@ - Total represents the total sum of the oxides before recalculation to 100%

Table X.
Ilmenite Analyses

Sample no.	5A	8B	8E	9D	22D	22L	23B
FeO*	46.712	44.61	43.13	47.28	44.32	45.40	41.91
TiO_2	50.62	50.19	52.50	50.94	50.55	51.49	50.36
MnO	1.26	3.94	2.67	0.90	2.69	2.15	6.28
MgO	.045	0.29	0.26	0.24	0.77	0.40	0.34
V_2O_3	0.18	nd	nd	nd	nd	nd	nd
Cr_2O_3	0.09	nd	nd	nd	nd	0.07	nd
ZnO	nd	nd	0.79	nd	1.01	nd	nd
Al_2O_3	0.29	0.30	0.24	0.29	0.47	0.18	0.30
SiO_2	0.39	0.44	0.33	0.29	0.19	0.27	0.26
CaO	nd	nd	nd	0.27	nd	nd	nd
Total@	100.87	99.26	102.55	100.04	100.02	101.03	99.34
Structural formula on the basis of 2 oxygens							
Fe^{2+}	0.963	0.920	0.911	0.974	0.923	0.943	0.869
Fe^{3+}#	0.013	0.015		0.013	0.012	0.010	0.014
Ti	0.952	0.947	0.998	0.958	0.960	0.973	0.955
Mn	0.027	0.084	0.057	0.019	0.057	0.046	0.134
Mg	0.017	0.011	0.010	0.009	0.029	0.015	0.013
V	0.004	nd	nd	nd	nd	nd	nd
Cr	0.002	nd	nd	nd	nd	0.001	nd
Al	0.008	0.009	0.007	0.008	0.014	0.005	0.009
Si	0.009	0.011	0.008	0.007	0.005	0.007	0.006
Sum	1.996	1.995	1.992	1.996	1.999	2.000	1.999

@ - Total represents the total sum of the oxides before recalculation to 100%
* - FeO represents all Fe calculated as Fe^{2+}
# - Fe in the structural formula has been divided into estimates of Fe^{2+} and Fe^{3+}

Table X. (continued)

Sample no.	23C	24B	44	55C	56A	135B
FeO*	48.03	46.79	47.38	43.98	36.96	48.24
TiO_2	50.65	51.16	50.06	50.33	50.81	50.51
MnO	0.31	1.14	1.71	4.32	10.79	0.29
MgO	0.27	0.25	0.25	0.34	0.28	0.18
V_2O_3	0.16	nd	nd	nd	nd	0.25
Cr_2O_3	nd	nd	nd	0.16	nd	nd
ZnO	nd	nd	nd	nd	nd	nd
Al_2O_3	0.31	0.37	0.31	0.22	0.28	0.25
SiO_2	0.25	0.29	0.30	0.33	0.36	0.22
CaO	nd	nd	nd	nd	nd	nd
Total@	101.26	100.80	101.35	100.79	100.72	101.55
Structural formula on the basis of 2 oxygens						
Fe^{2+}	0.993	0.970	0.975	0.911	0.765	1.000
Fe^{3+}#	0.014	0.011	0.016	0.014	0.012	0.015
Ti	0.955	0.966	0.942	0.952	0.962	0.950
Mn	0.007	0.024	0.036	0.092	0.230	0.006
Mg	0.010	0.010	0.009	0.013	0.010	0.007
V	0.003	nd	nd	nd	nd	nd
Cr	nd	nd	nd	nd	nd	nd
Al	0.009	0.011	0.009	0.006	0.008	0.007
Si	0.006	0.007	0.007	0.008	0.008	0.005
Sum	1.997	1.999	1.995	1.999	1.997	1.996

@ - Total represents the total sum of the oxides before recalculation to 100%
* - FeO represents all Fe calculated as Fe^{2+}
# - Fe in the structural formula has been divided into estimates of Fe^{2+} and Fe^{3+}

Table X. (continued)

Sample no.	141B	160	182A	183D	186A	210B
FeO*	46.19	46.20	48.21	44.57	44.54	46.52
TiO_2	50.38	50.78	49.70	52.59	50.14	50.52
MnO	0.46	1.76	0.91	2.56	3.69	1.75
MgO	1.66	0.33	031	nd	0.38	0.31
V_2O_3	0.52	0.28	nd	nd	0.27	nd
Cr_2O_3	0.15	nd	nd	nd	0.14	nd
ZnO	nd	nd	nd	nd	nd	nd
Al_2O_3	0.27	0.28	0.50	nd	0.29	0.53
SiO_2	0.31	0.29	0.63	0.13	0.51	0.26
CaO	nd	nd	nd	nd	nd	nd
Total(a)	100.39	100.77	100.25	99.97	100.29	100.98
	Structural formula on the basis of 2 oxygens					
Fe^{2+}	0.943	0.957	0.987	0.941	0.919	0.961
Fe^{3+}#	0.015	0.012	0.016		0.014	0.014
Ti	0.941	0.957	0.931	0.999	0.945	0.953
Mn	0.010	0.037	0.019	0.055	0.078	0.037
Mg	0.062	0.013	0.012	nd	0.014	0.012
V	0.010	0.006	nd	nd	0.006	nd
Cr	0.003	nd	nd	nd	0.003	nd
Al	0.008	0.008	0.015	nd	0.009	0.016
Si	0.008	0.007	0.016	0.003	0.013	0.006
Sum	1.9988	1.999	1.995	1.999	1.999	1.998

(a) - Total represents the total sum of the oxides before recalculation to 100%

* - FeO represents all Fe calculated as Fe^{2+}

# - Fe in the structural formula has been divided into estimates of Fe^{2+} and Fe^{3+}

Table X. (continued)

Sample no.	216	215A	231	239A	290B	D21B
FeO*	45.70	47.67	41.84	46.86	45.90	35.87
TiO_2	49.31	49.30	50.17	49.26	51.29	50.34
MnO	3.02	1.95	6.40	2.39	1.88	8.43
MgO	0.37	0.27	0.43	0.31	0.39	0.42
V_2O_3	nd	0.11	nd	nd	nd	0.13
Cr_2O_3	nd	nd	0.12	nd	nd	nd
ZnO	nd	nd	nd	nd	nd	nd
Al_2O_3	1.26	0.41	0.67	0.88	0.25	0.51
SiO_2	0.31	0.30	0.38	0.29	nd	2.55
CaO	nd	nd	nd	nd	nd	1.75
Total	100.33	99.69	100.28	100.74	100.60	98.40
Structural formula on the basis of 2 oxygens						
Fe^{2+}	0.936	0.979	0.857	0.959	0.953	0.752
Fe^{3+}#	0.016	0.018	0.015	0.017	0.012	
Ti	0.925	0.928	0.941	0.925	0.971	0.950
Mn	0.064	0.041	0.135	0.050	0.040	0.179
Mg	0.014	0.010	0.016	0.011	0.015	0.016
V	nd	nd	nd	nd	nd	nd
Cr	nd	nd	nd	nd	nd	nd
Al	0.037	0.012	0.020	0.026	0.008	0.015
Si	0.008	0.008	0.010	0.007	nd	0.064
Sum	1.999	1.998	1.996	1.996	1.997	1.979

@ - Total represents the total sum of the oxides before recalculation to 100%

* - FeO represents all Fe calculated as Fe^{2+}

# - Fe in the structural formula has been divided into estimates of Fe^{2+} and Fe^{3+}

Table XI.
Magnetite Analyses

Sample no.	8E	9D	22D	23B	23C	24B
Fe_2O_3	65.25	67.15	67.48	65.09	65.44	67.38
FeO	29.31	30.17	30.31	29.37	29.58	30.25
TiO_2	0.78	0.86	nd	0.42	0.30	0.20
MnO	nd	nd	nd	nd	nd	nd
MgO	0.42	0.24	0.23	0.42	0.31	0.25
V_2O_3	1.21	0.38	0.19	1.35	2.04	0.52
Cr_2O_3	1.41	0.17	0.21	2.21	1.67	0.44
ZnO	nd	nd	nd	nd	nd	nd
Al_2O_3	0.75	0.72	0.58	0.76	0.75	0.82
SiO_2	0.49	0.31	nd	0.37	0.40	0.28
Total(a)	102.29	99.82	99.26	102.95	101.95	99.26
Structural formula on the basis of 4 oxygens						
Fe^{3+}	1.860	1.860	1.956	1.789	1.852	1.846
Fe^{2+}	0.929	1.014	0.984	0.992	0.933	1.039
Ti	0.022	0.025	nd	0.012	0.008	0.006
Mn	nd	nd	nd	nd	nd	nd
Mg	0.024	0.014	0.013	0.024	0.017	0.014
V	0.037	0.012	0.058	0.041	0.062	0.016
Cr	0.043	0.005	0.006	0.066	0.050	0.013
Al	0.034	0.033	0.027	0.034	0.033	0.037
Si	0.019	0.012	nd	0.014	0.015	0.011
Sum	2.966	2.973	2.992	2.971	2.970	2.981

(a) - Total represents the total sum of the oxides before recalculation to 100%

Table XI. (continued)

Sample no.	44	56A	141B	182A	210B	215A
Fe_2O_3	67.92	64.58	56.84	66.79	66.59	66.39
FeO	30.65	29.14	25.65	30.01	30.05	28.29
TiO_2	nd	2.89	1.19	0.80	1.30	1.10
MnO	nd	0.39	0.06	nd	nd	nd
MgO	0.20	0.42	0.62	0.26	0.29	0.36
V_2O_3	nd	0.49	3.64	0.44	0.44	0.32
Cr_2O_3	nd	0.76	9.38	0.40	0.26	0.33
ZnO	nd	nd	nd	nd	nd	nd
Al_2O_3	0.68	0.68	2.19	1.04	0.77	1.13
SiO_2	0.24	0.50	0.33	0.28	0.31	0.42
Total@	101.52	103.08	100.75	101.70	103.13	101.90
Structural formula on the basis of 4 oxygens						
Fe^{3+}	1.943	1.687	1.381	1.844	1.826	1.804
Fe^{2+}	0.995	1.055	0.985	1.010	1.021	1.012
Ti	nd	0.082	0.033	0.023	0.037	0.032
Mn	nd	0.012	0.020	nd	nd	nd
Mg	0.011	0.024	0.034	0.014	0.017	0.020
V	nd	0.015	0.108	0.013	0.013	0.010
Cr	nd	0.023	0.273	0.012	0.008	0.010
Al	0.031	0.030	0.095	0.046	0.034	0.051
Si	0.009	0.019	0.012	0.011	0.012	0.016
Sum	2.989	2.946	2.923	2.972	2.968	2.954

@ - Total represents the total sum of the oxides before recalculation to 100%

Table XI. (continued)

Sample no.	216	231	239A	290B	D21B
Fe_2O_3	67.04	65.66	67.21	65.92	67.20
FeO	30.25	29.63	30.33	29.81	30.32
TiO_2	0.40	0.15	0.17	2.5	0.38
MnO	nd	nd	nd	nd	nd
MgO	0.32	0.38	0.29	0.31	0.27
V_2O_3	0.31	2.40	0.60	0.16	0.47
Cr_2O_3	0.25	0.59	0.17	nd	0.13
ZnO	nd	nd	nd	nd	nd
Al_2O_3	1.02	0.59	0.90	0.91	0.80
SiO_2	0.41	0.39	0.33	0.23	0.43
Total(a)	101.18	102.64	101.60	102.24	100.15
Structural formula on the basis of 4 oxygens					
Fe^{3+}	1.869	1.829	1.890	1.765	1.877
Fe^{2+}	1.002	0.989	0.995	1.047	1.005
Ti	0.011	0.004	0.005	0.071	0.011
Mn	nd	nd	nd	nd	nd
Mg	0.018	0.022	0.016	0.018	0.015
V	0.009	0.073	0.018	0.049	0.014
Cr	0.008	0.018	0.005	nd	0.004
Al	0.045	0.026	0.040	0.040	0.036
Si	0.016	0.015	0.013	0.009	0.016
Sum	2.978	2.976	2.982	2.955	2.978

(a) - Total represents the total sum of the oxides before recalculation to 100%

Table XII.
Hercynite Analyses

Sample no.	9D	22D	23C.	44	135B	239A	290A	290B
FeO*	39.35	26.68	37.05	40.65	40.46	42.78	37.38	37.07
TiO_2	nd	nd	nd	nd	nd	0.20	nd	nd
MnO	0.33	0.66	0.14	0.43	0.05	0.41	0.25	0.32
MgO	3.49	10.84	2.28	2.57	2.21	2.12	3.24	4.05
V_2O_3	nd	nd	0.22	nd	nd	nd	0.11	nd
Cr_2O_3	0.15	0.39	3.24	0.21	1.11	0.28	0.16	nd
ZnO	0.11	2.08	4.21	0.69	1.04	0.19	0.49	1.27
Al_2O_3	56.42	59.36	52.68	55.36	54.47	53.95	55.58	57.21
SiO_2	0.16	nd	0.19	nd	0.30	nd	nd	nd
Total@	100.67	99.73	100.41	99.59	99.37	100.42	99.74	99.38
	Structural formula on the basis of 4 oxygens							
Fe^{3+}	0.015	0.016	0.017	0.019	0.016	0.020		0.015
Fe^{2+}	0.923	0.588	0.887	0.959	0.967	1.017	0.924	0.864
Ti	nd	nd	nd	nd	nd	0.004	nd	nd
Mn	0.008	0.015	0.003	0.010	0.001	0.010	0.006	0.008
Mg	0.148	0.437	0.099	0.110	0.096	0.091	0.143	0.171
V	nd	nd	0.005	nd	nd	nd	0.003	nd
Cr	0.003	0.008	0.075	0.005	0.026	0.006	0.004	nd
Zn	0.002	0.041	0.091	0.015	0.022	0.004	nd	0.027
Al	1.895	1.892	1.811	1.877	1.864	1.842	1.935	1.913
Si	0.005	nd	nd	nd	0.009	nd	nd	nd
Sum	2.999	2.998	2.994	2.995	2.999	2.996	3.014	2.998

* - FeO represents all Fe calculated as Fe^{2+}

@ - Total represents the total sum of the oxides before recalculation to 100%

# - Fe in the structural formula has been divided into estimates of Fe^{2+} and Fe^{3+}

Table XIII.
Sphene Analyses

Sample no.	23B	55C	D4A	D10B	D10D
SiO_2	30.10	30.57	30.93	31.23	31.02
Al_2O_3	1.24	nd	1.44	2.42	2.15
TiO_2	39.32	38.33	36.75	37.38	37.71
FeO	nd	2.64	1.44	0.89	0.65
MnO	nd	nd	0.31	nd	nd
CaO	27.92	28.30	28.05	28.08	28.42
Total	99.65	97.69	98.23	95.99	97.29
Structural formula on the basis of 5 oxygens					
Si	0.986	1.010	1.016	1.015	1.010
Al	0.048	nd	0.056	0.093	0.082
Ti	0.970	0.954	0.909	0.915	0.924
Fe^{2+}	0.039	0.073	0.040	0.024	0.018
Ca	0.981	1.003	0.988	0.979	0.992
Sum	3.023	3.039	3.038	3.025	3.026

(a) - Total represents the total sum of the oxides before recalculation to 100%

Table XIV.
Rutile Analyses

Sample no.	55C	135B	210B	231	290B
TiO_2	96.98	95.91	95.05	86.80	96.31
FeO	1.20	0.72	3.92	11.74	3.27
MnO	nd	nd	nd	0.19	nd
MgO	0.22	0.48	0.20	0.14	nd
V_2O_3	0.29	0.70	nd	0.33	nd
Cr_2O_3	0.20	0.19	nd	0.12	nd
ZnO	nd	0.23	0.34	0.23	nd
Al_2O_3	nd	1.47	0.32	0.20	nd
SiO_2	0.37	0.31	0.19	0.18	nd
CaO	0.66	nd	nd	0.07	nd
Total	99.90	103.70	100.55	97.79	100.71
Structural formula on the basis of 2 oxygens					
Ti	0.980	0.964	0.970	0.920	0.981
Fe^{2+}	0.014	0.008	0.044	0.138	0.037
Mn	nd	nd	nd	0.002	nd
Mg	0.004	0.010	0.004	0.003	nd
V	0.003	0.008	nd	0.004	nd
Cr	0.002	0.002	nd	0.001	nd
Zn	nd	0.002	0.004	0.002	nd
Al	nd	0.023	0.005	0.003	nd
Si	0.005	0.004	0.003	0.003	nd
Ca	0.010	nd	nd	0.001	nd
Sum	1.017	1.020	1.029	1.077	1.021

[a] - Total represents the total sum of the oxides before recalculation to 100%

Table XV.
Prehnite Analyses

Sample no.	8B	22G	22L	D10A	D10C	D21B
SiO_2	42.10	43.59	43.15	43.12	42.45	42.58
Al_2O_3	22.39	24.02	23.68	21.53	21.53	21.99
TiO_2	1.28	0.21	1.07	nd	nd	nd
Fe_2O_3*	2.86	0.77	1.23	4.00	3.24	3.58
MnO	nd	nd	nd	nd	nd	nd
MgO	0.89	nd	0.50	0.80	0.54	1.63
CaO	24.89	26.99	25.60	25.44	25.80	24.35
Na_2O	0.18	nd	nd	nd	nd	nd
K_2O	0.06	0.09	0.23	0.19	0.18	0.23
V_2O_3	nd	nd	nd	0.11	0.21	0.21
Cr_2O_3	nd	nd	nd	0.21	0.28	0.23
H_2O	5.35	4.33	4.54	4.57	5.71	5.09
Total@	100.00	100.00	100.00	100.00	100.00	100.00
Structural formula on the basis of 22 oxygens						
Si	5.917	6.002	5.958	6.050	6.025	5.989
Al(IV)	0.083	nd	0.042			0.011
Al(VI)	3.628	3.899	3.812	3.562	3.602	3.635
Ti	0.136	0.022	0.112	nd	nd	nd
Fe^{3+}	0.336	0.089	0.142	0.469	0.385	0.422
Mg	0.187	nd	0.103	0.168	0.115	0.341
Ca	3.754	3.987	3.793	3.829	3.929	3.674
Na	0.048	nd	nd	nd	nd	nd
K	0.011	0.017	0.041	0.034	0.032	0.042
V	nd	nd	nd	0.012	0.023	0.023
Cr	nd	nd	nd	0.023	0.031	0.025
Sum	14.100	14.015	14.003	14.147	14.142	14.162

* - all Fe is represented as Fe^{3+}

@ - H_2O is calculated as the difference between the total sum of the oxides and 100%

Table XV.
Epidote and Grandite Analyses

Sample no.	5A	D14C	D21B	D10A**
SiO_2	38.99	38.16	37.47	35.02
Al_2O_3	28.09	21.61	21.96	8.53
TiO_2	nd	nd	1.90	1.02
Fe_2O_3	7.02	15.83	13.96	18.05
MnO	nd	nd	0.12	nd
MgO	nd	nd	nd	nd
CaO	23.48	22.86	22.56	34.79
H_2O	0.02	1.54	2.03	3.98
Total	100.00	100.00	100.00	100.00
Structural formula#				
Si	3.149	3.158	3.105	5.817
Al	2.675	2.109	2.146	1.671
Ti	nd	nd	nd	0.127
$Fe^{''}$	0.427	0.986	0.871	2.256
Ca	2.035	2.029	2.006	6.200
Sum	8.286	8.281	8.255	16.071

* - all Fe is represented as $Fe^{''}$

@ - H_2O is calculated as the difference between the total sum of the oxides and 100%

** - analysis of grandite; all other analyses are epidotes

# - structural formula for epidote is on the basis of 13 oxygens

# - structural formula for grandite is on the basis of 24 oxygens

Table XVI.
Rare Earth Element Analyses (rocks)

Sample no.	GAB	56A	141B	186A	22L
La	1.6±0.3	6.2±0.7	5.4±0.3	10±3	4.9±0.5
Ce	5.0±0.7	13.3±0.8	13.7±0.8	22.7±0.9	12.5±0.8
Nd	nd±	7±1	12±1	15±1	10±2
Sm	0.70±0.02	2.35±0.05	2.78±0.06	3.55±0.08	2.04±0.04
Eu	0.30±0.02	0.82±0.03	0.93±0.03	1.26±0.03	0.76±0.02
Tb	0.29±0.04	0.54±0.05	0.56±0.05	0.60±0.05	0.38±0.04
Tm	0.11±0.03	0.43±0.07	0.34±0.08	0.13±0.03	0.37±0.06
Yb	0.89±0.07	2.1±0.1	1.64±0.09	1.76±0.09	1.73±0.09
Lu	0.09±0.03	0.39±0.05	0.20±0.04	0.29±0.03	0.37±0.05
U	nd	0.23±0.05	0.19±0.03	0.22±0.05	0.13±0.05
Th	nd	nd	nd	nd	nd
Hf	nd	1.3±0.1	1.7±0.1	2.0±0.1	1.3±0.1
Ta	0.09±0.01	0.19±0.02	0.41±0.03	0.24±0.02	0.26±0.03

nd - not detected
Concentrations in ppm

Table XVI. (continued)

Sample no.	163D	1B	183B	23B	23C
La	26±1	77±3	12.0±0.7	45.0±2	34±1
Ce	67±2	160±3	29.6±0.9	93±2	75±2
Nd	44±2	80±2	16±1	38±2	30±2
Sm	9.8±0.2	12.6±0.3	3.60±0.08	8.0±0.2	6.3±0.1
Eu	1.62±0.04	2.98±0.07	1.68±0.04	1.33±0.04	0.41±0.03
Tb	1.42±0.09	0.93±0.06	0.30±0.03	1.8±0.1	1.52±0.09
Tm	0.63±0.08	nd	nd	1.8±0.2	2.0±0.2
Yb	4.0±0.2	1.4±0.1	0.67±0.08	15.7±0.5	17.2±0.6
Lu	0.55±0.05	0.23±0.05	0.11±0.02	2.1±0.1	2.5±0.2
U	0.32±0.07	1.5±0.1	1.07±0.08	1.7±0.1	1.7±0.1
Th	1.6±0.2	16.3±0.6	0.5±0.2	17.0±0.5	16.8±0.5
Hf	2.0±0.1	5.4±0.3	22.4±0.8	12.8±0.5	22.4±0.8
Ta	0.44±0.03	0.51±0.04	0.49±0.03	0.84±0.05	2.84±0.05

nd - not detected
Concentrations in ppm

Table XVI. (continued)

Sample no.	135B	290A	216	44	145B
La	33±1	67±2	41±1	52±2	8.4±0.5
Ce	66±1	127±2	86±2	106±2	16.7±0.6
Nd	28±1	52±2	37±2	43±1	9.2±0.9
Sm	5.0±0.1	8.4±0.2	6.7±0.2	7.3±0.2	3.11±0.07
Eu	1.24±0.03	1.84±0.04	1.25±0.03	1.50±0.03	1.20±0.03
Tb	0.86±0.05	0.56±0.03	0.78±0.05	0.63±0.04	0.68±0.04
Tm	0.45±0.05	0.06±0.03	0.19±0.04	0.16±0.03	0.26±0.05
Yb	2.6±0.1	0.55±0.05	2.1±0.1	1.43±0.08	2.11±0.09
Lu	0.41±0.04	0.10±0.03	0.25±0.03	0.16±0.03	0.19±0.03
U	0.99±0.07	1.03±0.07	1.23±0.08	1.22±0.09	0.21±0.04
Th	12.6±0.4	24.7±0.7	17.8±0.5	19.3±0.6	1.0±0.1
Hf	5.6±0.2	5.3±0.2	5.3±0.2	6.3±0.3	2.2±0.1
Ta	0.91±0.05	0.35±0.02	1.42±0.08	1.16±0.07	0.06±0.01

nd - not detected
Concentrations in ppm

Table XVI. (continued)

Sample no.	166D	122	92	233A	40A
La	11.0±0.6	26±1	20±1.0	75±3	3.0±0.5
Ce	23.9±0.8	47±1	55±1	142±3	4.9±0.3
Nd	17±1	14.4±0.8	21.6±0.9	54±1	nd
Sm	3.62±0.08	2.78±0.06	3.26±0.07	6.8±0.2	0.29±0.01
Eu	1.38±0.03	0.40±0.01	0.27±0.01	1.77±0.04	0.05±0.01
Tb	0.69±0.04	0.34±0.02	0.23±0.01	0.27±0.02	nd
Tm	0.36±0.05	0.20±0.03	0.10±0.02	0.11±0.02	nd
Yb	1.76±0.08	1.59±0.06	1.01±0.06	0.23±0.06	nd
Lu	0.12±0.03	0.17±0.02	0.14±0.02	0.07±0.02	nd
U	0.20±0.04	4.0±0.2	7.1±0.4	9.2±0.5	1.26±0.08
Th	nd±	17.7±0.5	19.5±0.6	20.7±0.6	nd
Hf	2.2±0.1	3.0±0.1	2.2±0.1	4.4±0.2	0.28±0.05
Ta	0.18±0.02	0.70±0.04	0.78±0.05	0.46±0.03	0.12±0.02

nd - not detected
Concentrations in ppm

Table XVI. (continued)

Sample no.	D4A	50:50*	75:25#
La	49±2	28.5	20.2
Ce	102±2	61.5	45.5
Nd	51±1	26.7	21.3
Sm	10.5±0.2	5.7	4.7
Eu	2.37±0.05	1.5	1.6
Tb	1.12±0.07	1.1	0.7
Tm	0.29±0.05		
Yb	2.3±0.1	8.2	4.4
Lu	0.33±0.03	1.1	0.6
U	0.24±0.05		
Th	2.5±0.2		
Hf	4.9±0.2		
Ta	0.17±0.02		

nd - not detected
Concentrations in ppm
* - 50:50 represents the calculated composition of a 50% melt and a 50% restite mixture
# - 75:25 represents the calculated composition of a 75% melt and a 25% restite mixture

Table XVII.
Rare Earth Element Analyses (minerals)

Sample no.	141B-p	186A-p	183D-p	GAB-p	183B-p
La	5.4±0.3	11.7±0.6	21.2±0.8	1.6±0.2	9.0±0.4
Ce	9.2±0.3	17.2±0.4	22.6±0.5	1.5±0.1	16.9±0.4
Nd	4.4±0.4	5.7±0.4	5.3±0.5	0.3±0.2	5.5±0.3
Sm	0.88±0.02	0.90±0.02	0.72±0.02	0.03±0.01	0.76±0.02
Eu	0.33±0.01	1.82±0.03	1.19±0.02	0.27±0.01	1.89±0.04
Tb	0.10±0.01	0.10±0.01	0.05±0.01	nd	0.06±0.01
Tm	0.03±0.02	nd	nd	nd	0.07±0.01
Yb	0.24±0.04	0.13±0.02	0.09±0.03	nd	0.03± 0.02
Lu	ndnd		nd	nd	nd±
U	0.15±0.02	0.17±0.03	nd	nd	0.07±0.02
Th	0.59±0.09	nd	nd	nd	nd
Hf	0.12±0.03	0.92±0.05	0.33±0.04	nd	0.31±0.02
Ta	nd	nd	0.1±0.01	0.1±0.01	nd
Eu/Eu*	1.3	7.0	6.4	30.4	

nd - not detected
Concentrations in ppm
Eu/Eu* - ratio of measured Eu to the theoretical Eu^{3+} value
p - under sample no. p stands for plagioclase

Table XVII. (continued)

Sample no.	290A-p	141B-o	186A-o	183D-o	GAB-o
La	23.0±0.8	0.6±0.3	0.66±0.04	0.7±0.2	3.6±0.5
Ce	40.8±0.8	1.6±0.5	3.9±0.7	5.3±0.5	1.5±0.6
Nd	14.1±0.5	nd	nd	3.5±0.8	1.4±0.9
Sm	2.26±0.05	0.25±0.01	0.71±0.02	0.74±0.02	0.08±0.01
Eu	1.10±0.02	0.09±0.02	0.14±0.02	0.09±0.02	0.05±0.02
Tb	0.15±0.01	0.06±0.02	0.18±0.04	0.16±0.03	0.07±0.03
Tm	nd	0.10±0.03	0.38±0.06	0.16±0.03	0.10±0.05
Yb	0.12±0.01	0.74±0.07	2.2±0.1	1.12±0.06	0.23±0.06
Lu	0.03±0.01	0.18±0.03	0.31±0.04	0.22±0.03	0.08±0.03
U	0.13±0.03	0.12±0.03	0.32±0.04	nd	nd
Th	0.91±0.05	0.09±0.05	nd	nd	0.2±0.1
Hf	1.19±0.05	0.59±0.08	7.5±0.3	0.32±0.07	nd
Ta	nd	0.02±0.01	0.09±0.02	0.04±0.01	0.02±0.01
Eu/Eu*	2.0	0.9	0.5	0.3	

nd - not detected
Concentrations in ppm
Eu/Eu* - ratio of measured Eu to the theoretical Eu^{3+} value
p - under the sample no. p stands for plagioclase
o - under the sample no. o stands for orthopyroxene

Table XVII. (continued)

Sample no.	141B-c	186A-c	183D-c	141B-h	183D-h
La	4.1±0.5	5.6±0.5	39±1	18±2	42±2
Ce	14.1±0.9	27±1	76±2	54±1	119±3
Nd	15±1	30±2	35±1	43±2	77±2
Sm	4.30±0.09	8.9±0.2	6.6±0.2	11.7±0.3	18.7±0.4
Eu	0.90±0.03	0.72±0.04	0.74±0.02	3.02±0.06	2.35±0.05
Tb	0.84±0.06	1.6±0.1	0.85±0.05	2.1±0.1	2.5±0.1
Tm	0.61±0.08	1.0±0.1	0.58±0.07	1.1±0.1	1.2±0.1
Yb	2.3±0.1	4.6±0.2	2.9±0.1	5.9±0.2	7.1±0.3
Lu	0.29±0.03	0.60±0.05	0.38±0.04	0.76±0.07	0.89±0.07
U	0.13±0.04	0.31±0.06	0.08±0.05	0.38±0.06	0.20±0.07
Th	0.3±0.2	nd	9.2±0.3	0.9±0.2	4.9±0.3
Hf	1.8±0.1	7.6±0.3	2.0±0.1	4.7±0.2	2.4±0.2
Ta	nd	nd	nd	0.51±0.04	0.69±0.04
Eu/Eu*	0.6	0.2	0.4	0.8	0.4

nd - not detected
Concentrations in ppm
Eu/Eu* - ratio of measured Eu to the theoretical Eu^{3+} value
c - under the sample no. c stands for clinopyroxene
h - under the sample no. h stands for hornblende

Table XVII. (continued)

Sample no.	GAB-h	186A-a	183D-a	GAB-a	183B-a
La	1.4±0.5	93±4	452±16	26±3	276±11
Ce	6.4±0.8	224±6	891±19	52±3	982±20
Nd	4±1	133±6	425±14	29±4	931±22
Sm	1.22±0.03	26.8±0.6	69±2	6.3±0.2	241±5
Eu	0.38±0.03	3.4±0.1	6.0±0.2	0.70±0.08	10.1±0.3
Tb	0.26±0.04	3.7±0.3	7.0±0.5	1.0±0.1	23±1
Tm	0.26±0.09	1.1±0.4	±	nd	3.3±0.7
Yb	1.34±0.09	6.3±0.4	12.5±0.8	1.4±0.2	24±1
Lu	0.23±0.04	0.9±0.2	1.8±0.3	0.13±0.09	1.7±0.2
U	nd	7.2±0.5	10.0±0.8	1.7±0.2	36±2
Th	nd	nd	26±2	nd	16±2
Hf	0.5±0.1	77±3	25±1	28±1	164±6
Ta	0.17±0.02	0.46±0.08	nd	0.32±0.05	1.2±0.2
Eu/Eu*	0.9	0.4	0.3	0.3	0.2

nd - not detected
Concentrations in ppm
Eu/Eu* - ratio of measured Eu to the theoretical Eu^{3+} value
h - under the sample no. h stands for hornblende
a - under the sample no. a stands for apatite

Table XVII. (continued)

Sample no.	183B-z	183B-g
La	11±2	nd
Ce	47±2	2±1
Nd	39±12	3±2
Sm	23.0±0.5	1.51±0.03
Eu	7.3±0.3	0.30±0.04
Tb	14.4±0.9	1.08±0.08
Tm	17±1	0.70±0.09
Yb	256±8	6.3±0.2
Lu	34±2	1.0±0.3
U	292±16	0.38±0.06
Th	85±4	nd
Hf	9783±342	9.9±0.4
Ta	59±3	0.05±0.02
Eu/Eu*	0.6	0.4

nd - not detected
Concentrations in ppm
Eu/Eu* - ratio of measured Eu to the theoretical Eu^{3+} value
z - under the sample no. z stands for zircon
g - under the sample no. g stands for garnet

Table XVIII.
Whole Rock Geochemical Analyses: Metasedimentary Lithologies

Sample no.	23C	73D	142C	210B	23B	59	156B
SiO_2	38.4	43.0	48.1	47.4	54.1	55.1	59.6
Al_2O_3	25.5	23.3	18.5	26.4	17.5	22.9	16.5
Fe_2O_3	6.2	6.0	6.4	4.6	3.6	2.3	1.3
FeO	15.9	10.4	10.1	7.7	11.1	8.5	5.7
MgO	5.71	4.56	6.47	2.99	3.9	3.04	4.35
CaO	0.36	1.54	1.77	0.45	3.21	1.30	3.55
Na_2O	nd	0.3	0.7	0.8	1.2	0.9	3.7
K_2O	1.15	5.43	2.99	2.92	1.32	3.44	2.02
TiO_2	2.57	1.78	1.77	1.14	0.94	1.00	2.02
MnO	0.62	0.11	0.20	0.09	0.56	0.18	0.16
S	0.12	0.01	0.03	0.01	0.04	0.09	0.17
P_2O_5	0.01	0.04	0.03	0.03	0.03	0.03	0.27
H_2O	2.40	2.0	1.8	5.4	1.40	1.20	1.2
CO_2	0.10	nd	0.2	nd	0.10	0.10	0.1
V	410	250	260	190	130	160	130
Cr	41	360	460	200	210	190	280
Ni	180	210	140	92	60	85	100
Cu	25	4.0	5.6	4.5	18	23	56
Co	50	49	51	32	30	35	27
Rb	89	356	168	167	73	189	166
Sr	37	230	250	100	310	250	200
Ba	730	2200	1500	990	550	1300	530
Zr	762	395	376	276	452	226	237
Nb	30	23	14	13	6	15	15
Y	83	30	28	31	110	70	44
Pb	13	41	27	16	23	34	26
U	9	6	0	1	3	0	0
Th	14	16	12	22	21	13	13

trace elements concentrations are given in ppm

Table XVIII. (continued)

Sample no.	183B	44	54D	62	83A	87A	88A
SiO_2	52.4	60.6	63.3	68.9	60.3	62.1	68.3
Al_2O	23.4	19.0	18.7	15.3	23.8	17.6	15.3
Fe_2O_3	0.7	4.9	1.0	1.1	nd	2.1	0.6
FeO	4.2	5.2	2.3	4.3	0.6	4.8	3.7
MgO	2.87	1.94	0.7	1.75	0.28	2.56	1.59
CaO	6.54	0.62	2.67	2.09	5.53	1.23	2.68
Na_2O	4.6	0.30	3.3	1.9	5.5	2.0	3.4
K_2O	2.76	3.01	6.41	1.76	2.33	2.72	1.57
TiO_2	0.79	0.94	0.08	0.61	0.05	0.66	0.51
MnO	0.05	0.23	0.28	0.21	0.03	0.18	0.09
S	0.07	nd	0.09	0.07	0.01	0.08	nd
P_2O_5	0.40	0.02	0.63	0.01	0.04	0.03	0.05
H_2O	0.9	2.7	0.5	1.6	0.7	2.8	1.5
CO_2	nd	nd	0.1	0.1	0.1	0.1	0.1=
V	110	130	27	78	34	89	50
Cr	20	150	10	95	17	120	71
Ni	10	62	nd	34	10	42	30
Cu	11	5.8	21	23	18	12	4.4
Co	20	37	9.7	23	nd	23	14
Rb	204	254	278	86	29	204	84
Sr	680	86	520	220	703	160	330
Ba	1300	780	1200	450	330	700	510
Zr	915	229	72	185	46	185	170
Nb	7	11	nd	7	2	11	11
Y	26	32	520	49	29	41	42
Pb	43	24	50	27	45	22	20
U	10	8	13	3	2	7	0
Th	17	16	9	10	12	18	14

trace elements concentrations are given in ppm

Table XVIII. (continued)

Sample no.	112B	134B	144A	152A	181B	202B	213B
SiO_2	63.1	69.8	67.4	67.5	63.5	69.4	68.8
Al_2O_3	15.1	15.4	13.9	15.5	18.5	15.3	15.3
Fe_2O_3	2.4	0.3	1.1	2.6	1.3	1.0	1.3
FeO	5.8	1.5	4.3	4.8	3.7	2.5	1.8
MgO	1.83	0.95	2.52	2.09	1.77	1.32	0.71
CaO	5.21	2.62	1.70	0.12	3.71	3.20	2.17
Na_2O	2.0	2.1	2.8	nd	4.0	2.5	2.6
K_2O	0.95	4.30	1.98	2.76	1.85	1.39	4.97
TiO_2	0.95	0.25	0.68	0.89	0.50	0.46	0.61
MnO	0.12	0.04	0.09	0.06	0.17	0.05	0.02
S	0.10	0.03	0.04	0.08	0.02	0.01	nd
P_2O_5	0.17	0.02	0.01	0.02	0.26	0.07	0.11
H_2O	1.7	1.0	2.1	3.6	1.0	1.4	0.7
CO_2	0.1	0.1	0.3	0.1	0.1	nd	0.1
V	230	27	81	110	67	48	40
Cr	20	12	93	150	27	14	9.1
Ni	15	nd	38	63	23	10	nd
Cu	18	31	26	27	11	12	8.7
Co	30	13	21	27	19	14	7.9
Rb	38	96	76	111	93	62	189
Sr	250	400	330	46	300	530	220
Ba	820	2500	750	840	340	510	1700
Zr	128	152	298	228	86	227	610
Nb	13	4	12	15	7	4	6
Y	59	29	33	46	46	28	nd
Pb	20	45	14	8	27	27	50
U	0	0	0	0	0	3	7
Th	2	6	16	8	1	22	79

trace elements concentrations are given in ppm

Table XVIII. (continued)

Sample no.	215	54A	54C	55C	88B	180A
SiO_2	67.7	74.0	72.0	71.5	73.4	71.4
Al_2O_3	15.2	14.2	15.0	13.8	14.1	14.5
Fe_2O_3	4.8	nd	0.2	1.0	0.1	0.9
FeO	4.0	0.3	0.5	4.3	0.9	1.7
MgO	1.89	0.13	0.32	1.37	0.38	0.76
CaO	0.14	0.48	0.70	0.55	0.38	2.02
Na_2O	nd	2.1	2.40	1.0	4.5	2.8
K_2O	2.22	8.05	7.68	3.93	3.65	3.48
TiO_2	0.98	0.07	0.10	0.61	0.14	0.30
MnO	0.08	0.01	0.01	0.07	0.02	0.07
S	0.04	nd	nd	0.08	nd	0.01
P_2O_5	0.02	0.13	0.13	0.05	0.05	0.04
H_2O	2.0	0.4	0.6	1.6	0.70	0.6
CO_2	nd	nd	nd	0.10	0.1	nd
V	96	18	22	67	17	32
Cr	140	nd	nd	100	nd	32
Ni	56	nd	nd	37	nd	10
Cu	16	5.7	7.0	52	12	7.7
Co	24	12	12	20	11	14
Rb	118	432	413	310	195	87
Sr	42	240	220	110	240	240
Ba	650	780	600	710	820	1000
Zr	279	7	57	189	81	122
Nb	10	2	15	17	3	4
Y	26	29	25	31	33	41
Pb	12	62	62	25	34	32
U	0	31	42	3	0	0
Th	17	6	12	13	3	4

trace elements concentrations are given in ppm

Table XIX.
Whole Rock Geochemical Analyses: Metaigneous Lithologies

Sample no.	78	200A	GAB	56B	97	113A	130
SiO_2	47.9	48.4	47.7	52.8	54.6	53.7	58.6
Al_2O_3	6.0	6.2	16.4	14.8	18.5	17.8	16.8
Fe_2O_3	4.0	2.6	1.7	6.1	2.3	3.5	2.1
FeO	7.3	10.1	7.0	8.3	5.6	4.9	5.1
MgO	16.6	21.2	11.0	6.16	4.08	4.55	3.70
CaO	10.7	3.96	11.5	7.49	4.52	7.06	5.85
Na_2O	nd	nd	0.6	0.7	1.6	3.3	1.2
K_2O	0.26	1.59	0.58	0.6	2.59	1.50	1.88
TiO_2	0.62	0.65	0.22	1.27	1.14	1.11	0.85
MnO	0.27	0.20	0.18	0.32	0.14	0.14	0.12
S	0.01	0.44	0.03	0.03	0.21	0.24	0.19
P_2O_5	0.05	0.06	nd	0.07	0.49	0.54	0.38
H_2O	4.5	4.8	2.7	1.50	3.9	1.4	1.4
CO_2	1.6	nd	0.1	0.10	0.2	0.10	0.1
V	160	130	170	450	130	180	100
Cr	2400	2000	460	27	25	56	150
Ni	600	1000	210	73	25	56	32
Cu	7.8	130	60	25	54	75	92
Co	78	220	57	54	21	27	23
Rb	3	115	290	23	890	45	93
Sr	32	36	130	130	540	750	580
Ba	39	65	43	140	1200	920	870
Zr	31	44	134	63	100	184	140
Nb	2	2	9	4	6	9	8
Y	43	38	35	46	39	43	39
Pb	14	11	45	18	15	21	28
U	4	0	0	3	0	0	0
Th	0	0	3	5	7	3	8

trace elements concentrations are given in ppm

Table XIX. (continued)

Sample no.	186A	200D	178	189A	145B	166C	166D
SiO_2	50.7	53.6	62.7	60.5	51.8	50.5	50.5
Al_2O_3	15.3	15.2	17.2	16.8	15.5	16.6	13.9
Fe_2O_3	1.3	1.5	2.2	1.0	2.7	2.1	2.2
FeO	9.1	7.1	3.5	5.2	9.5	9.0	10.2
MgO	7.35	7.96	2.37	4.52	4.92	4.63	6.33
CaO	9.49	6.12	5.03	4.76	8.78	5.66	7.76
Na_2O	2.0	0.1	3.0	2.1	2.1	2.9	1.7
K_2O	1.10	2.45	2.03	2.03	0.37	1.25	0.48
TiO_2	0.66	1.19	0.78	0.80	1.32	1.44	1.44
MnO	0.26	0.12	0.11	0.07	0.23	0.16	0.20
S	0.24	0.33	0.11	0.19	0.18	0.12	0.16
P_2O_5	0.13	0.43	0.22	0.19	0.08	0.15	0.12
H_2O	1.6	3.5	1.1	1.4	2.7	4.5	3.7
CO_2	nd	nd	0.1	nd	0.3	0.8	0.2
V	180	130	110	120	180	140	160
Cr	160	420	23	130	96	58	170
Ni	94	170	14	91	52	31	740
Cu	81	86	14	51	69	44	9
Co	40	39	20	29	96	33	45
Rb	34	147	122	121	5	38	11
Sr	250	530	720	530	150	440	240
Ba	370	1500	1600	1100	160	610	280
Zr	590	425	198	146	69	73	67
Nb	3	15	12	8	2	2	3
Y	38	36	43	36	26	39	37
Pb	19	34	26	55	9	11	11
U	0	11	0	6	0	0	0
Th	5	39	22	28	1	1	2

trace elements concentrations are given in ppm

Table XX.
Whole Rock Geochemical Analyses: Granitic Lithologies

Sample no.	35A	56E	65	71	81D	92	117A
SiO_2	74.9	75.0	74.5	75.3	73.8	73.8	74.9
Al_2O_3	14.0	14.7	14.6	13.7	14.5	14.8	14.0
Fe_2O_3	nd	0.1	0.2	nd	0.2	0.1	0.2
FeO	0.4	0.5	0.4	0.3	1.0	0.8	0.7
MgO	0.12	0.32	0.31	0.11	0.39	0.22	0.32
CaO	0.61	1.22	0.53	0.58	0.81	0.71	0.93
Na_2O	2.5	1.7	2.80	1.8	2.2	3.3	3.8
K_2O	6.80	5.51	5.69	7.32	5.76	4.95	4.44
TiO_2	0.04	0.08	0.09	0.04	0.28	0.12	0.07
MnO	0.02	0.02	0.01	0.01	0.02	0.07	0.06
S	nd	0.01	nd	nd	0.01	nd	0.07
P_2O_5	0.16	0.08	0.16	0.08	0.12	0.12	0.04
H_2O	0.4	0.50	0.6	0.30	0.8	0.4	0.4
CO_2	nd	0.10	nd	nd	nd	0.1	0.1
V	12	34	20	11	15	21	nd
Cr	nd	18	nd	nd	7.1	nd	nd
Ni	nd	nd	nd	nd	nd	nd	nd
Cu	6.4	13	5.5	7.1	6.2	12	5.8
Co	8.5	12	14	11	8.3	11	8.9
Rb	317	237	375	202	294	361	158
Sr	130	240	44	180	97	58	160
Ba	530	1900	150	41	490	240	580
Zr	9	51	25	3	165	73	48
Nb	4	1	9	1	13	14	6
Y	21	30	27	25	29	31	39
Pb	33	27	31	26	41	27	29
U	2	4	8	1	11	1	0
Th	4	9	4	2	42	4	0

trace elements concentrations are given in ppm

Table XX. (continued)

Sample no.	122	135A	135E	205	207
SiO_2	75.4	72.6	71.2	73.9	74.2
Al_2O_3	14.0	14.4	15.1	14.5	14.2
Fe_2O_3	0.4	0.2	0.3	0.2	0.2
FeO	0.8	0.6	0.6	1.0	0.3
MgO	0.46	0.38	0.45	0.34	0.05
CaO	0.72	1.16	0.67	0.79	0.3
Na_2O	3.5	2.2	1.5	2.3	3.3
K_2O	4.12	6.4	7.72	6.08	5.31
TiO_2	0.16	0.16	0.23	0.23	0.04
MnO	0.05	0.01	0.01	0.01	0.03
S	nd	nd	nd	nd	nd
P_2O_5	0.04	0.04	0.05	0.14	0.16
H_2O	0.7	0.3	0.6	0.7	0.4
CO_2	0.1	0.1	0.1	nd	nd
V	11	26	58	22	25
Cr	11	9.9	19	nd	14
Ni	nd	nd	nd	10	10
Cu	5.7	6.9	6.2	7.7	6.6
Co	9.8	14	14	8.4	7.4
Rb	161	180	217	298	358
Sr	160	360	390	71	38
Ba	640	4100	5900	300	82
Zr	92	189	95	137	4
Nb	8	5	4	11	4
Y	38	30	29	24	20
Pb	23	59	66	48	24
U	0	0	0	6	0
Th	9	13	13	22	0

trace elements concentrations are given in ppm